GEORGIA INSTITUTE OF TECHNOLOGY — OFFICE OF CONTRACT ADMINISTRATION

PROJECT ADMINISTRATION DATA SHEET

[X] ORIGINAL [ ] REVISION NO. _____

Project No. E-25-616 GTRI/~~GKK~~ DATE 12/19/83

Project Director: Dr. Thomas L. Eddy School/~~KMX~~ ME

Sponsor: National Science Foundation

Type Agreement: Grant No. CPE-8311325

Award Period: From 12/15/83 To 5/31/8~~6~~* (Performance) 8/31/85* (Reports)

Sponsor Amount:	This Change	Total to Date
Estimated:	$	$ 70,000
Funded:	$	$ 70,000

Cost Sharing Amount: $ 10,390 Cost Sharing No: E-25-314

Title: "Radiative Properties of Non-Local Thermodynamic Equilibrium Plasmas"

ADMINISTRATIVE DATA OCA Contact Lynn Boyd X4820

1) Sponsor Technical Contact:

Dr. Royal E. Rostenbach
National Science Foundation
Engineering Energetics Program
Washington, DC 20550

(202) 357-9606

2) Sponsor Admin/Contractual Matters:

Al Rice
National Science Foundation
Washington, DC 20550

(202) 357-9626

Defense Priority Rating: N/A Military Security Classification: None

(or) Company/Industrial Proprietary: _____

RESTRICTIONS

See Attached NSF Supplemental Information Sheet for Additional Requirements.

Travel: Foreign travel must have prior approval – Contact OCA in each case. Domestic travel requires sponsor approval where total will exceed greater of $500 or 125% of approved proposal budget category.

Equipment: Title vests with GIT - see section 8 of Grant General Conditions

COMMENTS:

* Includes usual six-month unfunded flexibility period.

Continuing grant - 1st year of 2

COPIES TO:

Project Director (Eddy)
Research Administrative Network
Research Property Management
Accounting
Procurement/EES Supply Services
Research Security Services
(Reports Coordinator (OCA))
Research Communications (2)
GTRI
Library
Project File
Other I. Newton

GEORGIA INSTITUTE OF TECHNOLOGY OFFICE OF CONTRACT ADMINISTRATION

SPONSORED PROJECT TERMINATION/CLOSEOUT SHEET

Date Dec. 8, 1987 .

Project No. E-25-616 School/~~DEPT~~ ME

Includes Subproject No.(s) N/A

Project Director(s) T. L. Eddy GTRC ~~GIT~~

Sponsor NSF

Title Radiative Properties of Non-Local Thermodynamic Equilibrium Plasmas

Effective Completion Date: 5/31/86 (Performance) 8/31/86 (Reports)

Grant/Contract Closeout Actions Remaining:

- [x] None
- [ ] Final Invoice or Final Fiscal Report
- [ ] Closing Documents
- [ ] Final Report of Inventions
- [ ] Govt. Property Inventory & Related Certificate
- [ ] Classified Material Certificate
- [ ] Other

Continues Project No. Continued by Project No.

COPIES TO:

Project Director
Research Administrative Network
Research Property Management
Accounting
Procurement/GTRI Supply Services
Research Security Services
Reports Coordinator (OCA)
Legal Services

Library
GTRC
Research Communications (2)
Project File
Other Duane Hutchison
Angela DuBose
Russ Embry

FORM OCA 69.285

FINAL REPORT

RADIATIVE PROPERTIES OF NON-LOCAL THERMAL EQUILIBRIUM PLASMAS

BY

T. L. EDDY
A. SEDGHINASAB
K. Y. CHO
R. V. FRIERSON
R. T. MURRAY

UNDER
NATIONAL SCIENCE FOUNDATION GRANT #CPE-8311325

FOR THE PERIOD OF DECEMBER 1983 THROUGH JUNE 1986

GEORGIA INSTITUTE OF TECHNOLOGY
A UNIT OF THE UNIVERSITY SYSTEM OF GEORGIA
THE GEORGE W. WOODRUFF SCHOOL OF MECHANICAL ENGINEERING
ATLANTA, GEORGIA 30332

1987

NATIONAL SCIENCE FOUNDATION
Washington, D.C. 20550

FINAL PROJECT REPORT
NSF FORM 98A

PLEASE READ INSTRUCTIONS ON REVERSE BEFORE COMPLETING

PART I—PROJECT IDENTIFICATION INFORMATION

1. Institution and Address	2. NSF Program	3. NSF Award Number
Georgia Tech Research Institute Atlanta, Georgia 30332		CPE-8311325
	4. Award Period From 12-83 To 6-86	5. Cumulative Award Amount $155,185

6. Project Title

PART II—SUMMARY OF COMPLETED PROJECT *(FOR PUBLIC USE)*

An experimental investigation of electric arc plasmas which are not in local thermodynamic equilibrium (LTE) has resulted in 1) an improvement in a multitemperature thermodynamic model to describe non-LTE plasmas, 2) a diagnostics method to determine the complete non-LTE plasma state from emission spectroscopy, 3) the experimental determination of the onset of LTE with increasing pressure or electron density, and 4) the reason for experimental variations in the atomic transition probability values of argon with corrected values having uncertainties of 5%. The study used a 30 Amp, argon, 3-mm dia., wall-stabilized arc at pressures from 0.1 to 10 bar. It is found that LTE is approached asymptotically at pressures above 1-atm. Small differences in the gas, electron, and total excitation temperature result in much larger differences in species particle densities; hence, LTE with respect to densities (within 10%) is near 5-atm ($N_e \gtrsim 1.5 \times 10^{17} cm^{-3}$) on the axis of the present arc. The improved or generalized multithermal equilibrium (GMTE) model was developed from a detailed study of hydrogen plasma. The model has also been applied to argon plasma. The resulting ArI transition probability values are within the range of the NBS 25% uncertainty values, but when properly corrected for non-LTE, they shift dependent upon upper energy level of the transition. This result can yield much different relative excitation temperatures than obtained previously.

PART III—TECHNICAL INFORMATION *(FOR PROGRAM MANAGEMENT USES)*

1. ITEM *(Check appropriate blocks)*	NONE	ATTACHED	PREVIOUSLY FURNISHED	TO BE FURNISHED SEPARATELY TO PROGRAM	
				Check (✓)	Approx. Date
a. Abstracts of Theses		1		2	March '88
b. Publication Citations		X			
c. Data on Scientific Collaborators	X				
d. Information on Inventions	X				
e. Technical Description of Project and Results		X			
f. Other *(specify)*					

2. Principal Investigator/Project Director Name *(Typed)*	3. Principal Investigator/Project Director Signature	4. Date
Thomas L. Eddy		11-18-87

NSF Form 98A (1-87) Supersedes All P

Form Approved OMB No. 3145-005

PART IV - SUMMARY DATA ON PROJECT PERSONNEL

NSF Division _____

The data requested below will be used to develop a statistical profile on the personnel supported through NSF grants. The information on this part is solicited under the authority of the National Science Foundation Act of 1950, as amended. All information provided will be treated as confidential and will be safeguarded in accordance with the provisions of the Privacy Act of 1974. NSF requires that a single copy of this part be submitted with each Final Project Report (NSF Form 98A); however, submission of the requested information is not mandatory and is not a precondition of future awards. If you do not wish to submit this information, please check this box ☐

Please enter the numbers of individuals supported under this NSF grant.
Do not enter information for individuals working less than 40 hours in any calendar year.

*U.S. Citizens/ Permanent Visa	PI's/PD's		Post-doctorals		Graduate Students		Under-graduates		Precollege Teachers		Others	
	Male	Fem.	Male	Fem.	Male	Fem.	Male	Fem.	Male	Fem.	Male	Fem
American Indian or Alaskan Native												
Asian or Pacific Islander					1							
Black, Not of Hispanic Origin												
Hispanic												
White, Not of Hispanic Origin	1				2						1	
Total U.S. Citizens	1				1						1	
Non U.S. Citizens					2							
Total U.S. & Non-U.S. ..	1				3						1	
Number of individuals who have a handicap that limits a major life activity.												

*Use the category that best describes person's ethnic/racial status. (If more than one category applies, use the one category that most closely reflects the person's recognition in the community.)

AMERICAN INDIAN OR ALASKAN NATIVE: A person having origins in any of the original peoples of North America, and who maintains cultural identification through tribal affiliation or community recognition.

ASIAN OR PACIFIC ISLANDER: A person having origins in any of the original peoples of the Far East, Southeast Asia, the Indian subcontinent, or the Pacific Islands. This area includes, for example, China, India, Japan, Korea, the Philippine Islands and Samoa.

BLACK, NOT OF HISPANIC ORIGIN: A person having origins in any of the black racial groups of Africa.

HISPANIC: A person of Mexican, Puerto Rican, Cuban, Central or South American or other Spanish culture or origin, regardless of race.

WHITE, NOT OF HISPANIC ORIGIN: A person having origins in any of the original peoples of Europe, North Africa or the Middle East.

THIS PART WILL BE PHYSICALLY SEPARATED FROM THE FINAL PROJECT REPORT AND USED AS A COMPUTER SOURCE DOCUMENT. DO NOT DUPLICATE IT ON THE REVERSE OF ANY OTHER PART OF THE FINAL REPORT.

Georgia Tech

THE GEORGE W. WOODRUFF SCHOOL OF
MECHANICAL ENGINEERING

Georgia Institute of Technology
Atlanta, Georgia 30332-0405

November 17, 1987

Dr. Robert Goulard
Thermal Systems and Engineering
Room 1126
National Science Foundation
1800 G. Street, Northwest
Washington, D.C. 20050

Dear Dr. Goulard:

Please find enclosed our final report for NSF Grant No. CPE-8311325 entitled "Radiative Properties of Non-Local Thermal Equilibrium Plasmas". The final results were completed, after funding expired, via the Ph.D. thesis of Ahad Sedghinasab. We both wished to provide NSF with a completed work and hence the delay in the submission of this final report.

Also enclosed are the following:

1. NSF Form 98A.

2. One abstract of a thesis for a student working on and related to the grant: A. Sedghinasab (Ph.D.). He should graduate in December 1987. R. Frierson assisted A. Sedghinasab and applied the GMTE diagnostics to his M.S. thesis on measurements of a rotating arc and obtained excellent results. He also should graduate in December 1987. R. Frierson's thesis abstract and an abstract from K. Y. Cho's Ph.D. thesis will be sent when available. Mr. Cho was instrumental in applying MTE to hydrogen and modifying it to GMTE from which we were able to obtain excellent non-LTE diagnostics and accurate argon transition probability values.

3. List of publication citations.

Sincerely,

Thomas L. Eddy
Associate Professor

TLE:cn

Experimental Determination of Argon Atomic Transition Probabilities using non–LTE Diagnostics

A THESIS

Presented to

The Faculty of the Division of Graduate Studies

By

Ahad Sedghinasab

In Partial Fulfillment

of the Requirements for the Degree

Doctor of Philosophy in Mechanical Engineering

Georgia Institute of Technology

October, 1987

Summary

A generalized multithermal equilibrium model (GMTE) based on the multifluid approach and the extension of the multitemperature mass action law is developed and used to study the argon atomic transition probabilities. For this purpose, arc experiments at 30A and 0.1 to 10 bar are performed. Measured line intensities are corrected for self-absorption and line wings. Stark broadening of H_β line of hydrogen is used to determine the electron density directly. The total excitation temperature, T_{exa}, the upper level excitation temperature, $T_{ex\beta}$, the gas temperature, T_g, and the electron temperature, T_e are calculated and plotted against the operating pressure and the electron density to determine the onset of the LTE condition. The LTE condition is found to exist at $n_e \geq 10^{17} cm^{-3}$. Accurate knowledge of the true LTE condition made possible the calculation of improved transition probability values for prominent argon lines. The new values of transition probabilities are compared to those given by the NBS. The difference is found to be energy level dependent, ranging from –38% for lines emitted from lower energy levels to +27% for lines emitted from higher energy levels. The model is also used to generate thermodynamic and radiative properties of argon at various nonequilibrium conditions. The Rydberg-Ritz relation is employed to predict the missing energy levels of the neutral argon and the first four ions for principal quantum numbers of up to 70.

LIST OF CITATIONS

PUBLICATIONS AND PRESENTATIONS:

Results of Research

1. T. L. Eddy, Multithermal Analysis of Subatmospheric Argon Arcs", 1984 IEEE International Conference on Plasma Science, St. Louis, May 14-16, 1984. IEEE Publ. No. 84CH1958-8, pp 19-20.

2. T. L. Eddy and A. Sedghinasab, "On the Utility of LTE Measurements in Non-LTE Electric Arcs", invited paper 1C-1, IEEE Int'l. Conf. Plasma Science, June 3-5, 1985; (Abstract) IEEE Publ. 85CH2199-8, p.7, 1985.

3. A. Sedghinasab and T. L. Eddy, "Composition and Thermodynamic Properties of non-LTE Argon Plasma", 37th Gaseous Electronics Conference, Boulder, CO, October 1984, (Abstract) Bull. Am. Phys. Soc., Ser. II, 30, 134, 1985.

4. A. Sedghinasab and T. L. Eddy, "New Transition Probability Scale for Argon", 38th Gaseous Electronics Conf., Monterey, CA, Oct. 15-18, 1985.

5. T. L. Eddy and K. Y. Cho, "Some non-LTE Diagnostic Methods for Hydrogen Plasmas", APS 6th Topical Conference on High Temperature Plasma Diagnostics, Hilton Head, SC, March 9-13, 1986.

6. A. Sedghinasab, T. L. Eddy, R. T. Murray and A. V. Larson, "An Arc Facility for Investigating non-LTE Thermodynamic and Transport Phenomena in Low and High Pressure Plasmas", Rev. Sci. Inst., 57 (8), 2903-5, 1986. Presented at APS 6th Topical Conference on High Temperature Plasma Diagnostics, Hilton Head, SC, March 9-13, 1986.

7. K. Y. Cho and T. L. Eddy, "Generalized Multi-Temperature Relations for Hydrogen Plasma", Paper EA-4, 39th Gaseous Electronics Conference, Madison, WI, October 7-10, 1986.

8. T. L. Eddy, "Generalized Multithermal Equilibrium Diagnostics of Hydrogen and Argon Arcs", Paper EA-2, 39th Gaseous Electronics Conference, Madison, WI, October 7-10, 1986.

9. A. Sedghinasab and T. L. Eddy, "GMTE Relations for Argon Plasma", Paper EA-3, 39th Gaseous Electronics Conference, Madison, WI, October 7-10, 1986.

10. T. L. Eddy and A. Sedghinasab, "Non-LTE Temperatures in Argon Arcs at Various Pressures", IEEE Int. Conf. Plasma Sci., June 1-3, 1987. To be submitted to IEEE Trans. Plasma Sciences.

11. A. Sedghinasab and T. L. Eddy, "Ambipolar Diffusion Effects in Non-LTE Arcs at Various Pressures", Proc. 18th Int. Conf. Phenon. in Ioniz. Gases, Swansea, Wales, July 13-17, 1987.

12. A. Sedghinasab and T. L. Eddy, "On the Transition Probability Scale Modification of AR I", Paper MB-2, 49th Gaseous Electronics Conference, Atlanta, Georgia, October, 1987. To be submitted to J. Quan. Spectrosc. Radiative Transfer.

Applications of Results

13. T. L. Eddy, A. Sedghinasab, and P. A. Johnson, "Effect of Cold Gas Injection on Plasma Temperature Measurements", Proc. 7th International Symposium on Plasma Chemistry, v.3, pp. 772-777 Eindhoven, The Netherlands, July 1985.

14. A. Sedghinasab and T. L. Eddy, "GMTE Relations for Argon Plasma", Paper EA-3, 39th Gaseous Electronics Conference, Madison, WI, October 7-10, 1986.

15. R. V. Frierson and T. L. Eddy, "Temperatures in an Arc Nozzle Produced by a Rotating Magnetic Field", Proc. 8th Int. Symp. Plasma Chem., Tokyo, Japan, August 31-September 4, 1987.

16. R. Frierson and T. L. Eddy, "Transient and Quasisteady non-LTE Diagnostics of a Rotating Argon Arc", Paper NB-3, 49th Gaseous Electronics Conference, Atlanta, Georgia, October 1987.

17. K. Y. Cho and T. L. Eddy, "Application of Generalized Multithermal Equilibrium Model to Collisional-Radiative Calculations for Nonequilibrium Hydrogen Plasma", Paper HA-4, 49th Gaseous Electronics Conference, Atlanta, Georgia, October 1987.

18. T. L. Eddy and K. F. Knoche, "Nonequilibrium in an 0.1 Bar Hydrogen Arc", to be submitted to J. Quant. Spectrosc. Radiative Transfer, 1985.

19 T. L. Eddy and C. J. Cremers, "Non-LTE Analysis of a Local Fluid Constricted Argon Arc", to be submitted to J. Appl. Phys., 1986.

RADIATIVE PROPERTIES

OF

NON-LOCAL THERMAL EQUILIBRIUM PLASMAS

T. L. Eddy
A. Sedshinasab
K. Y. Cho
R. V. Frierson
R. T. Murray

Final Report
National Science Foundation Grant CPE-8311325

October, 1987

George W. Woodruff School of Mechanical Engineering
Georgia Institute of Technology
Atlanta, Georgia 30332

TABLE OF CONTENTS

NOMENCLATURE

A_{mn}	Transition probability of an electron from state m to n
b_1	Departure coefficient of the ground state
c_s	Speed of sound
D_a	Ambipolar diffusion coefficient
E	Electrical field strength
E_o	Ground state energy level
E_I	Ionization potential energy level
E_m	Energy level of state m
g	Gibbs free energy
g_1	Degeneracy of the ground state
g_I	Degeneracy of the ionization potential
g_m	Degeneracy of state m
H_α	Alpha line of the hydrogen Balmer series lines
H_β	Beta line of the hydrogen Balmer series lines
H_γ	Gamma line of the hydrogen Balmer series lines
i_L	Line emission coefficient
I	Plasma radiation intensity
I_D	Direct intensity of the arc
I_{D+R}	"Direct plus reflected" intensity of the arc
$\bar{I}_{arc}$	Mean plasma intensity over the arc diameter
k_e	Thermal conductivity of electrons
m_e	Electron rest mass
n	Principal quantum number
n_1	Ground state population density
n_a	Neutral atom density
n_e	Electron density
n_i	Ion density
n_h	Total heavy particle density
n_m	Population density of a level m
NBS	National Bureau of Standards
P	Pressure
Q_{ea}	Total electron-atom collision cross section
Q_{ei}	Total electron-ion collision cross section
R_y	Rydberg constant

R_M	Mirror reflectivity
T_a	Atom translational temperature (K)
$\bar{T}_{arc}$	Arc mean transmisivity
T_e	Electron translational temperature
T_{ex}	Electronic excitation temperature
T_{exa}	Total electronic excitation temperature
$T_{ex\beta}$	Upper level excitation temperature
T_g	Gas translational temperature
T_i	Ion translational temperature
T_L	Lens transmisivity
T_{spec}	Total spectrometer transmisivity
T_{rot}	Rotational excitation temperature
T_{vib}	Vibrational excitation temperature
T_W	Window transmisivity
z_c	Compressibility factor
Z	Partition function
Z_{ex}	Electronic excitation partition function
Z_{exa}	Atomic excitation partition function
Z_{exi}	Ion excitation partition function
Z_{rot}	Rotational partition function
Z_t	Translational partition function
Z_{vib}	Vibrational partition function
ϵ_ν	Continuum emission coefficient
μ	Quantum defect
μ_o	Atomic weight
μ_r	Plasma refractive index
σ	Electrical conductivity
ξ	A continuum correction factor taking into account the deviation of the argon atomic level structure from that of hydrogen
ξ_{fb}	Continuum correction factor for free-bound transitions
ξ_{ff}	Continuum correction factor for free-free transitions

1.0 INTRODUCTION

1.1 Objectives

The major objective of this work is to determine accurate (true) and precise (low uncertainty) atomic transition probability (A_{mn}) values for argon and thereby develop a method for determining accurate and precise A_{mn} for other species. Argon was selected for the following reasons:

a) Experimental errors in ArI A_{mn} values are given as 7-15%; whereas, values among investigators vary by a factor of two or more.

b) Various corrections have been made to A_{mn} determinations in atmospheric arcs, resulting in a common A_{mn} scale [1-5], which differs from the recommended scale of the National Bureau of Standards [2]. These studies assume local thermal equilibrium (LTE), but there is ample evidence that LTE does not exist at atmospheric pressure in argon arcs. This will affect the A_{mn} scale.

c) The 25% uncertainty quoted for most ArI A_{mn} values [2] is the major contributing error in diagnostic analysis; hence, more accurate A_{mn} values must be found to provide an appropriate sensitivity for valid non-LTE diagnostics.

d) Though not usually a reactive component in plasma processing, argon is often used as a carrier or base flow gas. In addition, it is the most popular substance used in experimental studies of LTE/non-LTE arc/jet phenomena and analytical studies related to plasma mechanisms.

e) High pressure ($\gg$1atm), LTE arc experiments show that experimental continuum ξ_{fb} factors calculated with the commonly accepted A_{mn} scale [2] for argon differ by a factor of two from the theoretical ξ_{fb} scale of several different authors calculated by different methods. Dividing the A_{mn} scale by two, or equivilent modification of A_{mn} and/or ξ_{fb} would resolve this inconsistency.

The second major objective was to determine an accurate ξ_{fb} scale, which would follow from an accurate A_{mn} scale. Since the funding provided is less than half of that originally requested, the second objective is limited to a relative determination of the ξ_{fb} scale. The detailed experimental study of ξ_{fb} and its equivalent ς is therefore omitted. In

addition, the final year of study and final results of this project were completed under a Ph.D. thesis [6] in the absence of adequate funding.

1.2 Significance

Reported argon transition probability values differ by more than a factor of two [1-5] which greatly exceeds their reported error bounds. Most of the measurements have been made in 1-atm arcs which have been shown to deviate from local thermal equilibrium (LTE) [7-11]. Accurate atomic transition probability values are necessary to determine accurate level populations, temperature, and other properties which are needed to accurately calculate plasma heat and mass transfer. Relatively narrow engineering applications generally require greater accuracy than the relatively broad range of plasma calculations in physics and astrophysics. Uncertainties in the range of 15 to 50% are specified for most transitions of common atomic species (excluding H & He) [2]. The values should have uncertainties equivalent to those for other transport properties which are an order of magnitude smaller.

In this work, the calculated non-LTE property values and related tables, charts and/or non-LTE program itself will be used to determine the type and extent of non-LTE to help determine when LTE exists in the experiment. When only LTE methods are used, investigators often unknowingly compare variables which have similar ratios or values in both LTE and non-LTE under the conditions investigated [12]. The computer program will also allow the validation of the final results on the basis of consistency between various line, continuum, Stark broadening and pressure measurements to be completed in the second half of the project.

The continuum radiation is often used as a relatively simple measurement to determine the electron density [13-17] using a modification of the Kramers-Unsöld relation [18-19] and assuming LTE. More detailed relations [20-27] have allowed the separation of free-free and free-bound contributions as well as the extension to non-LTE plasmas [10]. Theoretical calculations of the free-bound ξ factor coefficients [21,26,27] agree with each other and with "1-atm" arc measurements (more or less) [10,28] but are a factor of 2-to-3 times lower than experimentally determined values in high pressure argon arcs [29-34]. Which values are correct? The free-bound contribution dominates much of the measurable continuum radiation in high pressure plasmas. Accurate ξ_{fb} values would allow accurate and convenient

diagnostics via the continuum radiation, as well as improve the accuracy of radiative transfer calculations.

The above objectives are related because a systematic error in the atomic transition probability value produces an equivalent systematic error or shift in the ξ_{fb} value in high pressure arc plasmas [10,35-38]. At present, the most commonly accepted set of values of the transition probabilities via NBS and the theoretically calculated ξ_{fb} values are in contradiction. Other recent work [5] using laser interferometry indicated that the correction of systematic errors in the use of Stark broadening to calculate the electron density may reduce to, but not eliminate, the extent of the contradiction. Most atomic transition probability and continuum ξ_{fb} experiments have not made the various necessary consistency checks to validate the accuracy (not precision) of the measurements.

2.0 BACKGROUND

2.1 Transition Probabilities

Argon is one of the most popular plasma substances because of its relatively low cost, high purity, long run duration capabilities, and its desirability as an electrode protectant while investigating more reactive substances. New plasma diagnostic methods are often tried with argon or substances are mixed with argon because of its stability, inert behavior and long run time capability. In spite of its popularity it is a paradox that the spectroscopic properties of argon (and other complex substances) are known with such little accuracy.

Wiese, Smith and Miles [2], present an extensive discussion on argon transition probability values determined from a variety of experimental methods, as well as by calculation, thereby justifying the values recommended by NBS in 1969. The extent of the discussion suggests the extent of the problem. Many investigators, including ourselves, have used the NBS recommended values with confidence, though the authors indicated that they had adopted a scale which appeared "to be the least objectionable one". The adopted scale is supported by a number of experimental measurements [1,39-45] prior to the publication of the data. A second scale, approximately 30% lower than the adopted scale was also supported by a number of experimental investigations [45-49].

Subsequent work was equally undecided with some investigations supporting the ArI values in one scale, but the ArII values in the other [5,13,16,17,49,50]. Some represent internal disagreements within a given scale [15] or agreement with either depending upon the method of analysis [4,5]. Fig. 2.1 presents selected values from these experiments which will be used for discussion below.

It appears that the scatter in the data may be related to at least one or more of the following factors.

1) The consideration of line wing contributions.
2) The accuracy of any electron density determination utilized.
3) The sensitivity of the method employed.
4) The type of plasma source.
5) The existence of local thermal equilibrium.

Wiese and Shumaker [51] have presented a method by which the contribution to the total line emission coefficient from the far wings can be included. Most investigations have not included this correction. Nubbemeyer [3] compares data from various investigators which have been so corrected. The data, presented in Fig. 2.2, are arranged as a function of the method applied. After line wing correction the major differences appear to be due to the sensitivity of the method applied.

The methods can be described briefly as follows. The method of best fit (MBF) compares a log-log plot of two experimentally obtained emission coefficients (neutral, ion, or continuum) with the theoretical LTE equivalent at that pressure but with reference A_{mn} values. The translation factors required to match the experimental and theoretical data yield the appropriate A_{mn} (or ξ) values. Hβ methods use the Stark broadening of the hydrogen β line to determine the electron density from which the LTE temperature (assuming LTE) can be determined, as well as the upper level populations. The latter are proportional to the measured line emission coefficient values through the unknown A_{mn}. Continuum (CONT) methods are similar to the Hβ method. The continuum ξ (λ,T) factor which is a weak function of T (assuming again LTE) is obtained from theory or experiment. Assuming LTE, the measured continuum emission coefficient is then related to N_e or T. A_{mn} is then calculated, as above, from the measured line emission coefficient and the calculated upper level density obtained from p and T, or equivalent. The laser interferometry (LI) methods are similar to the Hβ and

Fig. 2.1 : Selected values from experiments determining A_{mn}

Author(s)	Date	Reference	Plasma[3] Source	View	Method[4]	Pressure (atm)	Diameter (mm)	Current (Amps)	Est. Cur. Density (A/cm^2)	A_{mn} (per μs) without/with wing corrections AI 4158	AI4259	AI4300	AI6965	AI7147	AI7272	AiI4806	AII4347
Drawin	1956	118	A		Hβ	0.4-.85		200		1.67/	3.97/	.358/					
Gericke	1961	119	A	end						-1.2/	2.9/	.31/					
Olsen	1963	13	FBA	side	MBF	1.1	12	400	3-4	.655/	2.46/		5.31/		16.1/	78.6/	115/
Berge, et al	1965	30	TP		Hβ											111/	
Popenoe & Shumaker	1965	43	WSA	side	Hβ/GKS)	1	5	40-90	2-5	/1.6	/4.4	/.411	/7.1			/131	/240.
Richter	1965	48	A	end	MBF	1	4.1	2.5-125	.2-10			.31/.356				60/69.2	
Bott	1966	14	WSA	side	CONT[1]	1	10	35-150	.4-2	1.19/		.330/.376[2]					
Coates & Gaydon	1966	15	ST			1.2-1.8				-1.02/	3.1/	.317/.364	5.14/	.710/816	2.03/		
Malone	1966	120	RF	side								.318/					
Shumaker & Popenoe	1967	44	WSA		Hβ(GKS)	1	5	40-90	2-5				/7.28	/.706	/2.16		
Wiese	1967	1	WSA	side	Hβ(GKS)		5	50	2-3							78.8/	
Chapelle, et al	1968	49	PJ	side								.314/					
Wende	1968	47	WSA	end	MBF	1	7			1.1/	3.2/	.31/356					
Bues, et al	1969	46	A		Hβ							.43/					
Bues, et al	1969	46	A									.31/.356		/.521		~60/	
Shumaker & Popenoe	1969	16	WSA	side	MBF	1.02	3.2	135	16.8					/.522		87.2/	
Wujec	1969	121	A	end	Hβ							.366/.421					
NBS-NSRDS-22	1969	2								/1.45	/4.15	/.394	/6.7	/.65	/2.0	/79.0	/124.
v. Howelingen & Kruitkof	1971	50	A	side	T(Cont)	0.67	8	75-100	1-2			.308/.339				86/	
Shumaker & Popenoe	1972	17	WSA	side	MBF	0.2-5	3.2-4.8		2-4					/.557			
Nubbemeyer	1976	3	WSA	side/end	MBF	0.5-3	4-10	20-240	1-3			.340/.391		.566/.651		88.2/102	
Preston	1977	4	WSA	end	T(Kr)	1.75	3	60	8.5			.372/				74.9/	
Preston	1977	4	WSA	end	Hβ(KG)	1.75	3	60	8.5			.422/				120.8/	
Preston	1977	4	WSA	end	Hβ(VCS)	1.75	3	60	8.5			.369/				71.1/	
Baessler & Kock	1980	5	WSA	end	LI,Hβ(BK)	1	4	20-100	1-8			.32/				70/	
Baessler & Kock	1980	5	Ave of values corrected to Hβ(BK) scale:									.312/				70/80	

[1] Bott obtained the temperature from an AII absolute intensity, N_e from continuum.

[2] Nubbemeyer [3] suggests 0.376, Preston suggests 0.356.

[3] Plasma sources: FBA=free burning arc, WSA=wall stabilized arc, RF=radio frequency heating, TP-theta pinch, ST-shock tube, PJ=plasma jet, A=arc of unknown geometry.

[4] For method see Section II.B.1. T( ) indicates that the "LTE" temperature was obtained from ( ).

Fig. 2.2 Nubbemeyer's comparison of A_{mn} after line wing correction showning differences between methods (Nubbemeyer's ref. Nos.) from [3].

(a) Measured A_{nm} in s^{-1} (assuming LTE)

Author(s)	Method	A_{nm} for Ar(I) at 714·7 nm	A_{nm} for Ar(I) at 430·0 nm	A_{nm} for Ar(II) at 480·6 nm
COATES *et al.*[13]		$8{\cdot}16\times10^{5}\pm5\%$	$3{\cdot}64\times10^{5}\pm5\%$	—
RICHTER[10]	Miscellaneous	—	$3{\cdot}56\times10^{5}\pm10\%$	$6{\cdot}92\times10^{7}\pm15\%$
BOTT[11]	methods	—	$3{\cdot}76\times10^{5}\pm13\%$	—
WENDE[18]		—	$3{\cdot}56\times10^{5}\pm18\%$	—
BUES *et al.*[20]		$5{\cdot}21\times10^{5}\pm20\%$	$3{\cdot}56\times10^{5}\pm10\%$	—
OLSEN[26]	MBF (the normal	—	—	$9{\cdot}04\times10^{7}\pm10\%$
SHUMAKER *et al.*[19]	temperature was	$5{\cdot}22\times10^{5}\pm10\%$	—	$8{\cdot}72\times10^{7}\pm10\%$
SHUMAKER *et al.*[23]	exceeded)	$5{\cdot}57\times10^{5}\pm10$**	—	$7{\cdot}86\times10^{7}\pm10\%$**
NUBBEMEYER[this study]		$6{\cdot}51\times10^{5}\pm5\%$	$3{\cdot}91\times10^{5}\pm5\%$	$1{\cdot}02\times10^{8}\pm7\%$
DRAWIN[8]		—	$4{\cdot}12\times10^{5}\pm20\%$	—
POPENOE *et al.*[9]	Based on the	—	$4{\cdot}11\times10^{5}\pm11\%$	$1{\cdot}31\times10^{8}\pm23\%$
SHUMAKER *et al.*[15]	line broadening	$7{\cdot}06\times10^{5}\pm11\%$	—	—
WUJEC[21]	theory of H_β	—	$4{\cdot}21\times10^{5}\pm10\%$	—

*The results of Refs. (9, 15, 19, 23) have been corrected for line-wing errors by the authors. All other results have been corrected for line-wing errors by +15%, which is a rough approximation.
**Assumed uncertainties [see Ref. (19) for justification].

(b) Measured A_{nm} in s^{-1} (based on lifetime measurements*)

Author(s)	A_{nm} for Ar(I) at 714·7 nm	A_{nm} for Ar(II) at 480·6 nm
VEROLAINEN *et al.*[12]	$1{\cdot}04\times10^{6}$	—
NODWELL *et al.*[22]	$1{\cdot}20\times10^{6}\pm15{\cdot}5\%$	—
BUES *et al.*[20]	—	$5{\cdot}9\times10^{7}$
SCHNAPAUFF[28]	—	$5{\cdot}7\times10^{7}$
WIESE *et al.*[14]	$6{\cdot}5\times10^{5}\pm25\%$	$7{\cdot}9\times10^{7}\pm25\%$
NUBBEMEYER[25]	$8{\cdot}76\times10^{5}\pm16\%$	$6{\cdot}13\times10^{7}\pm19\%$

*Original lifetime measurements;[12,22] lifetime values taken from the literature.[20,28,14,25]

(c) Calculated A_{nm} in s^{-1}

Author(s)	A_{nm} for Ar(I) at 714·7 nm	A_{nm} for Ar(I) at 430·0 nm	A_{nm} for Ar(II) at 480·6 nm
GARSTANG *et al.*[1]	$1{\cdot}30\times10^{6}$	$1{\cdot}30\times10^{6}$	—
JOHNSTON[2]	$1{\cdot}40\times10^{6}$	$1{\cdot}40\times10^{6}$	—
STATZ *et al.*[3]	—	—	$8{\cdot}74\times10^{7}$
GARSTANG *et al.*[4]	—	—	$8{\cdot}36\times10^{7}$
MEINERS[5]	$1{\cdot}40\times10^{6}$	$2{\cdot}80\times10^{5}$	—
LUYKEN[6]	—	—	$9{\cdot}08\times10^{7}$
AYMAR *et al.*[7]	$8{\cdot}45\times10^{5}$	—	—

continuum methods but measure the index of refraction of the laser beam in the plasma to determine the electron density. Though the electron density determination is independent of LTE, the subsequent analysis usually employs LTE property values. Lifetime measurements record the exponential rate of decay of the radiation from a level after the maintaining energy source is cut off. The transition probability is calculated directly from the mean lifetime of the level. The lifetime technique is supposed to be independent of LTE.

Preston [4] has compared methods using pure argon diagnostics (MBF, CONT, and others) with those using a trace of hydrogen ($H\beta$) as shown in Fig. 2.3. For a proper comparison the A_{mn} values of all but Shumaker, et al. and Nubbemeyer should be increased by 10-15% to approximate the line wing correction. In spite of this correction the pure argon diagnostics show consistently lower values than those using $H\beta$ techniques. Most of the $H\beta$ experiments used the Griem, Kolb and Shen (GKS) broadening values [52]. Subsequent modifications have been made by Kepple and Griem (KG) [53] and Vidal, Cooper and Smith (VCS) [54]. A relative comparison of the half-widths predicted for the electron density measurement via 2λ laser interferometry by Baessler and Kock [5] are given in Fig. 2.4. Note that a given experimental half-width value would produce successively larger values of N_e as one proceeds down the table. Preston, as shown in Fig. 2.3, used both KG and VCS theories and found decreasing values of A_{mn} as one proceeds from KG to VCS fitting.

This is shown more explicitly by Baessler and Kock [5] whose A_{mn} values agree with the second or lower scale discussed above as shown in Fig. 2.5. Also shown are the date from $H\beta$ methods which have been corrected, using the experimentally determined half-widths found by comparison with LI obtained electron densities. It is notable that Baessler and Kock include most, if not all, significant investigations. The methods which vary most from the scale recommended by Baessler and Kock are the MBF and CONT. The sensitivity of these methods can be affected by non-LTE effects as will be shown next.

2.2 Continuum Emission Coefficient

The continuum emission coefficient relation can be written as a fraction of the free-free and free-bound contributions:

Reference	$A_{ki}/10^6$ s^{-1} for AI at 430 nm	$A_{ki}/10^6$ s^{-1} for AII at 480.6 nm	Method
Pure argon diagnostics:-			
GERICKE[73]	0.325† ± 15%	-	Arc plasma (end-on)
OLSEN[86]	-	78.6 ± 8%	Arc plasma (side-on)
RICHTER[6]	0.31 ± 10%	60 ± 15%	Arc plasma (end-on)
MALONE et al[74]	0.318 ± 1.3%	-	RF plasma (side-on)
BOTT[61]	0.330 ± 13%	-	Arc plasma (side-on)
CHAPPELLE et al[75]	0.314 ± 35%	78.8	Plasma jet (side-on)
COATES et al[60]	0.317 ± 5%	-	Shock-tube
FRISH[58]	0.098 ± 30%	-	Plasma jet (side-on)
WENDE[65]	0.31 ± 18%	-	Arc plasma (end-on)
SHUMAKER et al[68]	-	87.2 ± 10%	Arc plasma (side-on)
van HOUWELINGEN et al[62]	0.308 ± 8.5%	86 ± 13%	Arc plasma (side-on)
BUES et al[10]	0.31	-	Arc plasma
SHUMAKER et al[12]	-	78.6	Arc plasma (side-on)
NUBBEMEYER[11]	0.391 ± 5%	102 ± 7%	Arc plasma (end and side-on)
This study‡	0.372 ± 4% ± 10%	74.9 ± 9% ± 8%	Arc plasma (end-on)
Hβ diagnostics			
DRAWIN[76]	0.358 ± 20%	-	Arc plasma
POPENOE et al[47]	0.411 ± 11%	131 ± 23%	Arc plasma (side-on)
BERG et al[87]	-	111	Theta pinch
WIESE[63]	0.40§	-	Arc plasma
WUJEC[77]	0.366 ± 10%	-	Arc plasma (end-on)
BUES et al[10]	0.43	-	Arc plasma
This study‡			
KG fitting	0.422 ± 4%	120.8 ± 9%	Arc plasma (end-on)
VCS fitting	0.369 ± 10%	71.1 ± 8%	

†Derived from a mean of the photo-electric and photographic values.[73]

‡The first value for the quoted uncertainty is the standard error of the mean and the second is the systematic uncertainty based on a linear summation.

§Based on a relative intercomparison with the data of POPENOE and SHUMAKER.[47]

Fig. 2.3:
Preston's comparison of A_{mn} via pure argon versus $H\beta$ diagnostics (Preston's reference Nos.) from [4].

Fig. 2.4:
Reduced line widths of $H\beta$ from various theories, as well as the Baessler and Kock experiment from [5].

author	$\alpha_{1/2}$
GKS II	0.0885
KG	0.087
VCS	0.085
BK exp	0.0804

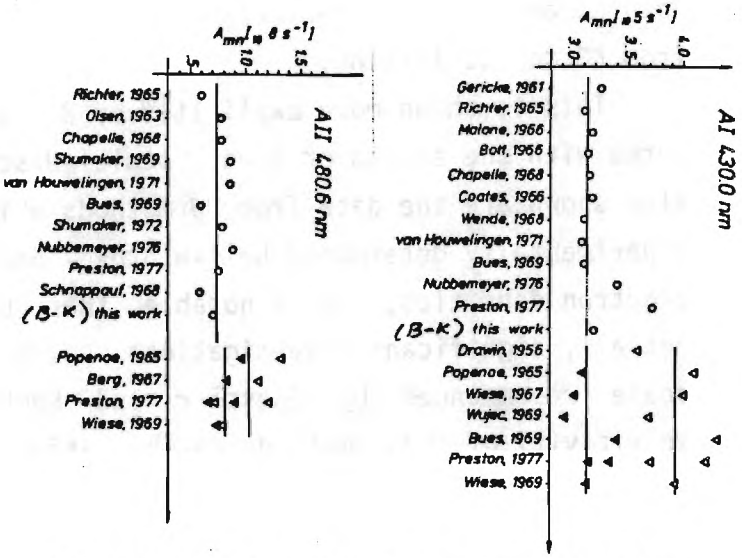

Fig. 2.5: Scale for A_{mn} recommended by Baessler and Kock from [5].

$$\epsilon_\nu = 5.44\times10^{-46}\ N_e\ N_i\ T^{-1/2} Z^2 \xi(\nu,T) \qquad (2.1)$$

where ξ is the "Biberman" ξ factor [20-22]. Writing ξ in the form given by Schlüter:

$$\xi = \frac{\eta}{z_{exi}}\ \xi_{fb}(\nu,T)\left[1-\exp\left(\frac{-h\nu}{kT}\right)\right] + \xi_{ff}(\nu,T)\ \exp\left(\frac{-h\nu}{kT}\right) \quad . \qquad (2.2)$$

The free-free coefficient (ξ_{ff}) is the well known free-free Gaunt factor [55,56]. Three theories [20,21,25-27] are in good agreement for the free-bound coefficient (ξ_{fb}), which are in substantial agreement with 1-atm experimental measurements [28,48,57-59] as shown in Fig. 2.6. In particular the experimental values of Schulz-Gülde [28] who used A_{mn} values equivalent to the Baessler and Kock scale are in excellent agreement with Schlüters theoretical values. Unfortunately, various high pressure argon arc experiments [29-34] yield values about a factor or two larger as shown in Fig. 2.7. It was found that correcting the data based on a common (in this case, NBS scale) A_{mn} reduced the scatter in the 1-atm data (see Fig. 2.8), as well as the high pressure data (see Fig. 2.9), but each at a different level.

For one set of experiments at 1-atm, both an LTE and a non-LTE analysis were employed. The LTE analysis (+) agrees well with the other 1-atm arcs assuming LTE analysis as shown in Fig. 2.8 and the non-LTE analysis (x) of the 1-atm arc agrees well with the high pressure ace measurements as shown in Fig. 2.9. Since the high pressure are measurements are "closer" to LTE than the 1-atm measurements, the initial conclusion is that the 1-atm measurements are in non-LTE.

2.3 Comparison of Effects

Additional complications occur since the high pressure experimental ξ_{fb} values do not agree with the theoretical ξ_{fb} values. It is found that a change in the value of ξ_{fb} is directly proportional to a change in A_{mn} [37,38]. Reducing the A_{mn} scale to about 70% of the NBS values (to the lower second scale recommended by Baessler and Kock and others) puts the 1-atm data on the theoretical curve for ξ_{fb} but drops the high pressure values only by an equivalent factor. The high pressure data can be lowered to the theoretical ξ_{fb} curves if the scale is reduced to 50% of the NBS value. If 1-atm argon arcs are indeed in non-LTE, then the transition probability

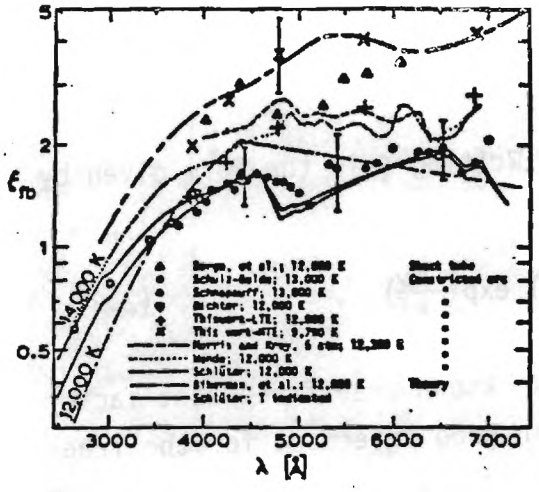

Fig. 2.6: ξ_{fb} values from theory and experiment at 1 atm and above (4-9 atm: Δ ; 5 atm: —— - ——) from [28,10].

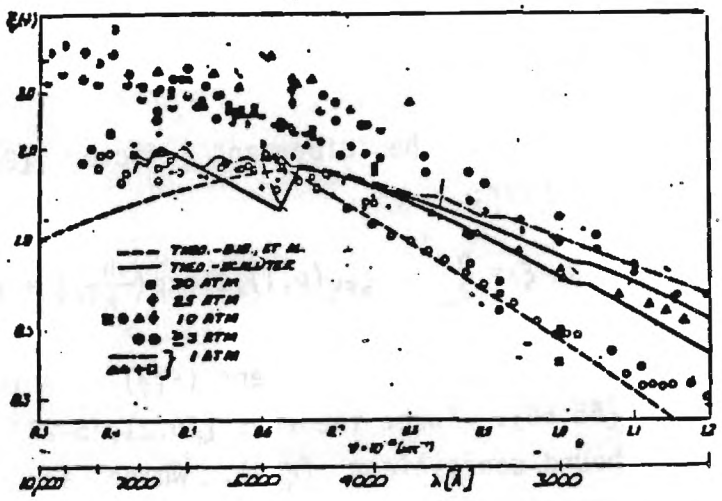

Fig. 2.7: Batenin and Minaev plot of ξ_{fb} at high (3-30 atm) low pressures (~atm). Symbols are: Ref 30 (●), 31 (◇, ◆), 32 (■ , ◪ , □), 33 (▲), 34 (◑ , ◒ , ○), 58 (— - —), and 59 (△).

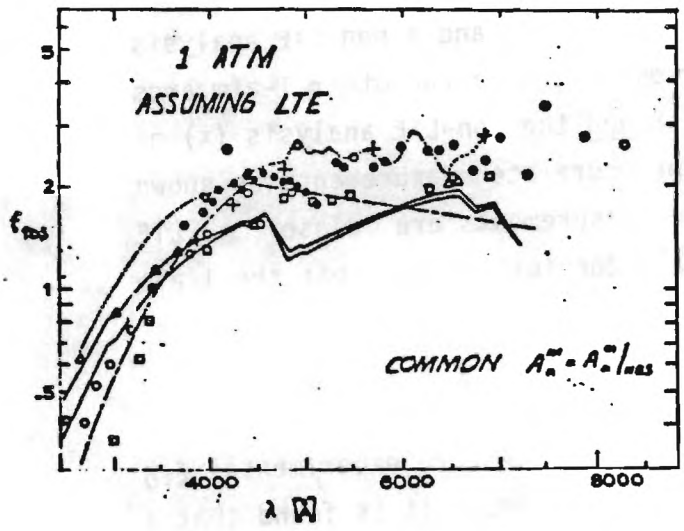

Fig. 2.8: ξ_{fb} values from 1-atm experiments normalized to NBS A_{mn} [2] after [37].

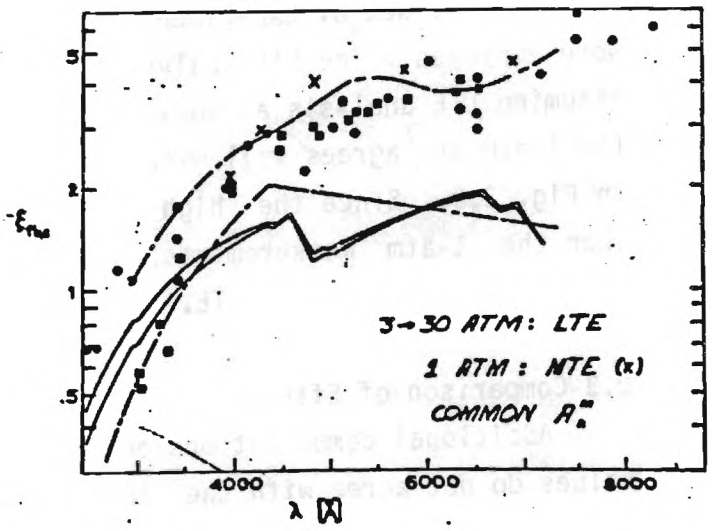

Fig. 2.9: ξ_{fb} values from 3-30 atm experiments assuming LTE and 1 atm experiment assuming MTE from [37].

values determined assuming LTE may well contain a systematic error of up to 20%, relative to the lower, second scale.

It must be noted that the theoretical ξ_{fb} calculations are not free from suspect. The calculation includes a partition function-like calculation with a non-hydrogenic Gaunt factor for each term. The Gaunt factor calculation procedure should be validated and the inclusion of "middle" levels not found in the usual tables of energy levels [60,61] but lying too low for inclusion as a hydrogenic sum. The inclusion of missing levels using the isoelectronic series is not a simple task and is often not performed even in partition function calculations. The omission of middle levels becomes significant at temperatures above the normal temperature.

The question of non-LTE was considered by Shumaker and Popenoe [17] in arc experiments at pressures from 0.2 to 4.98 atm. They used the MBF method with ArI 7147 and ArII 4806 as shown in Fig. 2.10. The experimental data at the three highest pressures (1.02 to 4.98 atm) were least squares fit to the equivalent LTE curves to determine A_{mn}. The value for the ion line agrees within 1/2% of the NBS value but the neutral line value is 14% below the NBS value and hence about 16% above the "second" scale value, though Hβ methods were not employed. Fig. 2.10 shows that much of the 0.5 atm data lies on or near the LTE curve with the exception of that below electron densities corresponding to about 5×10^{16} which is the general range of most of the analytical LTE criteria [24,62], higher than most experimental observations [63-65,11,14], but much less than the experimental results of Bober and Tankin [8] and predictions using the non-LTE model of Uhlenbush et al. [9].

Note that the MBF method using the Shumaker and Popenoe data results in the same transition probabilities whether 0.5 or 4.98 atm data is used. Contrarily, experimental ξ_{fb} factors obtained at 1 and 5 atmospheres would be different (and hence A_{mn} values would be different as shown in Figs. 2.8 and 2.9. No significant pressure dependence on ξ_{fb} values obtained at pressures larger than three atm is observed, though the data is precise enough to detect a distinct temperature dependence as shown in Fig. 2.11 (for a factor ξ within ξ_{fb} which excludes the obvious temperature dependence). It appears that the MBF method may not be sufficiently sensitive to non-LTE, (as pointed out as a possibility by Shumaker and Popenoe themselves). As further evidence, we compared 0.1 atm argon arc data [66] on an "Olsen" plot [67] but found the method to be insensitive to

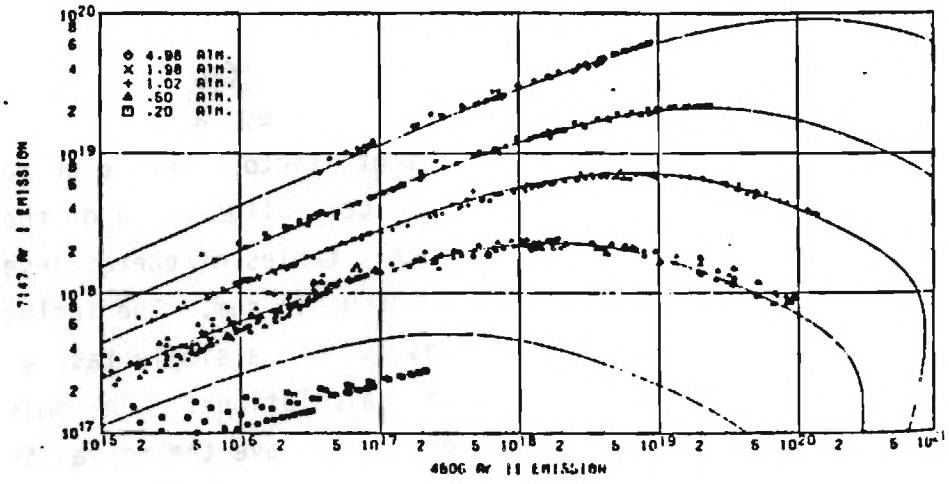

Fig. 2.10: Shumaker and Popenoe MBF plot from [17].

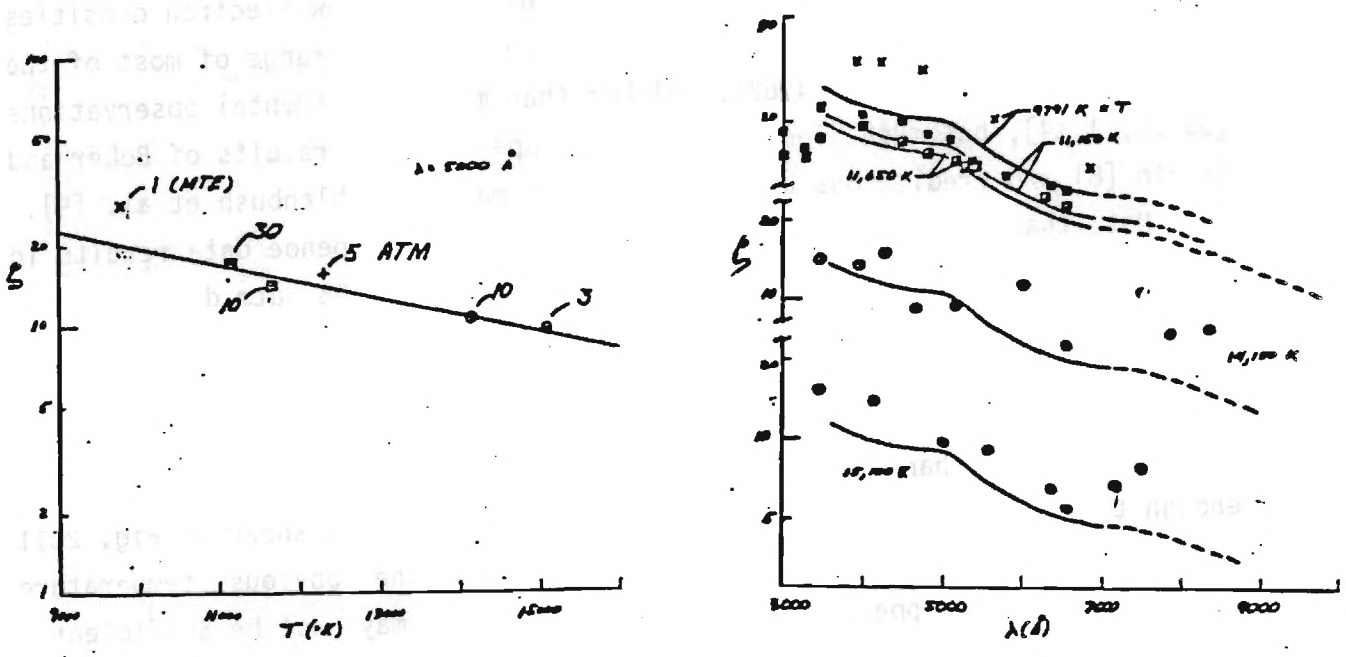

Fig. 2.11: Experimental values of the MTE free-bound factor ξ versus T ($T_{ex\beta}$) at 5000Å and versus λ by extrapolation of the Morris and Krey [29] experimental data (after [37]).

known non-LTE conditions and did not use it further. In addition, the MTE non-LTE model (to be discussed below), shown that electron-atom kinetic non-equilibrium shifts intensity and density curves the opposite way as electron-excitation non-equilibrium. Hence, especially for argon, the two effects could cancel each other out and end up near the LTE curve even though both types of non-LTE existed.

Baessler and Kock indicate that they do not know why their LI experiment yields stark broadening half-widths smaller than even the VCS theory. Our work shows that the Stark broadening theories for hydrogen should be fairly accurate (within $\simeq$ 20%) whether the 1-atm arcs employed to test the theory were in LTE or not. The same can not be said for helium for which our non-LTE analysis indicated that Stark half-widths greatly underestimated the electron density [68], presumably because the "calibration' was on a 1-atm helium arc assuming LTE electron densities. In both cases the continuum relations with hydrogenic and/or non-hydrogenic quantum mechanically derived Gaunt factors gave reliable electron densities consistent with other property values. The Baessler and Kock experimental half-width values may reflect another fine-tuning to account for non-LTE in 1-atm hydrogen arcs.

In summary, line wing corrections and experimentally based recommendations for Hβ stark broadening theory corrections appear to result in validation of a second consistent scale for argon transition probability values which is about 30% below the NBS recommended values for ArI and equivalent to the NBS scale for ArII. Experimental ξ_{fb} values from 1-atm arcs agree with theoretical values when the second A_{mn} scale is used. Contradictions occur from 3-30 atm arc measurements which indicate experimental ξ_{fb} values 20 to 30% larger. A non-LTE analysis of a 1-atm arc experiment gives ξ_{fb} values which agree with the high pressure values [10]. This suggests either the theoretical ξ_{fb} values are too low or the A_{mn} scale is too high, or both. The purpose of this work is to determine the "true" values of A_{mn} and ξ_{fb} utilizing appropriate non-LTE methods.

2.4 Electron Density Determination

The electron density can be one of the directly measured parameters of a plasma. Several techniques of differing precision have been developed for this purpose. Among the more established of these are determination of

electron density via continuum radiation, an appropriate broadening mechanism, and laser interferometry.

Provided the electrons have a Maxwellian velocity distribution, the electron and positive ion densities may be determined from a measure of the continuum intensity which is composed of radiation emitted from free-free as well as free-bound electron transitions. The experiments are done on an absolute basis, requiring a standard calibration light source. The continuum emission coefficient is related to electron density through the continuum relation (see Section 2.2). Although this relationship suggests that a prior knowledge of electron temperature is required, careful inspection of the equation reveals that the electron density is only a weak function of temperature ($\sim T^{1/4}$), which allows the use of a crude approximation for electron temperature. It has been shown [69] that in electron temperature range of 15,000 to 150,000 K, the value of $\epsilon_\nu/n_e^2\xi$ changes only by 10%. Although the electron density has the same functional dependency to ϵ_ν and ξ, the uncertainties in the absolute value of these two parameters are quite different.

Experimental uncertainties as low as 5% are easily realizable in continuum measurements, however the combined experimental and theoretical scatter in the values of ξ for argon are as high as 100%. Therefore, the precision and accuracy of the electron density is directly proportional to the accuracy of ξ.

Another source of uncertainty in electron density via continuum measurement is the contribution of line wings to the continuum intensity. Residual wing intensities superimposed on the continuum may cause the latter to appear much stronger than it actually is. The corrections necessary for precise intensity measurements may be obtained from line wing broadening theories.

Electron density is very often determined by measuring the spectral distribution of a line and relating the line shape or the line width to the electron density through an appropriate broadening theory. The dominant causes of line broadening in plasmas with no externally imposed magnetic field are Doppler and Stark broadening. The Doppler broadening which is the manifestation of the motion of a radiating particle towards or away from an observer is almost completely independent of electron density but is a strong function of plasma temperature. The full width at half maximum

intensity of a purely Doppler broadened line is given by [69]

$$\Delta\lambda_D = 7.16 \times 10^{-7}\lambda(T_g/\mu_o)^{1/2} \qquad (2.3)$$

where $\Delta\lambda_D$ and λ are in Å, T_g is the gas temperature, and μ_o is the atomic weight. In arc plasmas of moderate density, the Doppler effect is much weaker than the Stark effect, except for low density plasmas ($n_e \leq 10^{13}cm^{-3}$). Doppler broadening may also be caused by turbulence or gross mass motion in a plasma.

The predominant cause of line broadening in a dense plasma is the interactions of the emitters with the surrounding particles. This type of broadening is usually referred to as the pressure or the Stark broadening. The Stark broadening is a pressure broadening involving charged particles (i.e. electrons and ions). The Stark broadening theories have been developed from two different point of views, namely the impact theory and the quasi-static theory. The impact theory developed originally by Lorentz [70], and then refined by Kolb and Griem [71] states that a wave train of light emitted from an atom is perturbed by fast impacts, which disrupt the otherwise unperturbed wave train completely and cut it up into a number of smaller independent ones. The resulting intensity distribution is approximated by the "dispersion-type" or the Lorentzian shape, i.e.

$$I(\Delta\lambda) \sim \frac{1}{1 + (\Delta\lambda/\Delta\lambda_{1/2})^2} \qquad (2.4)$$

Unlike the impact theory, in quasi-static theory the particle is considered to be continuously under the influence of perturbers during the whole emission process. Furthermore, the perturbing particles are assumed to move so slowly during the time of emission that the perturbins field may be thought of as quasi-static. Spitzer [72] and Burkhardt [73] later realized that both approximations are part of the same general theory. This situation stimulated new theoretical activity and after some preliminary attempts, a refined Stark broadening theory was developed by Griem, Kolb, and Shen [52] for hydrogen and hydrogen-like lines.

For a long time the Stark broadening of the hydrogen lines has been one of the most important diagnostic tools for understanding of space as well as laboratory plasmas. The best available tabulations are those by Kepple and Griem [53] based on the "modified impact theory", and the most recent work

by Vidal et al. [54] utilized what is known as the "unified theory". The unified theory accounts for both the impact limit in the line center and the quasi-static limit in the line wings. At high electron densities of 10^{16}-$10^{17}cm^{-3}$ and electron temperatures of 12,000 to 20,000 K, the unified theory calculations give better agreement with the measured H_α, H_β, and H_γ profiles [54,74].

The refractive index of a uniform plasma can be related to electron density through relationships which take into account the contributions of atoms at ground state, excited atoms, ions, and free electrons to the index of refraction. Most often the effect of the free electrons on the refractive index is dominant, hence rendering the interpretation of refraction data more convenient. A typical relation used to deduce electron density from refractive index data is [75],

$$(\mu_r - 1) \simeq -4.46 \times 10^{-14}\lambda^2 n_e \qquad (2.5)$$

where λ is the wavelength of light in cm, and n_e is expressed in cm^{-3}. This method is known for its high precision and accuracy. Authors who use this technique for electron density determination claim an accuracy of about 1% which is much better than the quoted accuracy for Stark broadening of about 7-10%. In a recent paper Baessler and Kock [5] have used laser interferometry to correct the Stark broadening parameters of Griem, Kolb, and Shen [52], Kepple and Griem [53], and Vidal, Cooper, and Smith [54]. The correction to the electron densities obtained using these theories ranged from 9 to 15%. So, although it is very costly and complicated to set up an interferometry system, Stark broadening techniques corrected by laser interferometry scale of Baessler and Kock [5] can be used to obtain highly accurate electron density values.

9.1 EQUILIBRIUM AND NONEQUILIBRIUM CONSIDERATIONS IN MODELING

T. L. EDDY
Woodruff School of Mechanical Engineering
Georgia Institute of Technology
Atlanta, Georgia 30332

Equilibrium Versus Nonequilibrium

Consider the Boltzmann integrodifferential transport equation which permits the evaluation of the molecular energy distribution function of the i^{th} type of particles, f_i [1]:

$$\frac{\partial f_i}{\partial t} + c_i \frac{\partial f_i}{\partial r} + F_i \frac{\partial f_i}{\partial c_i} = \sum_{j=1}^{r} \left[\Gamma_{ij}^{(+)} - \Gamma_{ij}^{(-)} \right] \qquad (1)$$

where t is time, r is position, c_i is velocity, F_i is force/unit mass, and the Γ_{ij} net up-down collision integrals between i-type and j-type particles. The terms on the left represent transient, spacial gradient, and external body force effects on the distribution function f_i. The rhs represents the net effect of intermolecular collisions.

If the system being considered is isolated, then in sufficient time:

$$\frac{\partial}{\partial t} = \frac{\partial}{\partial r} = F_i = 0, \qquad (2)$$

and we obtain the equilibrium solution via intermolecular collisions, which for thermal plasma densities and specific energies is the Maxwell velocity distribution and the Boltzmann energy distribution. Hence

Equilibrium ≡ Thermodynamic Equilibrium

for an isolated or infinite system. Thermodynamic Equilibrium (TE) includes Radiative Equilibrium which requires all frequencies to satisfy the Planck function and hence be optically thick.

In thermal plasmas, transients, gradients and external body forces are often relatively weak so that a quasi-equilibrium locally finite state occurs called Local Thermodynamic Equilibrium (abbreviated here as LTDE to distinguish it from Local Thermal Equilibrium - LTE). Radiative Equilibrium does not hold because some transitions will be optically-thin and/or partially thick, otherwise the distribution functions will be Maxwell-Boltzmann (MB). As a result, Local Thermal Equilibrium (LTE) with all temperatures $T_i = T_j = \ldots$, Local Mechanical Equilibrium (LME) with all pressures $p_i = p_j = \ldots$ (not partial pressures), Local Chemical Equilibrium (LChE) with all chemical potentials $\mu_i = \mu_j = \ldots$, and so on will occur.

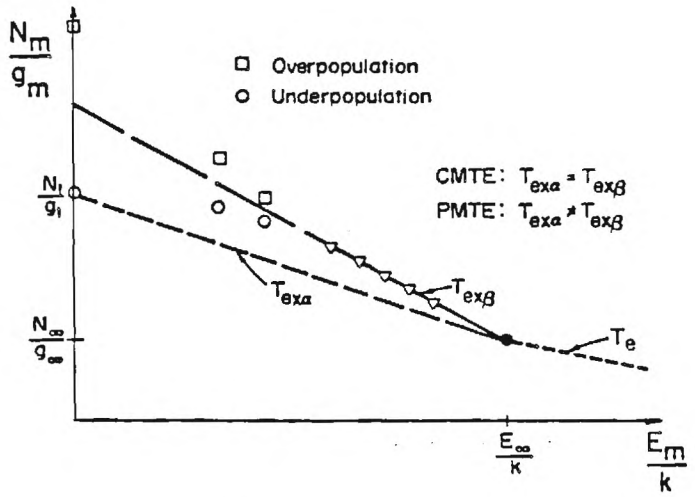

Fig. 1 Meaningful plasma temperatures:

- T_e ~ free electron translational temperature.
- T_g ~ atom, ion, or gas translational temperature.
- $T_{ex\beta}$ ~ upper level electronic excitation temperature.
- T_{exa} ~ total electronic excitation or Boltzmann temperature between m = 1 and m = ∞.

Nonequilibrium may occur when there are strong transient effects as in pulsed arcs, switching and afterglow; strong spacial effects as in plasma boundaries and with cold gas/particulate injection; and strong external body forces such as with magnetic or electric fields as found in cathode and anode fall regions. In low pressure plasmas, these effects alter the distribution function from the Equilibrium distribution and some non-MB distribution functions are used or the distribution function is treated as a variable function.

In high pressure plasmas, a MB distribution can usually be assumed because of the relatively small intermolecular relaxation times and mean free paths as well as the relatively stronger intermolecular forces. However, it is also experimentally found that different energy modes (translation, rotation, vibration, electronic, etc.) or species can have different distribution parameter values (e.g., $T_k \neq T_p$) within the same small local region, and that sometimes the energy mode follows the MB distribution over only part of the energy levels of the mode. This can be explained physically in terms of the ability of particular energy levels to equilibrate with each other or some other energy mode or species. To date, non-LTE is distinguished by different valued distribution parameters, but not non-LME or non-LChE. Chemical nonequilibria is usually handled with a "kinetic" method which assumes LTE, even though temperatures measured in reaction zones may vary between vibrational, rotational and translational energy modes. Future research should alleviate this paradox.

Description of Non-LTE Using f_{MB}

It has been shown for thermal plasmas near atmospheric pressure that the translational energy distribution is MB [2]. The electronic distribution functions may deviate from MB. Typical deviations will be discussed below in the discussion of selected non-LTE models.

Two-Temperature Models (2-T)

The 2-T models [3-5] usually assume that the electron (T_e) and heavy particle or gas (T_g) translational energy temperatures dominate as follows:

$$T_e = T_{exa} = T_{exi} = T_{ex\beta,a} = T_{ex\beta,i} \quad , \tag{3}$$

$$T_g = T_a = T_i = T_r = T_v \quad , \tag{4}$$

where (see Fig. 1) T_{exa}, T_{exi} are defined here as the Boltzmann temperatures between ground state and E_∞ (or E_I the lowered ionization potential) for the atom (a) and ion(i), respectively; $T_{ex\beta}$ is the ratio temperature of the highest excited levels; and T_r and T_v are the rotational and the vibrational excitation temperatures.

Typical equations for a 2-T model are given in Table I. The advantage of the model is that it adds only one variable (T_e) and hence one more equation, (the electron energy equation) to the LTE set of equations. Solutions can be obtained for fairly complex problems. The major disadvantages are that it may be too simple and that T_e and T_g values predicted are difficult to confirm. It is usually assumed via the Partial LTE (PLTE) model that $T_e = T_{ex\beta,a}$ however, diagnostic calculations using the PLTE ionization (Saha) equation have shown in general that [6]

$$T_{exa} \neq T_e \neq T_{ex\beta,a}. \tag{5}$$

The saving grace of the 2-T models is that $T_{ex\beta}$ is usually not employed. The GMTE multitemperature model (discussed later) shows that chemical equilibrium is mainly a function of T_e (and T_g), though the population of excited levels is mainly a function of T_{exa}. Therefore, T_e and T_g are the most appropriate two temperatures, so models based on these temperatures should give good results for transport properties and modeling the conservation equations. Problems or apparent contradictions arise when excited levels related to T_{exa} or $T_{ex\beta}$ are used to determine T_e (erroneously) for comparison of models with experiment. This is only valid in LTE which is often nonexistant. Both T_e and T_g are very difficult to measure (see Ch. 7.2). The specification of these temperatures as boundary conditions is convenient but of questionable merit when one can not confirm the values.

Many of the conservation relations are not affected explicitly by variations between similar models. They are affected by density and temperature value changes. The densities are usually controlled by the form of the ionization equation, as well as the equation of state. Table II compares the 2-T ionization equation with others. A major limitation is the exclusion of radiative transfer which could possibly be included using the methods of Lowke [7].

Table I: 2-T Plasma Modeling Equations.

Quasi-neutrality: $N_e = N_i$

State: $p = N_e k T_e + (N_i + N_a)\, k T_g$

Chem/Ioniz: $\dfrac{N_e N_i}{N_a} = 2\,\dfrac{Z_{exi}[T_e]}{Z_{exa}[T_e]}\left(\dfrac{2\pi m_e k T_e}{h^2}\right)^{3/2} \exp\left(\dfrac{-E_\infty}{kT_e}\right)$

Mass: $\vec{\nabla} \cdot \rho\, \vec{u} = 0$

Momentum: $\rho \vec{u} \cdot \vec{\nabla}\, \vec{u} = -\vec{\nabla} p + \vec{\nabla} \cdot \mu\, \vec{\nabla}\, \vec{u} + \vec{J} \times \vec{B}$

Gas Energy: $\vec{\nabla} \cdot \left[\dfrac{5}{2} k\, (N_a + N_e) T_g\, \vec{u}\right] = \vec{\nabla} \cdot \lambda_g \vec{\nabla} T_g + \dfrac{3}{2} k \left(T_e - T_g\right) N_e \dfrac{2m_e}{m_g} \bar{\nu}_{eg}$

Electron Energy: $\vec{\nabla} \cdot \left[\dfrac{5}{2} k T_e + E_{\infty,a}\right] N_e\, \vec{u} =$

$$\vec{\nabla} \cdot \lambda_e \vec{\nabla} T_e - \frac{3}{2} k \left(T_e - T_g\right) N_e \frac{2m_e}{m_g} \vec{\nu}_{eg} + \sigma_e E^2 + Q_{RAD}$$

Maxwell: $\mathrm{ROT}\ \vec{H} = j$

$\mathrm{ROT}\ \vec{E} = -\mu_o\, \partial \vec{H}/\partial t$

$\mathrm{DIV}\ \vec{B} = 0$

Table II. Comparison of Ionization Equations.

2-T or 2-T KINETIC METHOD

$$\frac{N_e^2}{N_a} = 2\,\frac{Z_{exi}[T_e]}{Z_{exa}[T_e]}\left[\frac{2\pi m_e kT_e}{h^2}\right]^{3/2}\exp\left[\frac{-E_\infty}{kT_e}\right]$$

PLTE/LCRE

$$\frac{N_e^2}{N_m} = 2\,\frac{Z_{exi}[T_e]}{g_m}\left[\frac{2\pi m_e kT_e}{h^2}\right]^{3/2}\exp\left[\frac{-(E_\infty - E_m)}{kT_e}\right]$$

MSE:PRIGOGINE (1940)

$$N_e\left[\frac{N_i}{N_a}\right]^{T_g/T_e} = 2\left[\frac{Z_{exi}[T_g]}{Z_{exa}[T_g]}\right]^{T_g/T_e}\left[\frac{2\pi m_e kT_e}{h^2}\right]^{3/2}\exp\left[\frac{-E_\infty}{kT_e}\right]$$

MSE:POTAPOV (1966)

$$N_e\left[\frac{N_i}{N_a}\right]^{T_g/T_e} = 2\left[\frac{Z_{exi}[T_e]}{Z_{exa}[T_e]}\right]\left[\frac{2\pi m_e kT_e}{h^2}\right]^{3/2}\exp\left[\frac{-E_\infty}{kT_e}\right]$$

MTE: EDDY, ET AL. (1973)

$$\frac{N_e^2}{N_a} = 2\left[\frac{Z_{exi}[T_{exa}]}{Z_{exa}[T_{exa}]}\right]\left[\frac{2\pi m_e kT_e}{h^2}\right]^{3/2}\exp\left[\frac{-E_\infty}{kT_{exa}}\right]$$

GMTE: EDDY & CHO (1986)

$$N_e\left[\frac{N_i}{N_a}\right]^{T_g/T_e} = 2\left[\frac{Z_{exi}[T_{exa}]}{Z_{exa}[T_{exa}]}\right]^{\frac{T_{exa}}{T_e}}\left[\frac{2\pi m_e kT_e}{h^2}\right]^{3/2}\exp\left[\frac{-E_\infty}{kT_e}\right]$$

Partial-LTE(PLTE) and Local Collisional-Radiative Equilibrium(LCRE) Models

The Partial-LTE (PLTE) Models [3,8-10] assume that the highest excited levels are distributed according to the electron temperature:

$$T_{ex\beta,a} = T_e \neq T_g \quad . \tag{6}$$

The PLTE assumption is usually coupled with a Collisional-Radiative model in order to determine lower energy level populations and the atom density, because the ground state is either over- or underpopulated based on $T_e = T_{ex\beta}$. The PLTE/LCRE ionization equation is given in Table II.

The collisional-radiative model includes various up/down collisional and radiative processes to determine the deviation of electronic levels from a Boltzmann distribution at T_e. The deviation is expressed in terms of a departure coefficient b_m for level m based on the upper level ionization equation such that [3]

$$\left(\frac{N_e^2}{N_m}\right)_{ACTUAL} \equiv b_m \left(\frac{N_e^2}{N_m}\right)^* \quad , \tag{7}$$

where

$$\left(\frac{N_e^2}{N_m}\right)^* = 2\,\frac{Z_{exi}}{Z_{exa}} \left[\frac{2\pi m_e kT_e}{h^2}\right]^{3/2} \exp\left[\frac{-(E_I - E_m)}{kT_e}\right] \tag{8}$$

and * indicates the PLTE (or "equilibrium") expression with T_e and N_e as independent variables. The physical meaning of b_n is more obvious from [9,10]:

$$1/b_m = \varsigma_m \equiv N_m/N_m^*(T_e, N_e) \quad , \tag{9}$$

where $N_m^*(T_e,N_e)$ is obtained from (8). The behavior of b_m is

$$b_m \to 1 \text{ as } m \to \infty \quad , \quad \text{and} \quad b_m \geq \text{ or } \leq 1 \text{ as } m \to 1. \tag{10}$$

The advantages of the PLTE/LCRE model is that the non-Boltzmann electronic energy level distribution can be determined and that calculations can even be made on a personal computer. The disadvantages are that LCRE, the model does not consider radiative transfer except as a specified self-absorption, e.g. via optically thick resonance lines [7] or specified Holstein escape factor values [3]. This can be relaxed with the non-local CRE model, which includes adiative transfer via variable radiation escape [11] or spectrally dependent radiative transfer [12]. A more serious disadvantage is that PLTE methods extrapolated to E_∞ or E_I [6] find $T_{exa} \neq T_e \neq T_{ex\beta,a}$ hence, the foundation of the model leading to the ionization equation used is questionable.

Non-Local Collisional-Radiative Equilibrium (non-LCRE) Models

These are considered separately from the PLTE/LCRE models because it is not necessary to use the PLTE constraint. The non-local aspect comes from the non-

local radiative transfer input through variable radiative escape factors [11] or spectrally dependent radiative transfer [12].

This category also includes collisional-radiative models which use the PLTE assumption at only very high lying levels so that measureable excited levels are not pre-determined [13,14]. The non-LCRE or CRE model is therefore, one of the best models available. Its limitations lie in the quality of the cross sections or rate constants available and the complexity of solution for multicomponent plasmas with arbitrary geometries.

Statistical Equilibrium and Radiative Transfer (SERT) Models

The SERT models parallel the development of LCRE and CRE models. The SERT models were the first to include radiative transfer seriously by writing the source function for a line (or continuum) [15, 16],

$$S_\nu = B_\nu \left[T_{ex}\right] = \frac{\int I_\nu \phi_\nu d_\nu + \epsilon B_\nu [T_e] + \theta}{1 + \epsilon + \Delta} \quad , \tag{11}$$

which is equal to the Planck function of an electronic excitation temperature, T_{ex}, in terms of the radiative field $\int I\phi d\nu$, collisional excitations $\epsilon B_\nu[Te]$ and de-excitation ϵ, collisional and radiative ionizations θ and recombination Δ, and radiative de-excitation 1, where all are normalized to the transition probability.

The advantages are similar to the non-LCRE models and include the capability to determine when $T_{ex} = T_e$ [6]. The disadvantages include the difficulties in solution over all significant frequencies which are further complicated with each additional level added to the multilevel atom solution.

Multitemperature Models

Most of the Multitemperature models are similar in that they are flexible as to the number of temperatures which may be used. The derivations are based on each subsystem k having its own temperature T_k. Prigogine [17] developed a MSE (Multitemperature Saha Equation) assuming each species had its own temperature:

$$T_a \neq T_e \neq T_i \ . \tag{12}$$

Potapov [18] developed a 2-T MSE based on T_e and T_g and equations (3) and (4), but obtained a different 2-T ionization equation than most 2-T models use, as shown in Table II. The $\theta_g = T_e/T_g$ powers can make tremendous differences between MSE and PLTE based 2-T species densities.

A Multithermal Equilibrium (MTE) model [19], based on experimental observations, extended the temperature identification to partial energy modes (see Fig. 1):

$$\text{Complete MTE(CMTE): } T_g \neq T_e \neq T_{ex\beta} = T_{exa}, \tag{13}$$

$$\text{Partial MTE(PMTE): } T_g \neq T_e \neq T_{ex\beta} \neq T_{exa}, \tag{14}$$

The MTE model has an ionization equation resembling the PLTE form as shown in Table II.

Recent work [20,21] has shown that the assumed equivalence of ensemble temperatures is an oversimplification, so that the MTE model is limited, like the PLTE model, to near-LTE situations. A generalized MTE (GMTE) model is also found to be a generalized extension of the MSE models and can be extended to the complete and partial energy modes (CMTE and PMTE) discussed above, whose concepts are still valid.

The general form of the law of mass action for the multitemperature models is [18]:

$$\prod_j N_j^{\eta_j kT_j} = e^{-\Sigma \eta_j E_{o,j}} \prod_j \left[Z_{t,j}^{\eta_j kT_{t,j}} \left(\prod_k^{int} Z_{k,j} \right)^{\eta_j kT_{k,j}} \right] , \qquad (15)$$

where η_j is the stoichiometric coefficient of species j, $E_{o,j}$ is the zero energy correction for partition function energies, and $Z_{t,j}$ is the translational partition function of species j. The k-product is over internal energy modes. From this equation, the various MSE, MTE and GMTE ionization equations can be written as in Table II. The PMTE relations are obtained by pivoting around the psuedo level density at E_∞ (or the lowered value E_I).

The advantage of the MSE and GMTE models is that the relations are rigorously derived from fundamental concepts and are based on experimental observations. They are flexible as to CMTE and PMTE and hence utilize physically meaningful temperatures in which the 2-T, PLTE, and CRE models can be expressed, including the b_n. The number of conservation equations must be increased to match the increase in temperature variables. This can be done by adding electronic excitation energy equations with collisional-radiative terms which can be evaluated as functions of the temperatures and species densities to facilitate solution [22]. Radiative transfer is included via radiation escape factors. The disadvantage is the additional complexity analogous to the CRE models.

Kinetic Methods

The kinetic method for determining species densities in plasmas [23] is a modified 2-T model which assumes that all reaction rates are functions of either T_e or T_g. The form for the reaction rate is

$$k_{f \text{ or } r} = C_1 T^{C_2} \exp(-C_3/kT), \qquad (16)$$

where k_f, k_r are the forward and reverse reaction rates and C_1, C_2, C_3 are constants obtained from experimental data. The measure of forward progress ξ of a reaction $\Sigma \eta_{fj} M_j \rightleftarrows \Sigma \eta_{rj} M_j$ is given by

$$\frac{d\xi}{dt} = \prod_j N_j^{\eta_{fj}} k_f - \prod_j N_j^{\eta_{rj}} k_r \quad . \qquad (17)$$

Steady state concentrations are then given by

$$\prod_j N_j^{\eta_j} = \frac{k_f}{k_r} = \exp\left(\frac{-\Delta E_o}{kT}\right) \prod_j Z_j^{\eta_j} \quad , \tag{18}$$

where the rhs is obtained only in LTE at T. A casual comparison of (18) and (15) suggests a contradiction; however, (18) is a rather simplistic expression and $k_{f,r}$ should also depend on the order of the reaction in which empirical consideration of species concentrations or densities enters. The view that kinetic methods are "pure" is somewhat of an illusion. Also the availability of reliable cross sections is the exception rather than the rule. More research needs to be done in this area.

A comparison [23] between values from Kinetic and MSE methods unfortunately misapplies the MSE method. When corrected, the two methods agree in steady state values at θ_g values considered ($\theta_g \sim 1.2 \rightarrow 1.4$). Aubreton [24] has compared the MSE method of Potapov [18] and a pseudo-kinetic method in the form of predicting non-LTE transport coefficients. The results are similar, but values at $\theta_g < 3$ differ by only 10-20%. In addition, the pseudo-kinetic method predicts that discontinuities appear at $\theta_g \gtrsim 3$ which is not the case with the MSE model. Similar discontinuities are found using GMTE diagnostic analyses with large θ_g.

Other kinetic methods use a collisional-radiative model in transient mode [25]. These models show that equilibrium of the ground state occurs at much, much longer times than the excited levels [26]. This result can greatly influence the modeling of circuit breakers and other transient plasma phenomena.

The advantages of the kinetic method are 1) in transient analyses involving relaxation processes and 2) in the convenient form of the non-LTE expression in (18). Many of the present 2-T applications neglect distributions of excited levels at other than T_e. It would be beneficial to look at multitemperature kinetic methods. A possible disadvantage of the kinetic method is that an ionization equation is replaced by an expression for which the reaction rates need to be determined from experiment or estimated. This may be an advantage in some complex plasma processes if the overall rates can be used, which would in most cases limit scaling or application to a different type of reactor.

Conclusion

The major questions that remain are what simplifications can be made in the ionization equation for a particular application to simplify the solution procedure and to resolve the application of a wide variety of ionization models and/or when do kinetic models need to be used. Future experimental work should include diagnostics to compare measured and diagnostically calculated electron and gas temperatures and both thermodynamic and transport property measurement to compare with theoretical calculations from various models.

Theoretical work should include property calculations or formulations via collisional-radiative features (to possibly express them as properties) and transport property calculations for other than 2-T models.

References

1. C. L. Tien and J. H. Leinhard, Statistical Thermodynamics, Revised Printing, Hemisphere Publ. Corp., Washington, D.C. (1979).

2. T. F. Morse, Phys. Fluids, 6, 1420 (1963).

3. M. Mitchner and C. H. Kruger, Jr., Partially Ionized Gases, Wiley-Interscience Publ., New York (1973).

4. A. V. Donskoi, V. M. Goldfarb and V. S. Klubuikin, Physics and Technology of Low Temperature Plasmas, S. V. Dresvin (Ed.), English translation by T. Cheron and H. V. Eckert, Iowa State Univ. Press, Ames, Ch. 8 (1977).

5. J. Mostaghimi, P. Proulx and M.I. Boulos, 7th Int. Conf. Plas. Chem., v. 3, 865-872 (1985) and Plas. Chem. Plas. Proc., 4 (3), 199-217 (1984).

6. T. L. Eddy, J. Quant. Spectrosc. Radiat. Transfer, 33 (3), 197-211 (1985).

7. J. J. Lowke, J. Appl. Phys., 41 (6), 2588-2600 (1970).

8. D. R. Bates, A. E. Kingston and R. W. P. McWhirter, Proc. Roy. Soc., Ser A, 267, 297 (1962) and 270, 155 (1962).

9. A. V. Potapov and L. E. Tsvetkova, Opt. Spectrosc., 38 (3), 253-255 (1975).

10. C. Park, J. Quant. Spectrosc. Radiat. Transfer, 22, 101-112 9 (1979).

11. R. J. Giannaris and F. P. Incropera, J. Quant. Spectrosc. Radiat. Transfer, 13, 167-181 (1973) and 13, 183-195 (1973).

12. J. P. Apruzese, D. C. Kepple, K. G. Whitney, J. Davis and D. Dustin, Phys. Rev. A, 24, 1001 (1981).

13. A. M. Gomes, J. Phys. D: Appl. Phys., 16, 357-378 (1983).

14. J. M. Anderson, "Collisional radiative recombination and net ionization in mercury vapor," General Electric Co., Tech. Inf. Series, No. 85 CRD 220 (1985).

15. R. N. Thomas and R. G. Athay, Physics of the Solar Chromosphere, Interscience, New York (1961).

16. R. N. Thomas, Nonequilibrium Thermodynamics, U. Colo. Press, Boulder, (1961).

17. I. Prigogine, Bull. Cl. Sc. Acad. R. Belg., 26, 53-63 (1940).

18. A. V. Potapov, High Temperature, 4, 48-51 (1966).

19. T. L. Eddy, E. Pfender, and E.R.G. Eckert, IEEE Trans. Plasma Sci., 1, 31-42 (1973).

20. T. L. Eddy, A. Sedghinasab, K. Y. Cho, R. Frierson, Radiative Properties in Non-LTE Plasmas, Final Report, NSF Grant CPE-8311325, 1987.

21. K. Y. Cho, Ph.D. thesis, Georgia Institute of Technology, Atlanta, in preparation.

22. D. W. Pruitt, "Heat transfer model for an arc plasma in multithermal equilibrium", M.S. Special Problem, Woodruff School of Mechanical Engineering, Georgia Institute of Technology, Atlanta (1984).

23. E. Richley and D. T. Tuma, J. Appl. Phys., 53 (12), 8537-8542 (1982).

24. J. Aubreton, "Etude de properiétés thermodynamiques et de transport dans des plasmas thermiques à l'équilibre et hors d'équilibre thermodynamiques: Applications aux plasmas de mélange Ar-H_2 et Ar-O_2, Thèse d'Etat, Université de Limoges (1985).

25. C. G. Braun, D. A. Erwin and M. A. Gunderson, Submitted to Applied Physics Letters (1986).

26. J. Kunc, personal communication (1986).

3.5 Criteria for Local Thermal Equilibrium (LTE)

A widely used model in plasma spectroscopy is the LTE model. The unique feature of the LTE model is that the temperatures describing the various processes such as ionization, excitation, dissociation, etc., are all equal. These circumstances may occur in dense, high temperature plasmas where there is a strong kinetic coupling between different species, so that collisions dominate the transitions between energy levels and equalize the particle temperature. It may also occur in tenuous plasmas with large optical depths (astrophysical plasmas) because of radiative equilibrium. In laboratory and industrial plasmas LTE often exists because some collisional and radiative processes work together to give LTE conditions. When LTE prevails, the level density distribution follows that of a system which is in complete thermal equilibrium at the same temperature, mass density, and chemical composition. The LTE model assumes that the population of atoms and ions in various excited states may thus be determined from the principle of equipartition, which does not require knowledge of atomic cross sections.

Spatial and thermal gradients in laboratory plasmas are often significant and cause diffusion of particles to the cooler walls. If the electron collision frequency is small (low electron density), the particles may not come to equilibrium with the local conditions before being diffused to cooler regions of the plasma. This leads to establishment of an electron density lower limit for which the equilibrium time is much smaller than the characteristic time for diffusion. Quantitative limits of electron density and temperature for which LTE exists have been repeatedly given by many authors, some of which are presented in Table 3.1. It can be noted that there is a wide range of conditions under which LTE is believed to occur.

Table 3.1: Selected Minimum Conditions for Establishment of LTE

Author	Minimum n_e for LTE (cm^{-3})
Wilson (1962) [77]	$n_e \geq 8.56 \times 10^{12} T_e$ T_e(K)
Griem (1964) [24]	$n_e \geq 3.5 \times 10^{12} T_e$
Schumaker & Popenoe (1968) [78]	$n_e \geq 2 \times 10^{17}$
Morris and Krey (1968) [79]	$n_e \geq 2 \times 10^{17}$
Evans et al (1970) [7]	$n_e \geq 10^{18}$
Bober & Tankin (1970) [8]	$n_e \geq 10^{18}$
Hey (1975) [80]	$n_e \geq 2.25 \times 10^{18}$
Preston (1977) [4]	$n_e \geq 9 \times 10^{16} - 2 \times 10^{17}$
Blades (1982) [81]	$n_e \geq 1.6 \times 10^{16}$

4.0 THE GMTE MODEL

4.1.1 Introduction

In this chapter, the generalized multithermal equilibrium (GMTE) model is derived and is applied to population and density as well as thermodynamic property determination in argon and hydrogen plasmas. GMTE diagnostic methods are also discussed in Chapter 6.

4.1 Argon

Thermodynamic property calculations based on statistical thermodynamics require accurate knowledge of partition functions which in turn depend on the atomic and ionic energy levels for their accuracy. Since the electronic energy levels of argon neutral and ions are not available at energies near the ionization level, various methods have been used to predict these levels [82-84]. It turns out that the values of partition functions at very high temperatures ($T > 15{,}000$ K) are sensitively dependent on not only the method used for prediction of these levels, but also on the neighbor-neighbor interactions. The major source of electronic energy level compilation has been the NBS circular no. 467 [85] which includes only a small fraction of these levels because it is based on experimental observations. Other recent publications [86,87] have contributed to the compilation of these levels, however, higher quantum number levels are generally missing because of the experimental limitations.

The proper form of the Rydberg-Ritz relation can be utilized to predict the unobserved energy levels. McBride and Gordon [84] and Gurvich et al [82] state that only a rough approximation of the energies of the upper levels is needed for the calculation of partition functions at high temperatures. This is true, if used in conjunction with a lowering technique which is dependent on the principle quantum numbers such as that given by Margenau and Lewis [88], and not on the value of the energy levels, such as Debye lowering after Griem [24]. Since the latter is used in this work, precise values of energy levels are required.

Careful studies in recent years [89-92] have indicated that argon electrical arcs deviate considerably from LTE. The determination of the extent of their deviation from LTE is only possible, if the diagnostic methods employed allow for such deviations and nonequilibrium conditions. Generalized multithermal equilibrium (GMTE) technique allows for such kinetic and excitation nonequilibrium.

4.1.2 Energy Levels and Partition Functions

The total partition function of a molecule is in general given by the product of all the partition functions associated with various energy modes,

$$Z = Z_t Z_{rot} Z_{vib} Z_{ex} \cdots$$

For a monatomic gas undergoing no chemical reaction, the partition function reduces to,

$$Z = Z_t Z_{ex}$$

where

$$Z_{ex} = \sum_{i=1}^{m} g_i e^{-E_i/kT_{ex}} \qquad (4.1)$$

here i=1 denotes the ground state, i=m is the last or the highest bound excited level, g_i is the statistical weight or degeneracy of a given energy level E_i, k is the Boltzmann constant and T_{ex} is the excitation temperature in degrees K.

The degeneracy of an energy level can be calculated using the iso-electronic series given by NBS [2]. Total degeneracy of each principal quantum number is the sum of the degeneracies for all the possible configuration of the atom at that level. For example, for n=4, it will include the degeneracies associated with the 4s, 4s', 4p, 4p', 4d, 4d', 4f, and 4f' configurations. Argon atom has two cores ($^2P_{3/2}$ and $^2P_{1/2}$), each having a different ionization potential 127109.7 cm^{-1} and 128541.3 cm^{-1} respectively. Argon atom ionized near its lowest ionization potential, indicating that only a few levels of the $^2P_{1/2}$ core which lie under the ionization potential of the $^2P_{3/2}$ core, have to be accounted for in the partition function calculations.

The missing energy levels of argon neutral and ions have been predicted using the Rydberg-Ritz equation for a given term series,

$$E_{n,l} = E_\infty - \frac{z^2 R_y}{(n - \mu)^2} \qquad (4.2)$$

where E_∞ is the ionization potential of each core, z is the effective charge (e.g. z-1 for neutral), R_y is the Rydberg constant (109735.8 cm^{-1} for argon), n is the integral quantum number corresponding to the hydrogenic principal quantum number, and μ is the quantum defect which is zero for hydrogen. The quantum defect for a non-hydrogenic atom is given by,

$$\mu = \alpha(l) + \frac{\beta(l)}{n^2} \tag{4.3}$$

where α and β are Rydberg and Ritz coefficients respectively. for a given atom these coefficients depend only on the azimuthal quantum number, l [93].

The second term in quantum defect expression losses its significance rapidly for large values of n. In addition, energy levels need to be calculated for higher quantum numbers, which simplified Eqn. (4.3) to the following form,

$$\mu=\alpha(l) \tag{4.4}$$

The coefficient α is predicted as follows. For each term series of a given core (e.g. s series in $^2P_{3/2}$ for argon neutral), the tabulated energy levels for that series for all the available quantum numbers are substituted in Eqn. (4.2). The resulting values of μ are then plotted vs. n (See Fig. 4.1). Next, the asymptotic value of this curve is determined for $n \to \infty$. This value is taken for the calculation of missing energy levels at large quantum numbers. Table 4.1 lists the values of the quantum defect for argon neutral and the first four ions.

At low temperatures ($T < 15{,}000$ K), only the low lying energy levels contribute significantly to partition functions. At high temperatures, on the other hand, the accuracy of high lying levels becomes increasingly important because of their role in determination of lowering of ionization potential. Fortunately, at large quantum numbers, the accuracy of quantum defect values becomes less significant and energy levels resemble hydrogenic levels. Values of energy levels determined by this method agree well with those given by Minnhagen [87] for argon neutral. The energy levels and degeneracies of argon neutral are presented in Appendix A.

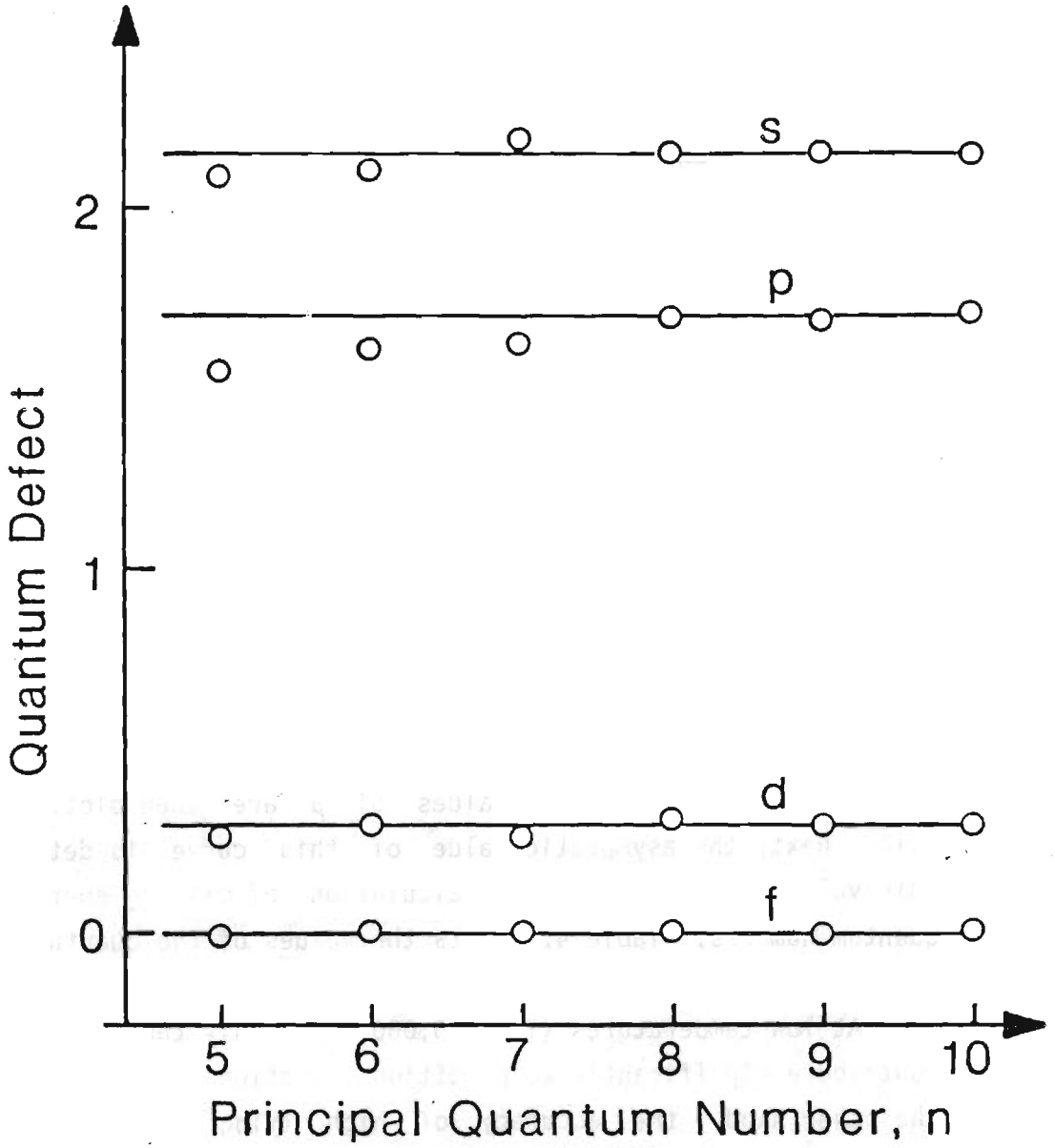

Figure 4.1: Quantum defect, μ, as a function of the principal quantum number

Table 4.1: Quantum Defect Values for Argon Neutral and Ions

Element	Branch	Ionization Potential (cm^{-1})	*Term series* s	p	d	f	≥ g
Ar I	$^2P_{3/2}$	127109	2.143	1.668	.333	.012	0[a]
	$^2P_{1/2}$	128541	—	—	—	—	—
Ar II	^3P	222820	1.52	0.91	0.354	0.041	0
(Cl I)[b]	^1S	236830	1.72	0.9	0.35	0.03	0
	^1D	256087	1.72	0.85	0	0	0
Ar III	$4S^\circ$	329965	1.3	0.7	0.1	0.01	0
(S I)	$2D^\circ$	351056	1.21	0.6	0.1	0.008	0
	$^2P^\circ$	364820	1.2	0.6	0.1	0.005	0
Ar IV	^3P	482400	*Assumed hydrogenic for the rest*				
(P I)	^1D	498701					
	^1S	502400					
Ar V	$^2P^\circ$	605100					
(Si I)	^4P	705100					

[a]Zero indicates that hydrogenic level structure is assumed
[b]Equivalent predicted term series of these elements are used in calculation of degeneracies

Calculations of partition functions as given by Eqn. (4.1) requires the summation over all energy levels below the ionization potential of the species considered. In practice, this presents a difficulty, in that, the given series diverge as $n \to \infty$, causing the value of partition function to be infinitely large. It must be noted that n only approaches infinity for an isolated single particle. In reality, however, only a finite number of levels contribute to the partition function due to the polarizing effect of the neighboring charged particles. This phenomenon manifests itself in the form of lowering of ionization potential. Evidence of lowering phenomenon has been previously documented [94]. This leads to the establishment of a criterion for terminating the partition function series at an energy level corresponding to the lowered ionization potential.

Of the various techniques available for calculation of lowering of ionization potential, the method given by Griem [24] is used in this work due to its inherent dependence on the value of energy levels and not explicitly on the principal quantum number. Greim's lowering is given by,

$$\Delta E_\infty = ze^2/\rho D \tag{4.5}$$

where z is the effective nuclear charge as seen by the excited electron and e is the electronic charge, and ρ_D is the Debye length given by [95],

$$\rho_D = \left[4\pi e^2 \left(\frac{n_e}{kT_e} + \frac{\Sigma_i z_i^2 n_i}{kT_a} \right) \right]^{-1/2} \tag{4.6}$$

where z_i is the effective ionic charge as seen by a free electron and the summation is over all charged heavy particles (ions). This method gives an order of magnitude smaller lowering than the nearest neighbor method [96], but a factor of 2 larger value than if the maximum Bohr radius is assumed equal to the Debye radius [97]. Griem's calculation is based on energy considerations due to coulomb field and seems to be the most appropriate method at this time. In Fig. 4.2 the internal partition function obtained in this work is compared to those of several other authors.

4.1.3 Generalized Multithermal Equilibrium Concept

When all the different energy modes of different species in a plasma are allowed to have their own equilibrium energy distribution and hence

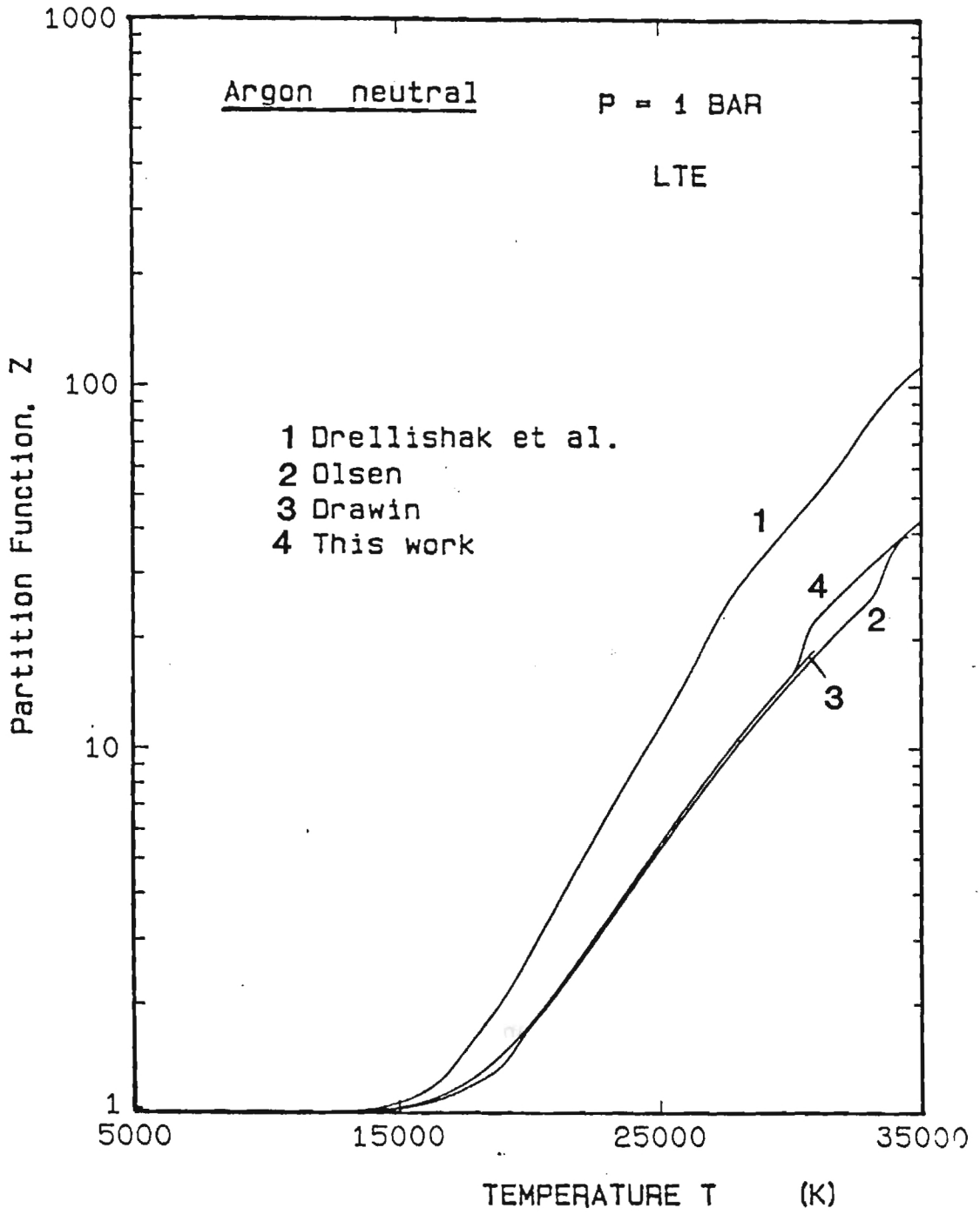

Figure 4.2: Internal partition function of argon neutral calculated by QDM as compared to other techniques

their own particular temperatures, a case of multithermal equilibrium would exist in which each energy mode is independent of other energy modes. Therefore, one can write,

$$T_e \neq T_a \neq T_i \neq T_{rot} \neq T_{vib} \neq T_{exa} \neq T_{exi} \neq T_{ex\beta,a} \neq T_{ex\beta,i} \neq \ldots$$

where T_{ex} is the total excitation temperature, and $T_{ex\beta}$ is the upper level excitation temperature. Some GMTE temperatures are illustrated in Figure 1 of Chapter 3.

Since the atoms and ions have equivalent masses, their kinetic energy distribution, in absence of strong electric fields, is often very similar, i.e. $T_a=T_i=T_g$. Furthermore, it is convenient to assume that $T_{exa}=T_{exi}$. This assumption is not necessary but little is known about typical values of T_{exa}/T_{exi}. Hence, for a singly ionized monatomic plasma one can write,

$$T_e \neq T_g \neq T_{exa} \neq T_{ex\beta,a} \neq T_{ex\beta,i}$$

The electron temperature (T_e), will usually be greater than or equal to the gas temperature (T_g), due to its longer free path. Likewise, $T_{ex\beta}$ is usually different than T_{exa}, because the ground state in a real plasma is seldom populated according to $T_{ex\beta}$. No further generalization can be made and the relation between any two temperatures will only be a function of the particular operating conditions (e.g. electron density, pressure, field strength, . . .).

The GMTE ionization equation is a generalized extension of MSE in which the assumption of $T_{exa}=T_e$ is relaxed. The resulting equation is very similar to that of MSE with the exception of the power term (T_{exa}/T_e) over the partition function ratios. Since the electronic partition function ratios, Z_{exi}/Z_{exa}, may differ appreciably from unity (e.g. 6 for argon), the power term may make a significant difference between the particle densities calculated by GMTE model and those calculated by MSE. The GMTE ionization equation is given as,

$$n_e \left[\frac{n_i}{N_a}\right]^{T_g/T_e} = 2 \left[\frac{Z_{exi}(T_{exa})}{Z_{exa}(T_{exa})}\right]^{T_{exa}/T_e} \left[\frac{2\pi m_e k T_e}{h^e}\right]^{3/2} \exp\left[\frac{-E_I}{kT_e}\right] \qquad (4.7)$$

Analogous to CRE model, an expression for the ground state departure coefficient can be written for GMTE in the following form,

$$b_1 = \left[\frac{n_i}{n_1}\right]^{1-(T_g/T_e)} \left[\frac{Z_{exi}}{Z_{exa}}\right]^{(T_{exa}/T_e)-1} \tag{4.8}$$

The GMTE ionization equation can be written for ionization from a pseudo level at the ionization limit, E_I,

$$n_e \left[\frac{n_i}{n_I}\right]^{T_g/T_e} = 2\left[\frac{Z_{exi}}{g_I}\right]^{T_g/T_e} \left[\frac{Z_{exi}}{Z_{exa}}\right]^{T_{exa}/T_e} \left[\frac{2\pi m_e kT_e}{h^e}\right]^{3/2} \exp\left[\frac{-E_I}{kT_e}\left(1-\frac{T_g}{T_{exa}}\right)\right] \tag{4.9}$$

This form of the ionization equation has the advantage of not strongly depending on n_a which is usually not known with a good accuracy. Instead, n_a is replaced by n_I which is readily determined by measuring the spectral emission coefficients of a few spectral lines.

4.1.4 Plasma Composition

Number densities of the argon species are calculated for a given pressure, T_{exa}, T_e/T_a, and T_e/T_{exa} using the following method. The electron number density as well as the heavy particle number densities are originally guessed and then used in Eqn. (4.3) to determine the Debye length, which is in turn used to calculate the corresponding lowering of the ionization potential. The lowered level is compared to the predicted energy levels and then the corresponding internal partition function is calculated using all the observed and the predicted levels below the lowered ionization potential. This is done for all the heavy particles present in the plasma. Using the modified law of mass action expressed in the following form, species concentration ratios are determined,

$$\left(\frac{n_i}{n_{i-1}}\right)^{T_g/T_e} = \frac{2}{n_e}\left(\frac{Z_{ex,i}}{Z_{ex,i-1}}\right)^{T_{exa}/T_e}\left(\frac{2\pi m_e kT_e}{h^2}\right)^{3/2} \exp\left(\frac{-E_{I,i}}{kT_e}\right);\ i=1,2,3,4$$

Since n_1 corresponds to the neutral atom number density. An updated value of heavy particle density n_h is then obtained using,

$$n_h = n_1 + \sum_{i=1}^{4}\left(n_1 \prod_{m=1}^{i}\frac{n_m}{n_{m-1}}\right)$$

Electron density is calculated from the quasi-neutrality assumption,

$$n_e = \sum_{i=1}^{4} i n_i$$

At this stage the total pressure can be calculated using,

$$p_{calc} = n_h kT_g + n_e kT_e \qquad (4.10)$$

This pressure is then corrected for atomic interactions at large densities using the Debye-Hückel relation [98] given below for high pressure gases,

$$\Delta pDH = p\left(24\pi p_D^3 \sum_{i=0}^{4} n_i\right)$$

This value is subtracted from the value obtained from Eqn. (4.10) to yield the corrected pressure, which is then compared to the given pressure. If the convergence criterion, $\Delta p/p < 10^{-6}$, is not reached, iteration process repeats starting from the Debye length calculation. It typically takes 10 to 14 iterations for this criterion to be satisfied.

4.1.5 GMTE Thermodynamic Properties

In the derivation of GMTE thermodynamic relations, it is assumed that each energy mode k of species j has an energy population distribution according to a mode temperature T_{kj}. It is also assumed that the various energy modes are weakly dependent on each other. Assuming a canonical energy distribution, the GMTE relations have been rigorously derived. Some of these relations used to generate thermodynamic properties are presented below.

The species partition function Z_j is obtained from the particle partition function and the species population,

$$\ln Z_j = \sum_k \ln Z_k^{N_j}$$

The ensemble partition function Z_N is found to be factorable over species j and energy mode k,

$$Z_N = \prod_j \frac{\prod_k Z_k^{N_j}}{N_j!}$$

where $N_j!$ accounts for the indistinguishability of the particles. Based on GMTE relations, the following properties can now be presented. The mass density p is calculated from,

$$\rho = \frac{(n_t - n_e)\, M_o}{N_o}$$

where n_t is the total particle number density, M_o is the atomic weight, and N_o is the Avogardro's number. The effective plasma atomic weight is given by,

$$M = \frac{(n_t - n_e)\, M_o}{n_t}$$

Although perfect gas is assumed, a compressibility factor, z_c, related to change in number of moles is defined as,

$$z_c = \frac{R}{R_o} = \frac{M_o}{M}$$

where R is the particular gas constant and R_o is the gas constant before dissociation or ionization. The ensemble translation temperature is then,

$$T_t = \frac{p}{z_c \rho R_o}$$

The Helmholtz function, Gibbs free energy, entropy, and enthalpy are calculated from,

$$a_N = \sum_j \frac{N_j k}{\rho} \left[T_{t,j} \left(\ln \frac{Z_{t,j}}{N_j} + 1 \right) + T_{exj} \ln Z_{exj} \right]$$

$$g_N = a_N + p/\rho$$

$$s_N = \sum_j (N_j/\rho) \sum_k \left. \frac{\partial g_{k,j}}{\partial T_{k,j}} \right|_p$$

$$h_N = \sum_j (N_j/\rho) \sum_k (g_{k,j} - T_{k,j} s_{k,j})$$

Some of these properties are shown in Fig. 4.3 through Fig. 4.9. Detailed derivation of these properties are given in refs. [100,110]. A species temperature based on the enthalpy can be written as,

$$T_{j,H} = \frac{\sum_k H_{k,j}}{\sum_k H_{k,j}/T_{k,j}}$$

where $H_{k,j}$ is the enthalpy associated with species j and energy mode k. An ensemble temperature based on the enthalpy can be similarly obtained from,

$$T_{N,H} = \frac{H_N}{\sum_j (H_j/T_j)}$$

where $H_N = \sum_j \sum_k h_{k,j}$.

Specific heats can be calculated from the following equations [110],

$$c_p = \left(\frac{\partial h_N}{\partial T_{N,H}} \right)_p = \sum_j (N_j/\rho) \sum_k \frac{\partial h_{j,k}}{\partial T_{k,j}}$$

Since properties are calculated for constant pressure cases, and not constant volume, the expression for c_v is therefore written in terms of c_p [97],

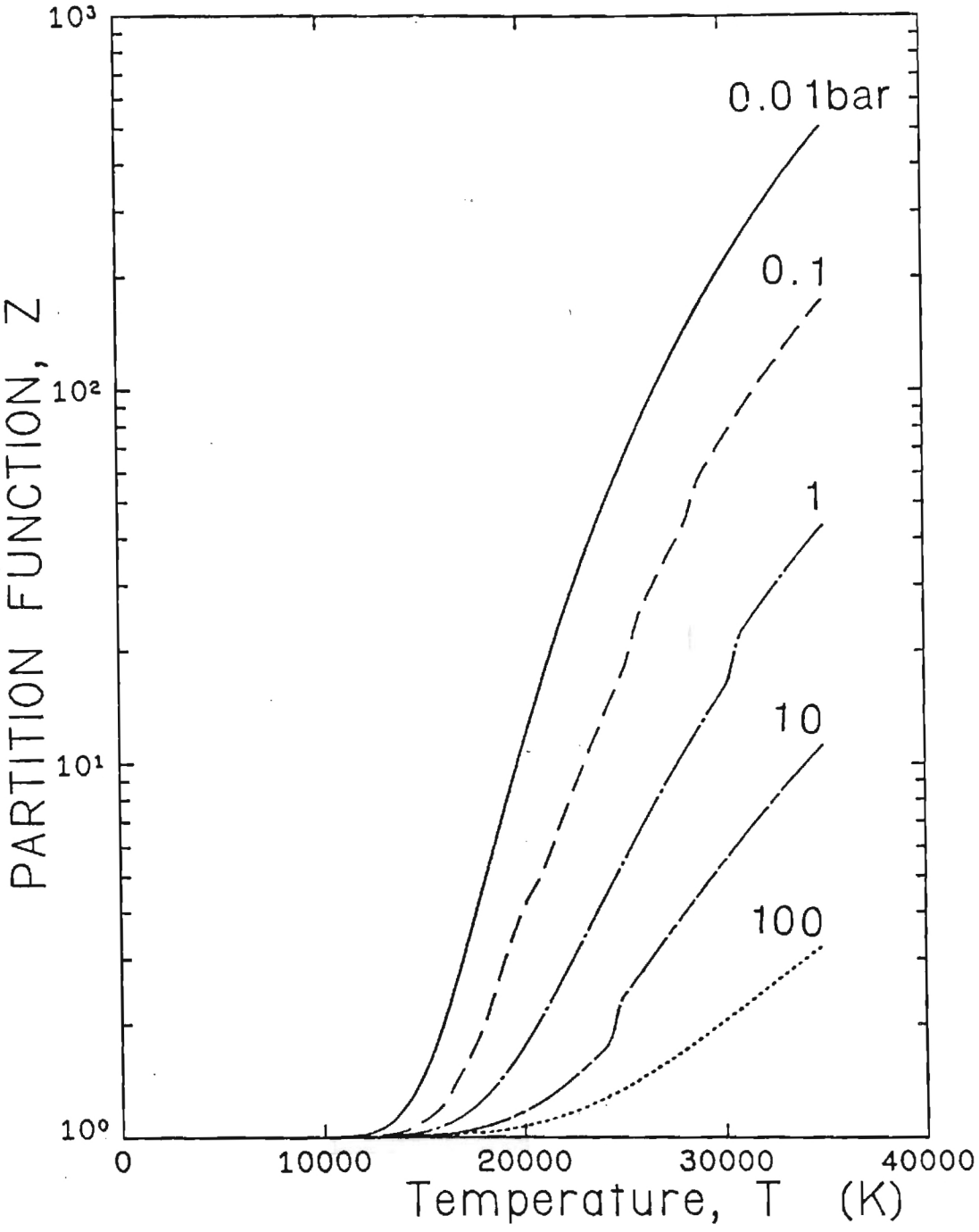

Figure 4.3: Partition function of neutral argon at LTE for various pressures

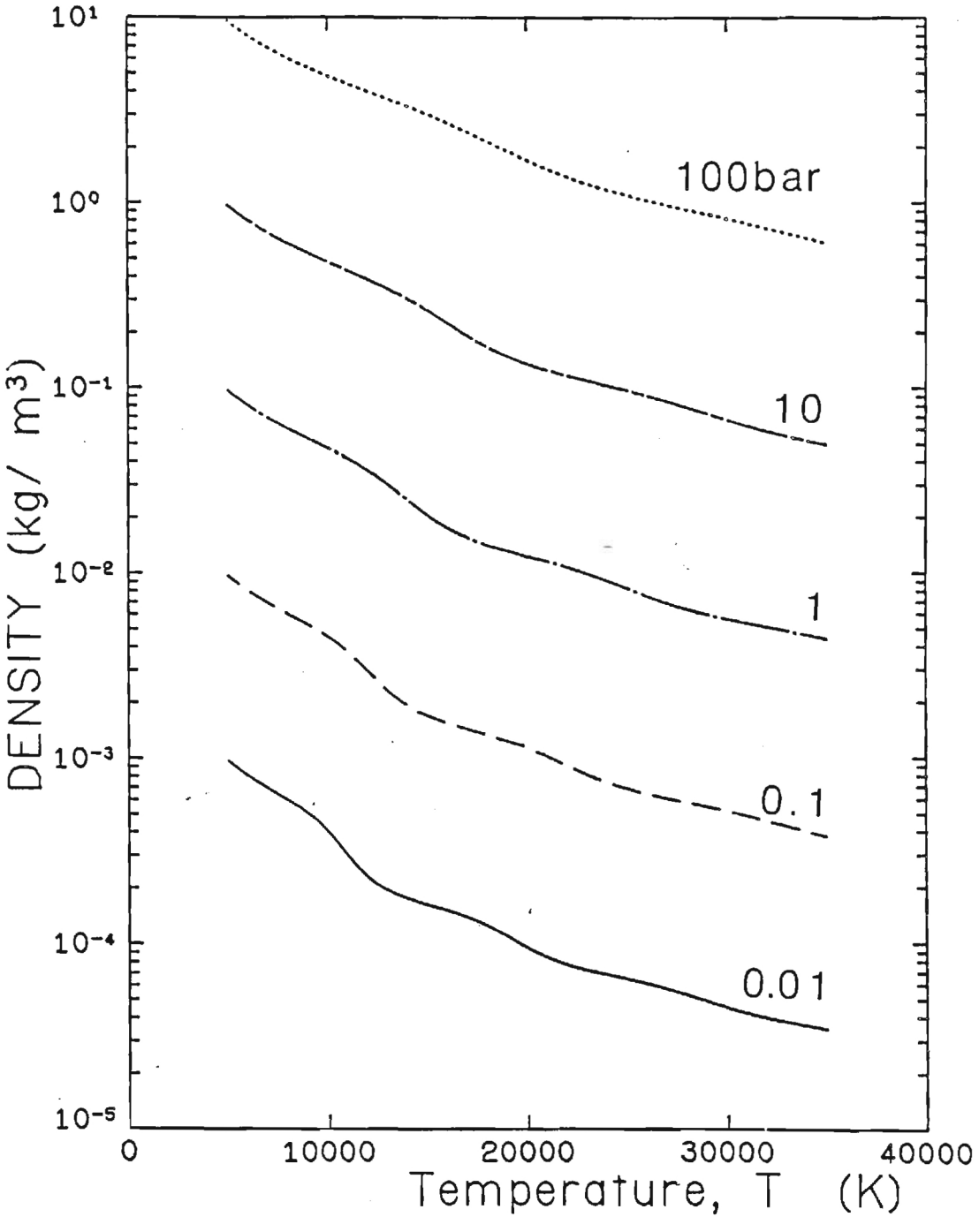

Figure 4.4: Mass density of argon at LTE for various pressures

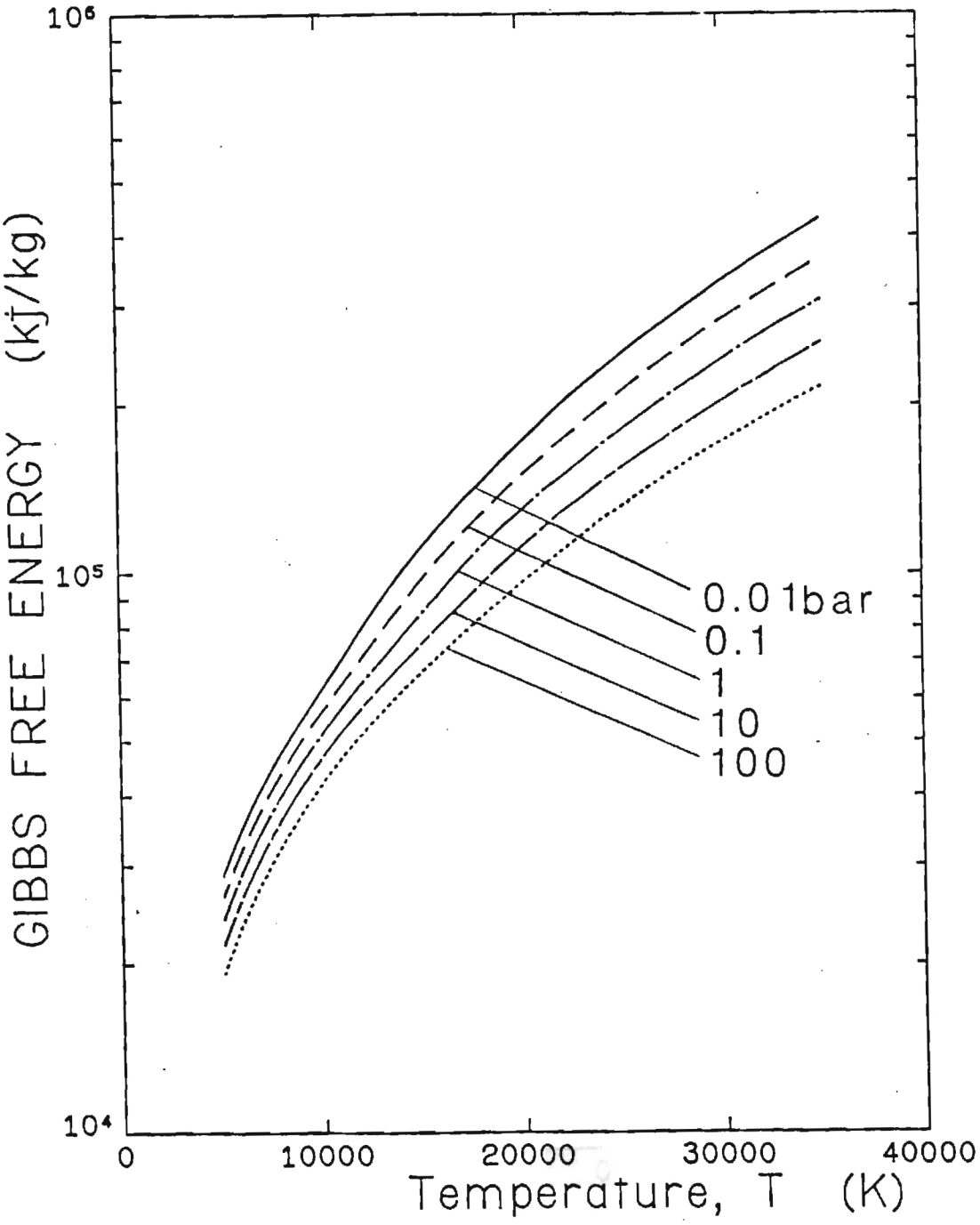

Figure 4.5: Gibbs free energy of argon at LTE for various pressures

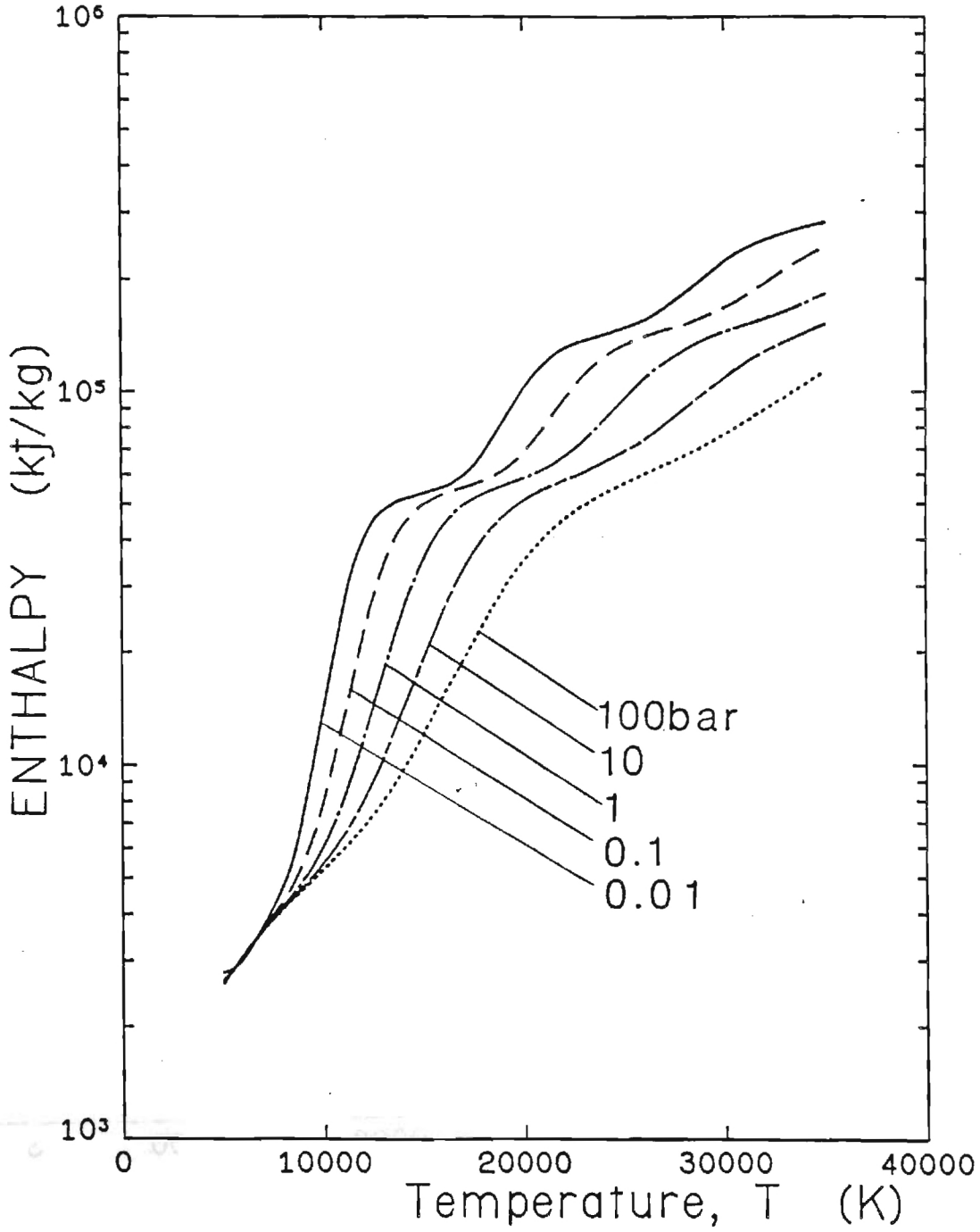

Figure 4.6: Enthalpy of argon at LTE for various pressures

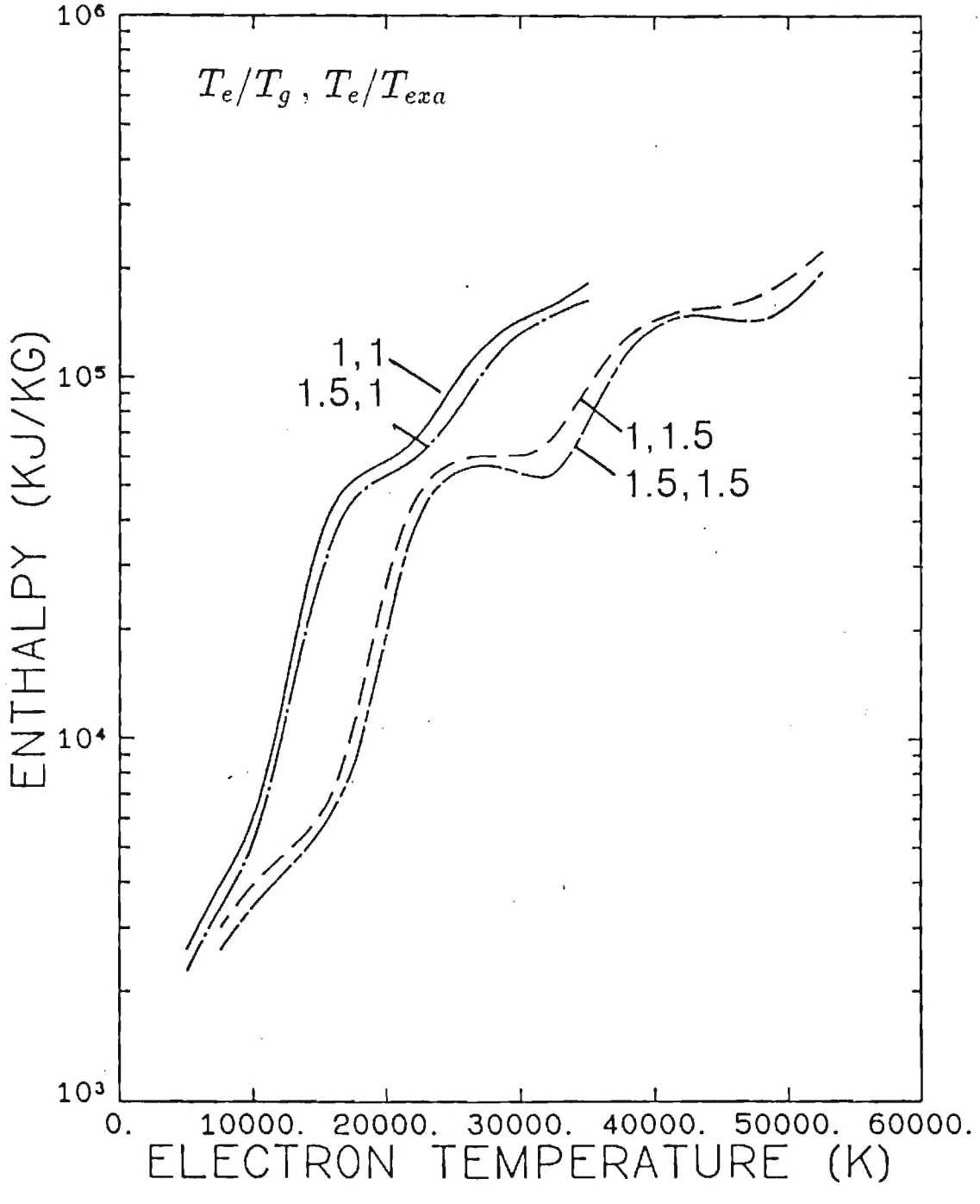

Figure 4.7: Enthalpy of argon at p=1 bar for various kinetic and excitation nonequilibrium

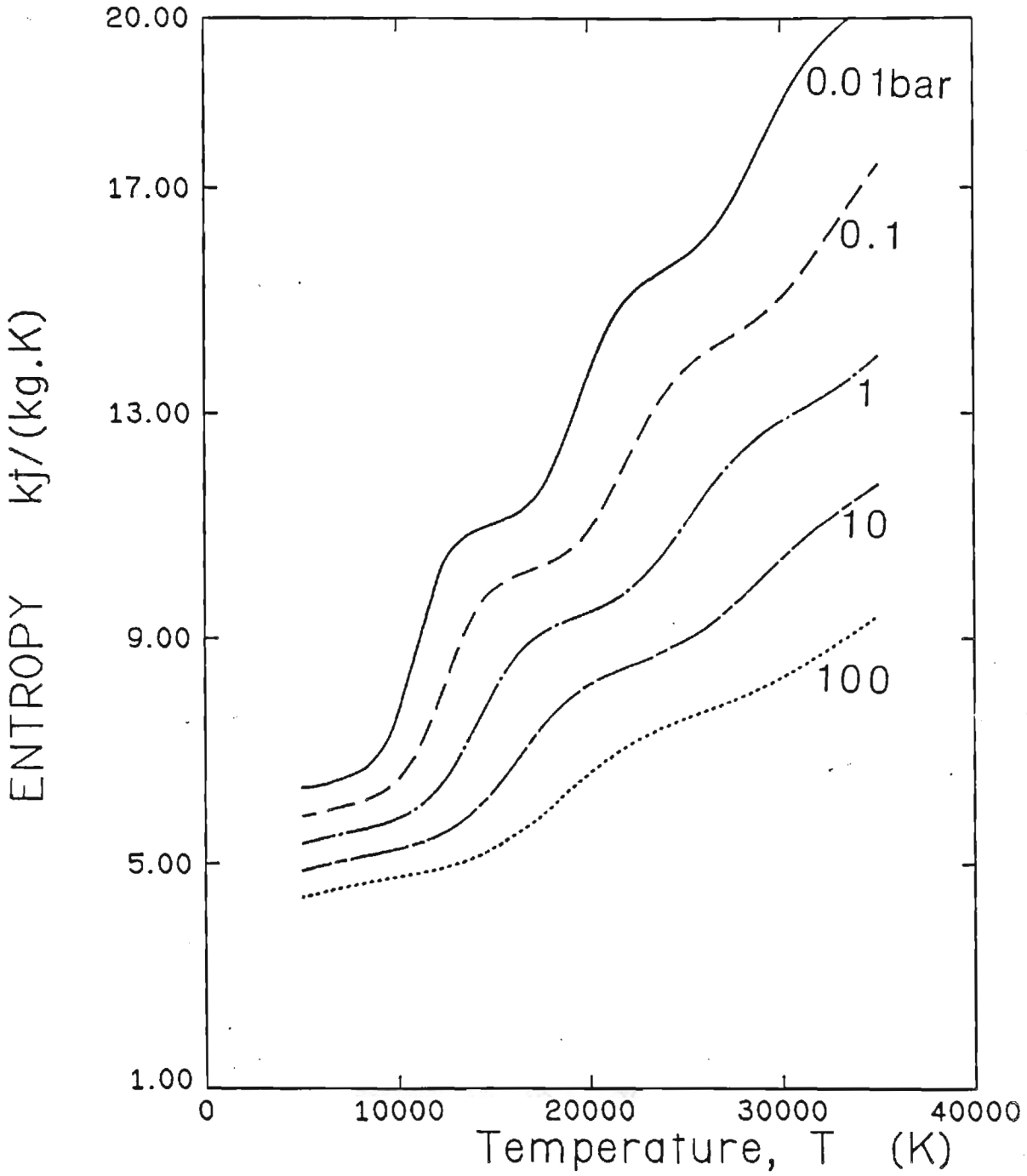

Figure 4.8: Entropy of argon at LTE for various presuures

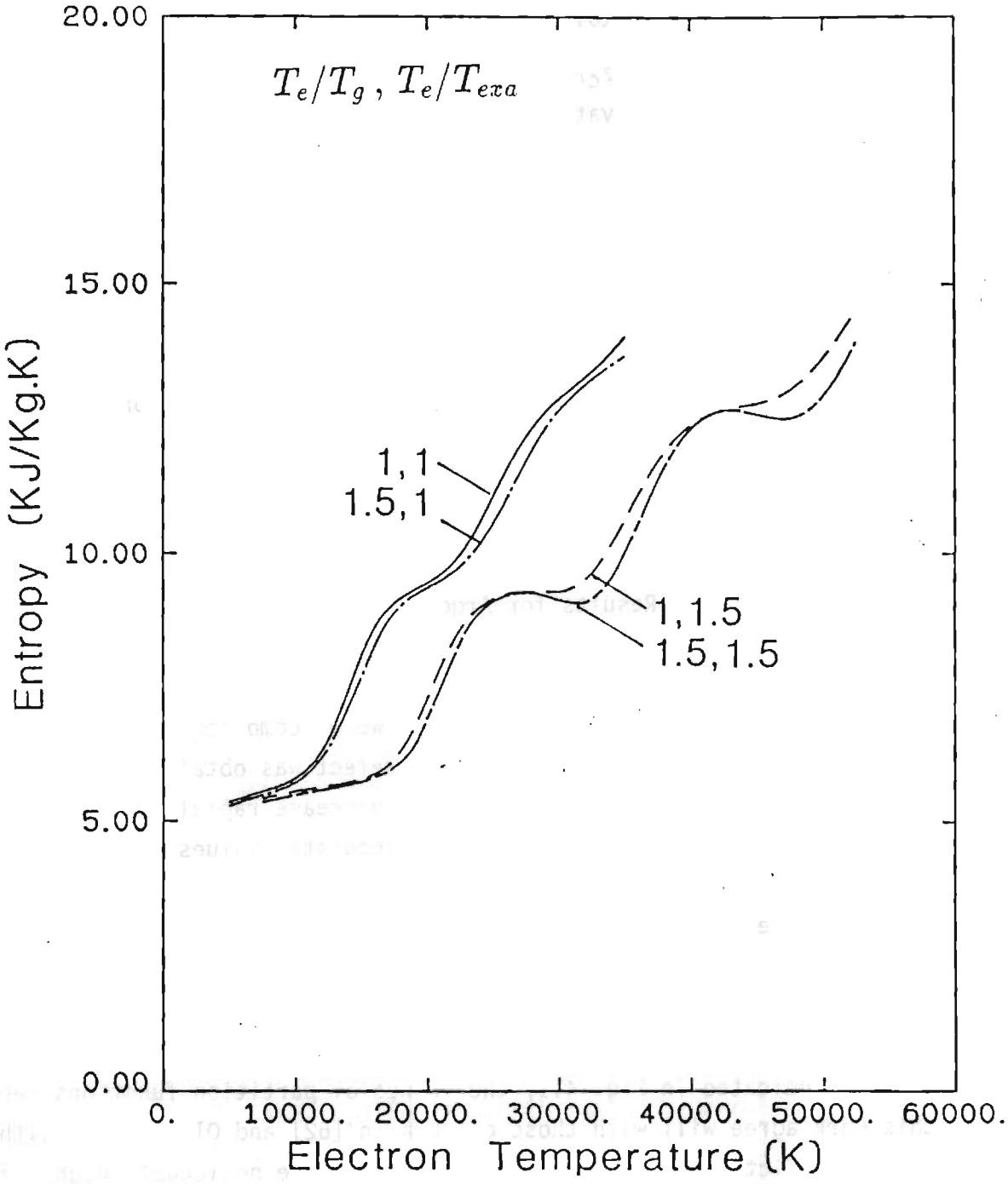

Figure 4.9: Entropy of argon at p=1 bar for various kinetic and excitation nonequilibrium

$$c_v = c_p - \frac{R\left[Z_c + \left(\frac{\partial z_c}{\partial \ln T}\right)_p\right]^2}{z_c - \left(\frac{\partial z_c}{\partial \ln p}\right)_T} = \sum_j c_p - \sum_j RZ_c$$

In order to evaluate $(\partial z_c/\partial \ln p)T$, properties are calculated for neighboring pressures and then derivative is taken over the pressure. As an example, for 1 bar, properties are calculated at 0.7, 1, and 1.2 bar, then $(\partial a_c/\partial \ln p)T$ is calculated using a quadratic equation which passes through z_c-lnp pairs for each temperature. Several curves of c_p are plotted as a function of the excitation temperature and are presented in Fig. 4.10. Having calculated c_p and c_v, the ratio of specific heats, γ, and the speed of sound, a, are calculated and shown in Fig. 4.11 and 4.12 respectively. Radiative properties such as line and continuum emission coefficients are also plotted for ArI 7147 and ArC 4200 and are shown in Figs. 4.13 through 4.19 as a function of T_{exa} and n_e. The program listing of ARGMTE along with a sample output is given in Appendix B.

4.1.6 Discussion of Results for Argon

The accuracy of the energy levels predicted using the quantum method is limited to the number of observed energy levels available for each species. Since a substantial number of levels were compiled for argon neutral, a fairly accurate value for the quantum defect was obtained. For argon ions, however, the number of observed levels decrease rapidly with higher degrees of ionization, resulting in less accurate values of energy levels. Fortunately, at the temperature range considered here ($5{,}000 < T_{exa} < 35{,}000$ K), the number density of second and higher ionic species are so low that even a crude approximation of their higher lying levels would be satisfactory. For this reason, hydrogenic levels could be used for most of the second, third, and fourth ion excited energy levels.

As indicated in Fig. 4.1, the values of partition functions reported in this work agree will with those of Drawin [62] and Olsen [67], although the values predicted by Drellishak et al [97] are noticeably higher for argon neutral and the first ion. The reason for this disagreement lies in the method of lowering used. Drellishak et al have used the following relation due to Margenau and Lewis [88], which, unlike the method used in this work, depends strongly on the principal quantum number,

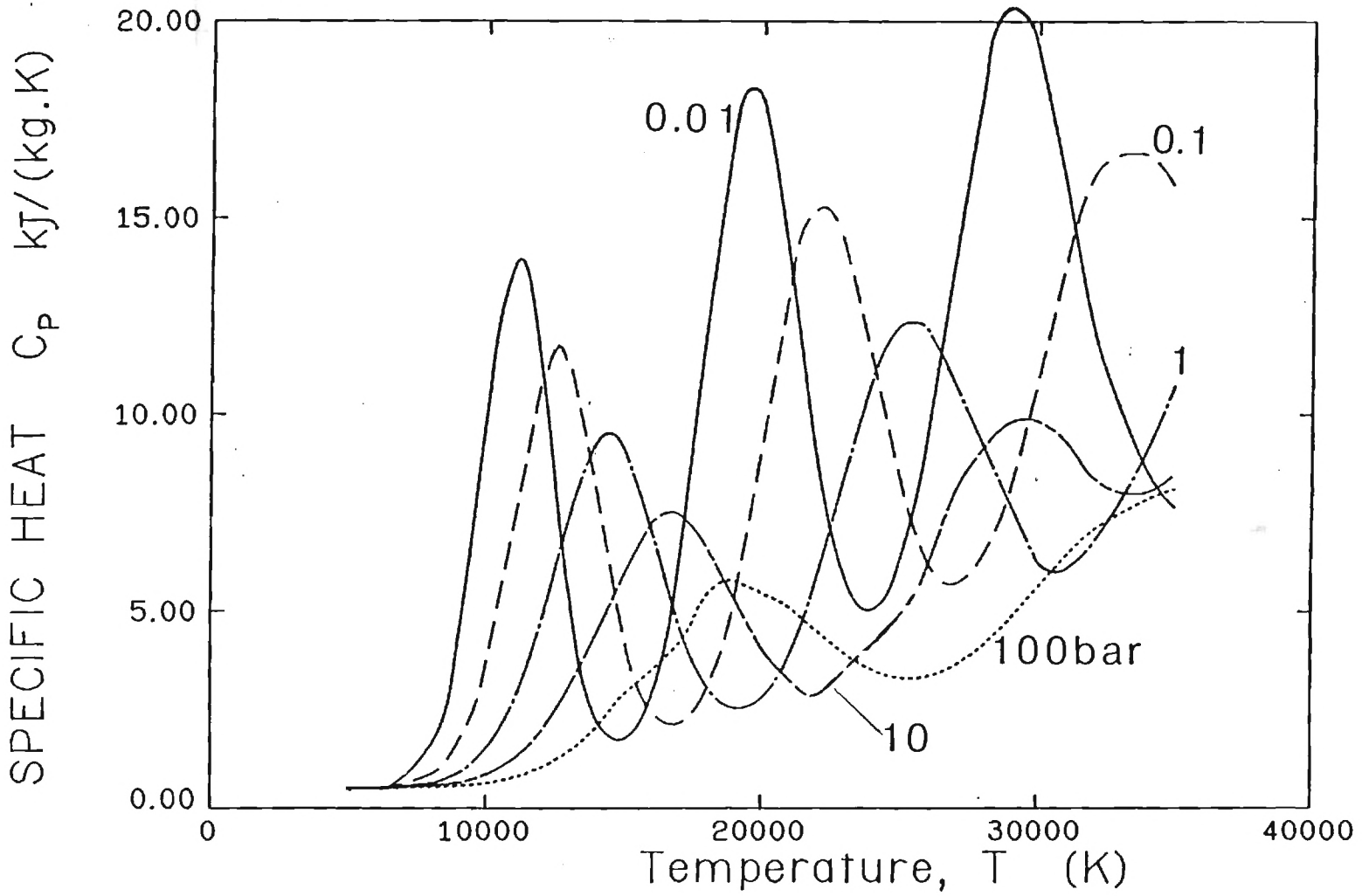

Figure 4.10: Specific heat of argon at LTE for various pressures

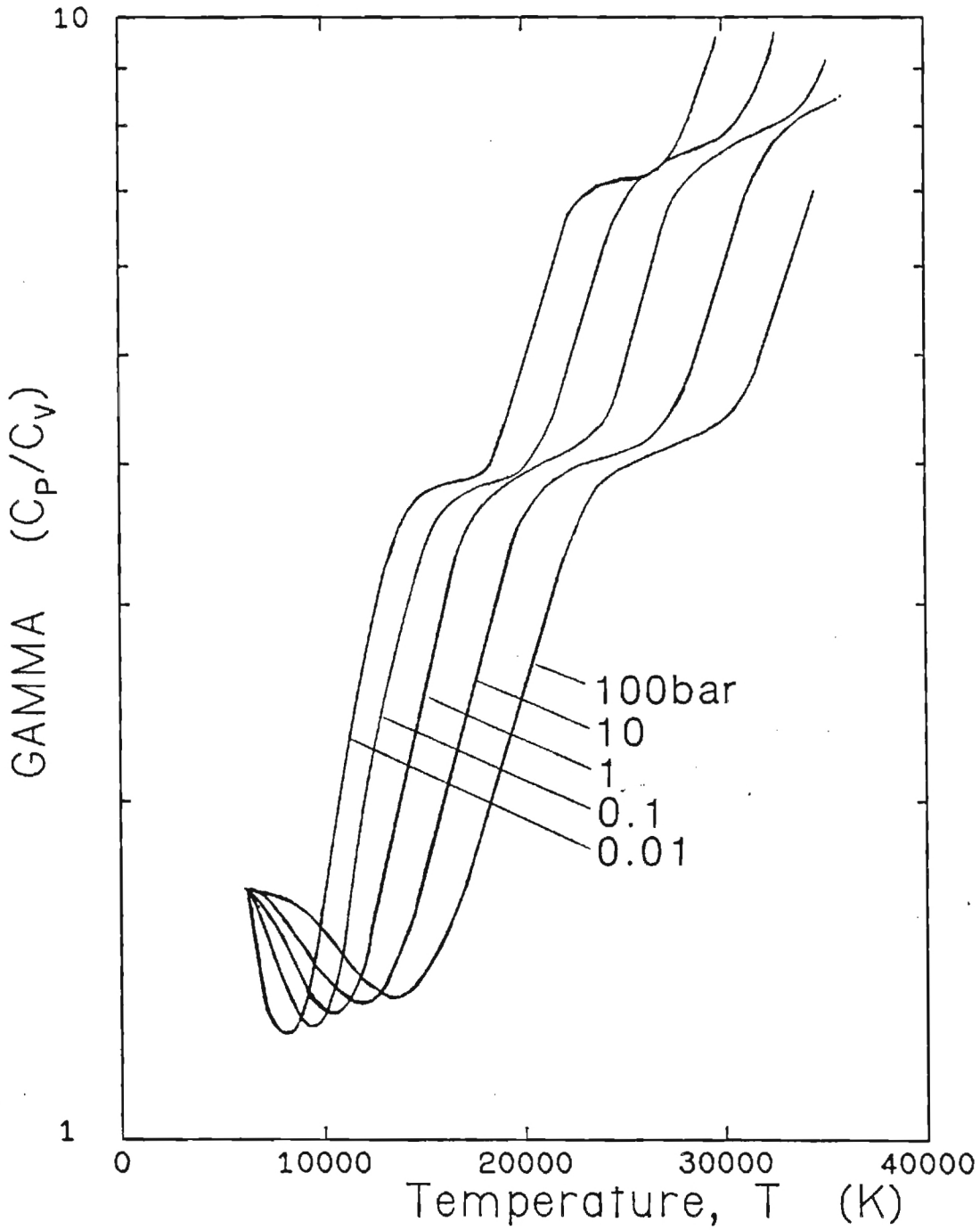

Figure 4.11: Ratio of specific heats of argon at LTE for various presuures

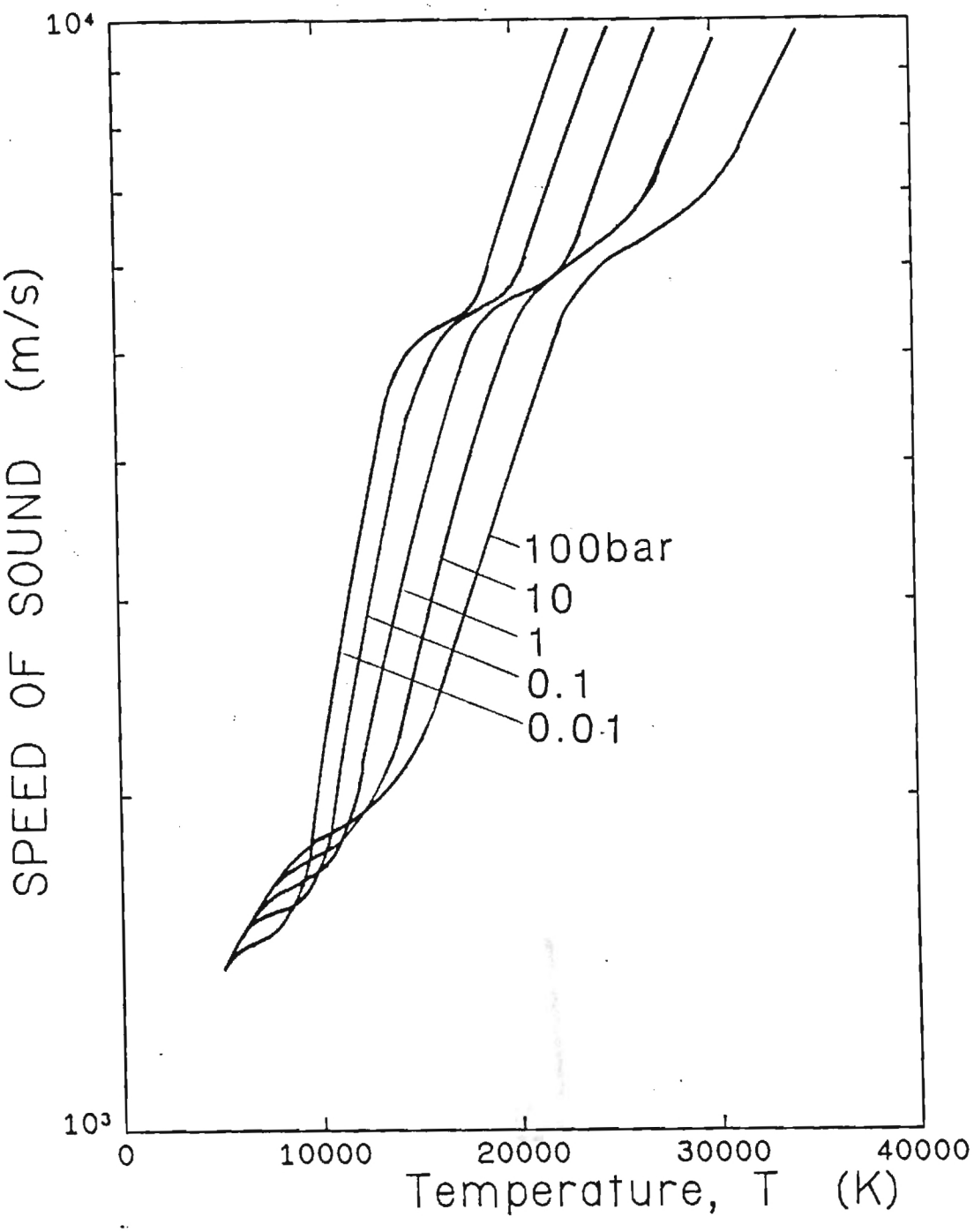

Figure 4.12: Speed of sound in argon at LTE for various pressures

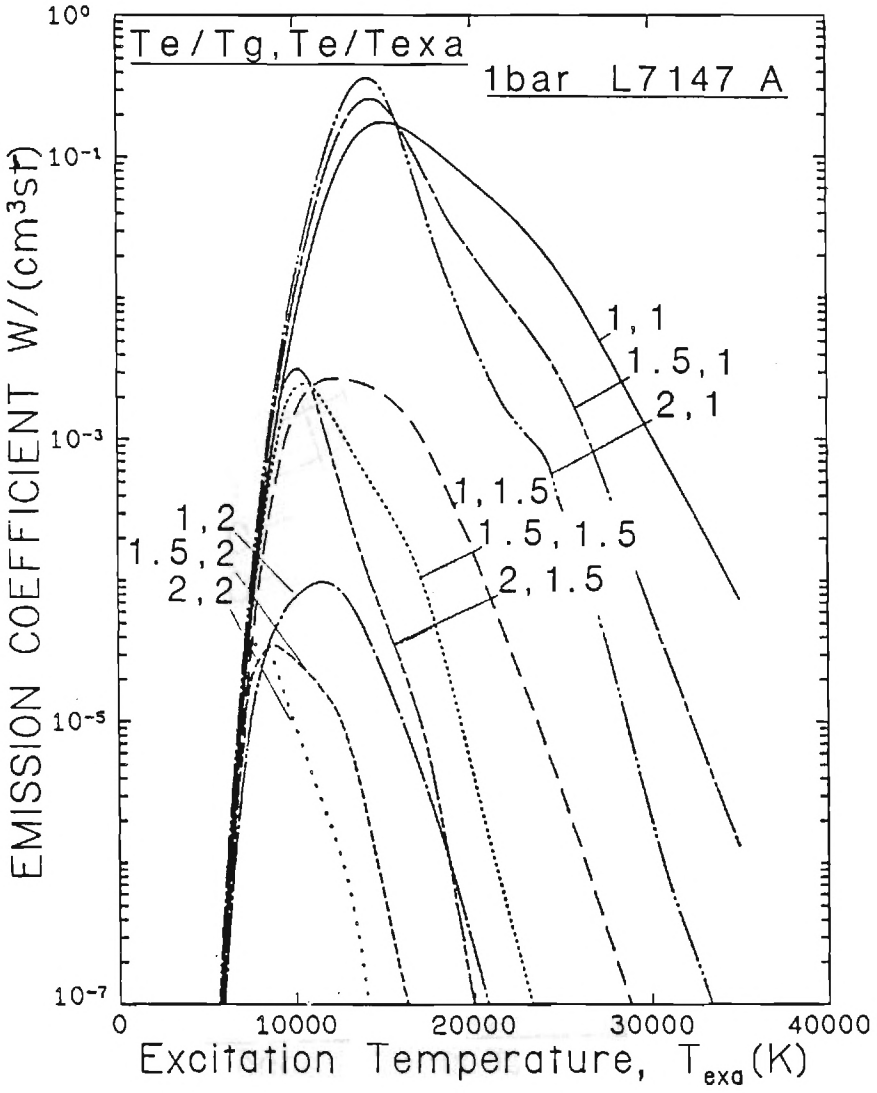

Figure 4.13: Emission coefficient of ArI 7147 as a function of excitation temperature for various kinetic and excitation nonequilibrium conditions, p=1 bar,$T_e/T_{exa} \geq 1$.

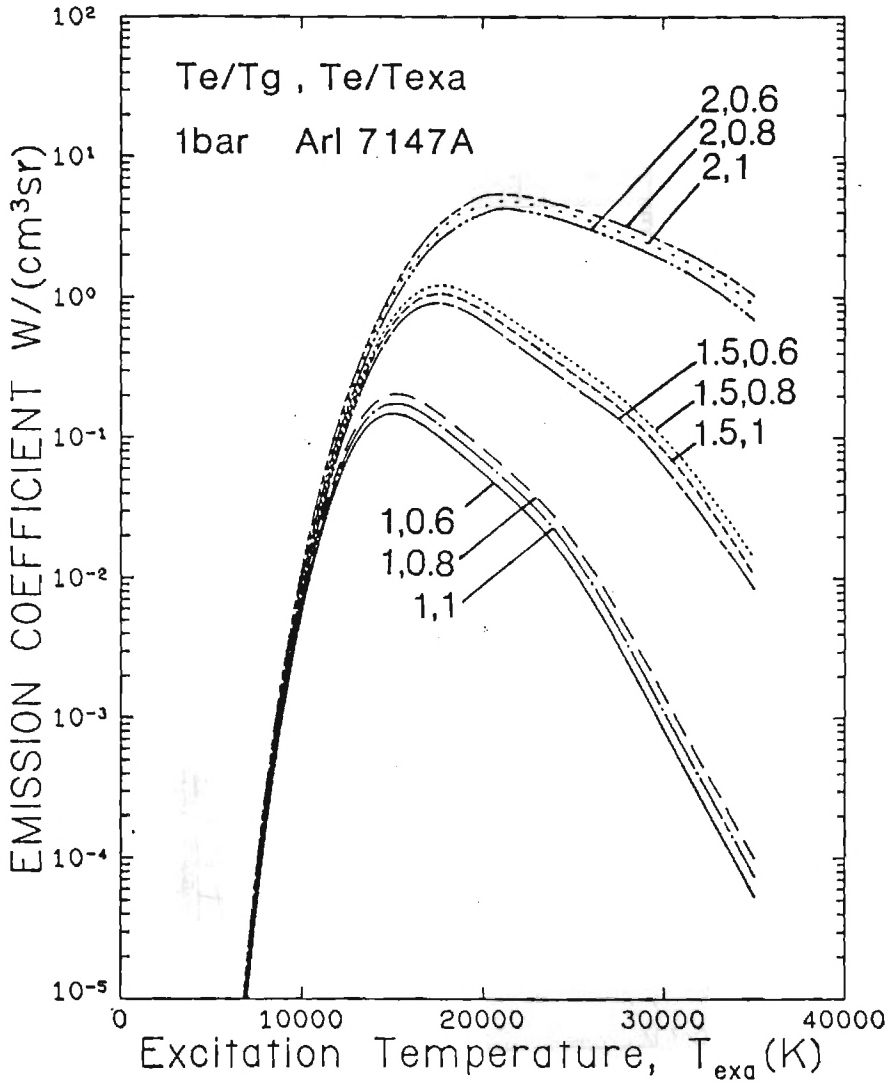

Figure 4.14: Emission coefficient of ArI 7147 as a function of excitation temperature for various kinetic and excitation nonequilibrium conditions, p=1 bar, $T_e/T_{exa} \leq 1$.

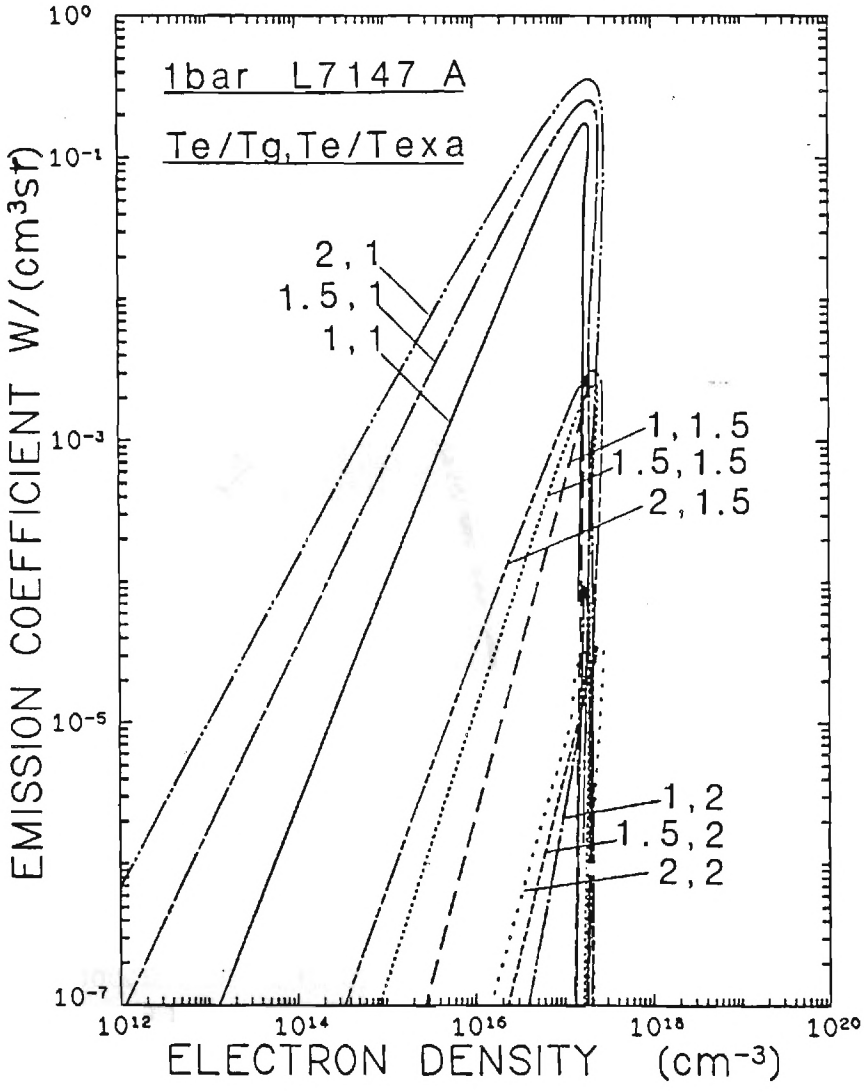

Figure 4.15: Emission coefficient of ArI 7147 as a function of electron density for various kinetic and excitation nonequilibrium conditions, p=1 bar

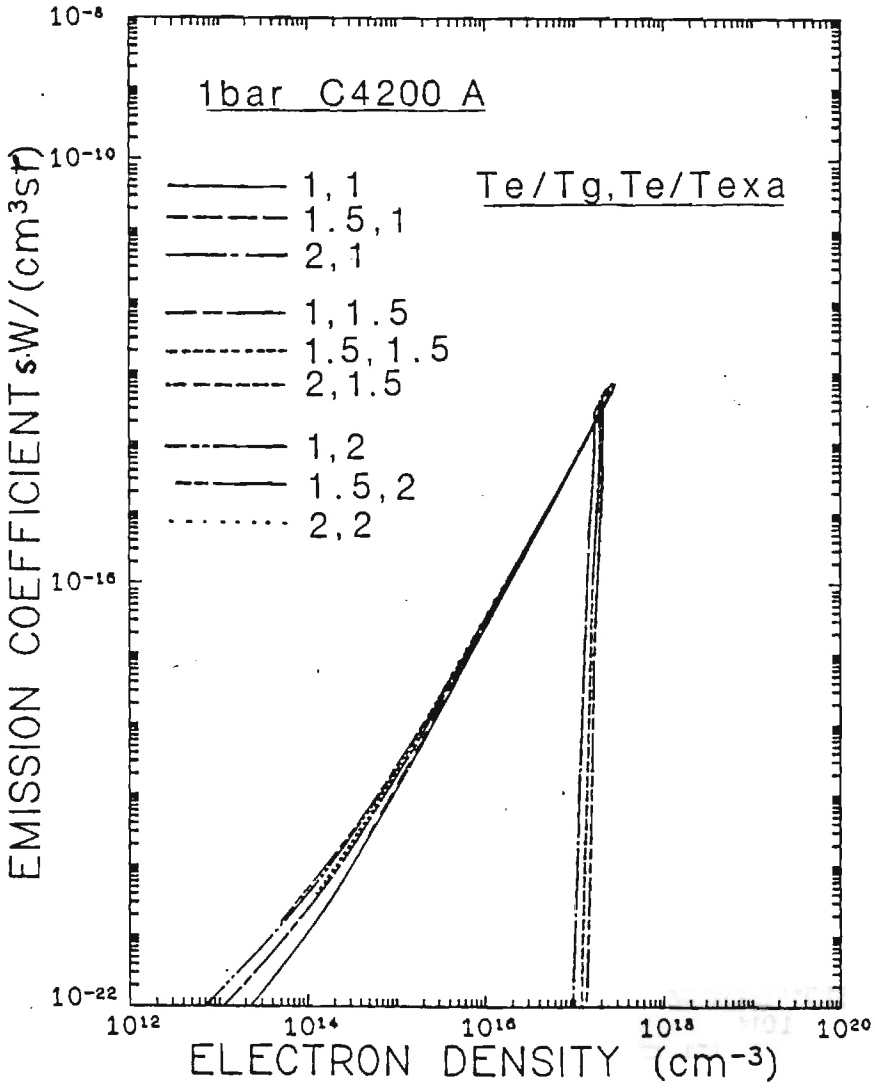

Figure 4.16: Emission coefficient of ArC 4200 as a function of electron density for various kinetic and excitation nonequilibrium conditions, p=1 bar

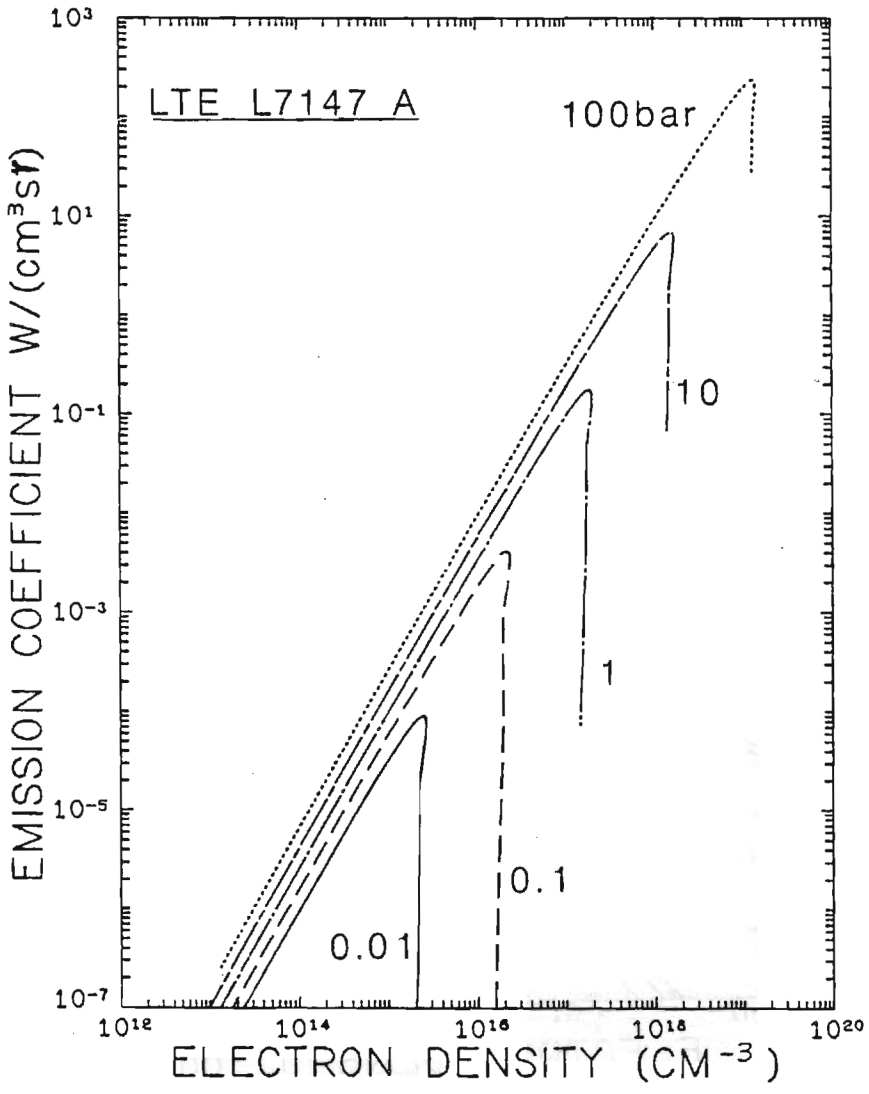

Figure 4.17: Emission coefficient of ArI 7147 at LTE as a function of electron density for various pressures

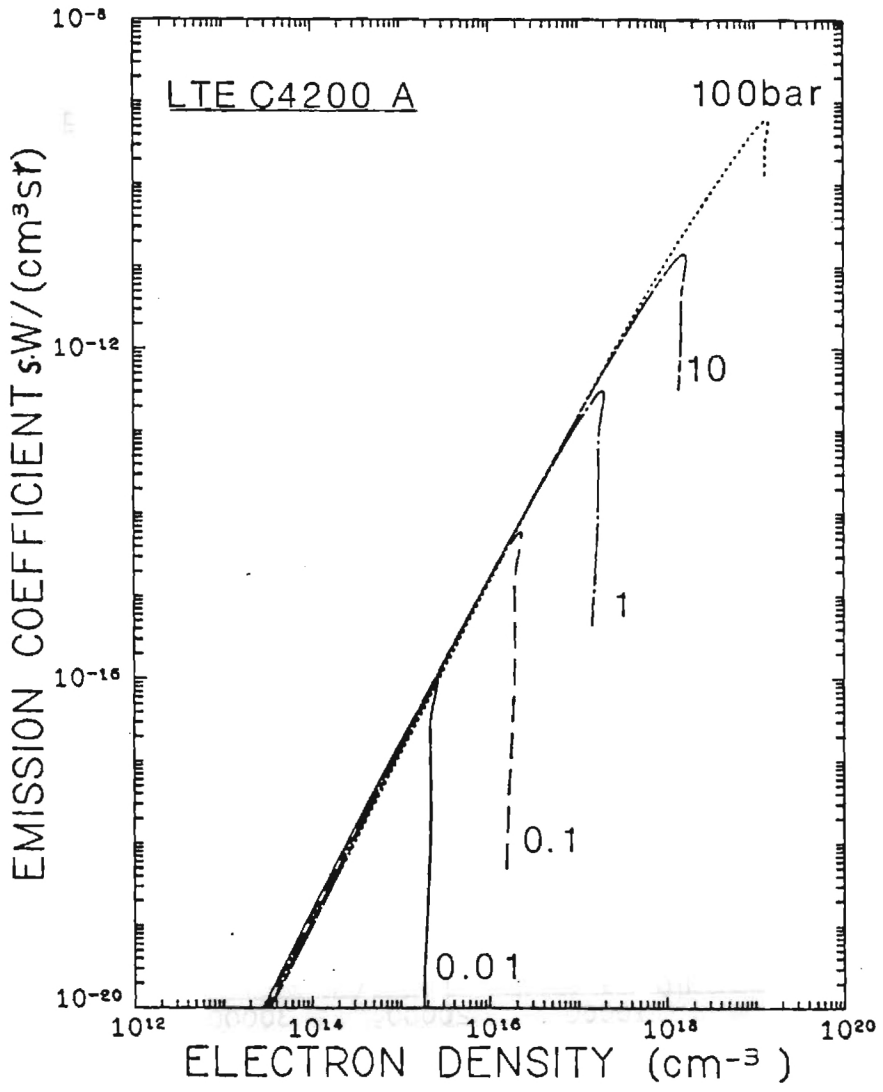

Figure 4.18: Emission coefficient of ArC 4200 at LTE as a function of electron density for various pressures

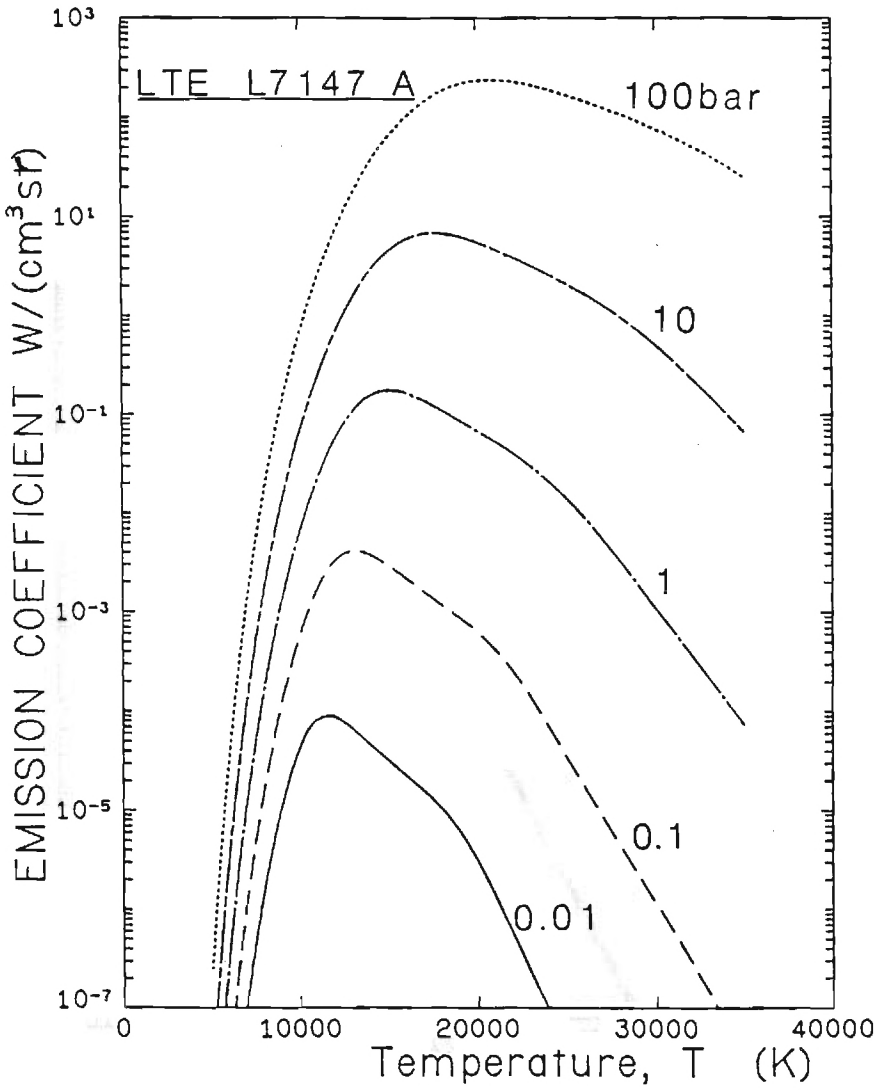

Figure 4.19: Emission coefficient of ArI 7147 at LTE as a function of excitation temperature for various pressures

$$n = 36.11 \times 10^3 \left[\frac{z_{eff}^2 T}{\sum_i n_i Z_i^2} \right]^{1/4}$$

This principal quantum number is then used in predicting the lowering of ionization level, assuming hydrogenic levels. The assumption of hydrogenic levels could result in considerable error in partition function for the atom due to the relatively large values of quantum defect for the first few term series.

An important application of GMTE method is the spectroscopic diagnostics of arcs and discharges where the line emission coefficients are the basis for temperature and density determinations. If kinetic or excitation nonequilibrium is present, then the normal temperatures will be quite different from an LTE equivalent depending on the extent of nonequilibrium and the spectral line considered. A noteworthy point is that, presence of kinetic nonequilibrium ($T_e > T_g$) results in values of line emission coefficients larger than the LTE value below the normal temperature (maximum emission coefficient) and lower than the LTE value above the normal temperature. See Fig. 4.13 and 4.14. Excitation nonequilibrium ($T_e \neq T_{exa}$) could result in a magnified shift from the LTE value. This shows that for equal temperature differences the effect of excitation nonequilibrium is stronger on the emission coefficient values. This would also mean that a right combination of kinetic and excitation nonequilibrium could resemble an LTE condition, leading the investigator to believe that LTE prevails in his system, while in reality, a severe case of nonequilibrium may exist.

Finally a comment is due concerning the specific heat calculations which consumed most of the investigation and computer time. The same discontinuity in partition function calculations as observed by Drellishak et al [97], was noticed in this work which led to various smoothing techniques applied to the generating function of c_p. Since C_p depends on second derivative of Gibbs free energy, the smoothness of Gibbs free energy was very essential. This problem was amplified at severe nonequilibrium situations such as $T_e/T_a = 3$ and $T_e/T_{exa} = 3$. Several smoothing functions including polynomials of different degrees were applied to partition functions and Gibbs free energy. This technique helped desensitize c_p to the roughness of generating function curves.

The ratio of specific heats, γ, and the speed of sound, c_s, are presented only in the LTE form in this work. Further extension of these relations to nonequilibrium conditions is rather complicated and involves resolving issues which are beyond the scope of this project. Further details and derivations are presented elsewhere [110].

4.2 Hydrogen

4.2.1 Partition Functions for Hydrogen and Hydrogen Levels

In statistical thermodynamics, the partition functions of a species are calculated with tabulated or calculated energy levels and degeneracies as explained in Section 4.1.2. In some calculations, it is necessary to use hydrogenic approximation for non-tabulated energy levels, especially at high energies. Partition functions are calculated m the following way [24].

$$Z(T) = \sum_{n=1}^{n'} g_n \exp(E_n/kT) + (2S_1+1)(2L_1+1) \sum_{n=n'+1}^{Nmax} 2n^2 \exp\left[-(E_\infty - E_H/n^2)/kT\right], \quad (4.11)$$

where $n < (z^2 E_H/\Delta E_\infty)^{1/2} \leq n_{max}$; z=1 for neutral atoms, z=2 for singly charged atoms, etc; S_1 and L_1 are spin and orbital momentum of the ground state of the next higher ionization stage; and ΔE_∞ is lowering of ionization energy. The first summation is done with tabulated values of g_n and E_n. The second summation uses hydrogenic approximation for high energy levels. Griem [24] estimates the integrated formula for the hydrogenic approximation with:

$$Z(T) = \sum_{n=1}^{n'} g_n \exp(-E_n/kT) + (2/3)\,(2S_1+1)\,(2L_1+1) A^3 \exp\left[-(E_\infty - \Delta E_\infty)/kT\right] \quad (4.12)$$

where $A=(z^2 E_H/\Delta E_\infty)^{1/2}$. In this derivation, the approximation that $E_\infty - z^2 E_H/n^2 = E_\infty - \Delta E_\infty$ is used. Griem indicated that errors in various computational simplifications and cutoff exceed errors from using (4.12) and that the choice of n' is not critical. This is true at subatmospheric pressures and low (below the normal temperature) temperatures in argon. The present study

shown that the approximation in (4.12) can give serious errors, especially at high pressures for high temperature thermodynamic properties, if it is used with improper n' selection.

For the purpose of checking the error from this approximation, partition functions for hydrogen plasma are calculated by two methods:

a) summation up to the lowered ionization energy level. (Equation (4.11)). The fractional effect between n and A is considered by linear proration of the next energy level contribution [101].

b) summation up to a certain energy level + approximation formula up to the lowered ionization energy level. (Equation (4.12)).

The results are given in Table 4.2. The error from using the approximation of equation (4.12) are significant when n_{max} is quite a bit larger than n'.

It is recommended that Equation (4.11) be used to get the partition functions. The summation in Equation (4.11) is calculated by a prorating scheme [101] in which the fractional contribution between n_{max} and A is considered to avoid stepwise change of the partition function values.

Two lowering methods are used. For hydrogen plasma, the Debye lowering is:

$$\Delta E_\infty = \frac{e_o^2}{\rho_D} \qquad \text{where} \quad \rho_D = \sqrt{\frac{kT}{8\pi e_o^2 n_e}} \tag{4.13}$$

and the Bethe lowering is:

$$\Delta E_\infty = \frac{a_o}{\rho_B} \text{ Ry} \qquad \text{where } \rho_B = \left[\frac{3}{4\pi(n_i+n_a)}\right]^{1/3} \tag{4.14}$$

Table 4.2. Comparison of partition functions.
(z_Σ and $z_\int$ are calculated by equation (1) and (2) respectively.)

				n' = 10		n' = 50	
p(atm)	T(K)	A	z_Σ	$z_\int$	$(z_\Sigma-z_\int)/z_\Sigma$	$z_\int$	$(z_\Sigma-z_\int)/z_\Sigma$
	10000.	35.4	2.0045E+00	2.0045E+00	3.2976E-05	2.0045E+00	1.7111E-05
.01	20000.	38.5	1.7085E+01	1.6984E+01	5.9263E-03	1.7054E+01	1.8221E-03
	30000.	47.3	3.8276E+02	3.9137E+02	3.6093E-03	3.8252E+02	6.2316E-04
	10000.	25.4	2.0018E+00	2.0018E+00	1.8184E-05	2.0017E+00	7.0537E-05
.1	20000.	21.5	4.7909E+00	4.7566E+00	7.1556E-03	4.4658E+00	6.7651E-02
	30000.	26.4	7.0820E+01	7.0282E+01	7.6029E-03	6.9211E+01	2.2725E-02
	10000.	18.7	2.0008E+00	2.0008E+00	8.9464E-06	2.0004E+00	1.8138E-04
1.	20000.	12.0	2.5686E+00	2.5630E+00	2.1746E-03	1.1110E+00	5.6731E-01
	30000.	14.6	1.4859E+01	1.4729E+01	1.0454E-02	6.5847E+00	5.5687E-01

The larger values of ΔE_∞ are used.Figure 4.20 gives the excitation partition functions for a 1-bar hydrogen plasma.

4.2.2 Chemical Equilibrium and Densities

For hydrogen plasma, ($H = H^+ + e$), the equations to calculate densities are the following.

Chemical equilibrium from Equation 4.7 with temperatures T_e, T_g, T_{exa} ($=T_{exi}$) and $Z_{exi}=2$

$$n_e \left[\frac{n_i}{N_a} \right]^{T_g/T_e} = 2 \left[\frac{Z_{exi}}{Z_{exa}} \right]^{T_{exa}/T_e} \left[\frac{2\pi m_e k T_e}{h^2} \right]^{3/2} \exp\left[- \frac{E_\infty - \Delta E_\infty}{k T_e} \right] \qquad (4.15)$$

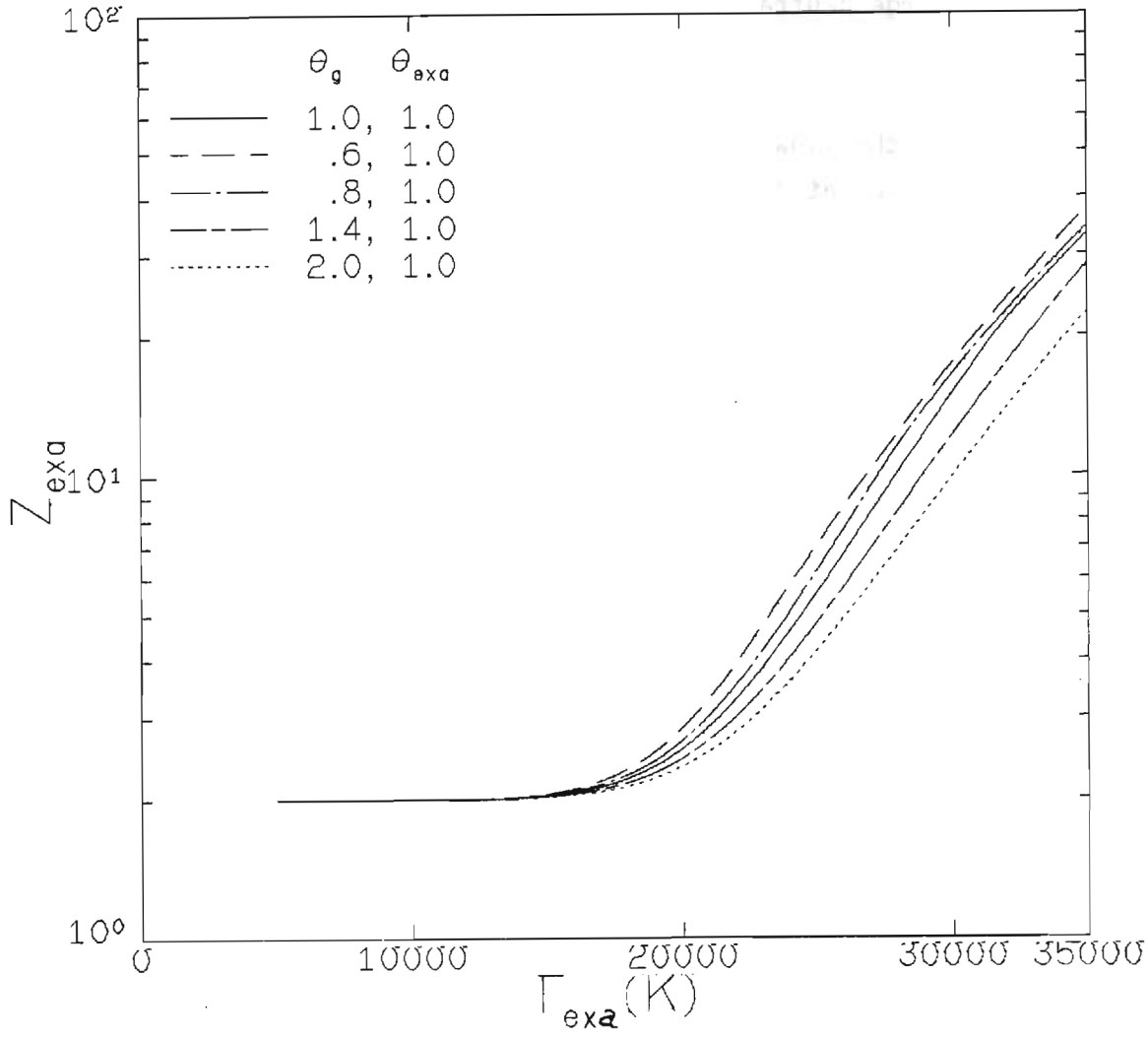

Fig. 4.20: Excitation Partition Function for 1-Bar Hydrogen Plasma

Equation of state with Debye-Hueckel approximation:

$$p = (1 - \Delta P_c)\ (n_e kT_e + (n_i+n_a)kT_g) \tag{4.16}$$

where $\Delta p_c = \left[24\pi\rho_D^3\ (n_a + n_i + n_e)\right] -1$,

and From Charge neutrality:

$$n_e = n_i \ . \tag{4.17}$$

With ΔE_∞ the (lowering of ionization energy) from Section 4.2.1, n_e, n_i, and n_a are calculated for given P, T_e, T_e/T_{exa} and T_e/T_g.

The GMTE state diagram is shown in Figure (4.21). Compared to MTE state diagram (Figure 4.22), the excitation temperature effect on composition is small for θ_g=1, θ_{exa} = 0.8 to 2.0 and the constant pressure lines for these conditions are on the top of LTE line (θ_g=1, θ_{exa}=1).

4.2.3 Thermodynamic Properties

For hydrogen, the thermodynamic properties are given by the following equations. For unit volume,

$$a = \sum_j a_j$$

$$n_a k \left[T_g\left(\ln Z_{ta}+1.0\right)+ T_{exa}\ln Z_{exa} +1.0\right]$$

$$+ n_{ik} \left(T_g\left(\ln Z_{ti}+1.0\right)+T_{exa}E_{ia}\right) + N_e kT_e\left(\ln Z_{te}+1.0\right) \tag{4.18}$$

$$g = \sum_j G_j = a + p/\rho \tag{4.19}$$

$$s = \sum_j \sum_k s_{k,j}$$

$$s = n_a k \left(\ln Z_{ta} + \ln Z_{exa} + 2.5\right) + n_i k \left(\ln Z_{ti} + 2.5\right)$$

$$+ n_e k \left(\ln Z_{te}+ 2.5\right) +\left(\partial_{gexa}/\partial T_{exa}\right)_p \tag{4.20}$$

$$h = \sum_j \sum_k h_{k,j} = g + \sum_j \sum_k T_{k,j}s_{k,j} \tag{4.21}$$

$$u = h - p/\rho \tag{4.22}$$

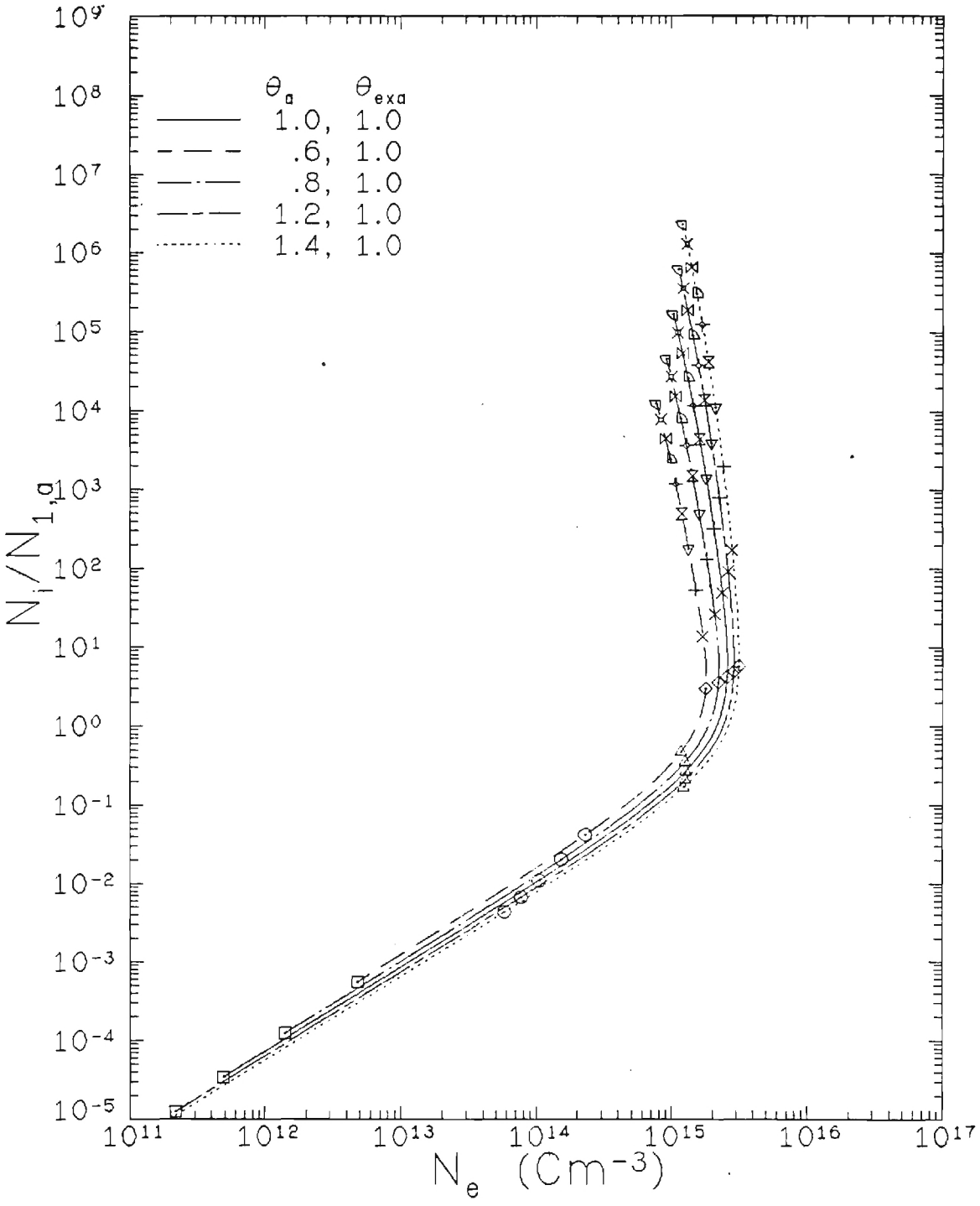

Fig. 4.21: GMTE State Diagram

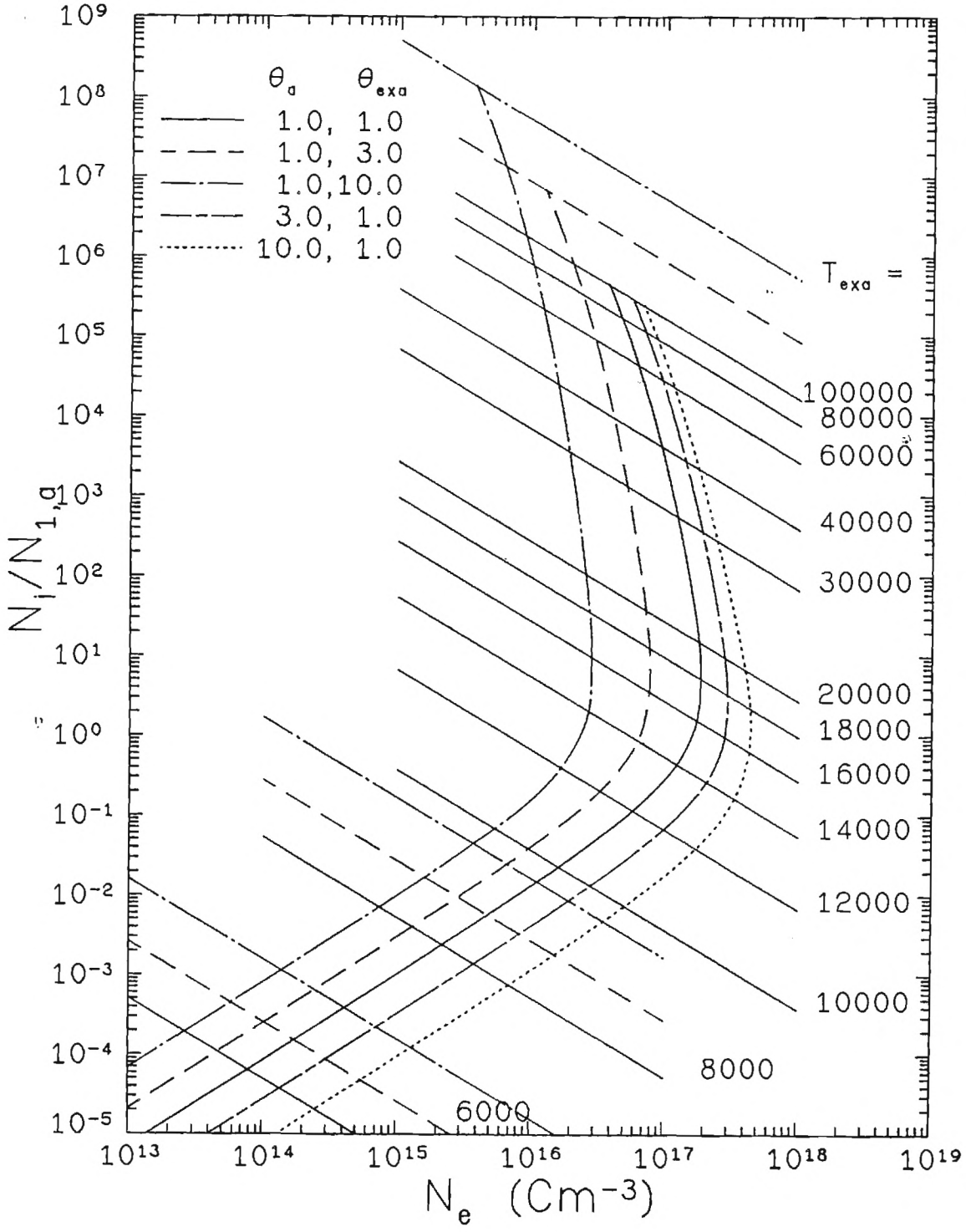

Fig. 4.22: MTE state diagram

In Table 4.3, the thermodynamic properties of 1-bar hydrogen plasma are given for θ_g=1 and θ_{exa}=1. The LTE results are within 1% of the results of Patch [101].

4.2.4 Line Emission Coefficients

The line emission coefficient of hydrogen atom for transition from m to n is given by:

$$i_L = \frac{hc}{4\pi\lambda} A_{mn} N_{m,a} \tag{4.23}$$

where $\begin{cases} N_{m,a} = \dfrac{N_a}{Z_{exa}} g_m \exp\left[\dfrac{-E_m}{kT_{exa}}\right] \\ A_{mn} : \text{transition probability} \end{cases}$

Figs. 4.23a & b show the line emission coefficients of Hα for a 1 bar hydrogen plasma. The Figure shown that at low temperature ($T_{exa} < T_{norm}$), the temperature determined by LTE diagnostics is not equal to T_e but is approximately equal to T_{exa}. This suggests the usual assumption of T_e=T_{exa} in diagnostics should be confirmed before using T_{LTE} from i_L as the election temperature.

4.2.5 Continuum Emission Coefficient

The continuum emission coefficients for hydrogen are reduced from the equations in Section 6.2:

$$\epsilon_\nu = \left[5.44\times10^{-46} \frac{Ws}{cm^3 st}\right] n_e n_i T_e^{-1/2} (\xi_A + \xi_B) \tag{4.24}$$

where $$\xi^{fb} = \frac{\beta_c}{Z_{exi}} \frac{E_H}{kT_e} \varsigma(\nu, T_{ex\beta}) \exp\left[-\frac{h\nu}{kT_e} - \frac{\Delta E_\infty}{kT_{ex\beta}}\right]$$

$$\varsigma(\nu, T_{exa}) = \sum_{ml} \frac{g_{ml}\,\sigma_{ml}}{m^5 \sigma_m} \exp\left[\frac{E_{I,a} - E_m}{kT_{ex\beta}}\right]$$

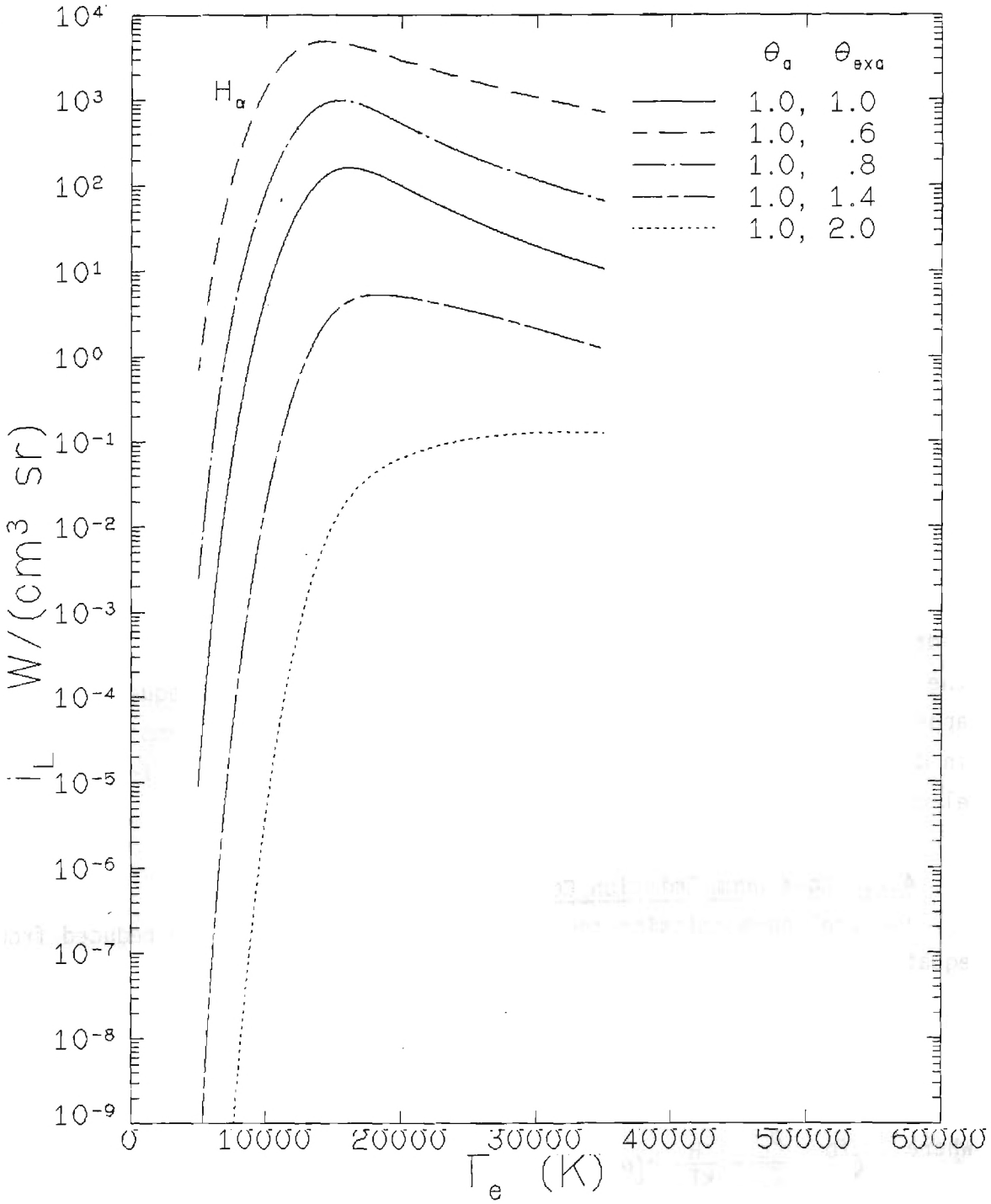

i_L vs T_e λ = 6562.80 A

Fig. 4.23a: Line Emission Coefficient

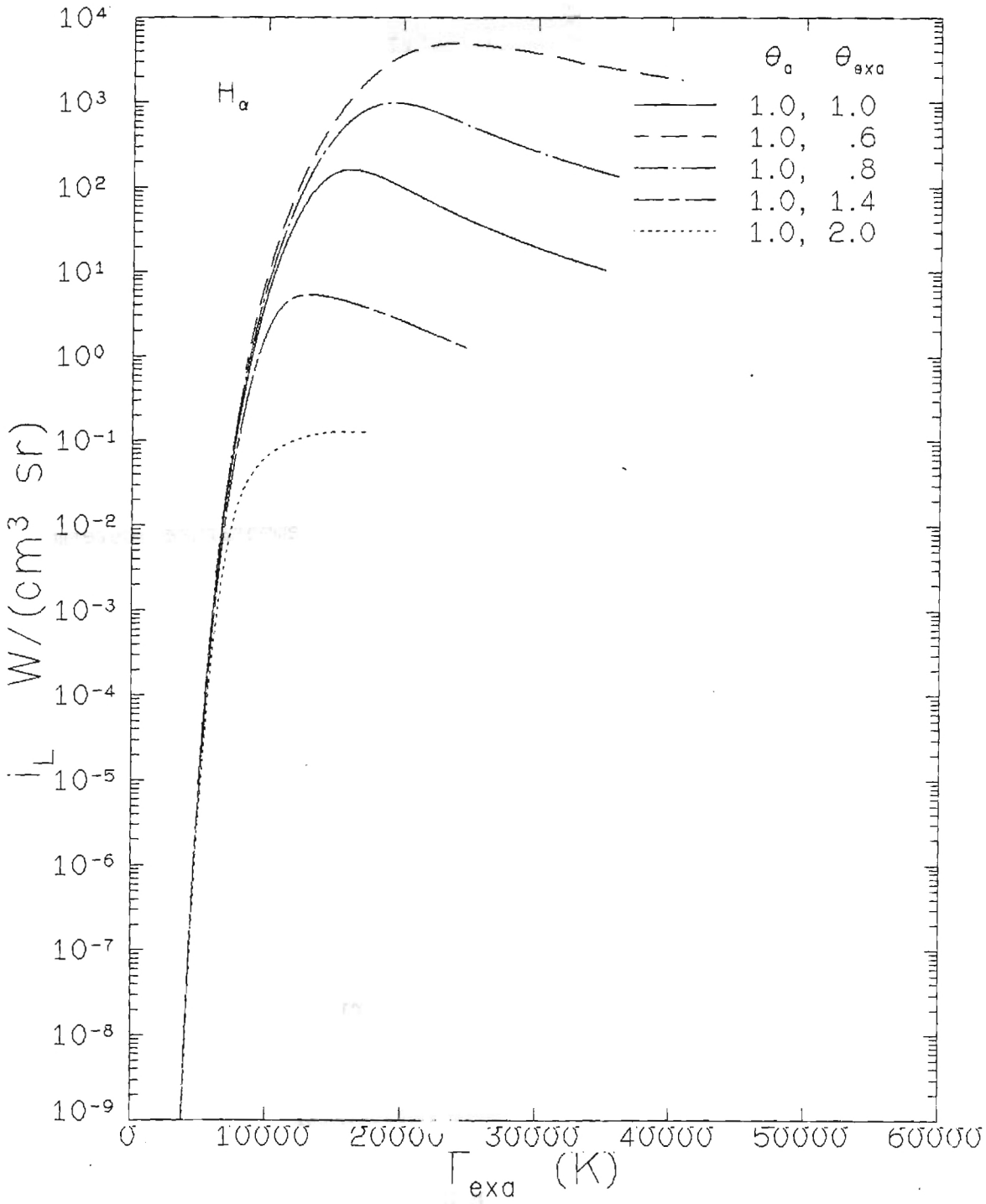

i_L vs T_{ex} λ = 6562.80 A

Fig. 4.23b: Line Emission Coefficient

$$+ \sum_m \frac{G_m}{m^3} \exp\left[\frac{E_H}{m^2 k T_{ex\beta}} \right]$$

$$\xi^{ff} = \bar{G}_f \exp\left(\frac{\Delta E_s - h\nu}{kT_e} - \frac{\Delta E_\infty}{kT_{ex\beta}} \right)$$

$$\beta_c = \left(\frac{Z_{exa}}{Z_{exi}} \right) \frac{T_{exa}}{T_g} - 1 \left[\frac{n_e}{2 \left(2\pi m_e kT_e / h^2 \right)^{3/2}} \right]^{\theta_g - 1}$$

$$\cdot \exp\left[\frac{E_{I,a}}{kT_{exa}} \left(\frac{T_{exa}}{T_g} - 1 \right) \right] .$$

In Figure 4.24, continuum emission coefficients of a 1 bar hydrogen plasma are given for λ=3780Å. For θ_g=1 (Figure 4.24) the temperatures determined by LTE diagnostics are approximately equal to the electron temperature for θ_{exa} = 0.8 to 2.0.

5.0 EXPERIMENTS

5.1.1 Equipment

The study of plasmas which deviate from local thermal equilibrium (LTE) requires rapid and accurate measurements of the plasma radiation. The existing arc facility in the High Pressure Plasma Laboratory has been automated and computerized to yield intensity measurements with a relatively high speed, precision, and accuracy. The hardware is also modified to operate at pressures as low as 10 torr. The original facility is described in detail by Bauder and Stephens [102], prior to its installation at Georgia Tech.

The plasma generator is a wall stabilized Maecker type [103]. The present channel consists of 16 individually cooled, high conductivity, oxygen free copper plates with engraved cooling channels. The arc apparatus is enclosed in a cylindrical steel chamber, for pressures up to 200 atmospheres. The cathode is a 1/4 in, 2% thoriated tungsten rod with a 90° included angle. The test gas is injected tangentially to the cathode

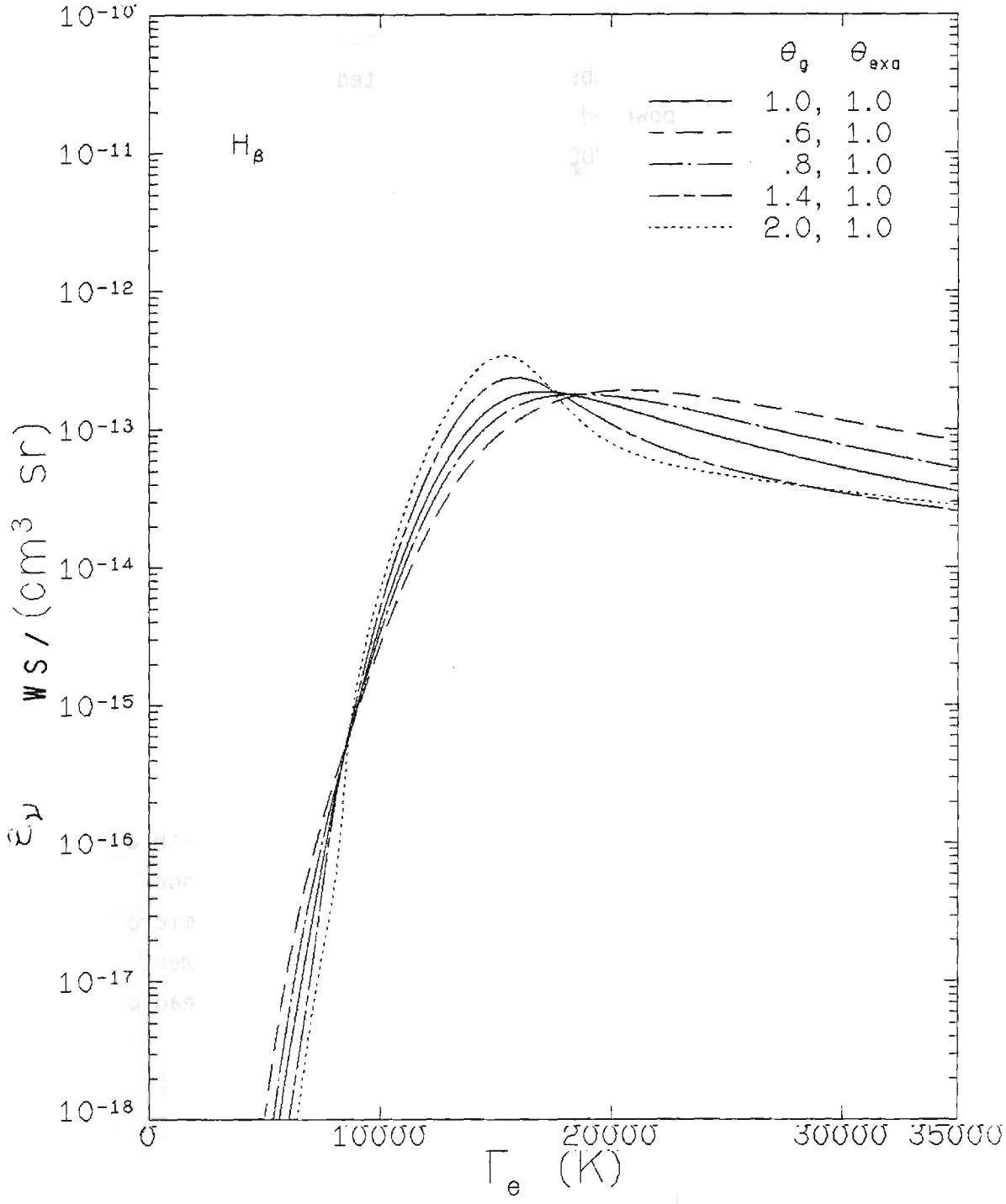

ε_ν vs T_{ex} λ = 3780.00 A

Fig. 4.24: Continuum Emission Coefficient

housing to create a vortex and minimize instabilities. Argon protects the electrodes when reactive substances are tested.

The facility is powered by a series of four A.O. Smith (A2500-10SP) rectifiers, rated at 1000 VDC open circuit and 250A at 100% duty cycle. The electrical circuit includes ballast resistors and a Π filter for the reduction of the current ripple to about 1%.

5.1 Instrumentation

The arc chamber pressure is sensed by Celesco P2G750 and P2G5000 pressure transducers (750 and 5000 psi max) and read via a Celesco CD25A readout unit. The chamber pressure is also read by a Wallace-Tiernan FA 233 absolute pressure gauge for subatmospheric pressures. Chamber pressures below 20 torr are read by a thermocouple gauge to within 0.2 torr.

The copper cascade plates also serve as electric potential probes. The voltage induced in each of the plates is routed to an HP3455A digital voltmeter (DVM) via a series of Preston wide-band floating differential amplifiers in rejection mode. The slope of the potential voltage versus distance from cathode gives the electrical field strength, which varies between 10 and 20 V/cm depending on the operating conditions.

Plasma lateral intensity measurements are made by translating the chamber with a Slo-Syn stepper motor (200 steps/rev), with a resolution of less than 1μm/step and controlled by a Slo-Syn preset indexer. The start-stop and direction signals are sent from a HP9825 microcomputer via a HP98032A 16-bit parallel interface. The chamber movement is sensed by a Bourns precision linear potentiometer and the output is read by the DVM.

As shown in Fig. 5.1, the radiation leaving the chamber is reflected by a front surface mirror (M_1), passes through a diaphragm (D), and is focused on the entrance slit of the monochrometer by a 2-inch magnesium floride coated lens (L). The diaphragm is set so that the depth of field of the optics includes the entire 3mm diameter bore. A typical radiation solid angle is shown in Fig. 5.2. The monochrometer is a 1-m McPherson 2051, Czerny-Turner type, with an effective aperture of f/8.6. The grating has 1200 lines/mm and first order Littrow blaze at 5000 which makes it suitable for visible and near infrared measurements. The inverse dispersion varies from 7.8 Å/mm near the UV to about 6.8 in the IR region (Fig. 5.3). The McPherson 788 programmable automatic wavelength scanning unit (AWS) is

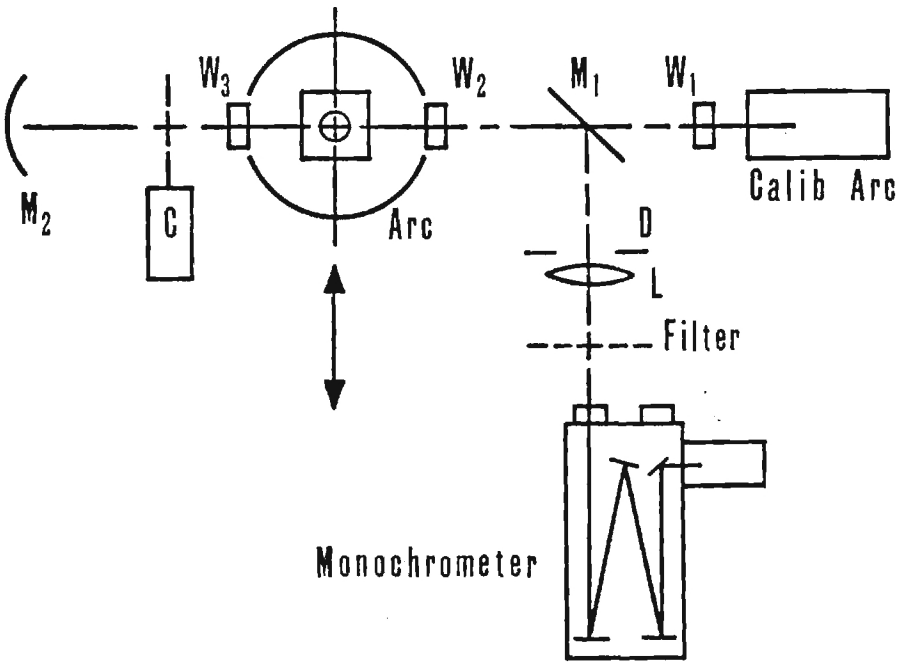

Figure 5.1: Schematic of the optical arrangement

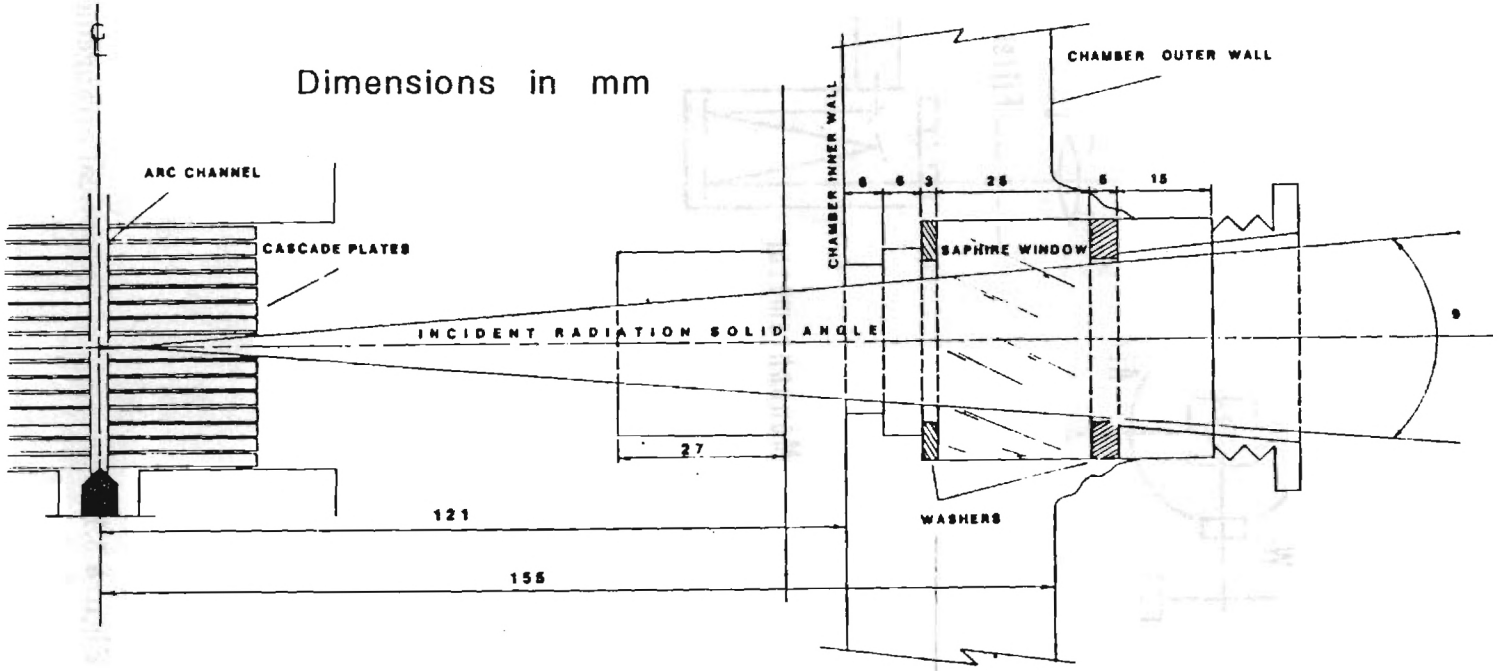

Figure 5.2: Detailed sketch of the arc pressure chamber window port indicating the maximum possible solid angle

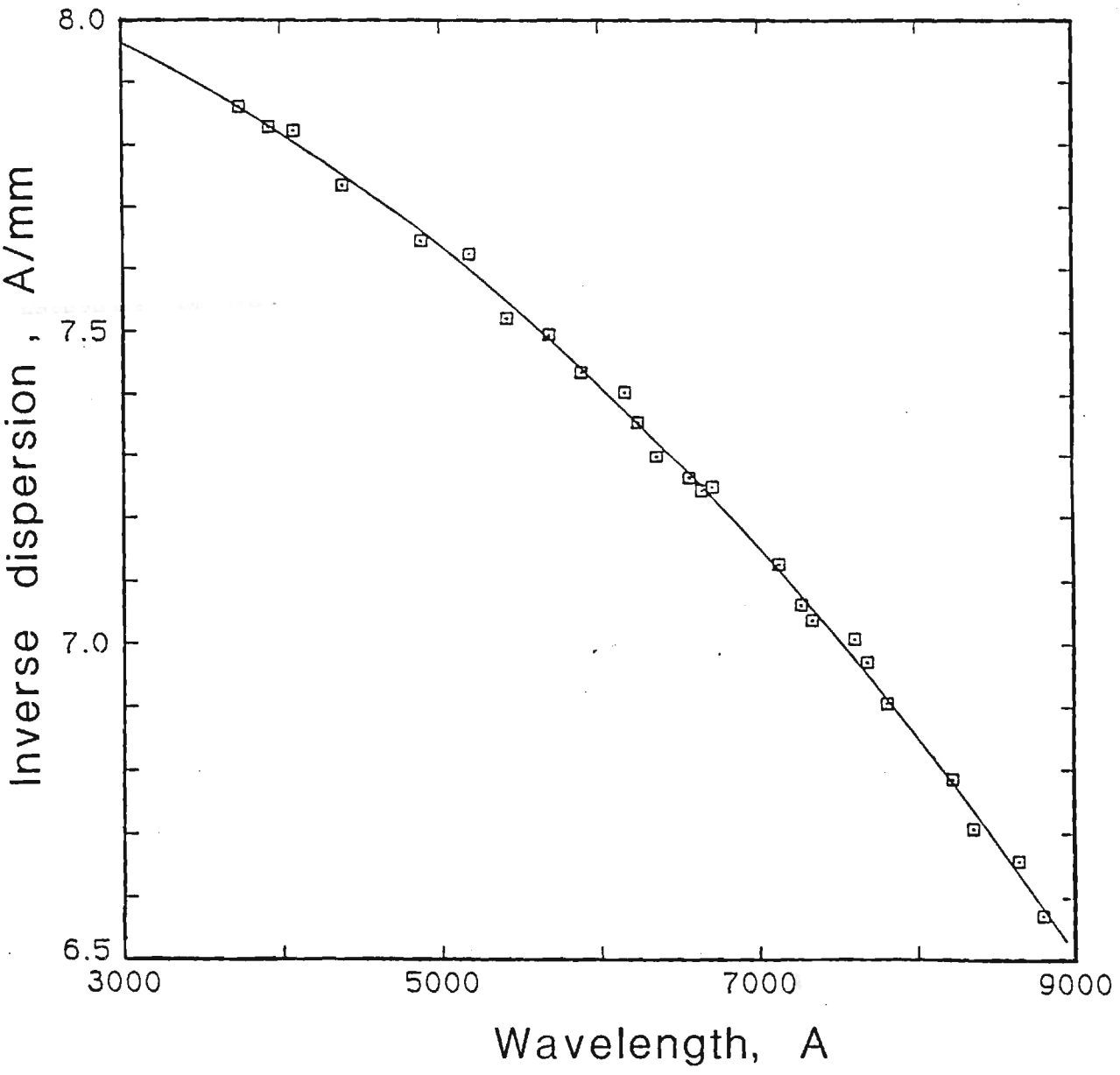

Figure 5.3: Inverse dispersion of the McPherson 2051 monochrometer in A/mm

also installed. Speed ranges of 0.05 Å/min to 5000 Å/min can be achieved. The AWS is controlled by the microcomputer through an HPIB (IEEE-488) interface and can be programmed for the desired location, scan speed, direction, acceleration, and deceleration rates.

The monochrometer has vertical slits variable from 5μm to 2mm. The refracted radiation is detected by a photomultiplier tube (EMI 9658B) which has an S-20 spectral response with enhanced red sensitivity. The signal from the PM tube is routed to a Kiethley 416 high speed picoammeter and then to a Mark 250 Gould strip chart recorder or to a HP3495A scanner, DVM, and the microcomputer.

5.2 Absorption Measurements

Spectral lines with partial absorption are corrected with the optical setup shown in Fig. 5.1. The radiation leaving the plasma is focused back onto the plasma by means of concave mirror (M_2). A chopper (C) is mounted to alternately interrupt the radiation to the concave mirror. Direct intensity measurements are effected by the transmission (T) and reflection (R) factors of each component. Hence,

$$I_D = \bar{T}_{arc}\bar{I}_{arc}(T_{spec}T_L R_{M_1} T_{W_2})$$

$$= \bar{T}_{arc}\bar{I}_{arc}(T_1)$$

where an overbar indicates the mean value over the arc cross section in the direction of optical alignment. Direct plus reflected intensity is then,

$$I_{D+R} = T_1\bar{T}_{arc}\bar{I}_{arc} + T_1 T_{arc}(T_{W_3})^2 R_M \bar{T}_{arc}\bar{I}_{arc}$$

$$= I_D(1+R_{M_2}(T_{W_3})^2\bar{T}_{arc})$$

$$= I_D(1+R_2\bar{T}_{arc})$$

$$= I_D(1+\tau)$$

where R_2 is the effective reflection efficiency for the additional absorption path, and τ is an overall transmission coefficient . τ is best obtained from experiments where absorption is insignificant or $\bar{T}_{arc} = 1$ (e.g. low current, low pressure, and continuum wavelengths). The mean value

for τ is calculated over the optical path. Once the value of τ is established, any value of I_{D+R}/I_D less than $1 + \tau$ is an indication of absorption and should be corrected using,

$$I_{D,corr} = I_D \left[\frac{1 + \tau}{I_{D+R}/I_D} \right]$$

The alignment of the concave absorption mirror is very critical The image across the arc must be symmetric and have the maximum possible intensity. This is accomplished by scanning the arc and adjusting the mirror to improve the trace (Fig. 5.4) on a computer monitor. This also acts as a fine adjustment on the general alignment.

The quality of the absorption correction method is indicated in Fig. 5.5. The data is for a 5 bar, 30 A, wall stabilized argon arc of 3mm diameter. The Boltzmann plot includes populations from ArI lines which are strongly (7948Å), partially (6965,6871Å), and slightly (4158, 4259, 7147, 7272Å) absorbed. This data is part of some preliminary experiments which were performed before the system was completely fine tuned. The Boltzmann plots for the final set of experiments (see Figs. 7.1 through 7.7) indicate the improvement in the optical system.

5.3 Refraction Effects

Refractive-ray bending in axially symmetric plasma sources has been the subject of a number of scientific investigations [104-106] due to its importance in correcting potentially serious systematic errors in spectroscopic measurements. A fairly recent study of refraction effects in high pressure argon arcs [107] has shown that these effects are significant only at pressures higher than 30 bars.

Refraction experiments performed on the 3mm wall stabilized argon arc at pressures between 1 and 30 bar and 15A indicate that refraction effects a 1 bar are not observable. As the pressure increases above 2 bar, the refractive effects become detectable and are a function of pressure and the region of the arc emitting the radiation. when a lens is used to focus the arc image onto the monochrometer slit, the lens also focuses the refracted rays to the extent that 6the refractive effects are not visually detectable, even at the higher pressures used in this study.

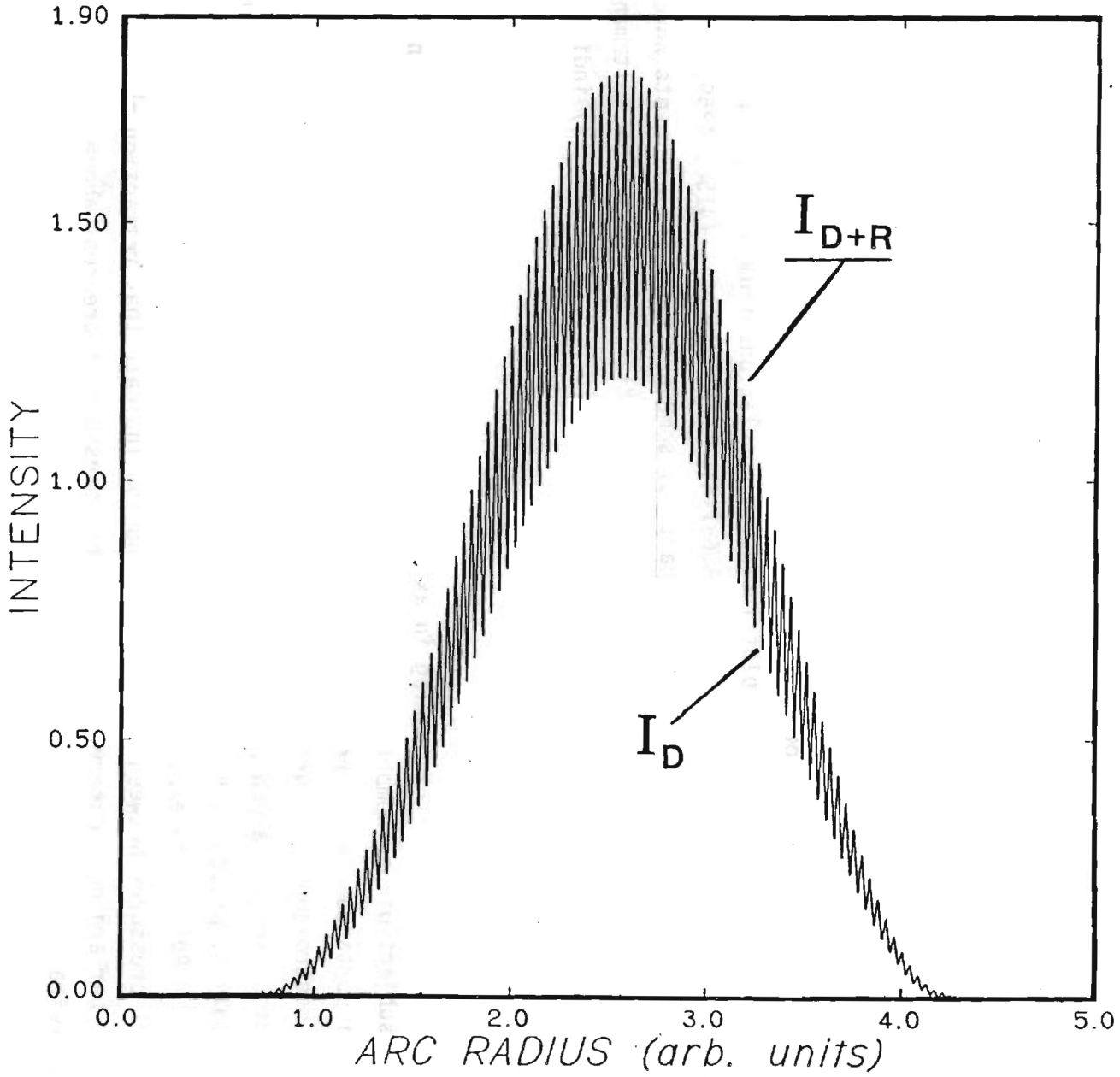

Figure 5.4: A typical lateral scan of the arc showing the alternating "direct" and

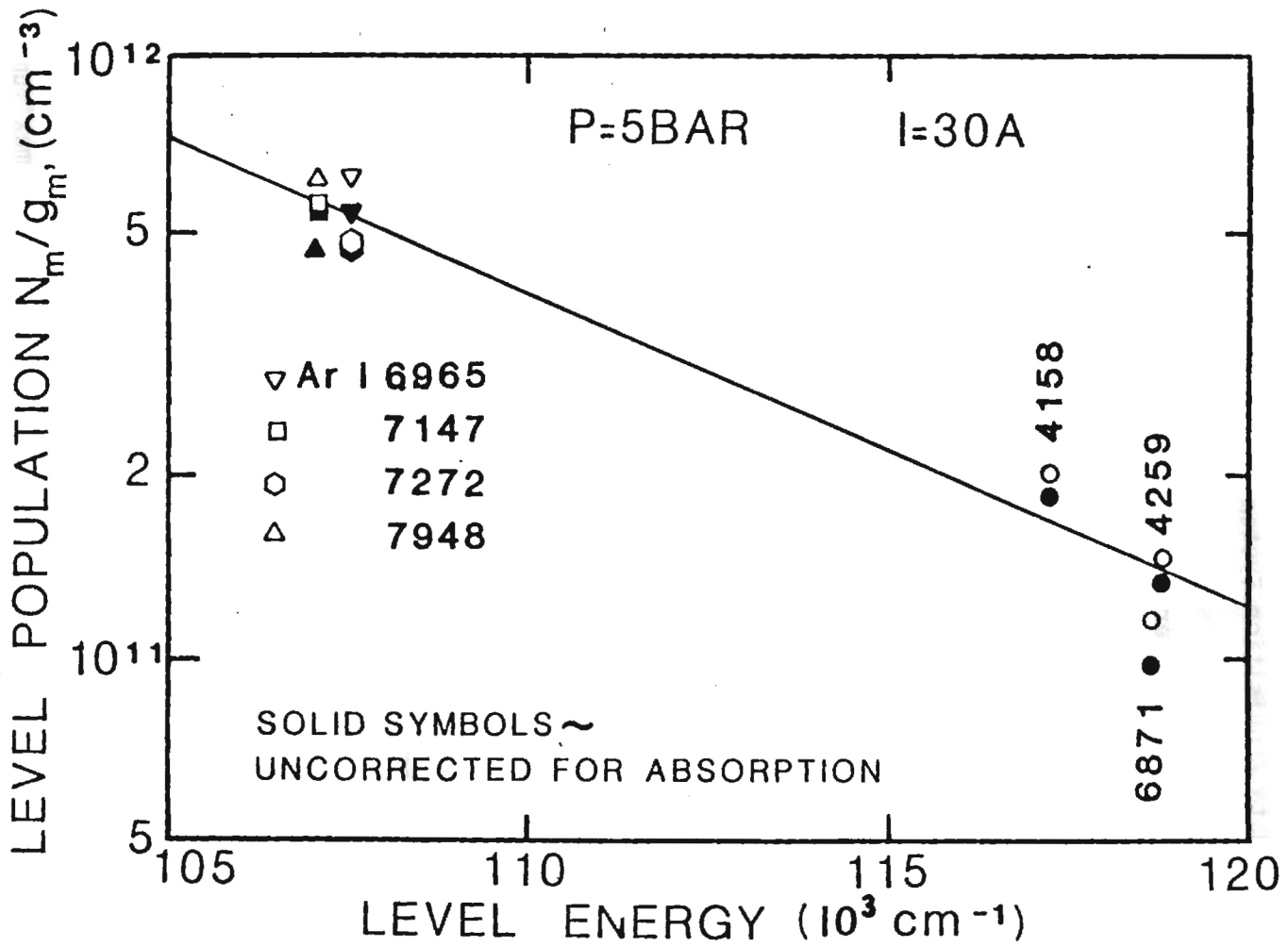

Figure 5.5: Boltzmann plot showing populations from lines with various degrees of absorption

Ray tracing techniques (explained in detail in Appendix C) shows that the image size and hence effective magnification factor at 30 bar and for the region of maximum refraction is affected by no more than 3%. Since most of the data is at much lower pressures and at regions with much lower refraction, the refractive effect has been neglected in the diagnostics.

5.4 Data Acquisition System

The date acquisition system (DAS), shown in Fig. 5.6, includes the HP9825 microcomputer (which serves as the controller and data collector), HP3455 DVM, HP3495A scanner, HP59308A timing generator, HP59309A clock, and the HPIB 16-bit parallel I/O, and BCD interface cards. The HPIB interface is used to switch scanner inputs to the DVM and read DVM data. The parallel I/O card is used to control the chamber movement and trigger the cascade plate voltage stepper switch. The BCD interface reads the monochrometer wavelength setting. The information fed to the scanner includes chamber pressure, arc current, plate voltage, chamber position, and the picoammeter signal.

For lateral arc scans, the chamber is set at the leftmost position and is then commanded to move to the right at a speed preset by the stepper motor indexer while that data collection begins. After the specified number of samples are taken, the chamber is stopped and initial and final positions of the chamber and the data are recorded. Similar procedures are used for wavelength scans, only the AWS scans the line. The arc chamber is then indexed to the next position and the process is repeated. This usually involves about 50 equal interval locations across the arc.

The intensity data as well as other relevant information are recorded on tape cartridges which are transferred to a CDC Cyber for reduction and analysis.

5.5 Data Evaluation

The data set for an individual spectral line intensity and one or two adjacent continua are initially smoothed by employing a 4-interval, third-order polynomial scheme (2 intervals on each side). The resulting profile is used to fine the arc position where the maximum intensity occurs (center). If necessary, the smoothed data is routed through a self-absorption correction scheme using the method outlined in Section 5.2. The

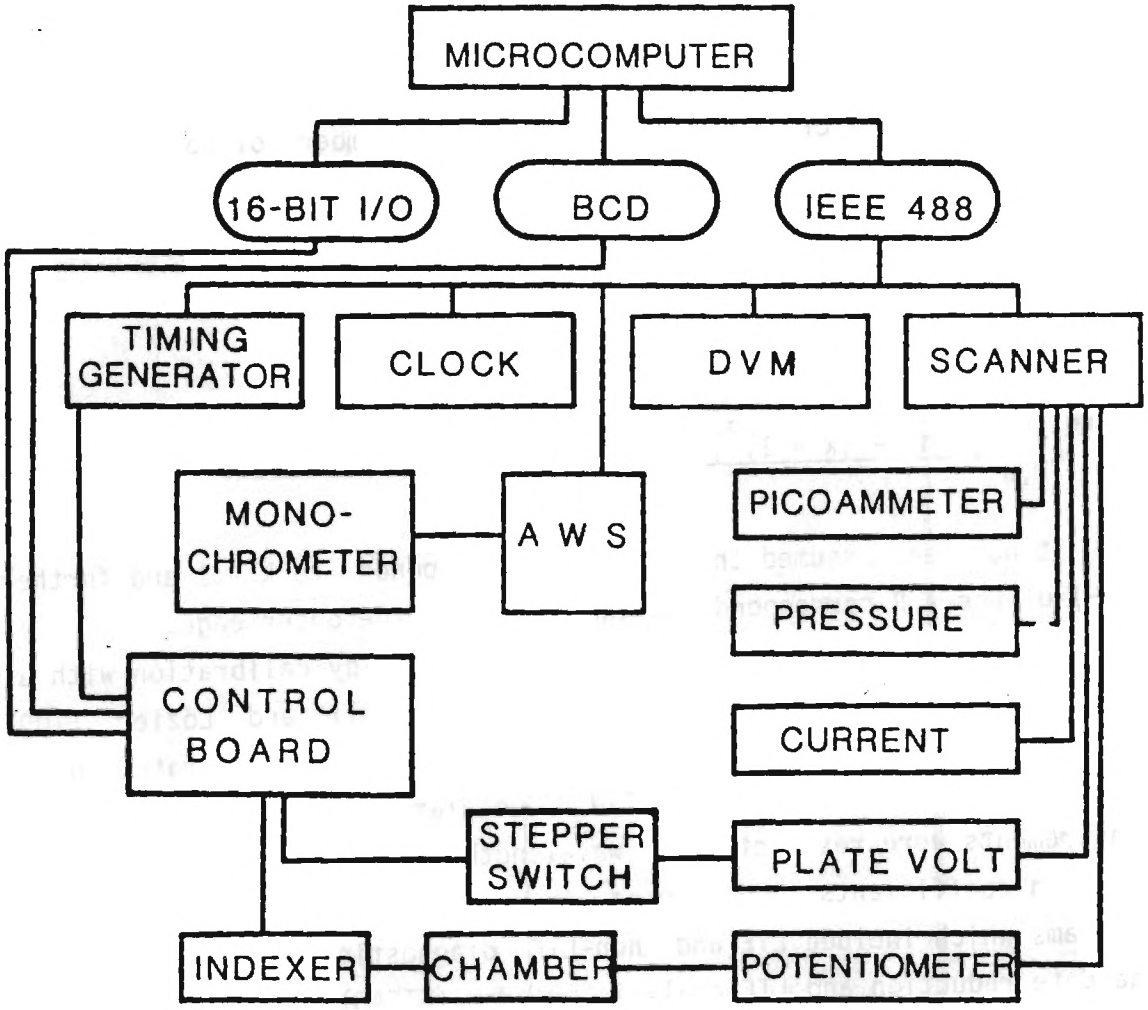

Figure 5.6: Schematic of the data acquisition and wavelength scanning instrumentation

corrected profile is folded about its center. The adjacent continua are prorated by wavelength, averaged, and subtracted from the line intensity. The resulting lateral net line intensities are converted to radial emission coefficients using the Abel transform after Nester and Olsen [108] using the following relationships,

$$i_k(r) = -2/\pi a \sum_{n=k}^{N-1} I_n(x) B_{k,n}$$

where n is the lateral position index, k is the radial position index, a lateral position increment, N is the total number of points, and $B_{k,n}$ is given by,

$$B_{k,n} = A_{k,k} \quad \text{for } n = k$$

$$B_{k,n} = A_{k,n-1} - A_{k,n} \quad \text{for } n \geq k + 1$$

where

$$A_{k,n} = \frac{[n^2 - (k-1)^2]^{1/2} - [(n-1)^2 - (k-1)^2]^{1/2}}{2n - 1}$$

It has been assumed that center corresponds to k - 1 and furthermore, $I_n(R)=0$, where R corresponds to the radium at the outer edge.

Absolute emission coefficients are obtained by calibration with a Mole-Richardson Molarc Lamp, Model 2371, after Null and Lozier [109] at a temperature of 3803±20 K. Since the calibration arc is operated in air, the spectrum of the arc contains C-N modecular bands (see Fig. 5.7). The measurements were restricted to wavelengths free of molecular bands. The emission coefficients are stored in a file for input to the analysis programs which include LTE and non-LTE diagnostic methods. The listing of the date reduction and LTE analysis program (NTSAD) is given in Appendix C.

5.6 Operating Conditions

Based on numerous preliminary experiments at currents ranging from 30 to 200A and pressures ranging from 0.1 to 20 bar, it was decided to run at 30A based on the following reasons. In order to demonstrate the validity of the GMTE model for resolving nonequilibrium conditions, one has to simulate cases which significantly deviated from LTE - low electron densities. Operating at low currents provided such a case. In addition, high current

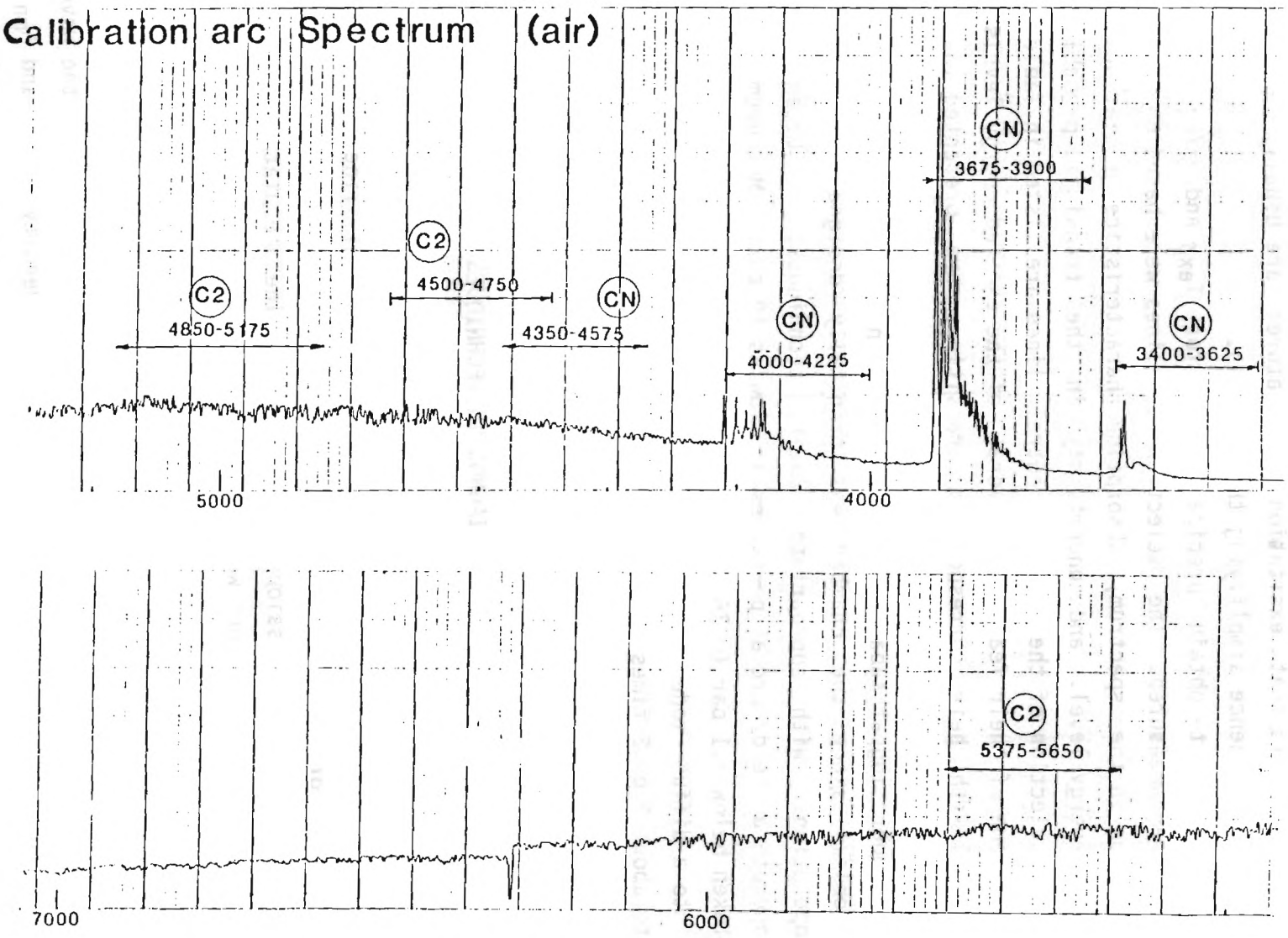

Figure 5.7: Spectrum of carbon calibration arc operated in air

arcs (I > 75A) tended to rapidly deteriorate the stabilizing plates. This effectively meant untolerable downtown periods, which could easily be prevented by operating at low currents. Another advantage of operating at low currents is that excitation temperatures are usually below the normal temperature, hence simplifying the analysis.

In order to obtain precise values for $T_{ex\beta}$ and n_I/g_I, many spectral lines were measured. The selection of lines were based on their relative location in the spectrum, absorption characteristics, radiation intensity, upper energy level, and uncertainty in the transition probability. The final selection of the measured neutral lines are listed in Table 5.1 along with some of their features. Several of the excited energy levels of argon neutral with their corresponding transitions are presented in a Grotrian diagram in Fig. 5.8.

Operating at subatmospheric pressures initially presented many hardware problems, since the chamber was originally designed for high pressure operation. With appropriate sealing techniques, it became possible to operate a steady arc at pressures as low as 10 torr. Measurements were not taken below 0.1 bar (~ 76 torr). Below this pressure, the arc would change into a diffuse mode and expand significantly at the cascade window section to about 2 or 3 times the channel bore size. The higher limit for pressure is 10 bar, because it was found that the LTE condition was reached at about 5 bar.

6.0 DIAGNOSTIC TECHNIQUES

6.1 Line Emission Coefficients

Spectral line intensities of several neutral lines (up to 9) were measured, corrected for absorption, and inverted via the Abel transform to yield radial line emission coefficients. The population density of the corresponding transitions were calculated using,

$$i_L = \frac{hc}{4\pi\lambda} n_m A_{mn}$$

where i_L is the line emission coefficient (W $cm^{-3}sr^{-1}$), λ is the wavelength of the transition (A), n_m is the upper level density (cm^{-3}) and A_{mn} is the transition probability (1/sec) from level m to n which is usually known and tabulated in various sources [3,47,99].

Table 5.1: List of Studied Spectral Lines of Argon Neutral

Wavelength ($\AA$) ref.[99]	$E_m(cm^{-1})$ ref.[68]	g_m ref. [68]	A_{mn} ($\times 10^8$) ref.[99]	Transition (Paschen notation)
3947.505	118469.117	5	6.3×10^{-4}	$1s_5 - 3p_3$
3948.979	118459.662	3	0.00467	$1s_5 - 3p_2$
4044.418	118469.117	5	0.00346	$1s_4 - 3p_3$
4158.59	117183.654	5	0.0145	$1s_5 - 3p_6$
4200.674	116942.815	7	0.0103	$1s_5 - 3p_9$
4259.362	118870.981	1	0.0415	$1s_2 - 3p_1$
4272.17	117183.387	5	0.0145	$1s_5 - 3p_6$
4300.101	116999.389	5	0.00394	$1s_4 - 3p_8$
4510.73	117563.020	1	0.0123	$1s_2 - 3p_5$
6871.289	118651.447	3	0.0290	$2p_{10} - 4d_5$
6937.664	118512.17	1	0.0321	$2p_{10} - 4d_6$
6965.43	107496.463	3	0.067	$1s_5 - 2p_2$
7030.25	119683.113	5	0.0278	$2p_9 - 3s_5$
7067.22	107289.747	5	0.0395	$1s_5 - 2p_3$
7147.042	107131.755	3	0.0065	$1s_5 - 2p_4$
7272.936	107496.463	3	0.0200	$1s_4 - 2p_2$
7635.106	106237.597	5	0.274	$1s_5 - 2p_6$
7948.176	107131.755	3	0.196	$1s_3 - 2p_4$
8521.44	107131.755	3	0.147	$1s_2 - 2p_4$

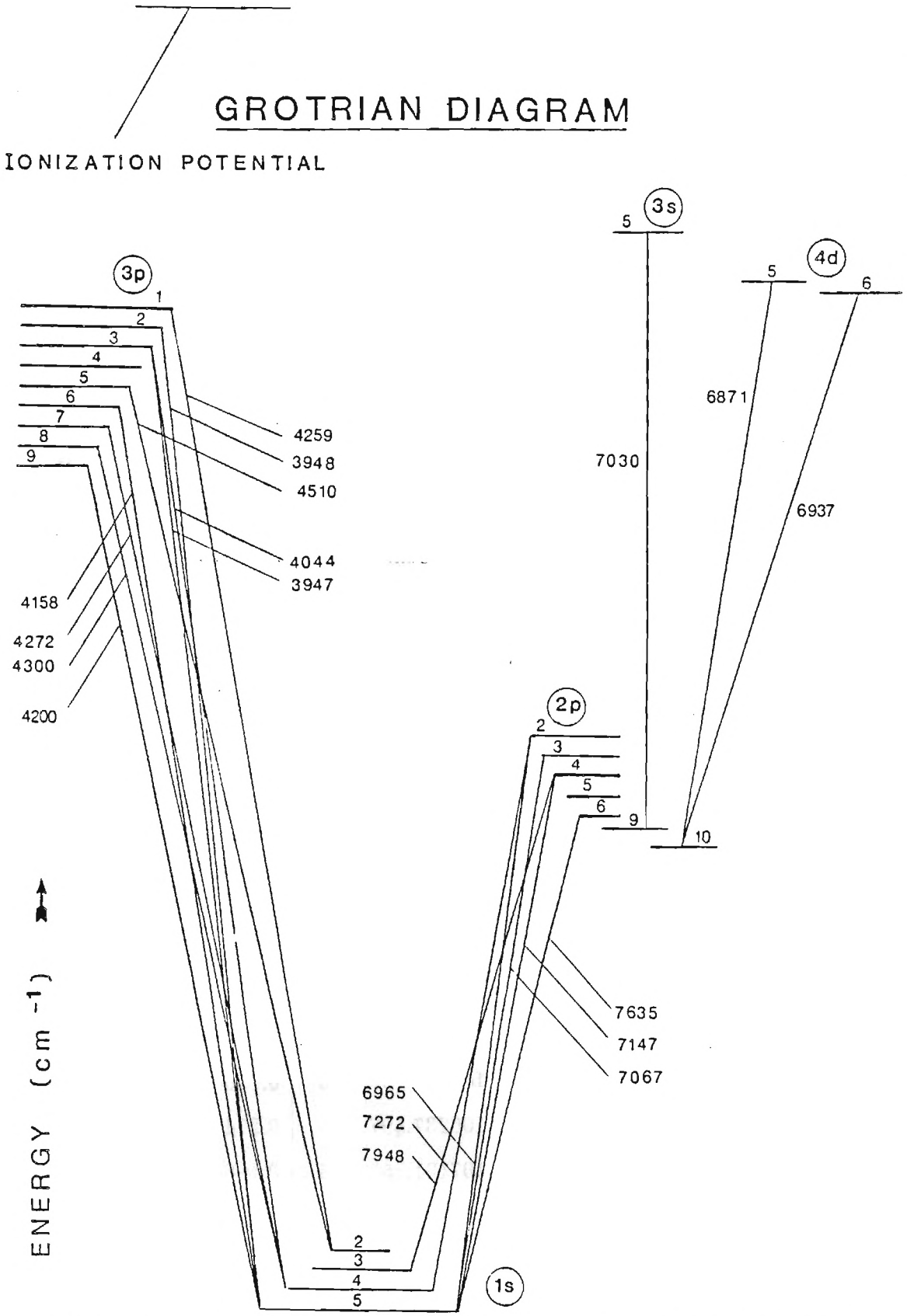

Figure 5.8: Grotrian diagram for argon neutral showing some of the excited levels, wavelengths in A.

Plotting the level densities of a Boltzmann plot and fitting a straight line through the measured levels would result in upper level excitation temperatures ($T_{ex\beta}$) —— sometimes referred to as the distribution temperature. Extrapolating $T_{ex\beta}$ to the lowered ionization level yields n_I/g_I, which is later used in the calculation of the electron temperature.

6.2 Continuum Emission Coefficients

In an argon arc, the continuous emission is composed of the recombination (free-bound) and the bremsstrahlung (free-free) continuum, since the plasma contains neither molecules nor negative ions. If the plasma is in LTE, the continuum emission coefficients can be written as [10],

$$\epsilon_\nu \; 5.44\text{x}10^{-46} n_e n_i T^{-1/2} z^2 \xi \quad \frac{W - s}{cm^3 st}$$

The ξ factor is a weighted sum of photoabsorption cross sections, taking into account the difference of the atomic energy level structure of argon as compared to that of hydrogen. ξ is given by [10],

$$\xi = \frac{\gamma}{Z_{exi}} \xi_{fb}\left[1 - \exp\left(-\frac{hc}{\lambda kT}\right)\right] + \xi_{ff}\exp\left(-\frac{hc}{\lambda kT}\right)$$

In this expression γ is the statistical weight of the parent ion (γ=6 for the heavy rare gases). The factor ξ_{fb} has been introduced by Biberman et al [20] using the quantum defect method developed by Burgess and Seaton [111]. Later Schlüter [26] recalculated the ξ_{fb} factor taking into account the effects of high electron energies and using exact Coulomb functions. Hofsaess [27] obtained similar results using the scaled Thomas-Fermi method including the polarization effects.

In GMTE the continuum equation takes a more complicated form due to the dependence of the ξ factor to many variables such as T_e, T_g, T_{exa}, $T_{ex\beta}$, and frequency. The GMTE continuum emission coefficient is given by [112],

$$\epsilon_\nu = 5.44\text{x}10^{-46} z^2 \exp\left(\frac{-\Delta E_\infty}{kT_{ex\beta}}\right)\left\{n_e n_i T_e^{1/2} \bar{G}_f \exp\left(\frac{\Delta E_s - h\nu}{kT_e}\right)\right.$$
$$\left. + 4\left(\frac{n_I}{g_I}\right)\left(\frac{2\pi m_e k}{h^2}\right)^{3/2} \frac{z^2 E_H}{k} \varsigma(\nu, T_{ex\beta}) \exp\left(-\frac{h\nu}{kT_{ex\beta}}\right)\right\}$$

where $\bar{G}_f$ is the overall e-i free-free Gaunt factor. The term $\exp[(\Delta E_s - h\nu)/hT_e]$ accounts for lines merged into the continuum by advancing the series limit. ς is given by [112],

$$\varsigma\left(\nu, T_{ex\beta}\right) = \sum_{ml}^{\nu} \frac{g_{ml}\sigma_{ml}}{m^5\sigma_m} \exp\left(\frac{E_I - E_{ml}}{kT_{ex\beta}}\right) + \sum_{m}^{\nu} \frac{G_m}{m^3} \exp\left(\frac{z^2 E_H}{m^2 kT_{ex\beta}}\right)$$

where g_{ml} is the statistical weight of a level with quantum numbers m and l. σ is the classical absorption cross section calculated by Griem [24], and E_H is the ionization potential for hydrogen. Here the first sum is over nonhydrogenic contributing levels and the second sum is over hydrogenic contributing levels. The value of ς can be back calculated from the values of ξ_{fb} given by various authors and tabulated as a function of ν and $T_{ex\beta}$ for convenience.

6.3 Stark Broadening of H_β

Electron density was deduced from direct measurement of the broadening extent of the hydrogen Balmer H_β line. For this reason hydrogen gas was introduced to the arc at less than 1% of argon volumetric flow rate. In the range of pressures and densities encountered in the course of these experiments, the Stark broadening was the most dominant broadening mechanism, therefore, the contribution of other broadening mechanisms such as natural, Doppler, Zeeman, and instrument broadenings were neglected.

The halfwidths of the H_β line were used to obtain electron density using the 'Unified Theory' of line broadening developed by Vidal, Cooper and Smith [54] which generates normalized profiles covering the entire profile from the impact limit in the line center to the quasi-static limit in the line wings. Several rigorous experimental investigations [74,113,114] verify the theory, although 2-λ interferometric measurements of Baessler and Kock [5] indicate that the electron densities calculated using the VCS theory must be corrected using the ratio of the reduced line widths, $\alpha_{1/2}$ of H_β line using the following relation:

$$n_{e,corr} = \left(\frac{\alpha_{1/2,vcs}}{\alpha_{1/2,B\text{-}K}}\right)^{3/2} n_{e,vcs} = \left(\frac{.085}{.0804}\right)^{3/2} n_{e,vcs} = 1.087\, n_{e,vcs}$$

The correction to electron density given by the B-K scale was adapted and used in this work.

6.4 LTE Analysis Method

In the LTE method of analysis, the equivalent optically thin line-emission coefficient, i_L, and the pressure are the experimentally determined quantities. Withe the knowledge of transition probability of a spectral line, the population density of its upper level of transition can be determined from:

$$n_m = i_L \frac{4\pi\lambda}{hc} \frac{1}{A_{mn}} \quad . \tag{4.25}$$

Assuming a double ionized plasma, the following five equations can be solved simultaneously to yield electron, neutral, first ion, and second ion density as well as the corresponding LTE temperature.

$$\text{Boltzmann: } \frac{n_m}{n_a} = \frac{g_m}{Z_{exa}} \exp\left[\frac{-E_m}{kT}\right] \tag{4.26}$$

$$\text{Saha I: } \frac{n_e n_i}{n_a} = \frac{2Z_{exi}}{Z_{exa}} \left[\frac{2\pi m_e kT}{h^2}\right]^{3/2} \exp\left[\frac{-E_I}{kT}\right] \tag{4.27}$$

$$\text{Saha II: } \frac{n_e n_{ii}}{n_i} = \frac{2Z_{exii}}{Z_{exa}} \left[\frac{2\pi m_e kT}{h^2}\right]^{3/2} \exp\left[\frac{-E_{II}}{kT}\right] \tag{4.28}$$

$$\text{Quasi-neutrality: } n_e = n_i + 2n_{ii} \tag{4.29}$$

$$\text{Ideal gas law: } P = \left(n_a + n_e + n_i + n_{ii}\right) kT \tag{4.30}$$

There are two sets of solutions that satisfy Eqns. 4-26 through 4-30. The solutions correspond to temperatures below and above the normal temperature of the plasma for a given pressure. If LTE prevails, and the plasma temperature is at or above the normal temperature, then the two solutions will cross over. At arc periphery, the arc temperature is low, therefore the low-T solution is selected. As we go toward the center of a

cylindrical arc the two solutions approach each other. If the solutions crossover, from the point of crossing to the center of the arc the high-T solution is selected.

In experiments performed in a 3-mm bore size and up to 200 amp, the second-ion population is observed to be insignificant.

6.5 GMTE Analysis

Line emission coefficients, pressure, field strength, and electron densities were fed into the GMTE analysis routine to determine the upper level excitation temperature, total excitation temperature, electron temperature, gas temperature and neutral atom density. The GMTE equations employed in the analysis are,

State:

$$P = k(n_e T_e + n_i T_g + n_a T_g)$$

Quasi-Neutrality:

$$n_e = n_i$$

Line emission coefficient:

$$i_L = \frac{hc}{4\pi\lambda} n_m A_{mn}$$

Upper level excitation temperature from Boltzmann factor:

$$\frac{n_m}{n_n} = \frac{g_m}{g_n} \exp\left[- \frac{E_m - E_n}{kT_{ex\beta}} \right]$$

Boltzmann factor to the ground state:

$$\frac{n_I}{n_a} = \frac{g_I}{Z_{exa}} \exp\left[\frac{-E_I}{kT_{exa}} \right]$$

Upper level ionization equation:

$$n_e \left[\frac{n_i}{n_I}\right]^{T_g/T_e} = 2\left[\frac{Z_{exa}}{g_I}\right]^{T_g/T_e} \left[\frac{Z_{exi}}{Z_{exa}}\right]^{T_{exa}/T_e} \left[\frac{2\pi m_e kT_e}{h^2}\right]^{3/2} \exp\left[\frac{-E_I}{kT_e}\left[1 - \frac{T_g}{T_{exa}}\right]\right]$$

Electron energy equation (see Appendix E):

$$\sigma E^2 = (3m_e/m_g)k(T_e - T_g)n_e(3kT_e m_e)^{1/2}(n_e Q_{ei} + n_a Q_{ea})$$
$$- \frac{1}{r}\frac{d}{dr}\left(rk_e \frac{dT_e}{dr}\right) - \left(\frac{5}{2}kT_e + E_I\right)\frac{1}{r}\frac{d}{dr}\left(r\, AD_a \frac{dn_e}{dr}\right) + q_{rad,e}$$

In addition to being implicit and highly nonlinear, these equations also require the knowledge of electron temperature and density gradients, dT_e/dr and dn_e/dr. In order to solve this system of nonlinear equations, a trial and error technique has been adapted in which densities, temperatures, and their gradients are initially assumed to be those of an equivalent LTE case. At each iteration process, the values of T_e, T_g, T_{exa}, and n_a are updated for all the radial positions. Then new values of dT_e/dr and dn_e/dr are calculated and the iteration scheme is repeated until the electron temperature and density would not change by more than 0.01%. This usually requires only 3 or 4 iterations since the electron temperature and density gradients highly resemble those of the LTE case.

6.6 T - p Plot

T-p plots have been traditionally used [115-117] to quantitatively demonstrate the kinetic nonequilibrium effect. This technique has been extended to illustrate kinetic as well as various excitation nonequilibrium effects and their extent. It also helps find a lower limit for the LTE condition. In GMTE T-p plots all the pertinent temperatures (T_e, T_g, T_{exa}, $T_{ex\beta}$, and T_{LTE}) are used to give a complete picture of the nonequilibrium.

At non-LTE conditions, the various temperatures differ from each other significantly depending on the extent of non-LTE. As the LTE conditions are approached, the temperatures are expected to converge to a single value (T_{LTE}). It is also possible for temperatures to approach each other and before complete convergence, continue parallel to each other. This could be the cast if the transition probabilities were inaccurate. Hence, T-p plots can be utilized to demonstrate inaccuracies in atomic parameters used in the analysis.

7.0 PRELIMINARY RESULTS

7.1 Boltzmann Plots

The experimental conditions for this study have been described in

detail in Chapter 5. The emission coefficients of numerous neutral argon lines were measured to yield precise upper level excitation temperature, $T_{ex\beta}$. Typical Boltzmann plots at various radii are shown in Fig. 7.1-7.7 for all the different pressures. Whenever possible, the same set of lines was measured for all the pressures, although at higher pressures the extensive broadening of the lines and the consequent overlapping with other neighboring lines forced us to modify the selection of the measured lines. This was done very judiciously. For example, since ArI 7948 was too broad to be measured with the maximum exit slit setting (3mm), ArI 8521 was chosen instead. It has the same upper level and therefore would be an alternate representative of the same level in a Boltzmann plot.

Absence of any noticeable scatter in the Boltzmann plots implies the extreme precision and caution exercised in performing the experiments. For instance, in cases where lines of a common upper level energy are measured (e.g. 7272 and 6965 or 7147 and 7948 Å) the level intensities coincide, indicating a very high level of reproducibility in intensity measurement. To validate this point further, every measurement was repeated three times and the average of the three was calculated. In none of the cases, was the deviation of any one single measurement larger than 0.5% of the calculated average. Although if the entire set of an experiment was repeated three times, it would have had the advantage of long term temporal averaging in addition to short term averaging, but the uncertainty in repeatability of the wavelength position setting would have introduced a larger effective error.

The scatter in level densities becomes noticeable only at outer edges of the arc (plasma-cole gas interface), where the intensity becomes at least two orders of magnitude smaller than the centerline intensity and therefore the background noise becomes as large as 30% of the measured intensity. This is specially true at lower pressures, where the arc intensity is small to begin with.

The temperatures shown in the Boltzmann plots are calculated by fitting a straight line to the measured level densities. Transition probabilities given by NBS have been used in calculating the level densities. The measured lines in this study have upper level energies ranging from 105,000 to 120,000 cm^{-1}. The reason for not measuring any line with higher upper energy level was that these lines generally lie in the 5000-6000 Å region of the spectrum where the continuum has a "bumpy" structure due to the

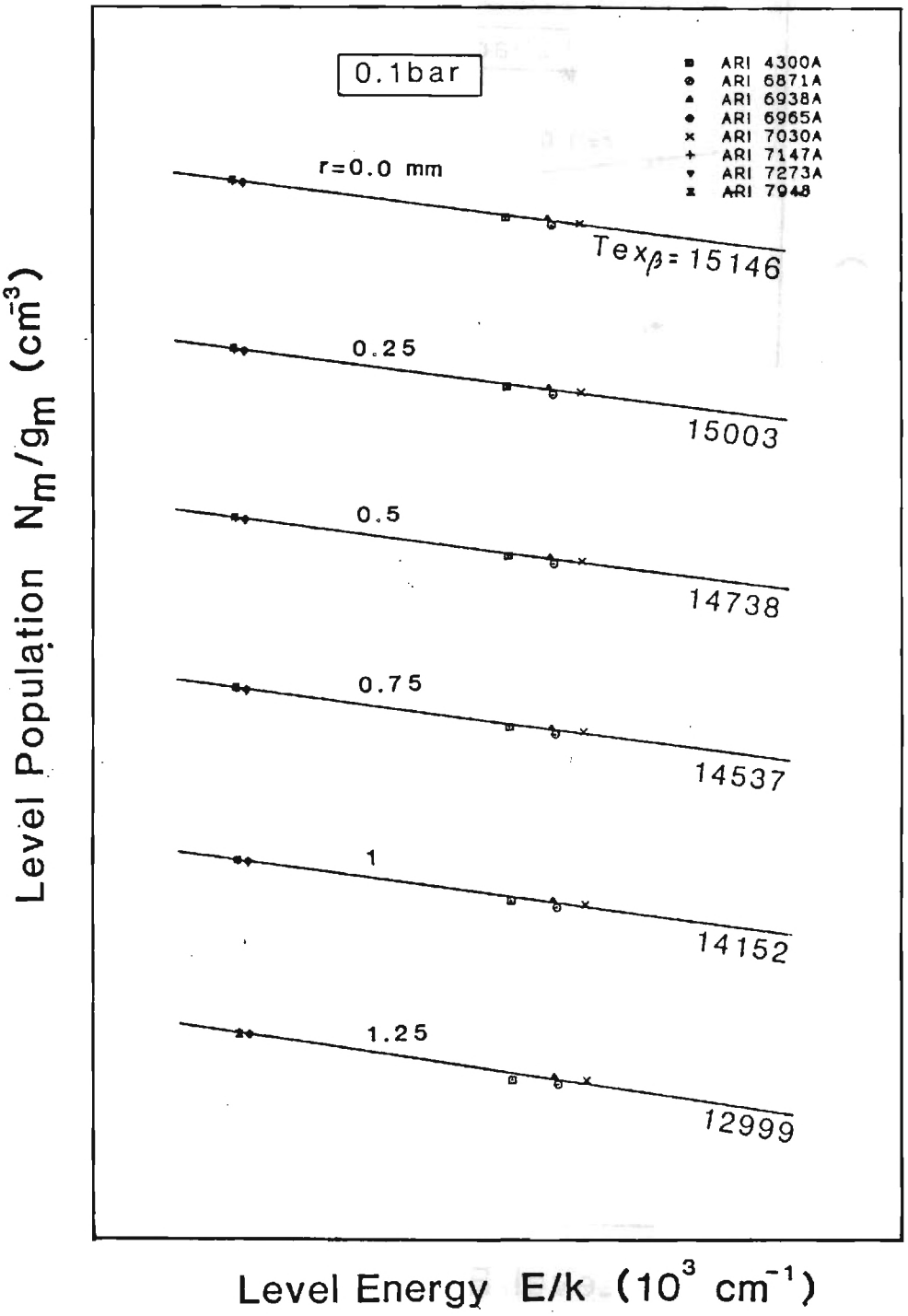

Figure 7.1: A Boltzmann plot showing the ratio temperature ($T_{ex\beta}$) at various arc radii for p=0.1 bar

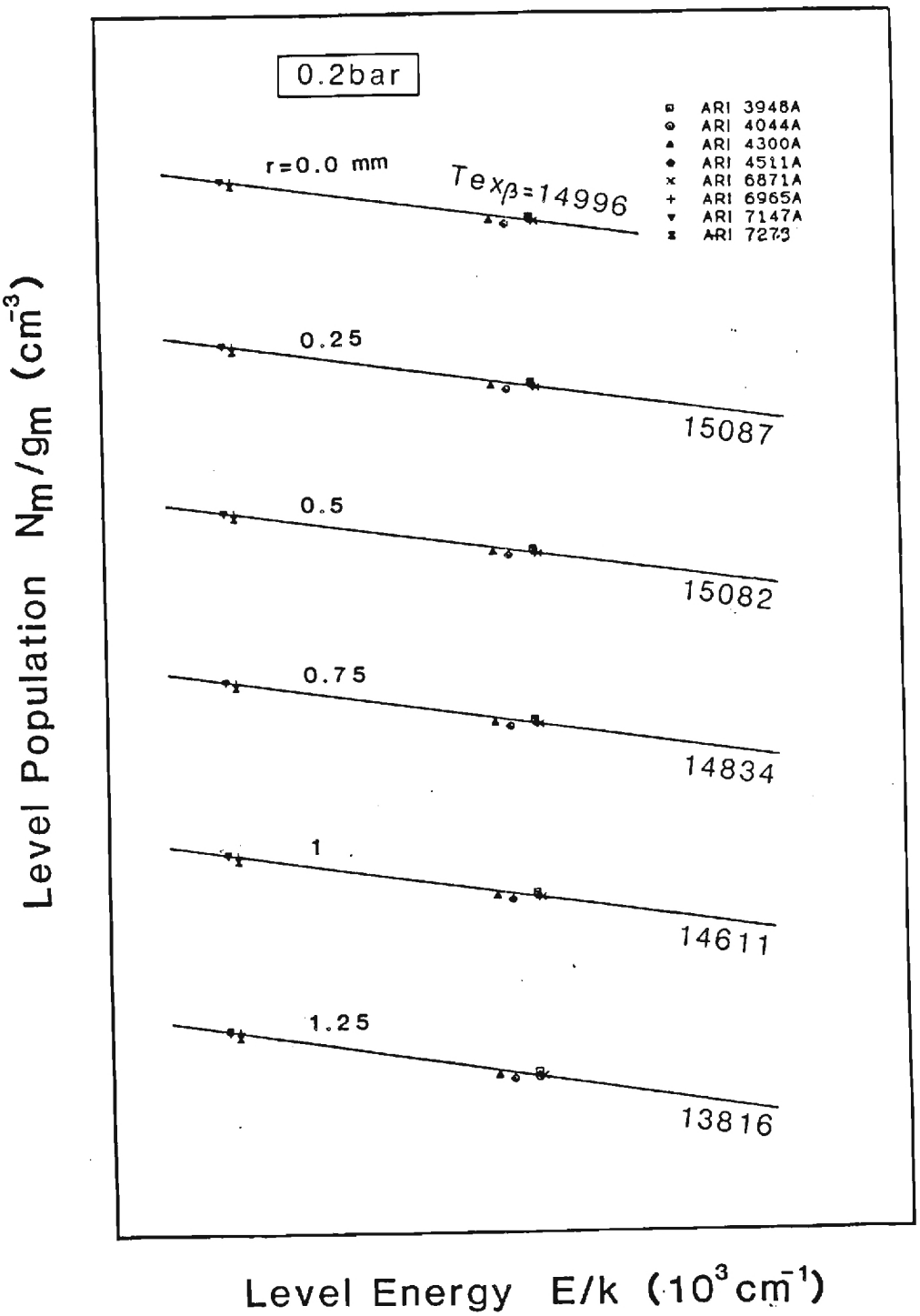

Figure 7.2: A Boltzmann plot showing the ratio temperature ($T_{ex\beta}$) at various arc radii for p=0.2 bar

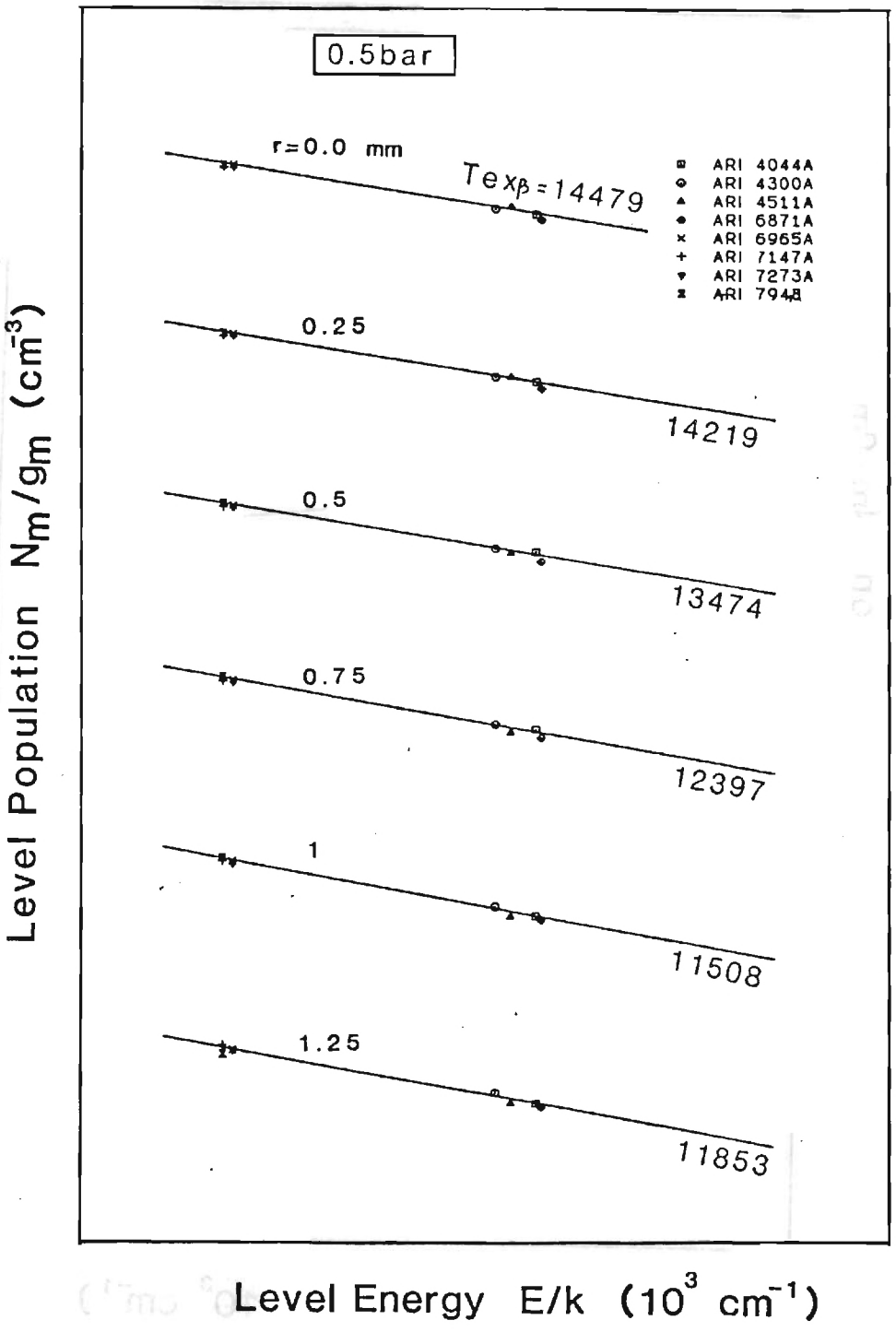

Figure 7.3: A Boltzmann plot showing the ratio temperature ($T_{ex\beta}$) at various arc radii for p=0.5 bar

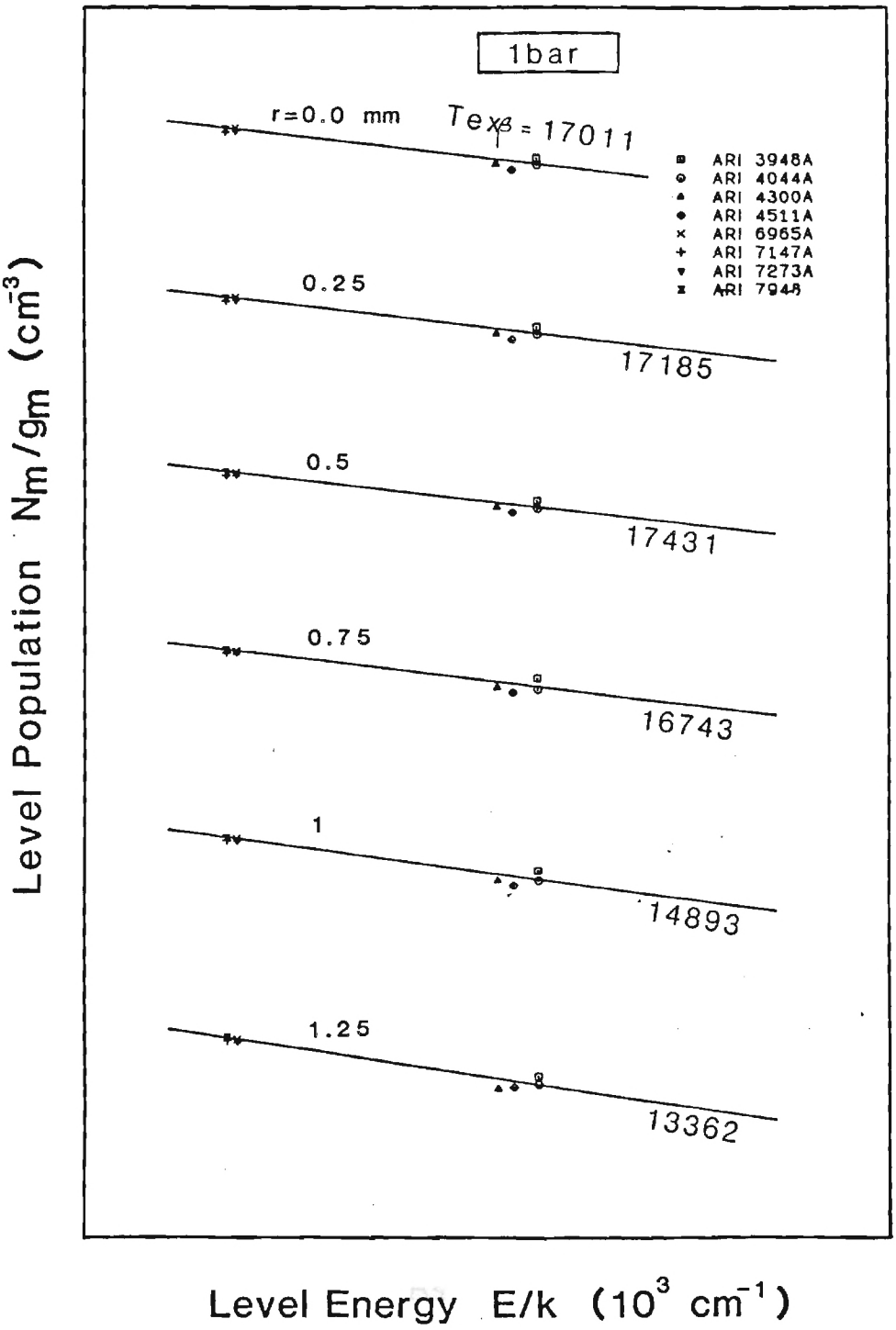

Figure 7.4: A Boltzmann plot showing the ratio temperature ($T_{ex\beta}$) at various arc radii for p=1 bar

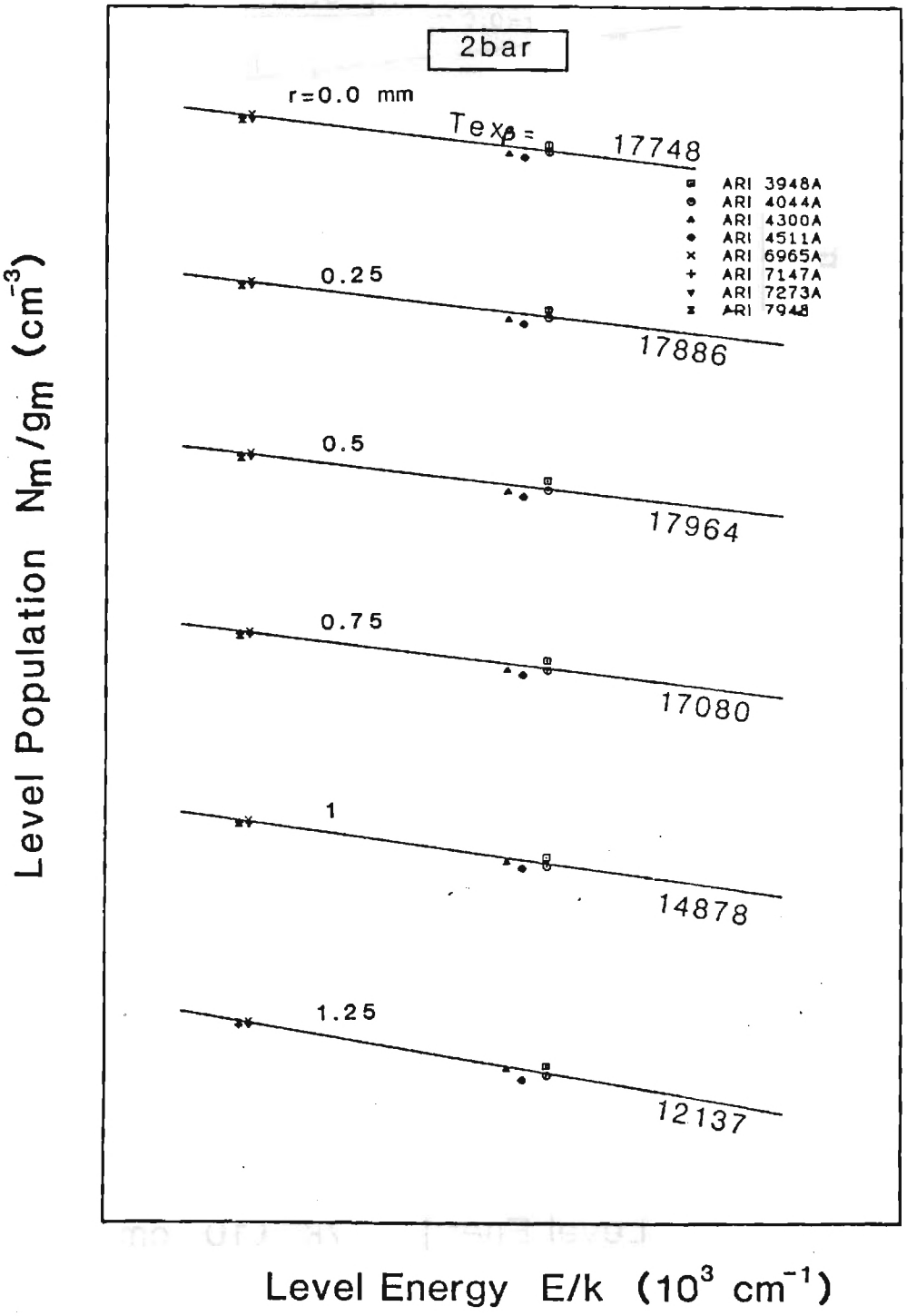

Figure 7.5: A Boltzmann plot showing the ratio temperature ($T_{ex\beta}$) at various arc radii for p=2 bar

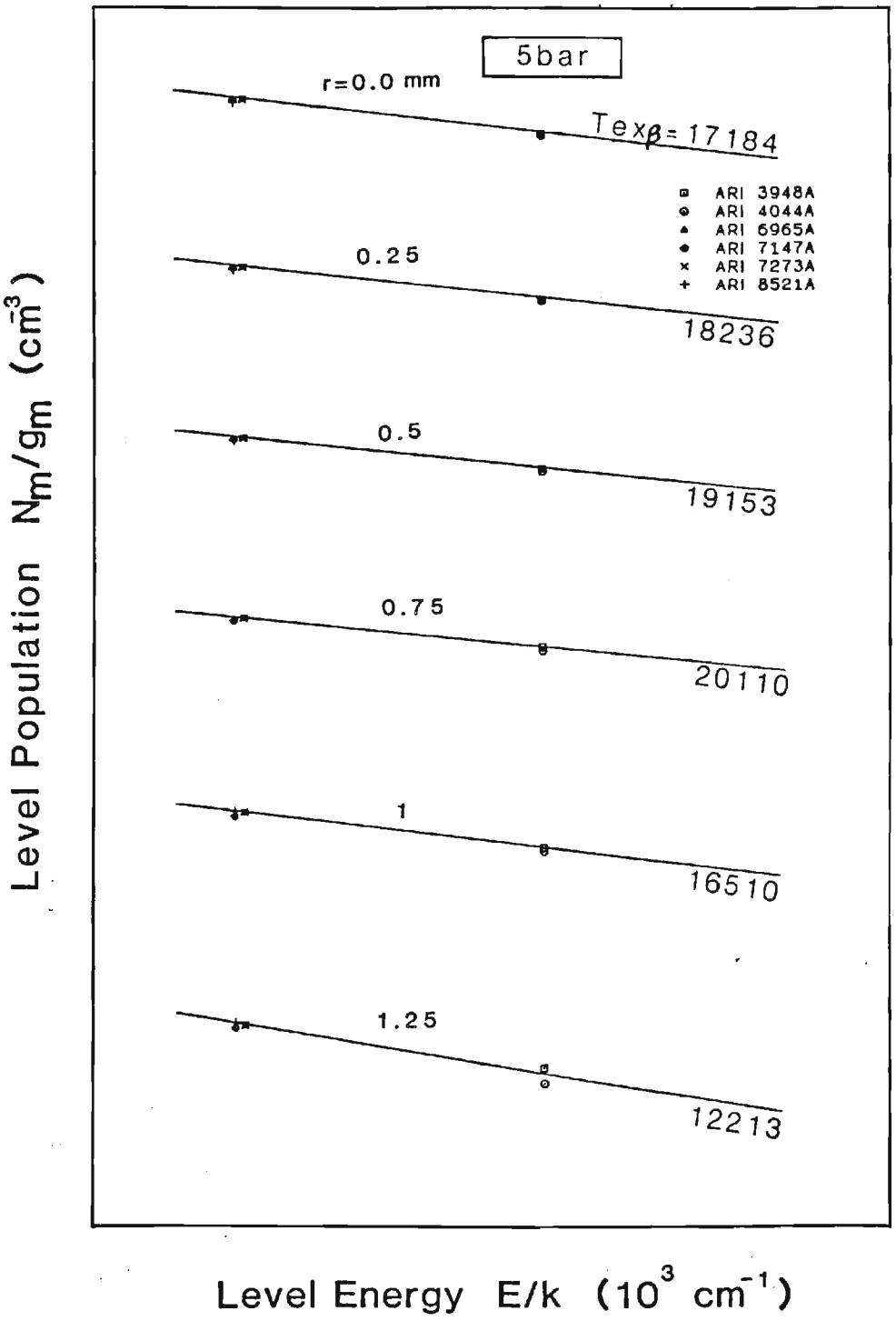

Figure 7.6: A Boltzmann plot showing the ratio temperature ($T_{ex\beta}$) at various arc radii for p=5 bar

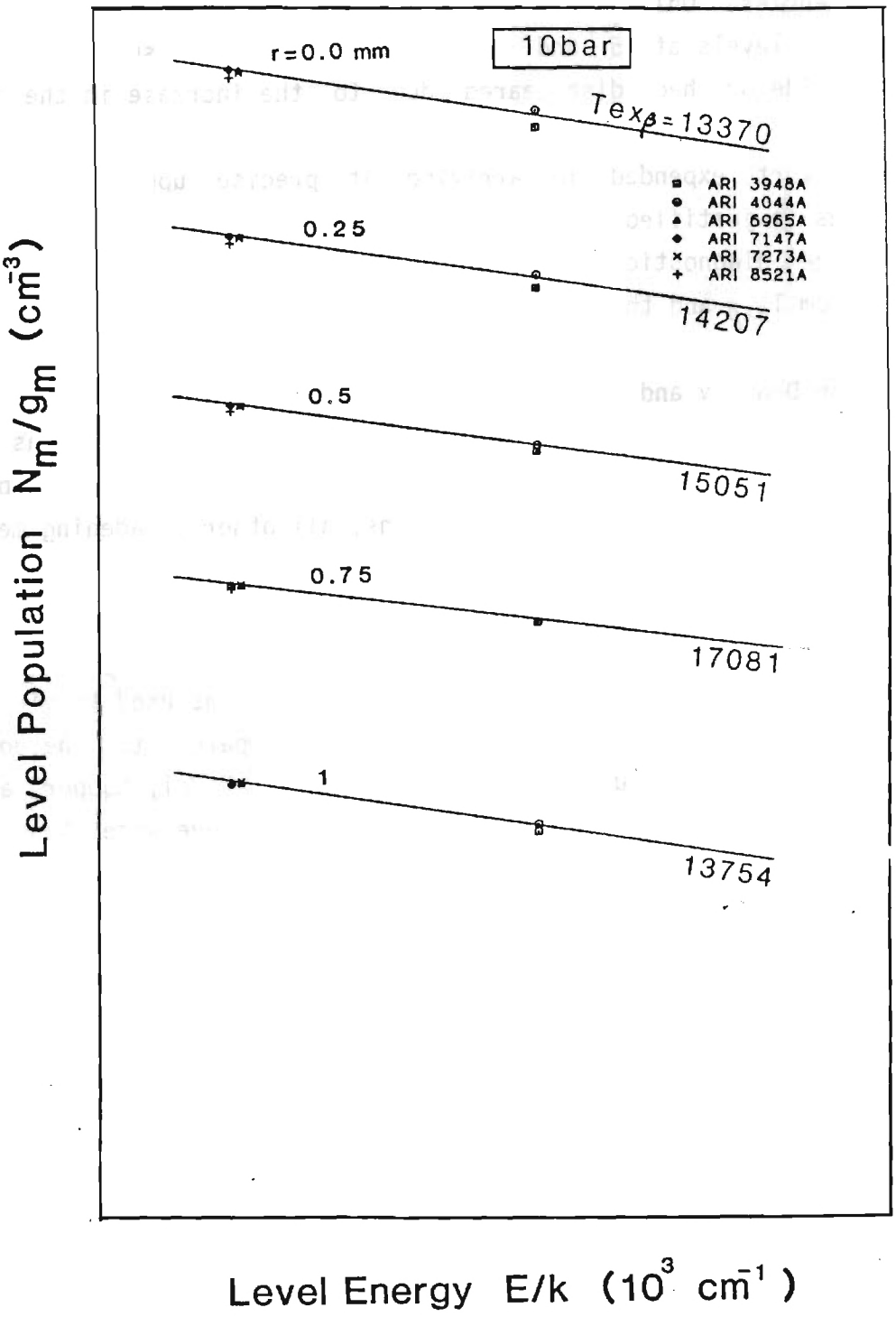

Figure 7.7: A Boltzmann plot showing the ratio temperature ($T_{ex\beta}$) at various arc radii for p=10 bar

recombination of free electrons to various energy levels which coincide with these frequencies. Only ArI 3948 and 4044 were selected to represent the higher energy levels at 5 and 10 bars, since other suitable lines were either too wide or had disappeared due to the increase in the continuum intensity.

The effort expended in arriving at precise upper excited level temperatures is justified due to the fact that n_I/g_I which is an important input to the diagnostic relations presented in Chapter 6, is directly obtained from $T_{ex\beta}$ and the excited level populations.

7.2 Electron Density and LTE Results

Electron density as a function of radius for each pressure was directly obtained by measuring the halfwidth at half maximum of the Stark broadened H_β line. Based on preliminary calculations, all other broadening mechanisms (specially Doppler broadening at lower pressures) were negligible compared to the extent of the broadening due to the Stark effect. The arc was laterally scanned at different wavelengths over the entire H_β line and parts of the adjacent continuum. Then Abel transform was used to yield radial profiles. The halfwidth was measured and compared to the normalized theoretical halfwidth deduced from the works of Vidal, Cooper, and Smith [54]. The electron densities obtained by this technique were then corrected to the 2-λ interferometric scale given by Baessler and Kock [5].

LTE analysis was performed on all the measured intensities to obtain an overall understanding of the plasma parameters. Using a line intensity and the pressure, LTE parameters such as n_e, n_a, and T can be obtained. Figs. 7.8-7.14 show the $n_{e,LTE}$ obtained for all the measured lines at various pressures. Shown also in these figures in the electron density from the H_β line broadening. The spread in $n_{e,LTE}$ is about 20% for a given pressure. In general, lines originating from higher energy levels (e.g. 3948, 4044, 6871 Å) yield higher LTE electron density. This is due to the fact that since the ground state is overpopulated relative to $T_{ex\beta}$, LTE temperatures calculated from levels closer to ionization potential would be larger. Larger LTE temperature would in turn result in higher $n_{e,LTE}$.

Figs. 7.15-7.21 depict the LTE temperatures for each line at each pressure. At a given pressure and low degrees of ionization one can see

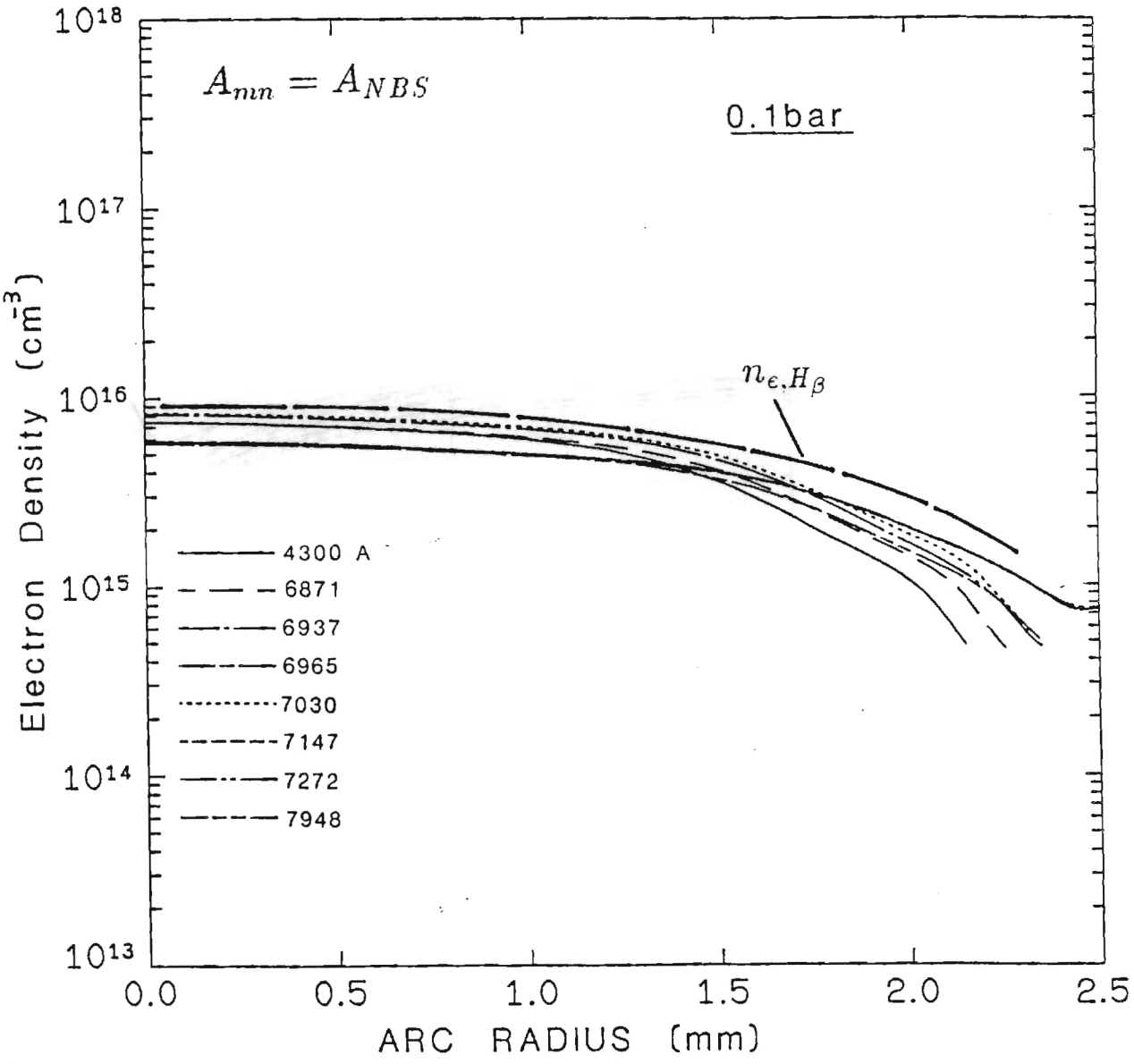

Figure 7.8: Electron density obtained using the LTE diagnostics, p=0.1 bar

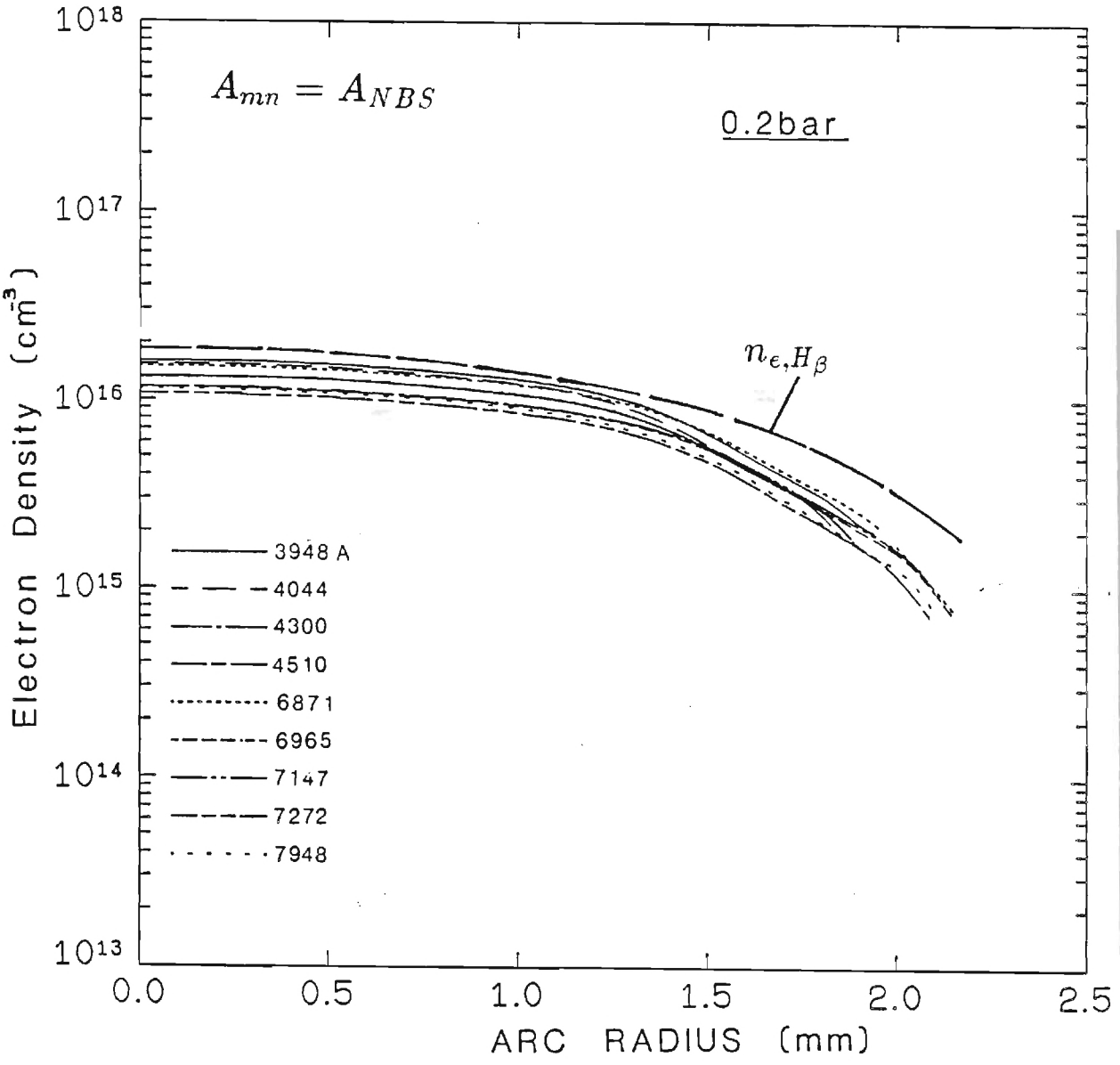

Figure 7.9: Electron density obtained using the LTE diagnostics, p=0.2 bar

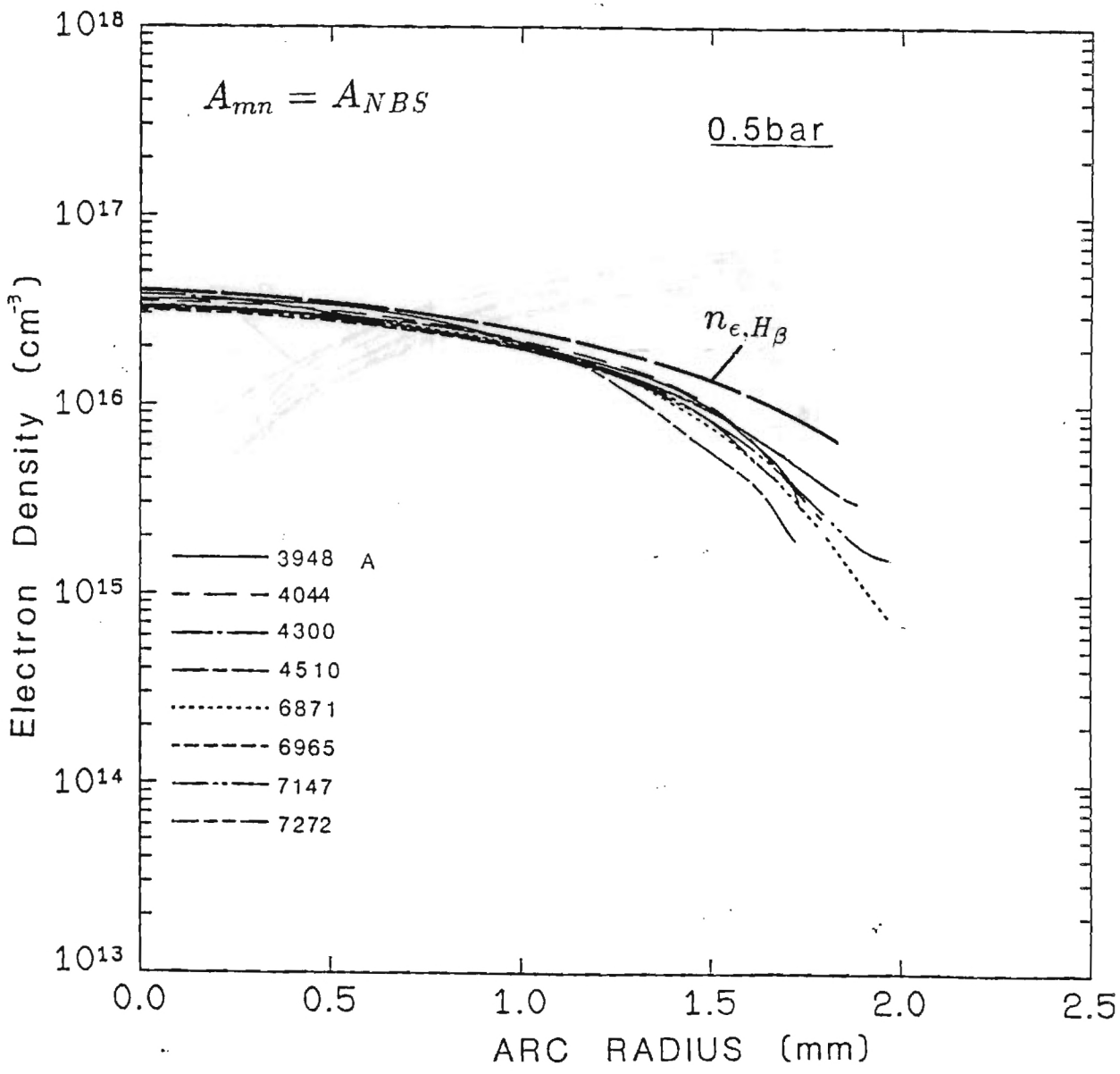

Figure 7.10: Electron density obtained using the LTE diagnostics, p=0.5 bar

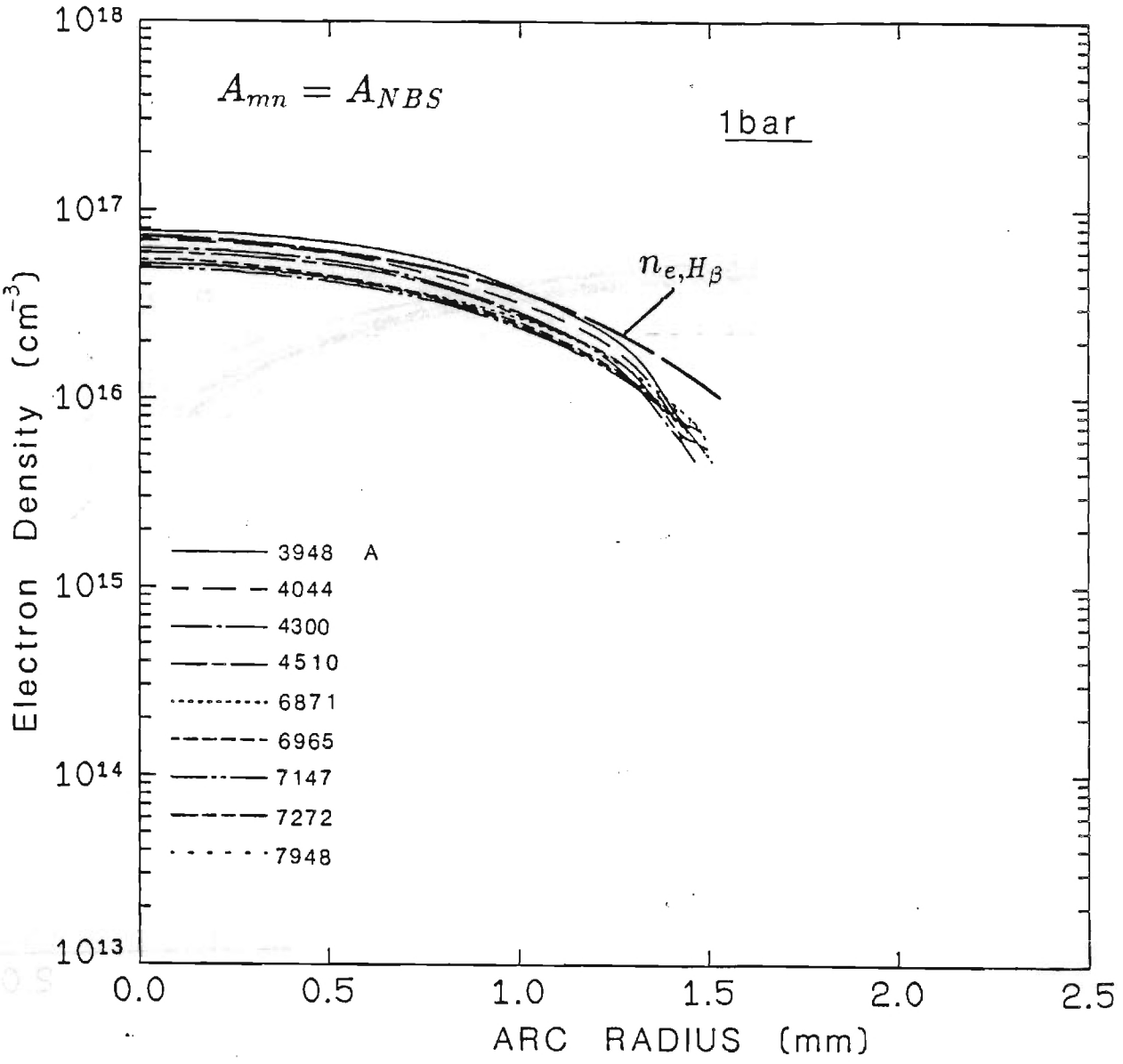

Figure 7.11: Electron density obtained using the LTE diagnostics, p=1 bar

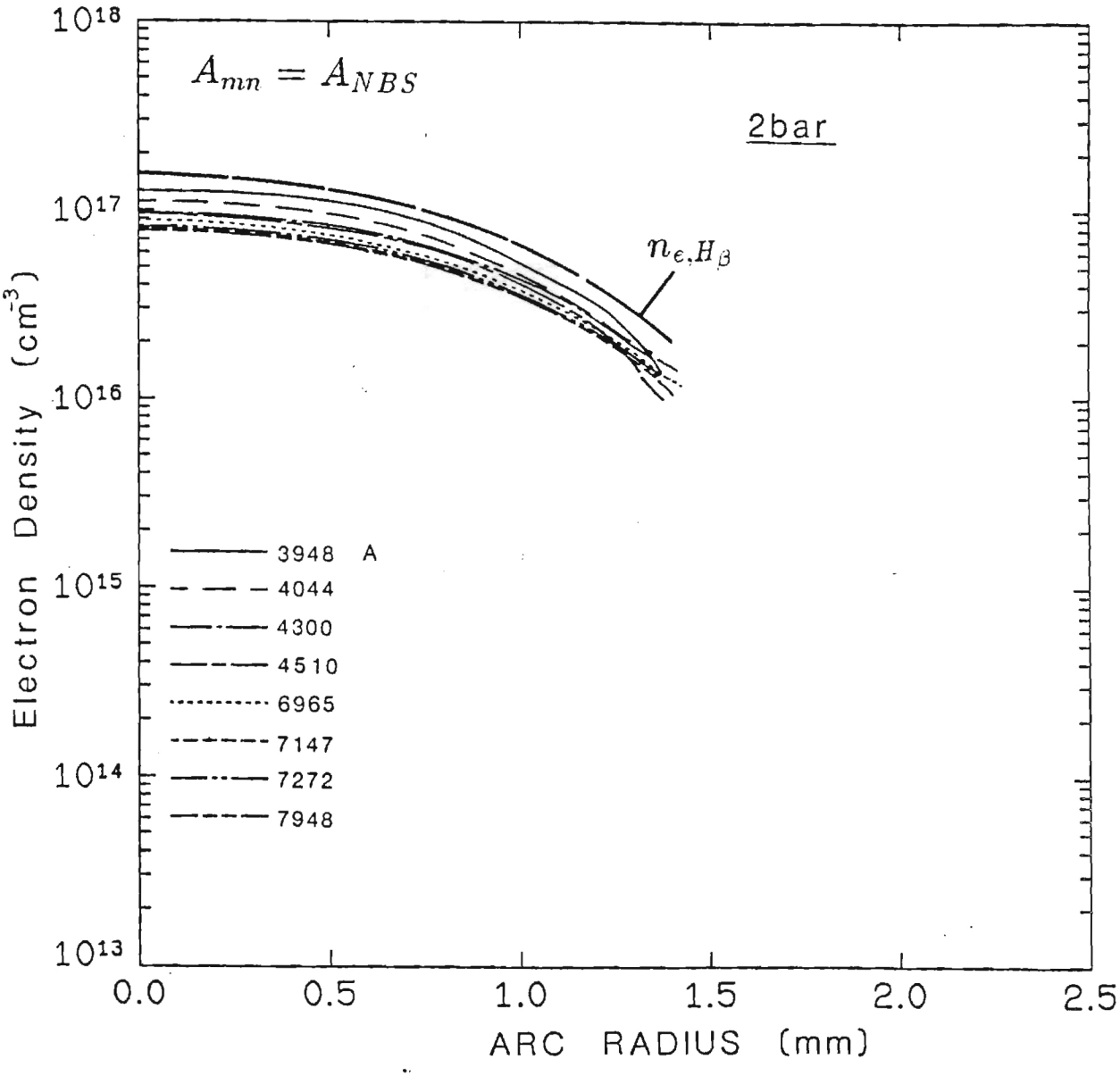

Figure 7.12: Electron density obtained using the LTE diagnostics, p=2 bar

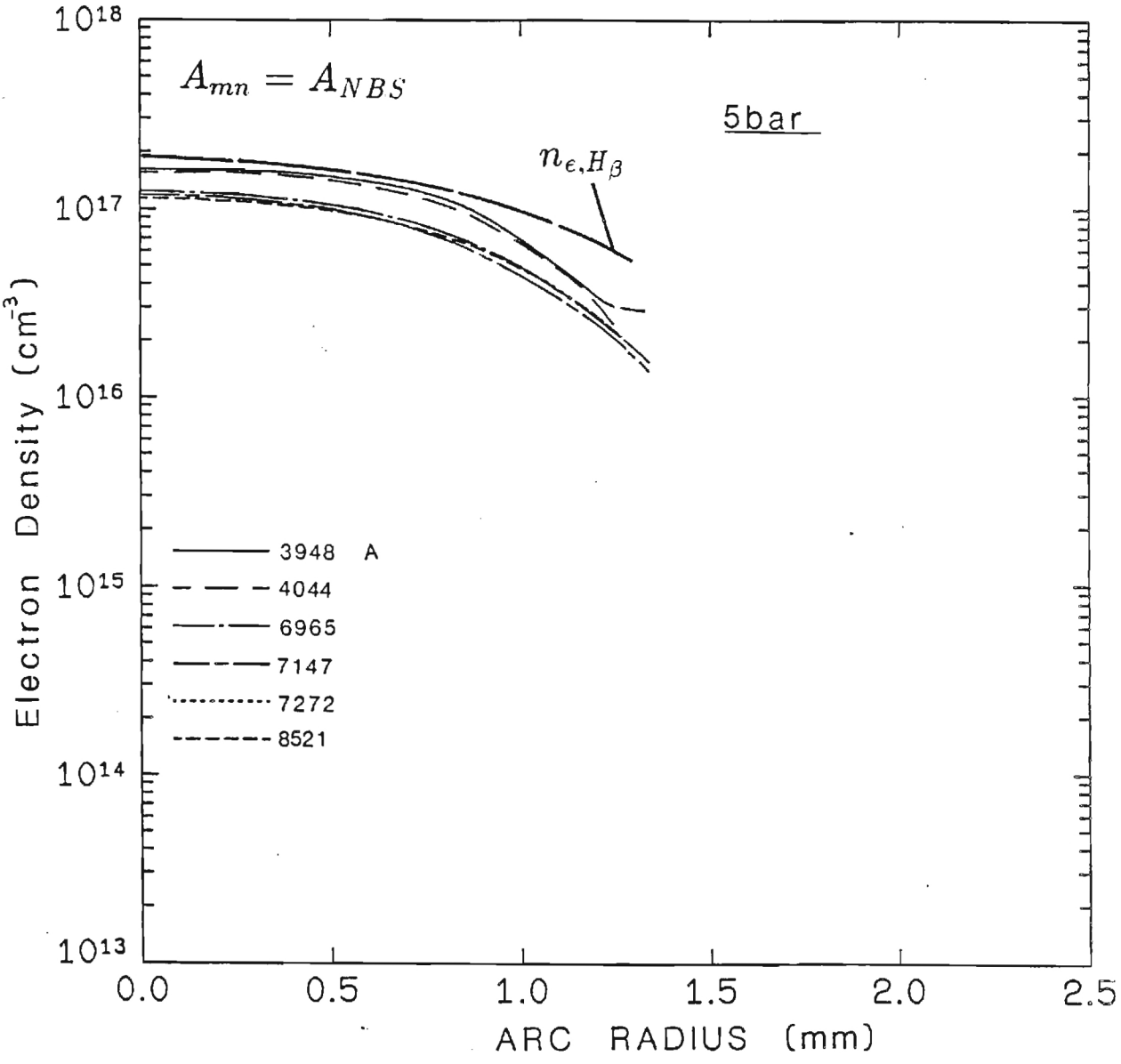

Figure 7.13: Electron density obtained using the LTE diagnostics, p=5 bar

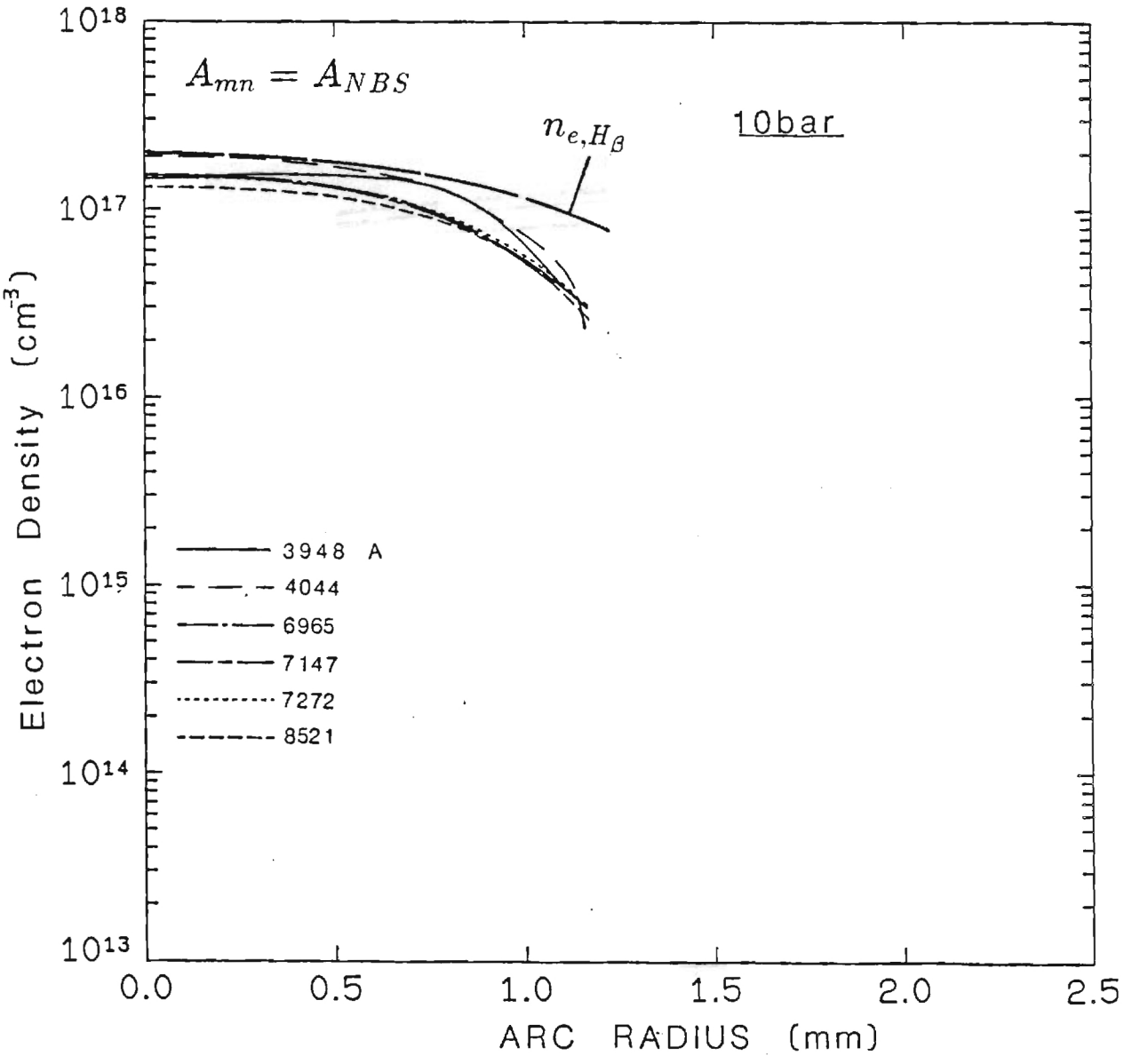

Figure 7.14: Electron density obtained using the LTE diagnostics, p=10 bar

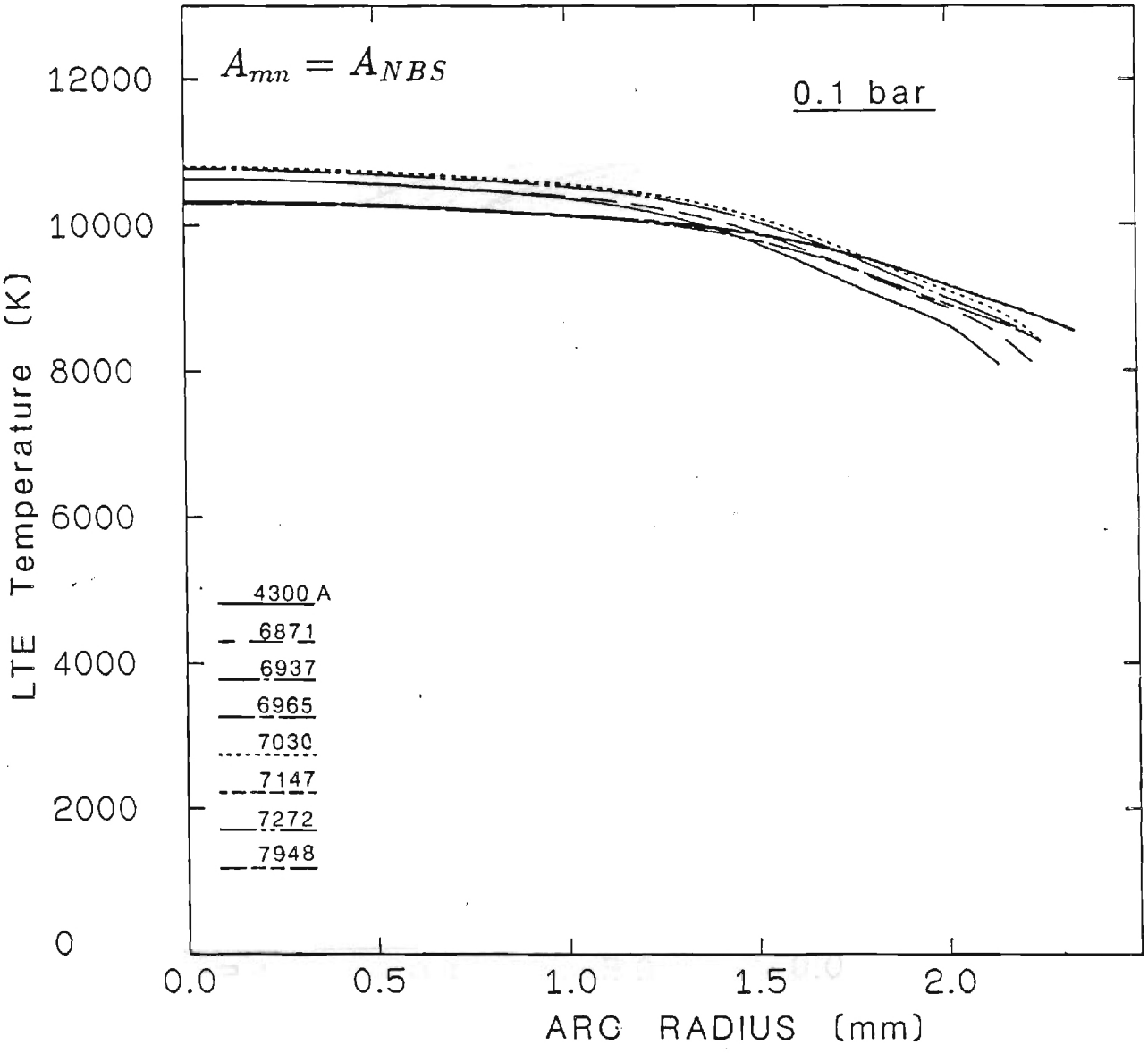

Figure 7.15: Plasma temperature obtained using the LTE diagnostics, p=0.1 bar

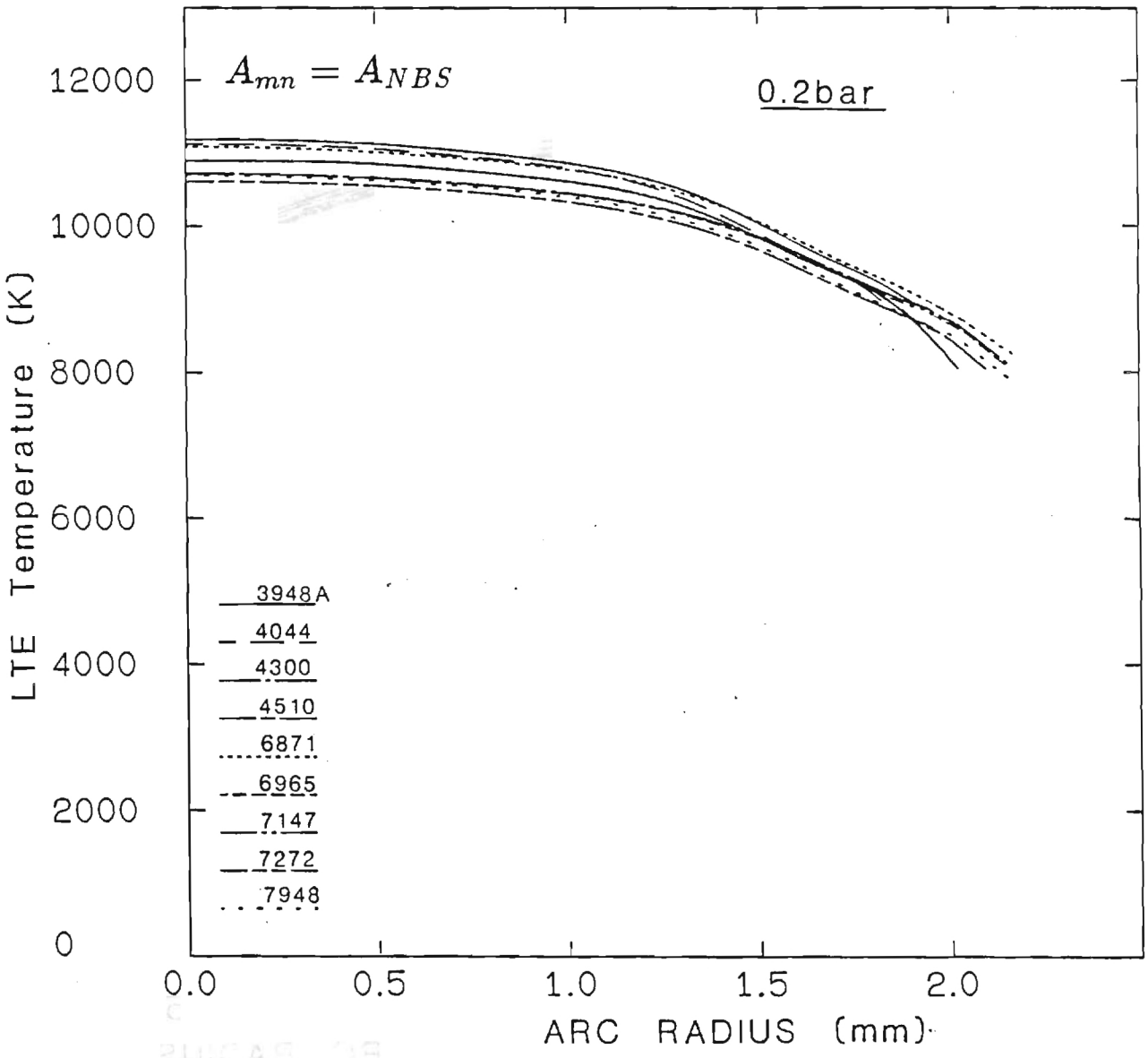

Figure 7.16: Plasma temperature obtained using the LTE diagnostics, p=0.2 bar

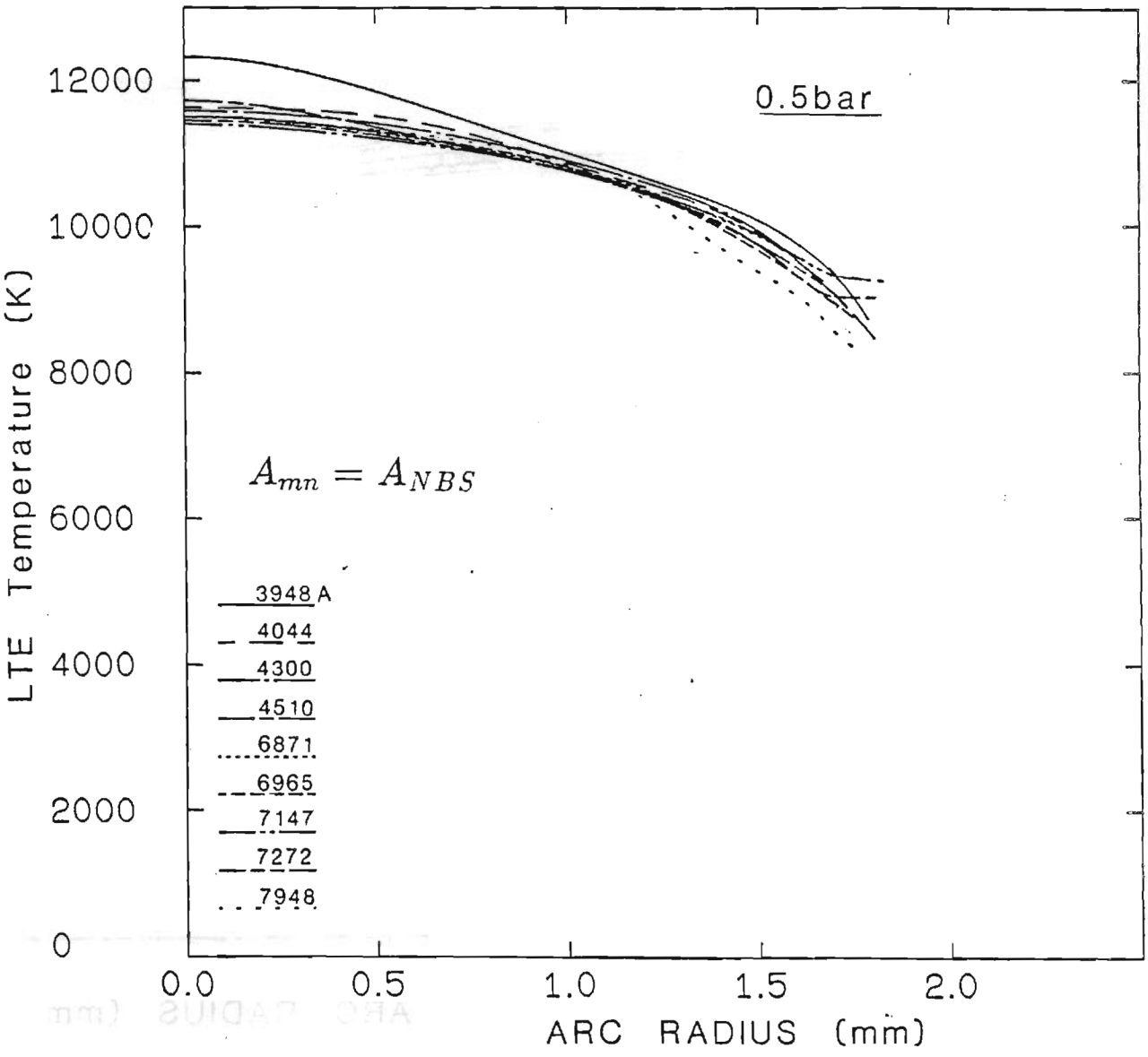

Figure 7.17: Plasma temperature obtained using the LTE diagnostics, p=0.5 bar

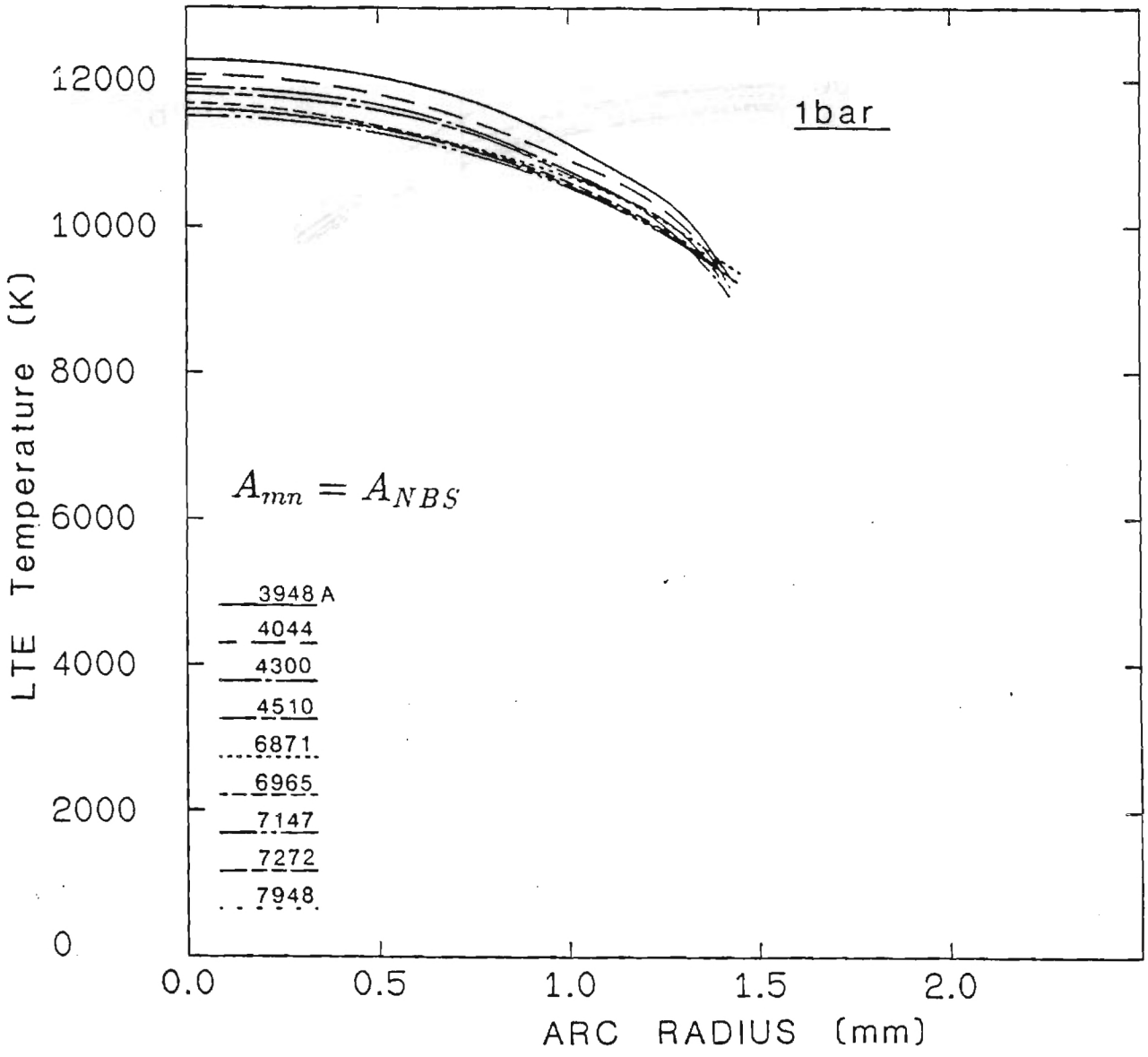

Figure 7.18: Plasma temperature obtained using the LTE diagnostics, p=1 bar

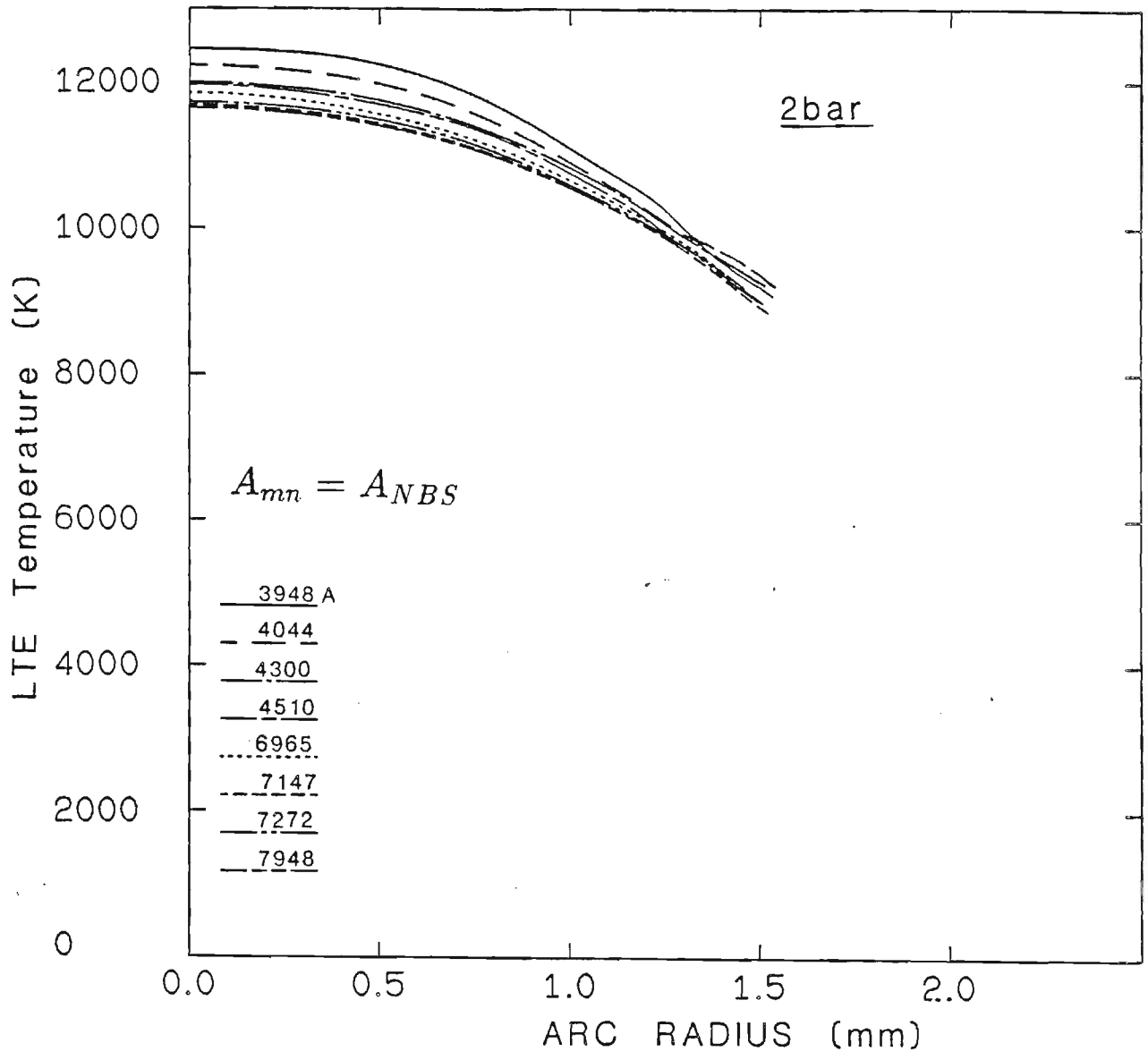

Figure 7.19: Plasma temperature obtained using the LTE diagnostics, p=2 bar

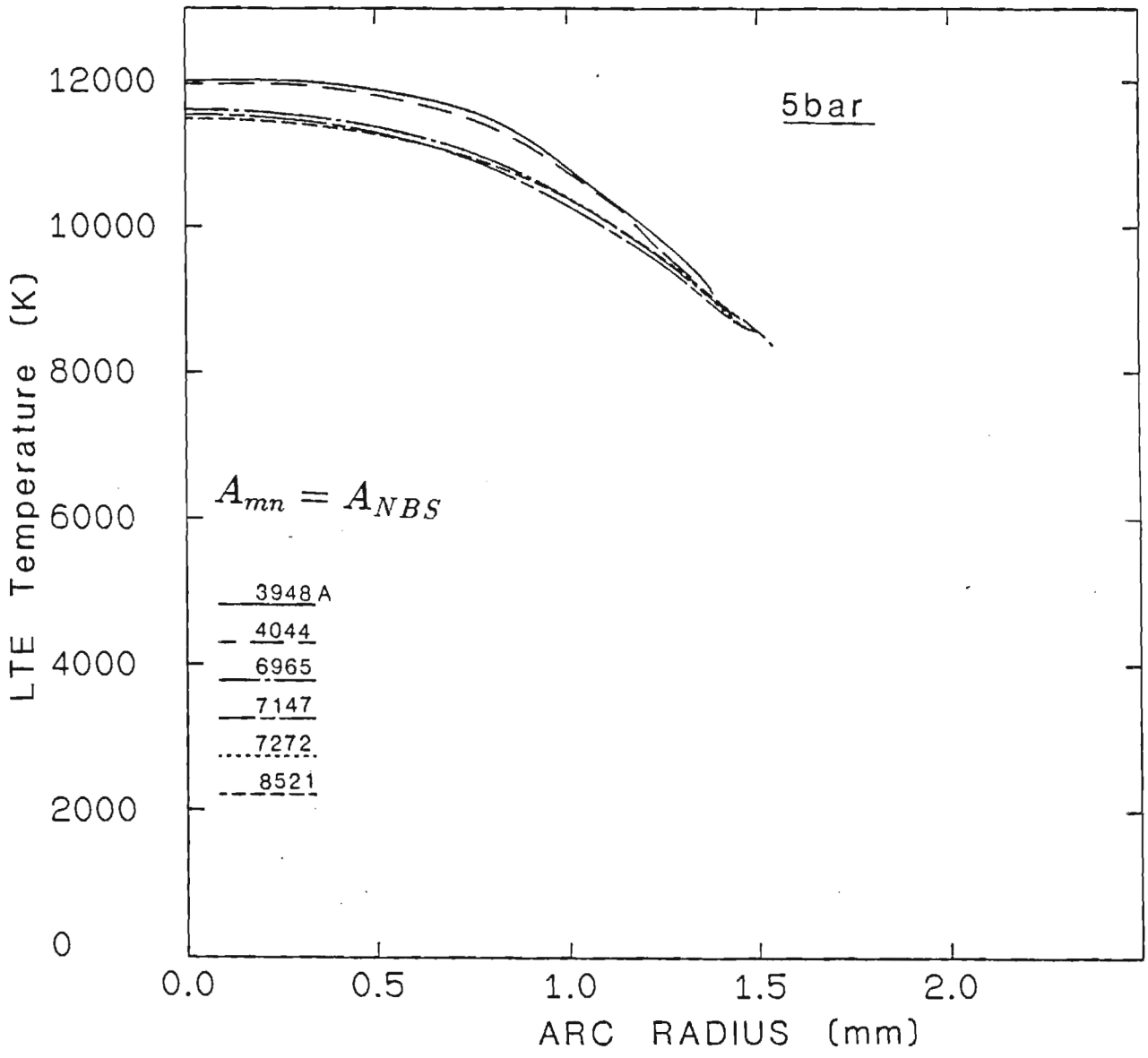

Figure 7.20: Plasma temperature obtained using the LTE diagnostics, p=5 bar

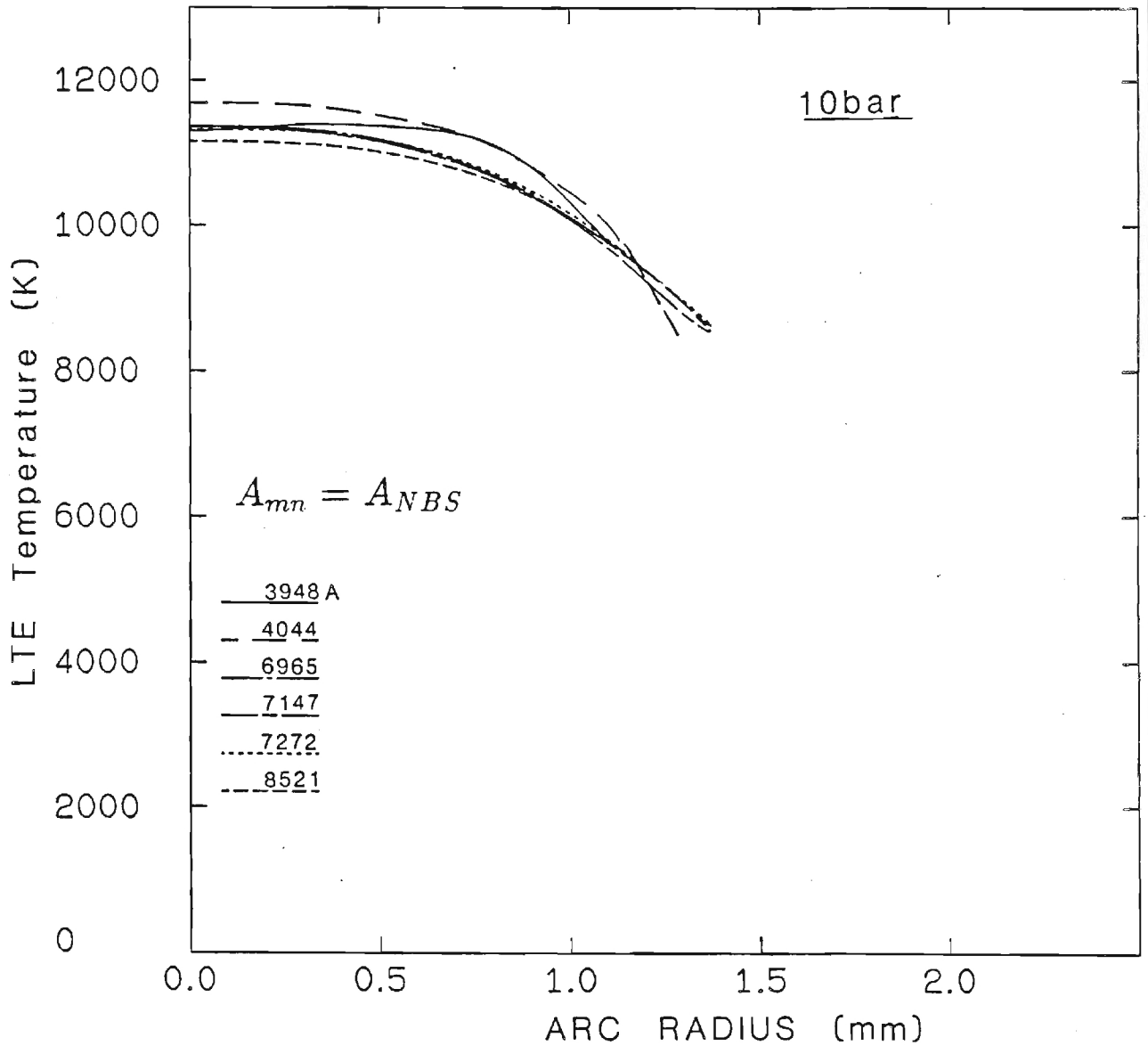

Figure 7.21: Plasma temperature obtained using the LTE diagnostics, p=10 bar

from the Saha equation that a change in T would result in a corresponding change in n_e. Of course, this is only true below the normal (peaking) point where the line emission coefficient has a maximum value. Beyond this point, the electron density remains relatively constant with temperature until the second stage of ionization becomes significant. LTE electron densities range from $6x10^{15}$ cm^{-3} to $2x10^{17}$ cm^{-3} at the centerline.

In both sets of Figures 7.8-7.14 and 7.15-7.21, the increase in arc radius for decreasing pressures is evident. This phenomenon was one of the reasons for deciding against any measurements below 0.1 bar. The arc diameter at 0.05 bar would become as large as three times the channel diameter at the observation port. This expansion at the port violated the assumption of one dimensionality (radial direction) of the analysis.

8.0 RESULTS OF GMTE ANALYSIS

8.1 Electron Density Comparison

Using the line emission coefficient, pressure, electron density, and the field strength, the diagnostics relations presented in Section 6.5 were solved to yield the significant temperatures and densities of the plasma. The NBS transition probability scale [2] was used for these calculations. Fig. 8.1 shown the electron density at the centerline as a function of the pressure. An average LTE electron density for each pressure is also shown and compared to the directly measured n_e, via H_β. It is noticed that the deviation of the two electron densities is about 10-15% which is very close to the combined theoretical and experimental error bound of the two techniques. The $n_{e,LTE}$ is expected to correspond to n_eH_β when LTE prevails and correct atomic parameters are used in the analysis.

8.2 Temperature Determination with $A_{mn}=A_{NBS}$

The various excitation and translational temperatures along with a typical LTE temperature are presented in Figs. 8-2-8.8 for each pressure. In all cases T_{LTE} remains very close to T_{exa}, while the other temperatures vary significantly depending on the pressure. In general,

$$T_{LTE} \simeq T_{exa} > T_e > T_g$$

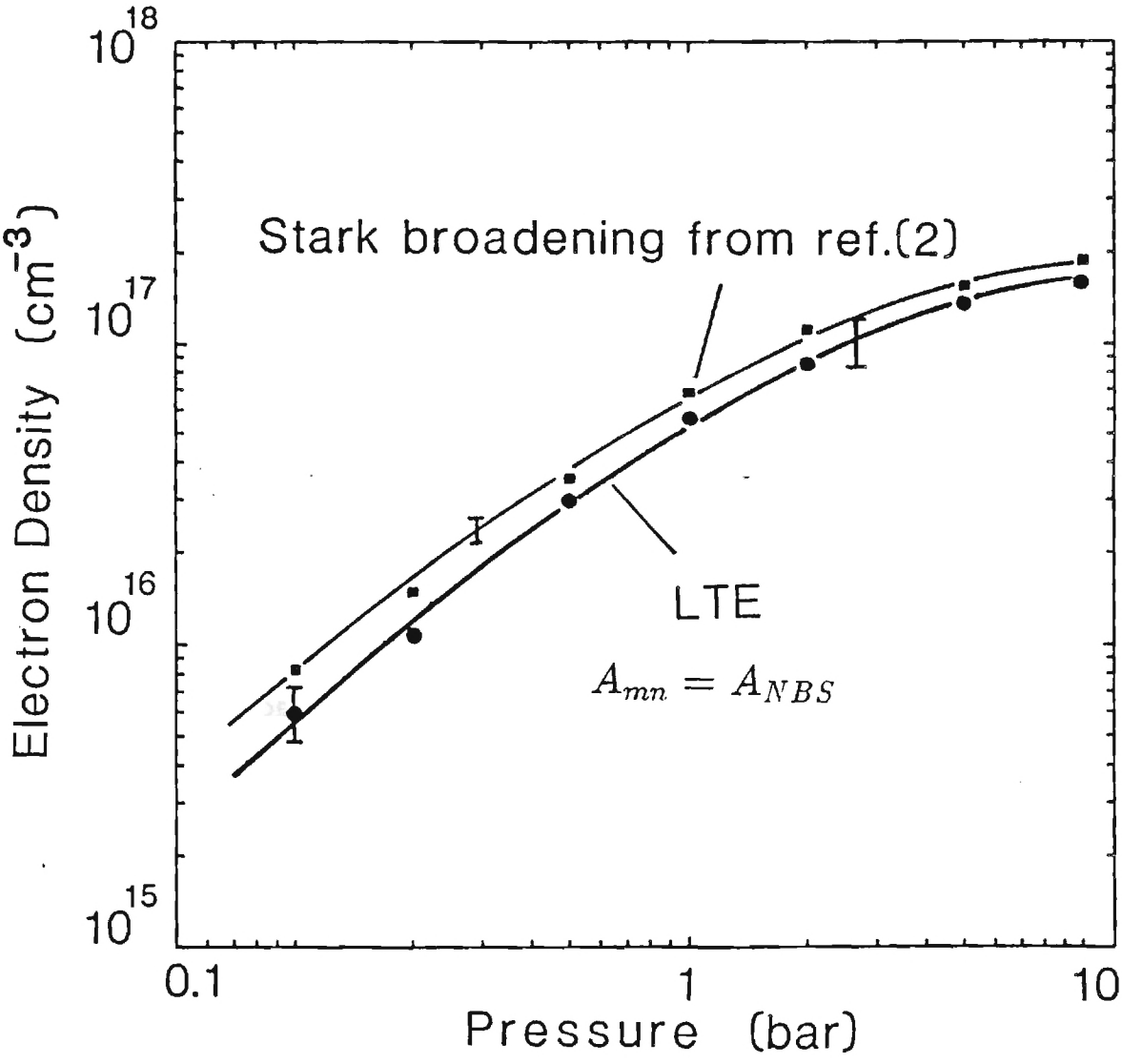

Figure 8.1: Electron density from LTE analysis and from direct measurement of the Stark broadening of the hydrogen H_β as a function of the arc chamber pressure (r=0).

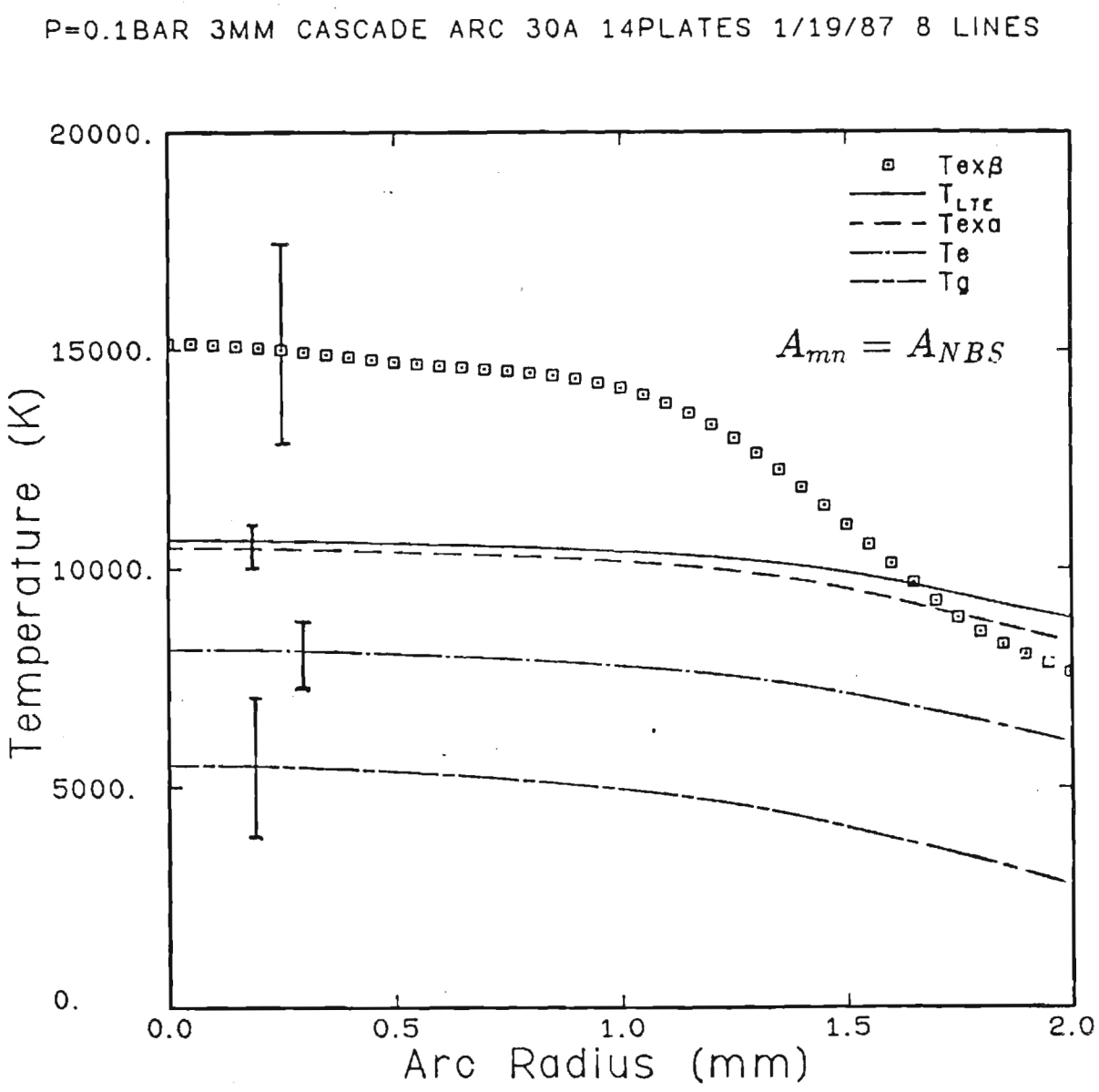

Figure 8.2: Various excitation and kinetic temperatures of the plasma as a function of arc radius, p=0.1 bar

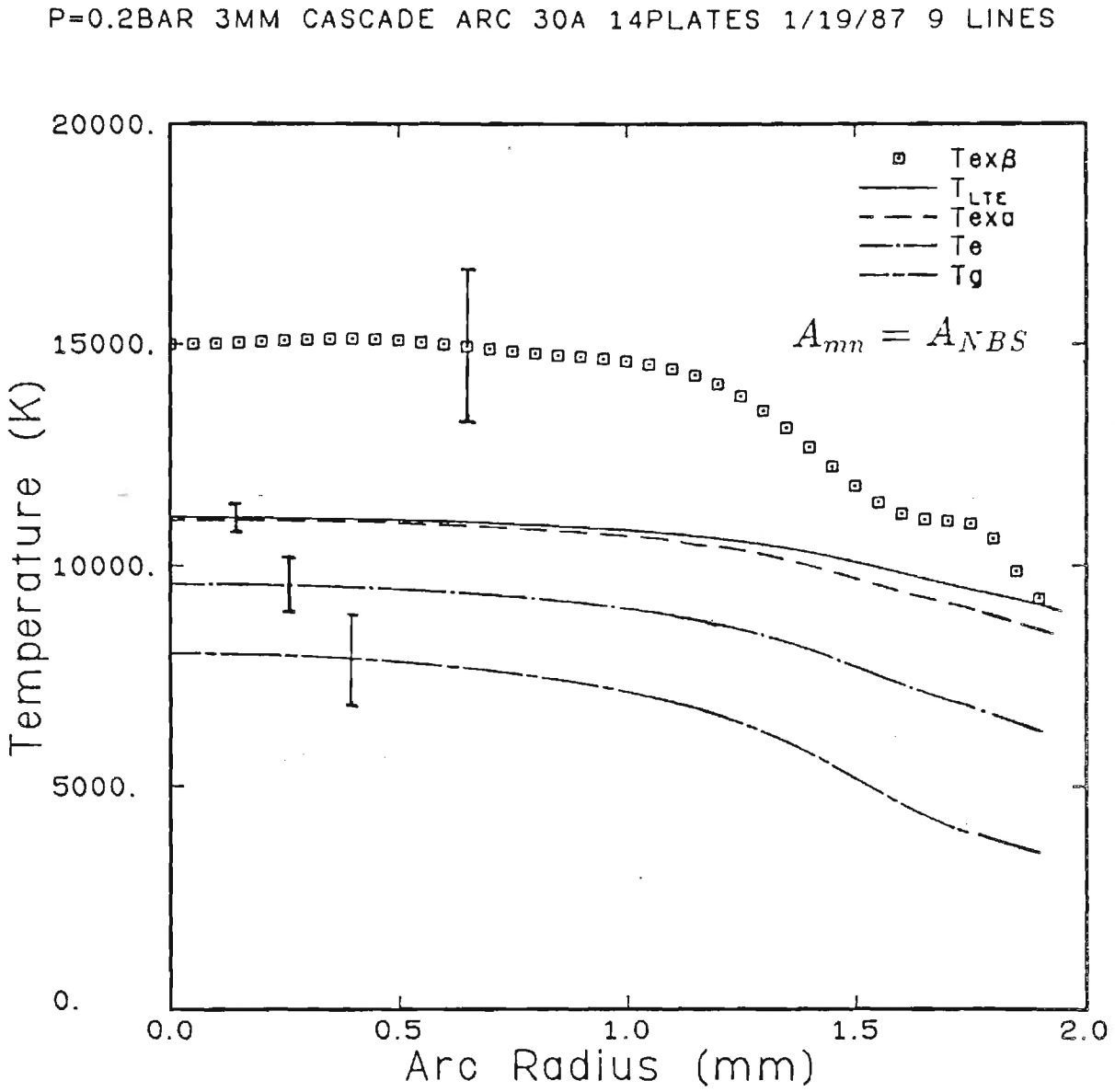

Figure 8.3: Various excitation and kinetic temperatures of the plasma as a function of arc radius, p=0.2 bar

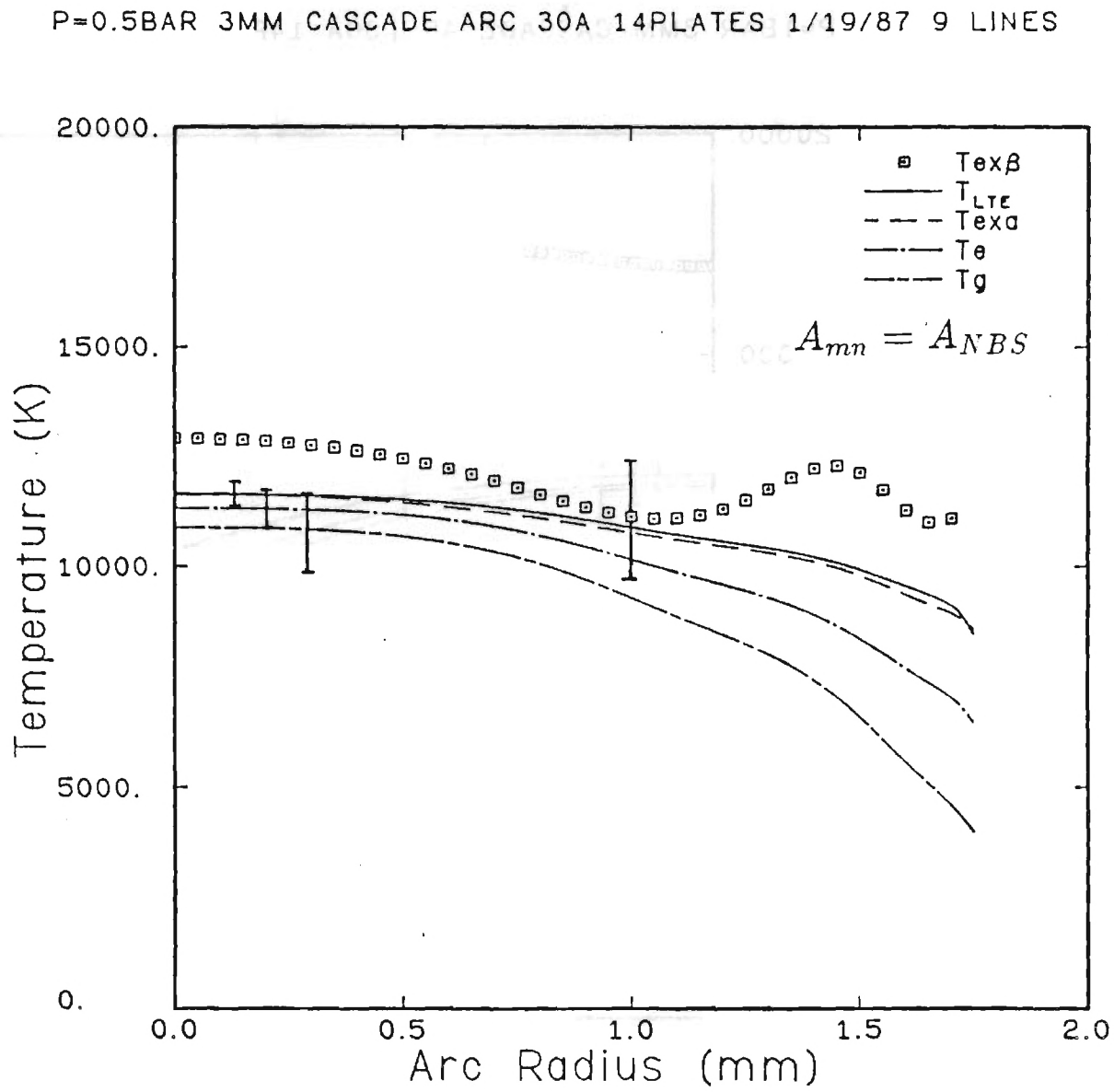

Figure 8.4: Various excitation and kinetic temperatures of the plasma as a function of arc radius, p=0.5 bar

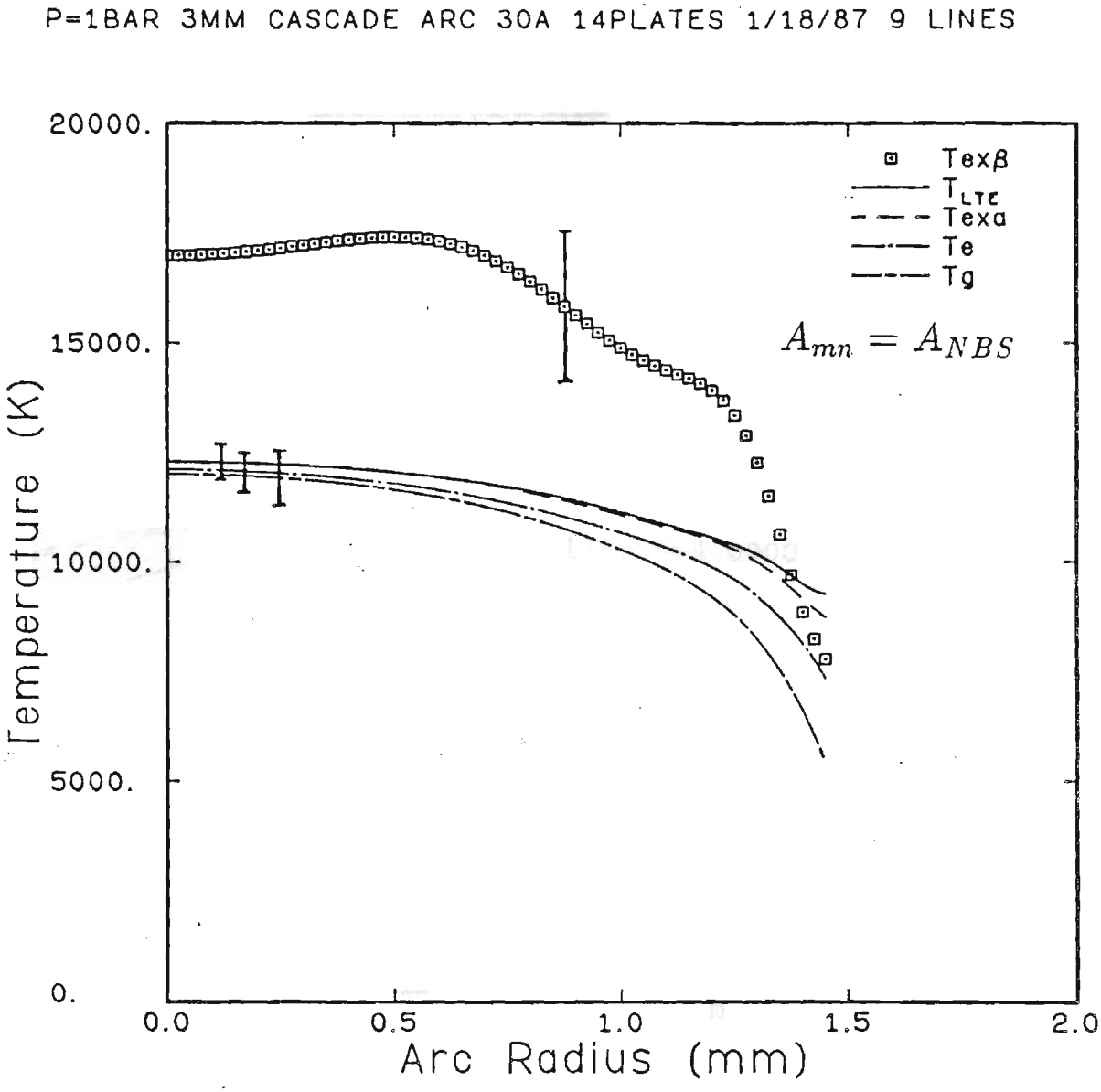

Figure 8.5: Various excitation and kinetic temperatures of the plasma as a function of arc radius, p=1 bar

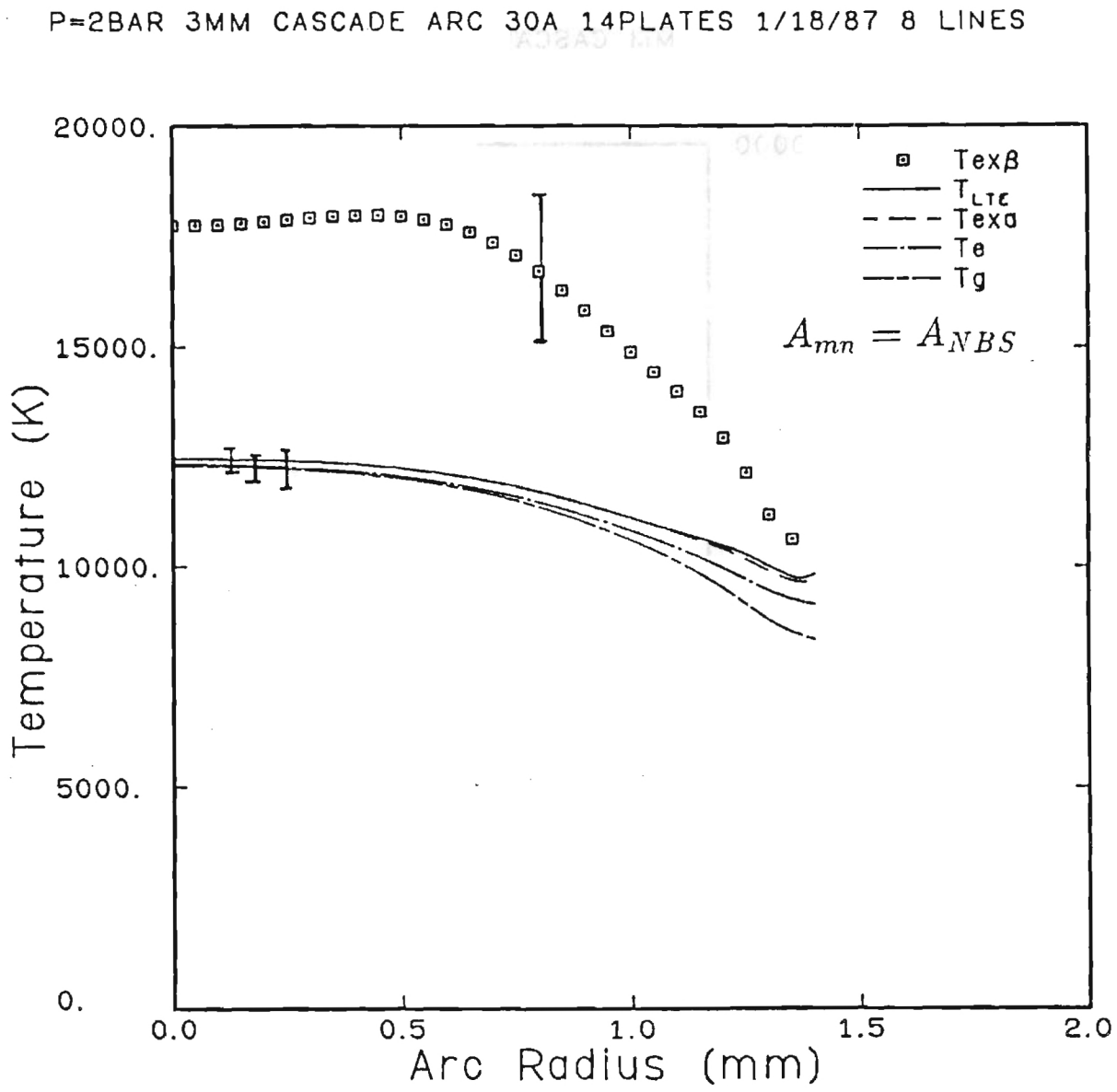

Figure 8.6: Various excitation and kinetic temperatures of the plasma as a function of arc radius, p=2 bar

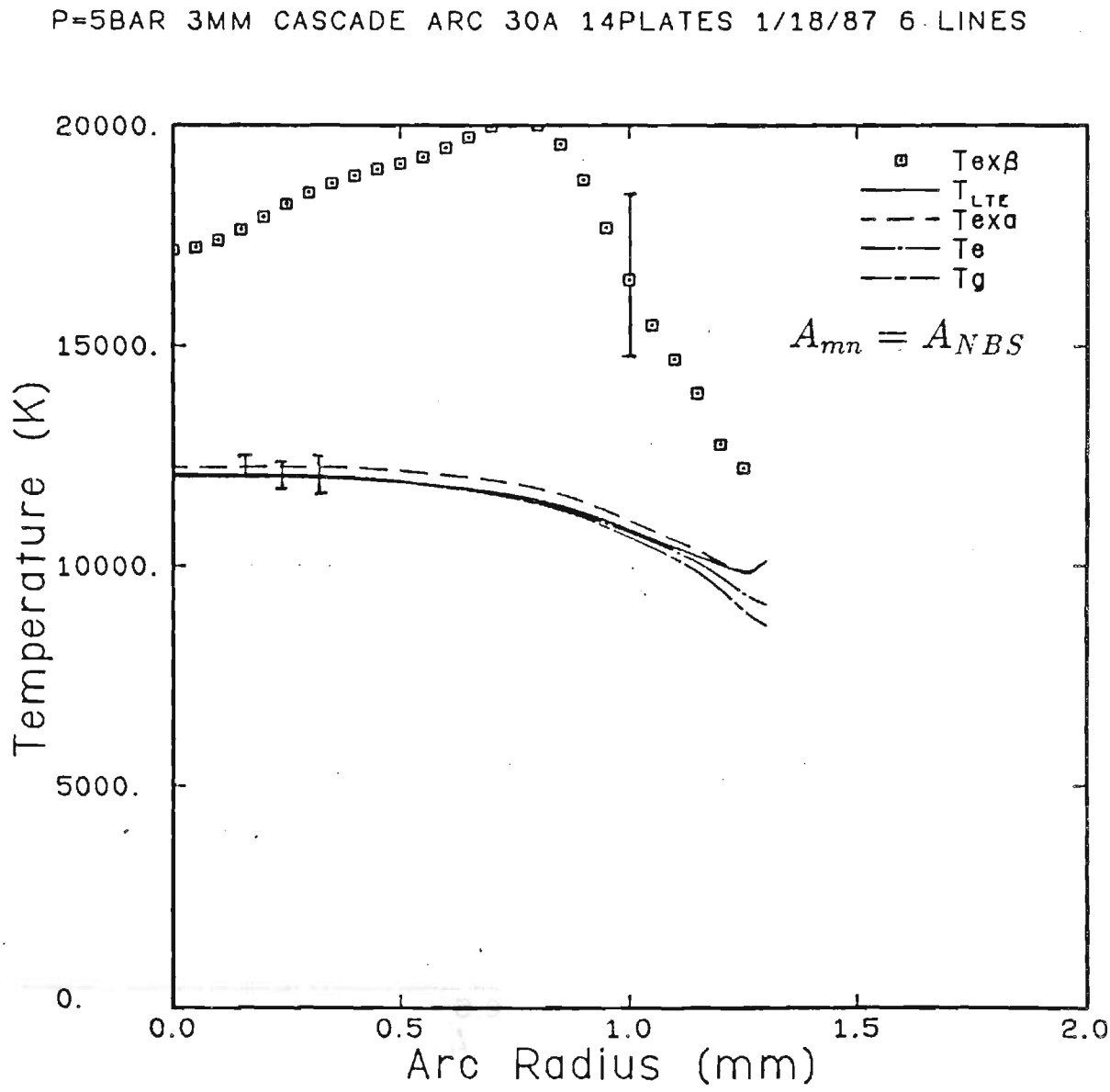

Figure 8.7: Various excitation and kinetic temperatures of the plasma as a function of arc radius, p=5 bar

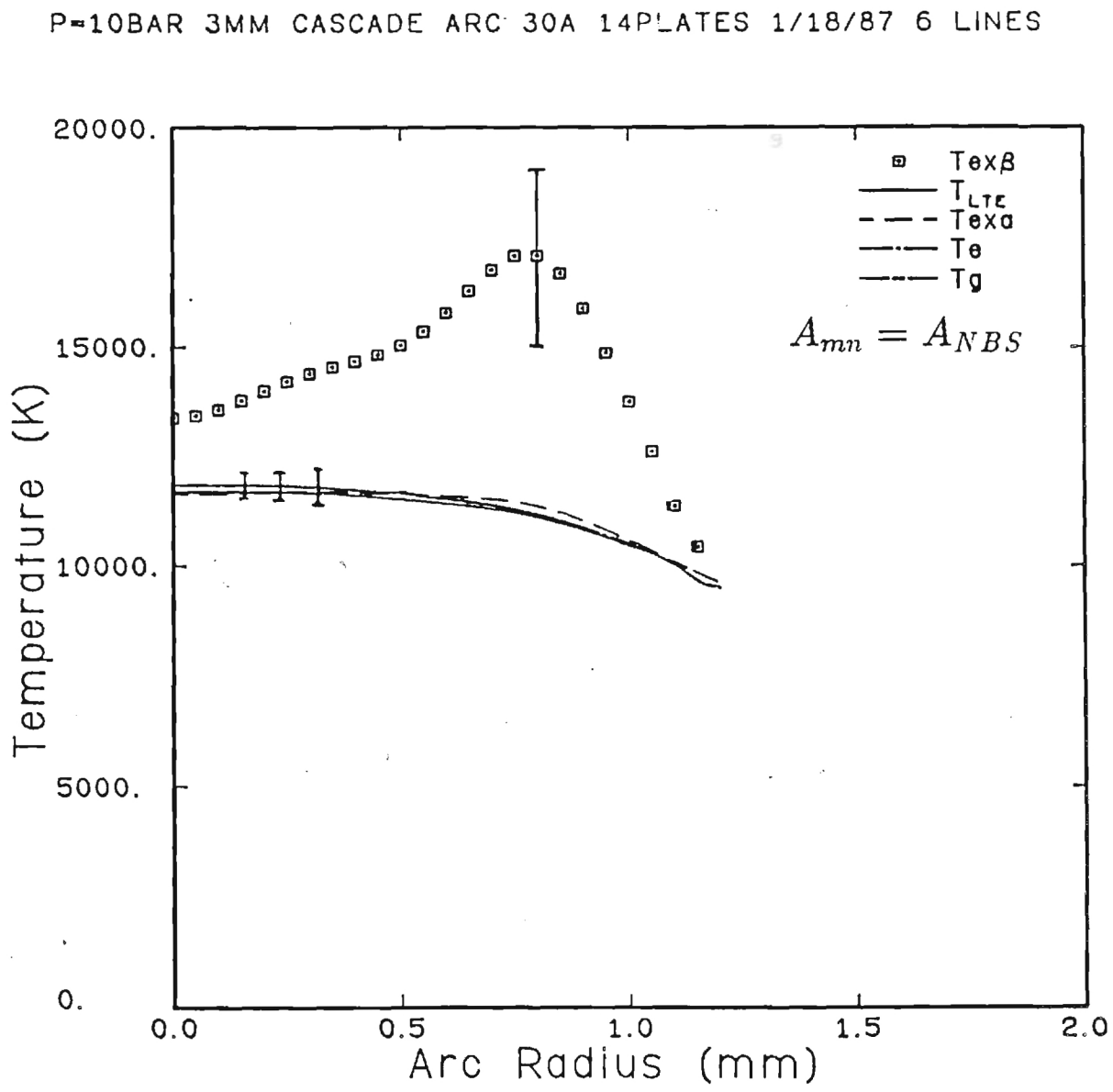

Figure 8.8: Various excitation and kinetic temperatures of the plasma as a function of arc radius, p=10 bar

At 0.1 bar, the gas temperature is about half the excitation temperature, and $T_e \simeq 3/4 T_{exa}$. These differences decrease steadily at higher pressures. The equilibrium conditions extends to larger radii at higher pressures, such that at 5 bar and up, even at the outer edges of the arc LTE seems to prevail (except for $T_{ex\beta}$). The temperatures are relatively insensitive to the transition probability scale used, therefore, these conclusions are valid, even if there is a factor of two difference in the transition probability values. One can presume that LTE exists at pressures as high as five bar which means that $T_{ex\beta}$ should coincide with other temperatures, but as it is evident from these results $T_{ex\beta}$ is almost 50% higher than the other temperatures, which suggests errors in relative values of the transition probability. This may be possible since Wiese et al [2] have used Klose's lifetime measurement date for the red lines (usually emitted from the lower energy levels) and Shumaker and Popenoe's [44] arc data for blue lines (emitted from higher energy levels) to arrive at the final values of the transition probabilities. Normalization of the arc date from each set of lines has also been performed to give agreement with the life-time measurements. In addition, arc experiments have the possible disadvantage of mistakes in line wing corrections, as discussed later, which would give rise to more relative error between the red and the blue lines. The subject of the transition probability will be discussed later in more detail.

8.3 Energy Transport Mechanisms

The electron energy equation was used as one of the diagnostic relations for determining the GMTE plasma parameters. This equation can also be used to demonstrate the relative magnitude of energy transferred to various processes. Figs. 8.9-8.15 show the percentage breakdown at the input field energy into electron-heavy particle collisions (equivalent to heavy particle conduction), electron conduction, continuum radiation, and ambipolar diffusion. The fraction of energy lost through ambipolar diffusion is relatively small in all instances due to the small overall gradients of electron temperature and density in the arc except for the outer edges. The continuum radiation increases markedly at higher pressures such that at 10 bar, almost 70% of the input energy is lost via radiation at

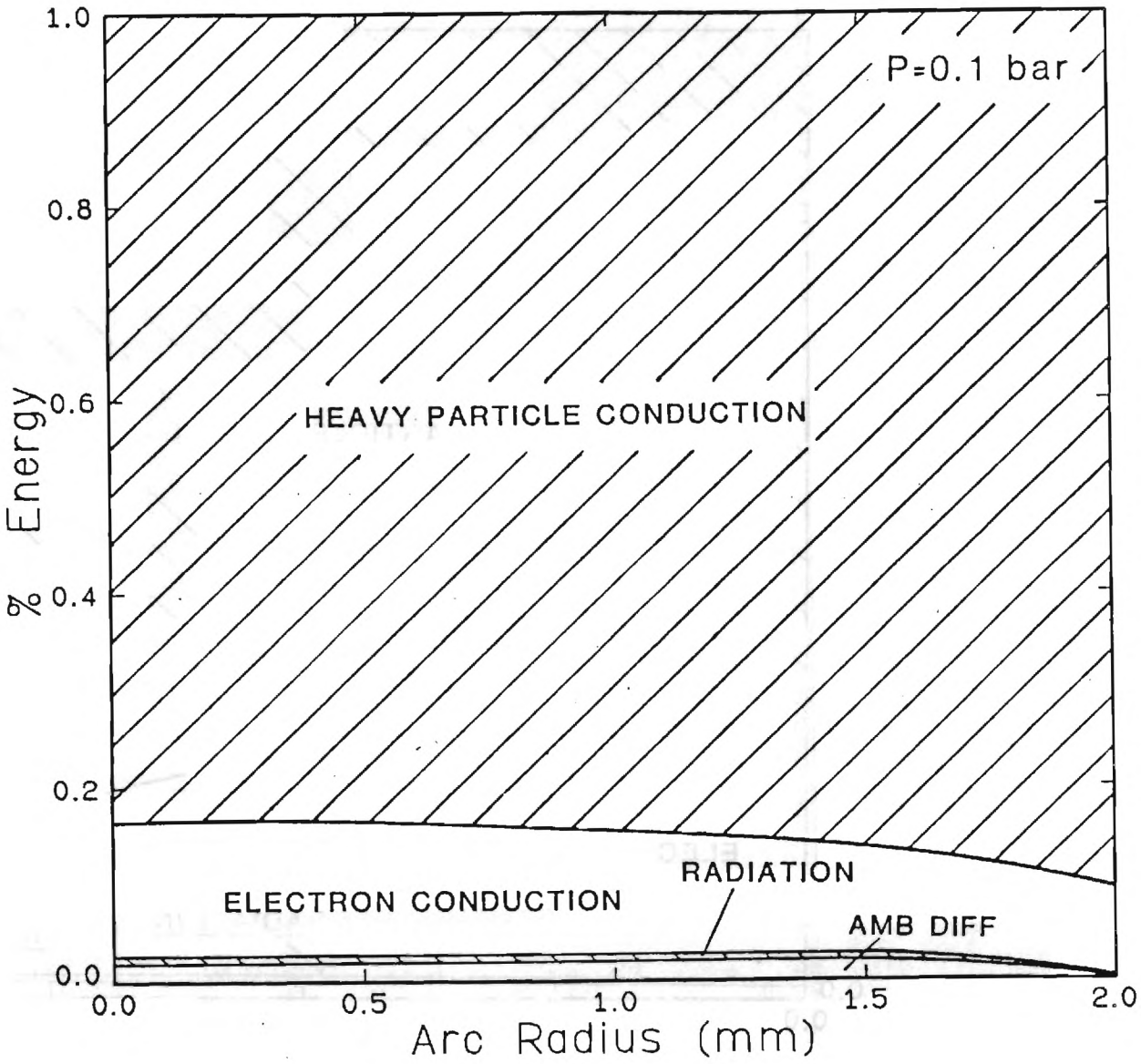

Figure 8.9: Distribution of the electron energy gained from the electric field to various loss mechanisms, p=0.1 bar.

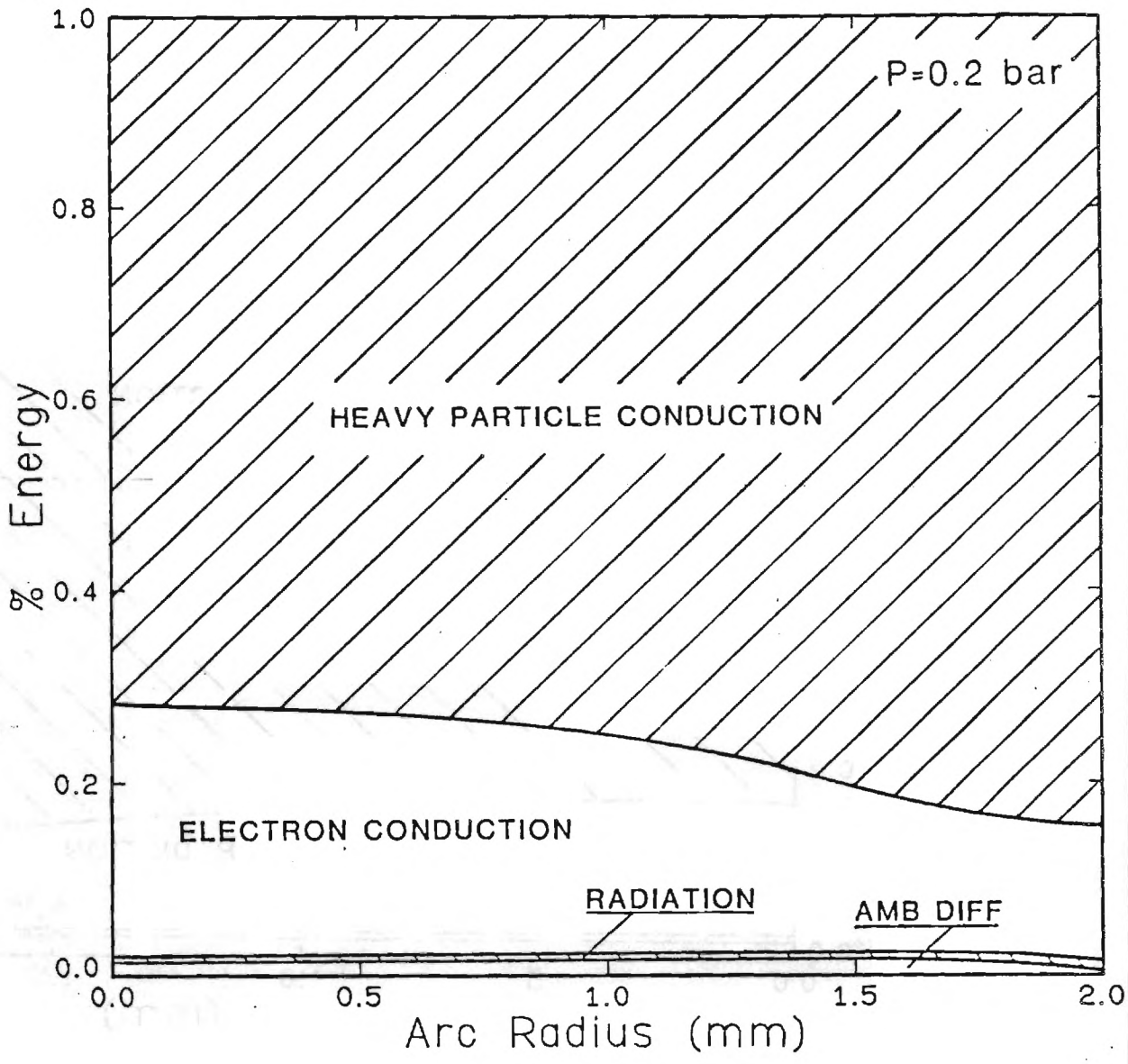

Figure 8.10: Distribution of the electron energy gained from the electric field to various loss mechanisms, p=0.2 bar.

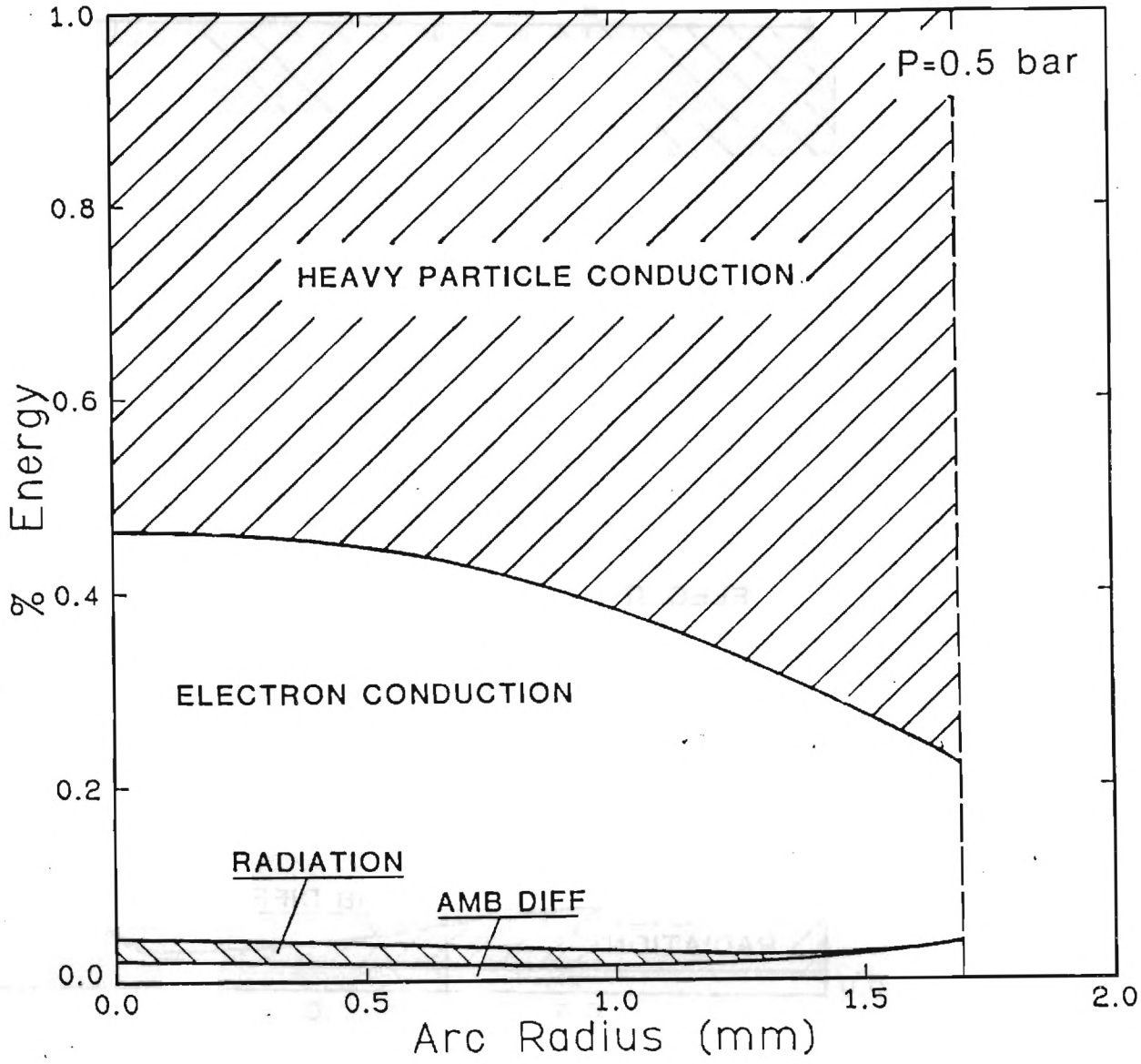

Figure 8.11: Distribution of the electron energy gained from the electric field to various loss mechanisms, p=0.5 bar.

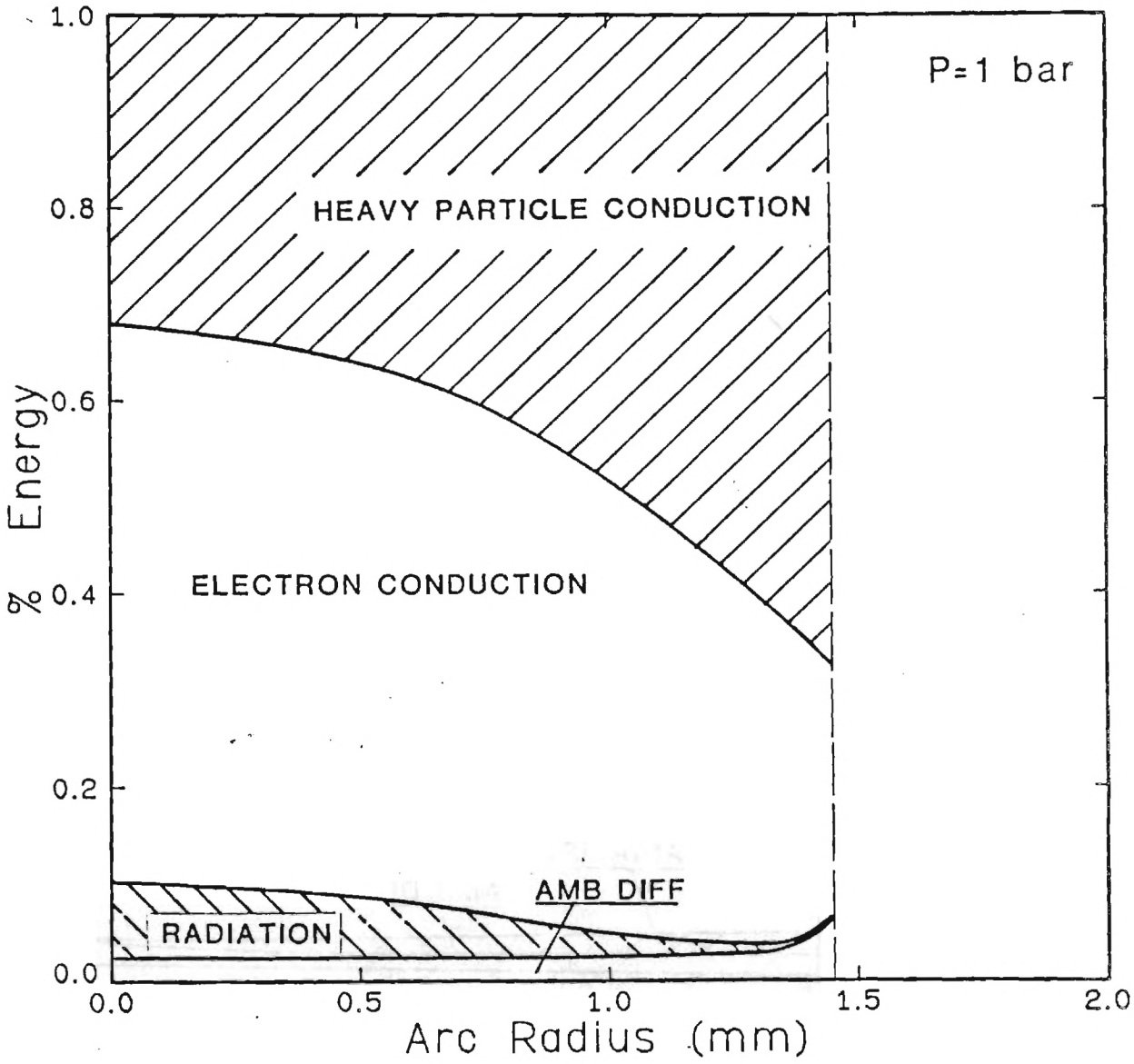

Figure 8.12: Distribution of the electron energy gained from the electric field to various loss mechanisms, p=1 bar.

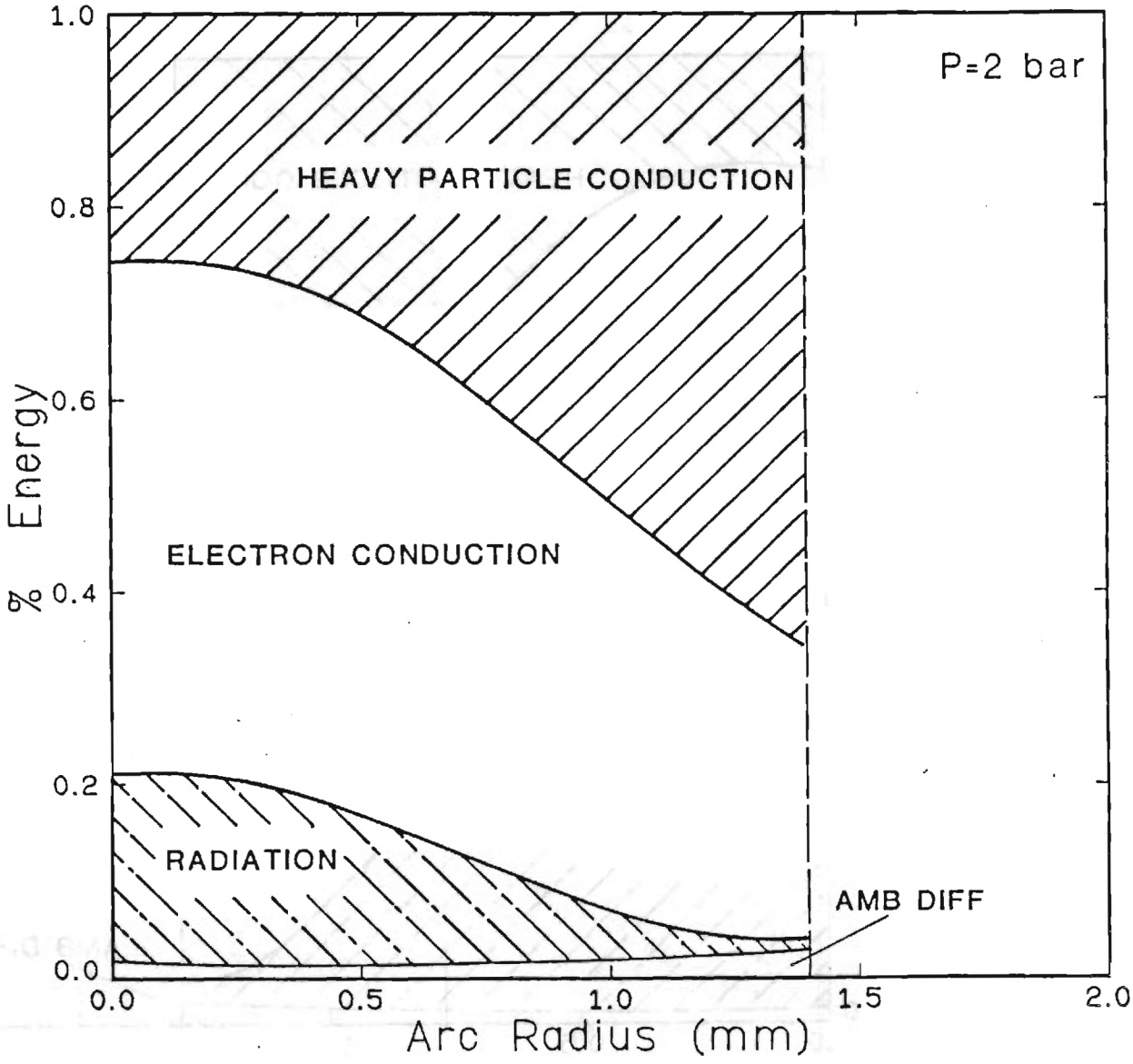

Figure 8.13: Distribution of the electron energy gained from the electric field to various loss mechanisms, p=2 bar.

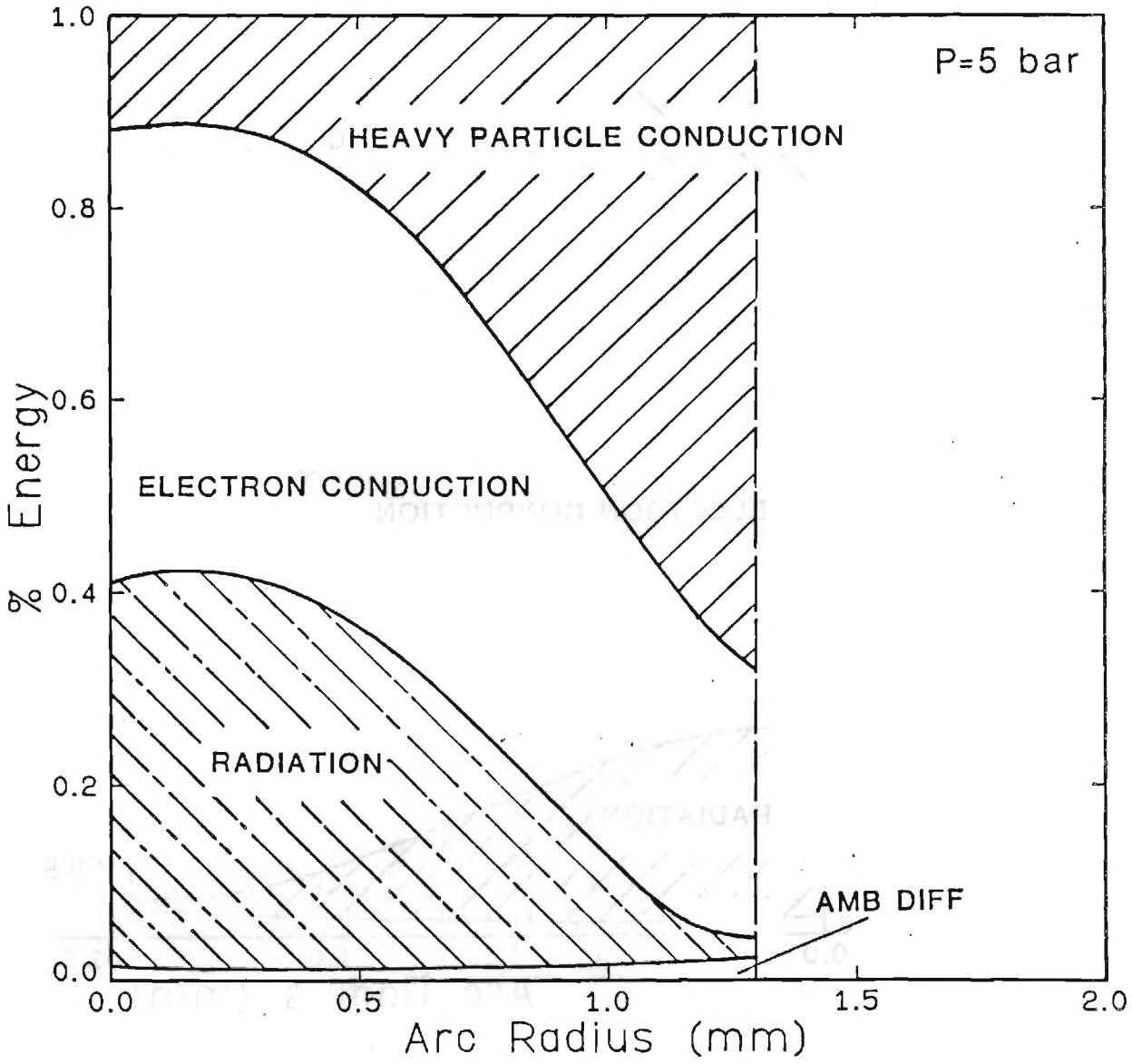

Figure 8.14: Distribution of the electron energy gained from the electric field to various loss mechanisms, p=5 bar.

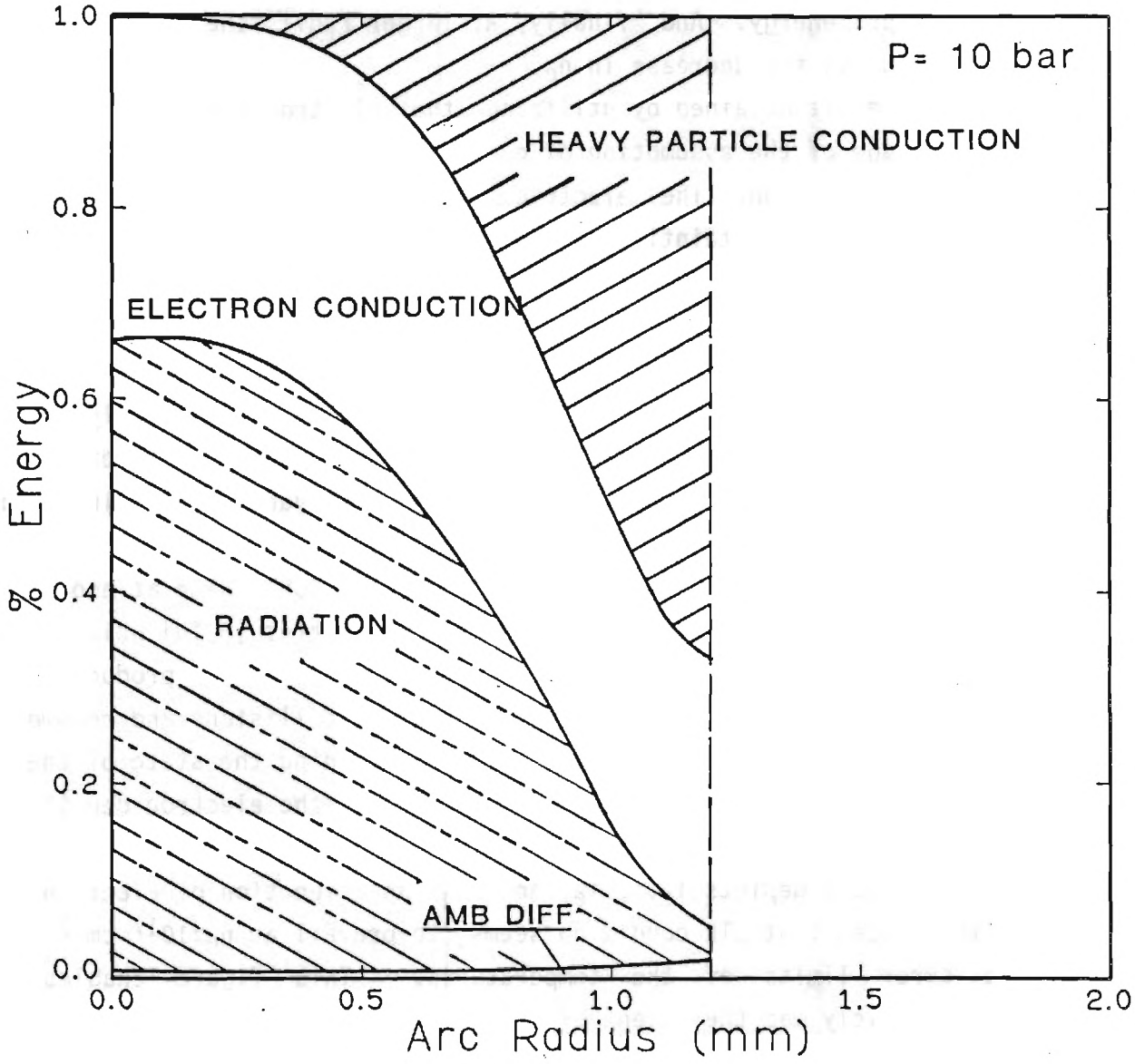

Figure 8.15: Distribution of the electron energy gained from the electric field to various loss mechanisms, p=10 bar.

r = 0. At higher pressures, electron-heavy particle tranlational equilibration occurs; hence, $T_e \simeq T_g$. Electron conduction is a function of both the electron conductivity and the electron temperature gradient. Since electron temperature variation as a function of pressure is only about 20%, the energy loss through electron conduction stays constant at about 20-30% of the input energy. And finally, at larger radii, the radiation decreases rapidly due to the decrease in n_e.

The result obtained by utilizing the electron energy equation has the disadvantage of the assumption of constant electric field strength, E, at a given cross section. The electric field may vary at larger radii, giving rise to larger uncertainties in the temperature and density determination at these regions.

8.4 T-p and T-n_e Plots with $A_{mn}=A_{NBS}$

The results of this set of experiments can be more fully appreciated when various temperatures are plotted against the operating pressure. The resulting T-p plot, Fig. 8.16 has the unique advantage of illustrating the extent of nonequilibrium as well as the onset of the LTE. At R - 0, various temperatures (except for $T_{ex\beta}$) approach a common value at about 2-5 bar. This is consistent with many studies of argon arcs [8,10] which argue that LTE exists at $p > 1$ bar. The same type of plots can be produced for radii other than r = 0, Fig. 8.17. Since electron collisions and recombinations are responsible for most of the processes governing the state of the plasma, the various temperatures may be plotted against the electron density to show the entire range of pressures and densities.

Fig. 8.18 depicts T_{exa}, T_e, and T_g as a function of electron density. It is noticed that LTE condition seems to prevail at $n_e \simeq 10^{17}$ cm^{-3} to within the error limits of the temperatures. This figure enables one to quantitatively map the extent of non-LTE.

8.5 The Determination of Improved A_{mn} Values

Assuming LTE, the values of transition probabilities can now be calculated for all the measured lines as a function of pressure to demonstrate their deviation from the values given by NBS. Fig. 8.19 shows the ratio of the calculated A_{mn} to those of NBS. It was originally expected that if any deviation existed between the new values and those by NBS, the

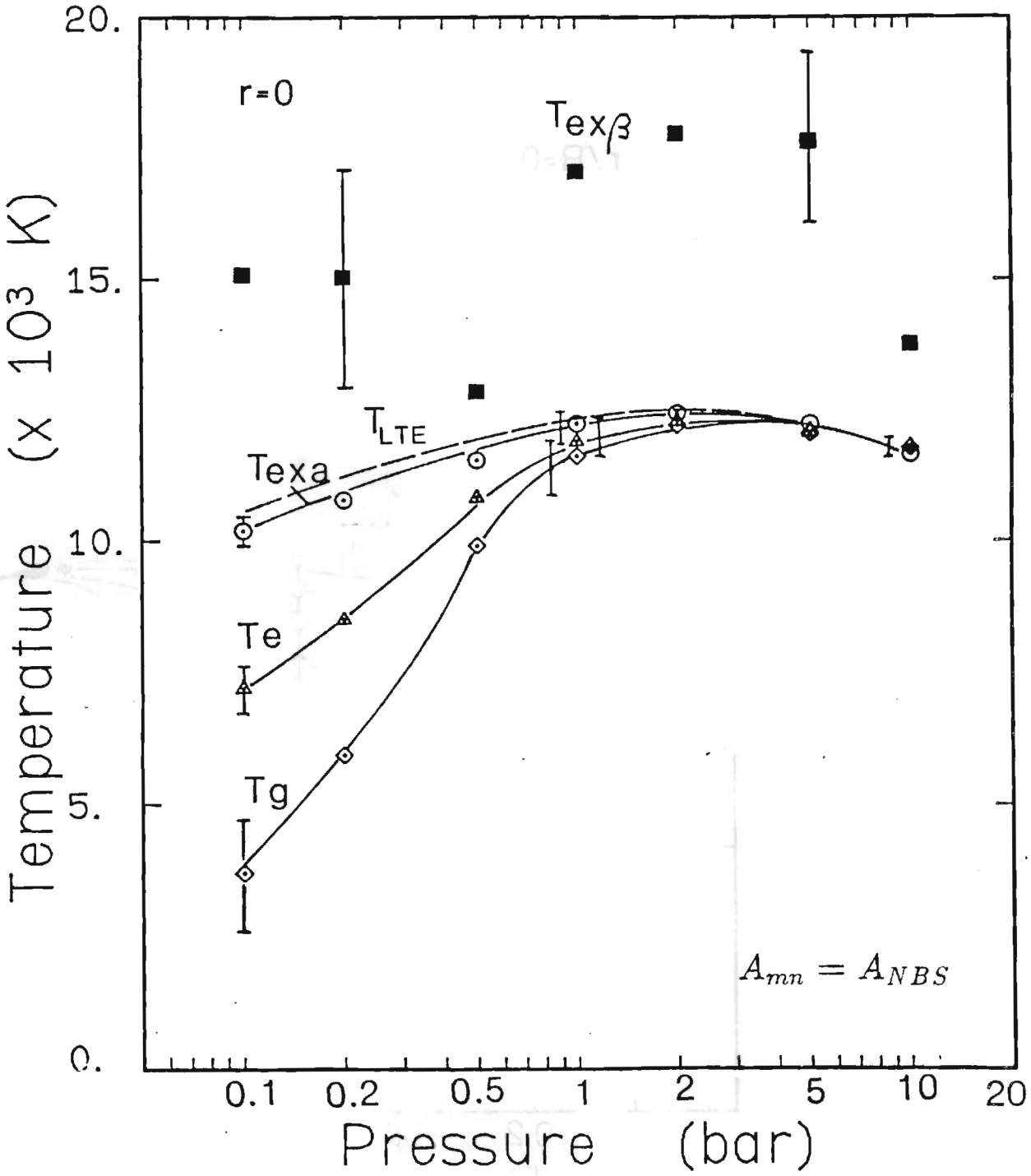

Figure 8.16: T-p plot: various excitation and kinetic temperatures as a function of pressure, r/R=0.

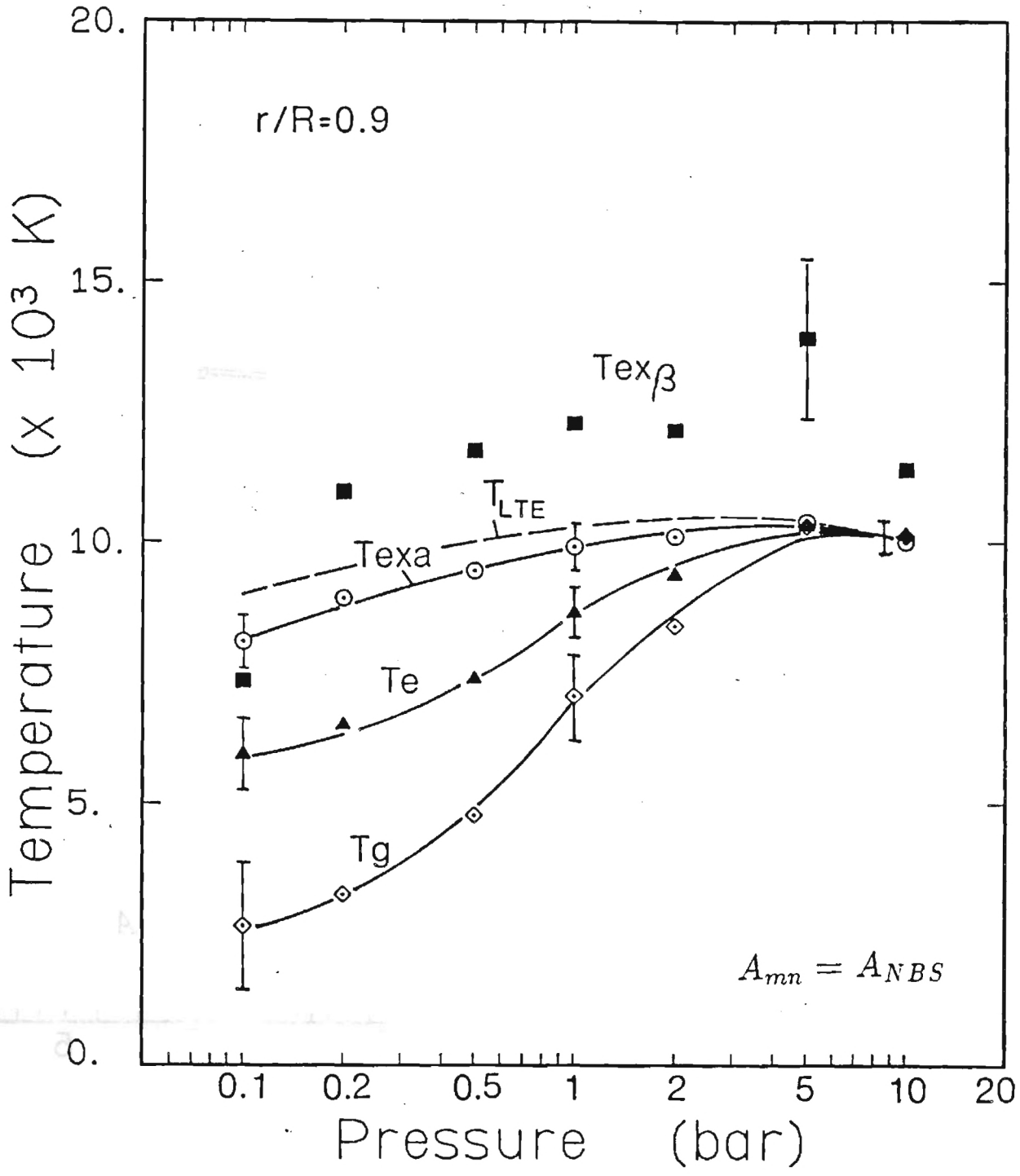

Figure 8.17: T-p plot: various excitation and kinetic temperatures as a function of pressure, r/R=0.9.

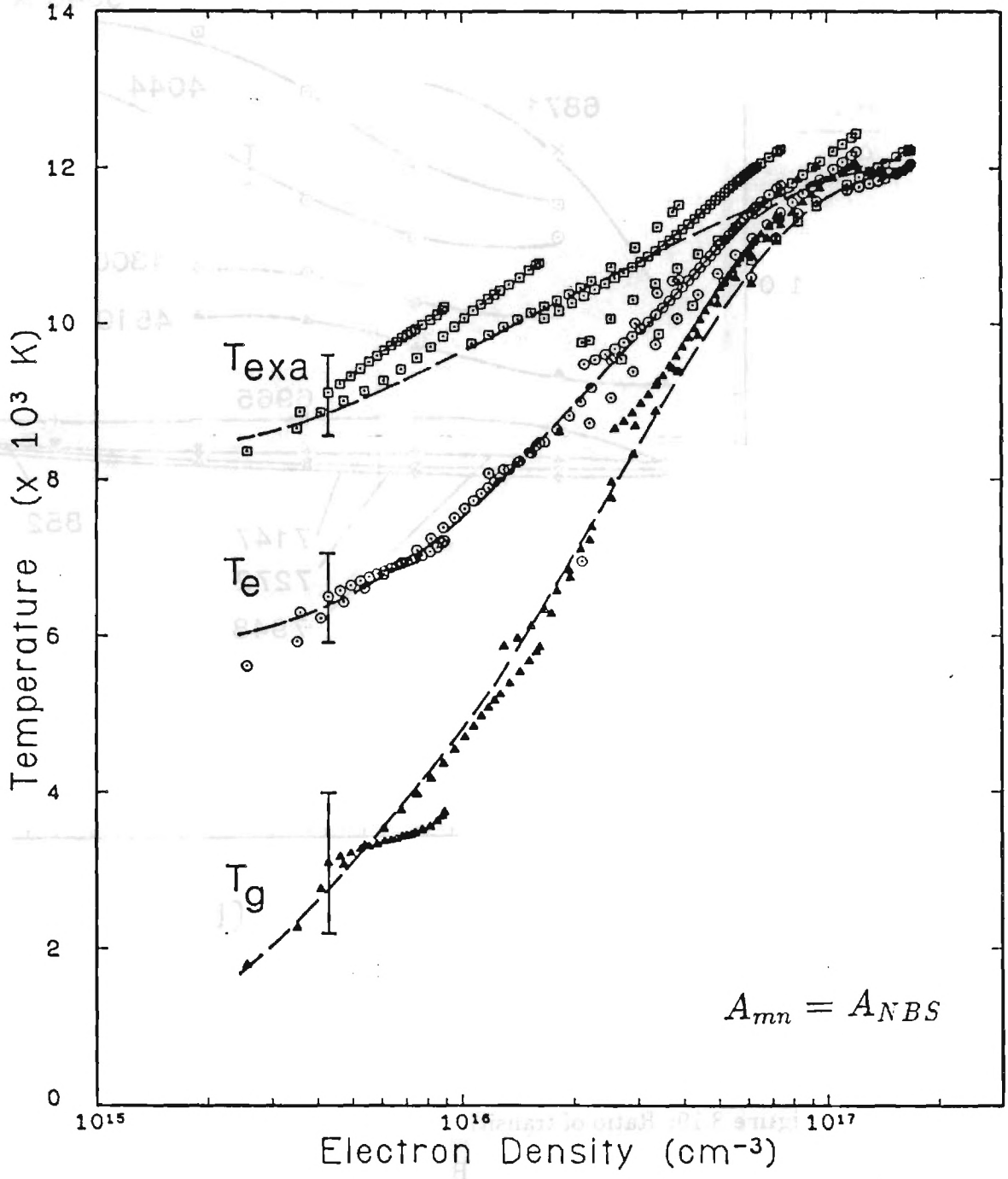

Figure 8.18: T-n_e plot: various excitation and kinetic temperatures as a function of electron density for all pressures and radii.

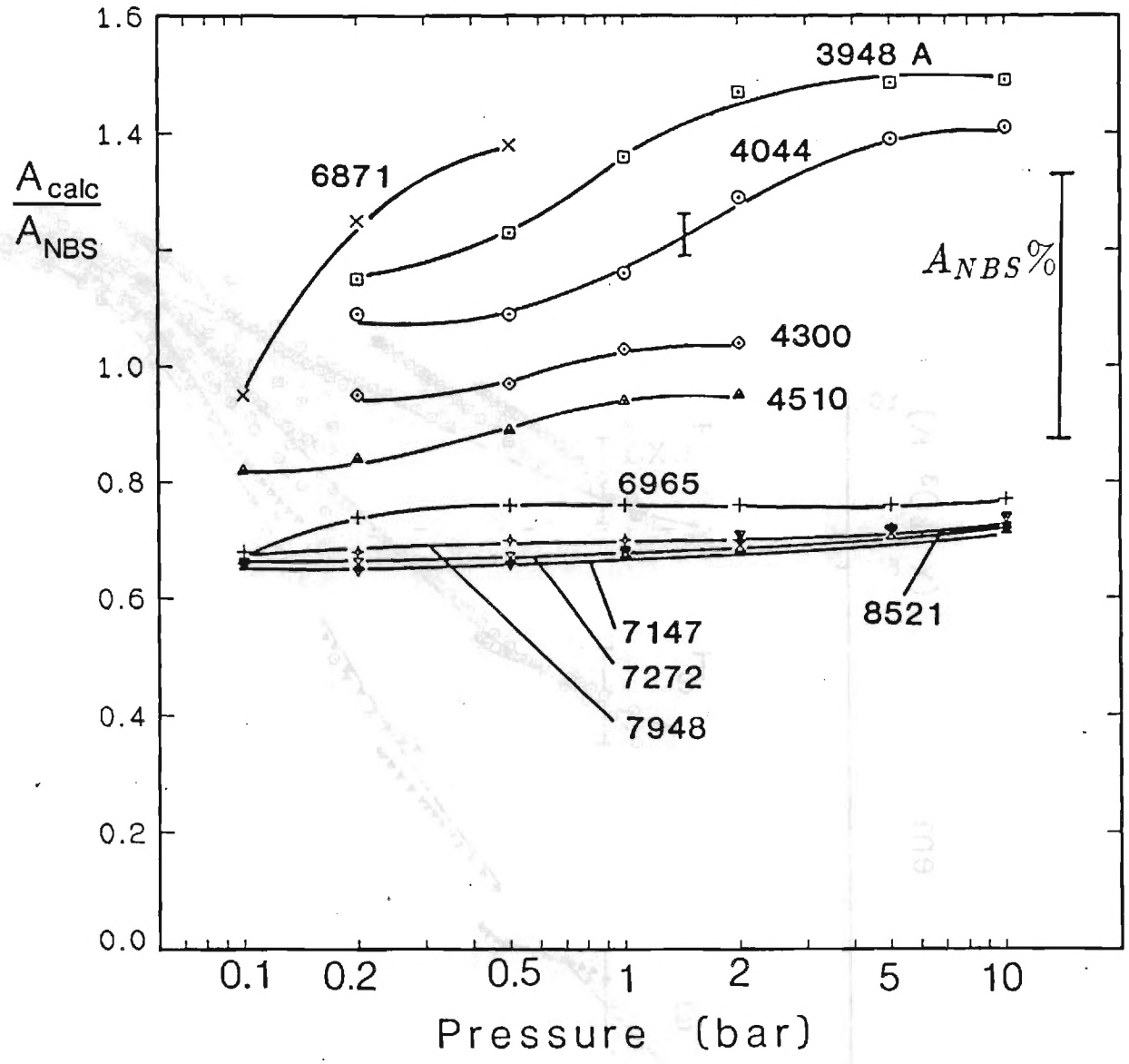

Figure 8.19: Ratio of transition probabilities obtained in this work to those of NBS for all the measured lines. NBS values have been corrected for H_β parameters as suggested by ref. [5].

deviation would be a constant factor for all the lines. In other words, the entire scale would be off by a certain percentage. Surprisingly, the deviation of A_{cal}/A_{NBS} was totally energy level dependent with transitions from low levels grouping at about 30% below the A_{NBS}, medium levels at about same values as the A_{NBS}, and high levels almost 30% higher than the A_{NBS}. Error limits include the experimental errors plus the theoretical uncertainties associated with the electron density determination. The uncertainly bound given for $A_{mn,NBS}$ is also shown on the right side of Fig. 8.19.

After studying all the probable causes for this energy level dependence, conclusion was drawn that the assumption of LTE in the analysis of non-LTE arc experiments may have significantly contributed to this behavior. Notice that the transition probabilities for ArI 4300 is in fairly good agreement with that of NBS. If the test arc plasma deviates from LTE, the ground state will be overpopulated with respect to the excited levels. Now, if one takes the ArI 4300 as the reference energy level, lines with higher upper energy levels will be overpopulated with respect to their LTE values and lines with low upper energy levels will be underpopulated with respect to their LTE values. This in turn translates to smaller than actual vales of A_{mn} for high level lines and larger than actual vales of A_{mn} for low level lines. This means that the correct values of the transition probabilities are their asymptotic limit at high pressures (or electron densities). These new values have been determined and compared to the NBS values and those given by Wende [47] in Table 8.1. The uncertainty quoted for the NBS transition probabilities used here are 25% which is an indication of the scatter in the values of the various authors and is usually two to three times larger than the errors given by each author. The errors associated with the new values take into account the experimental and the H_β broadening errors.

The new values of transition probabilities are obtained by precise line emission measurements with average experimental error of about 2%. The electron densities are corrected by the 2-λ interometric scale which reduces the theoretical errors of determining H_β line width to about 1%. Using the new values, the T-p plot at r = 0 can be redrawn to show the more accurate picture of the deviation from LTE, Fig. 8.20. Since at the true LTE

Table 8.1: Transition probabilities obtained in this work compared to those given by NBS [99] and Wende [47] for prominent neutral argon lines.

Wavelength	*Transition probability* $(\times 10^7) sec^{-1}$				
(Å)	NSRDS-NBS-22	Wende	This work	$\Delta_{NBS}\%$	$\Delta_{Wende}\%$
3948	$0.0467 \pm 25\%$	$0.035 \pm 23\%$	$0.0595 \pm 5\%$	27	71
4044	$0.0346 \pm 25\%$	$0.028 \pm 23\%$	$0.0419 \pm 5\%$	21	50
4300	$0.0394 \pm 25\%$	$0.031 \pm 18\%$	$0.0346 \pm 6\%$	-12	13
4510	$0.123 \pm 25\%$	$0.10 \pm 18\%$	$0.1157 \pm 6\%$	-6	16
6871	$0.290 \pm 25\%$	—	$0.2327 \pm 5\%$	-20	—
6965	$0.67 \pm 25\%$	—	$0.4430 \pm 4\%$	-34	—
7147	$0.065 \pm 25\%$	—	$0.0409 \pm 4\%$	-37	—
7272	$0.200 \pm 25\%$	—	$0.1328 \pm 4\%$	-34	—
7948	$1.96 \pm 25\%$	—	$1.22 \pm 5\%$	-38	—
8521	$1.47 \pm 25\%$	—	$0.9114 \pm 5\%$	-38	—

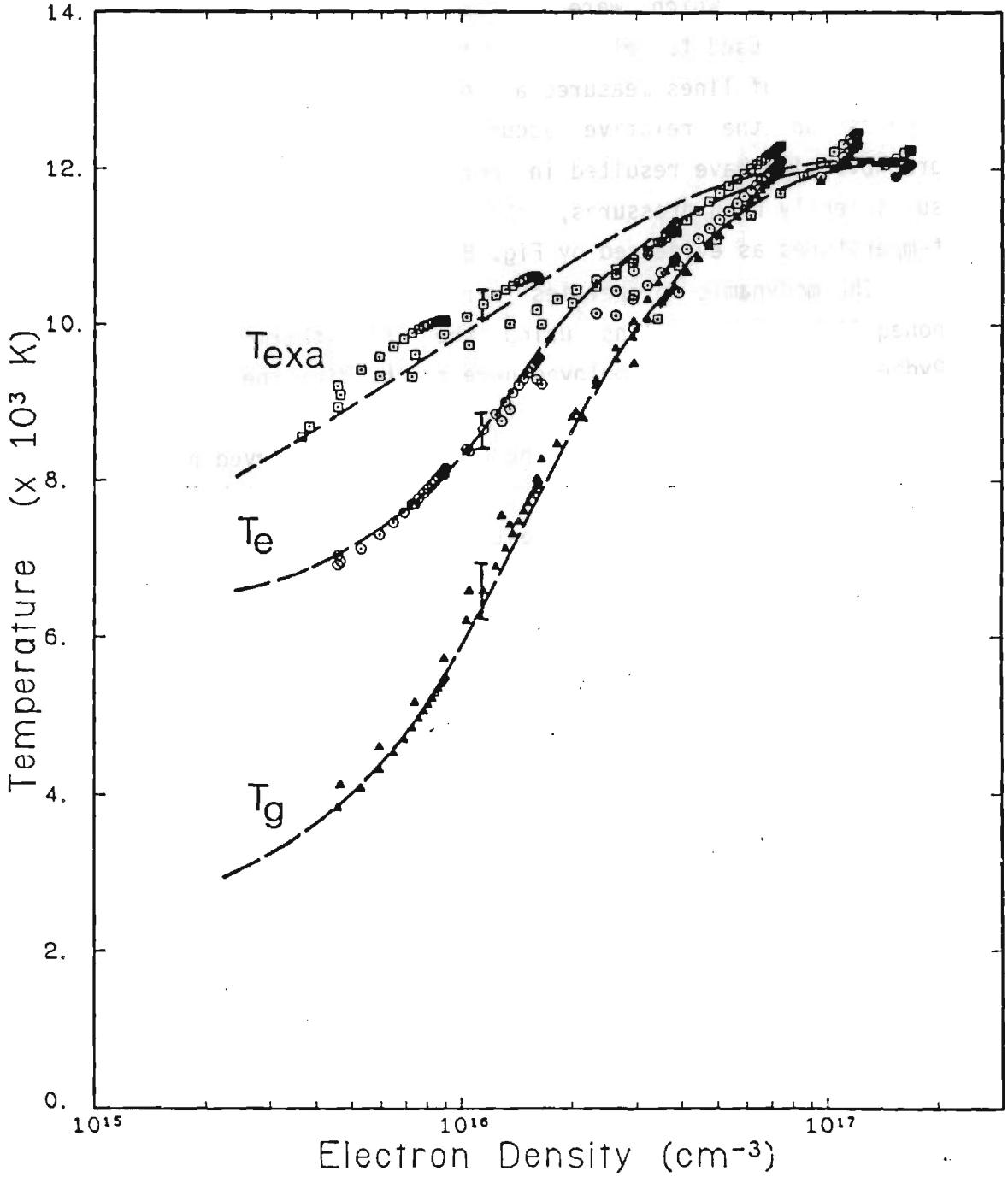

Figure 8.21: T–n_e plot: using the accurate transition probabitities obtained in this work

The correction from the $A_{mn,NBS}$ values was a strong function of upper energy level of the corresponding transition, which suggests that various arc experimental data used in compilation of ref. [2] were obtained in non-LTE conditions.

For lines which were not measured at higher pressures, Boltzmann factors were used to relate their transition probabilities to the transition probability of lines measured at $p \geq 5$ bar. The accuracy of this technique depends on the relative accuracy of the $T_{ex\beta}$. The new transition probabilities have resulted in more accurate values of $T_{ex\beta}$, so that at sufficiently high pressures, this temperature corresponds to other plasma temperatures as evidenced by Fig. 8.20.

Thermodynamic properties were generated for various pressures and nonequilibrium conditions using the GMTE thermodynamic relations. The Rydberg-Ritz relation employed here to predict the unobserved energy levels of argon neutral and the first four ions for argon, gave results which were in very good agreement with the available observed high energy levels (to within 1%).

Finally, we can make an estimate of the appropriate value of the ξ_{fb} scale based on the new A_{mn} values. Most LTE temperatures in previous high pressure continuum experiments were determined from lines involving lower level transitions. If these A_{mn} are corrected by -37% as per Table 8.1, experimentally determined ξ_{fb} values in Fig. 2.9 would decrease almost identically. This is almost equal to the factor of 0.50 to get very good agreement between experimental and theoretical ξ_{fb} values. This provides additional support to results obtained and eliminates the contradiction discussed in Chapter 2 and is well within the experimental error bounds involved.

10.0 REFERENCES

1. Wiese, W.L., Proc. Eight Int'l. Conf. of Phenomena in Ionized Gases, Vienna, p. 447 (1967).

2. Wiese, W.L., Smith, W.M., and Miles, B.M., NSRDS-NBS-22, U.S. Govt. Printing Office, Washington, D.C., (1969).

3. Nubbemeyer, H., JQSRT 16, pp. 395-404, (1976).

4. Preston, R.C., JQSRT 18, pp. 337-60 (1977).

5. Baessler, P. and Kock, M., J. Phys. B 13, pp. 1351-1361 (1980).

6. Sedghinasab, A., Ph.D. Thesis, Georgia Institute of Technology, Atlanta, December (1987).

7. Evans, D.L., Marchand, J.M., Braun, W.G., and Oss, J.P., AIAA Paper 70-42, 8th Aerospace Sciences Meeting, N.Y. (1970).

8. Bober, L, and Tankin, R.S., JQSRT 10, p. 991 (1970).

9. Uhlenbush, J., Fischer, E., and Hackmann, J., Z.Physik 239, p. 120 (1970).

10. Eddy, T.L., Cremers, C.J. and Hsia, H.S., "The MTE Continuum Relation with Application to an Argon Arc at Atmospheric Pressure", JQSRT, 17, pp, 287, 296 (1977).

11. Giannaris, R. J. and Icropera, F.P., JQSRT 11, p. 291 (1971).

12. Eddy, T.L., "Critical Review of Plasma Spectroscopic Diagnostics via MTE", IEEE Transactions of Plasma Sciences, 4, pp. 103-111 (1976).

13. Olsen, H.N., JQSRT, 3, pp. 59-76 (1963).

14. Bott, J.F., Physics of Fluids 9, pp. 1540-7 (1966) and JQSRT 6, pp. 807-22 (1966).

15. Coates, P.B. and Gaydon, A.G., Proc. R. Soc. A 293, ppo. 452-68 (1966).

16. Shumaker, J.B., Jr. and Popenoe, C.H., J. Opt. Soc. Am. 59, pp. 980-85 (1969).

17. Shumaker, J.B., Jr. and Popenoe, C.H., NBS J. Res A 76, pp. 71-6 (1972).

18. Kramers, H.A., Phil. Mag 46, p. 836 (1923).

19. Unsöd, Ann. Physik 33, p. 607 (1938).

20. Biberman, L.M. and Norman, G.E., Opt. Spectrosc. 8, p. 230, (1960).

21. Biberman, L.M. and Ulyanov, K.N., Opt, Spectrosc. 10, p. 297, (1961).

22. Norman, G.E., Opt. Spectrosc. 14, p. 277 (1963).

23. Anderson, A.D. and Griem, H.R., Proc. 6th Int'l. Conf. on Ioniz. Phenom, in Gases, Vol. 3, pp. 293-298, North Holland, Amsterdam (1963).

24. Griem, H.R., Plasma Spectroscopy, McGraw-Hill, New York (1964).

25. Schlüter, D., Z. Astrophysics, 61, p. 67 (1965).

26. Schlüter, D., Z. Physik, 210, p. 80 (1968).

27. Hofsaess, D., JWSRT, 19, pp. 339-352 (1978).

28. Schulz-Gulde, E., Z. Physik, 230, p. 449 (1970).

29. Morris, J.C. and Krey, R.V., JQSRT, 9, pp. 1633-1636 (1969).

30. Berge, O.E., Bohn, A., and Rehder, L., Z. Naturforsch 20a, p. 122 (1965).

31. Golubev, V.A., and Klimkin, V.F., "Teplofizika Vysokikh Temperatur, 9, p. 683 (1971).

32. Goldbache, C., Nollez, G, and Peyturaux, R., JQSRT, 12, pp. 1089-1104 (1972).

33. Knovov, A.A. and Kulagin, S.G., "Teplofizika Vysokikh Temperatur, 11, p. 1062 (1972); 12, 3 (1974).

34. Batenin, V.M. and Minaev, P.V., JQSRT, 18, pp. 171-177 (1977).

35. Ernst, W.E. and Schulz-Gulde, E., Physica 93C, pp. 136-144 (1978).

36. Baessler, P., Obbarius, H.U., and Schulz-Gulde, E., Physica 96C, pp. 147-154 (1979).

37. Eddy., T.L. and Fentress, M.L., "Additional Validation of the MTE Continuum Relation for non-LTE Plasmas", Bull. Am. Phys. Soc., Ser. II, 24, pp. 118, (1979).

38. Eddy, T.L., "High Pressure Continuum Radiation Measurements Indicate That Argon Transition Probability Values May Be Too Large", Bull. Am. Phys. Soc., Ser. II, 24, p. 774, (1979).

39. Klose, J.Z., J. Opt. Soc. Am. 57, pp. 1242-1244, (1967).

40. Klose, J.A., J. Opt. Soc. Am. 58, pp. 1509-1512, (1968).

41. Osherovich, A.L., and Veroleinen, Y.F., Leningrad, Vestnik, Univ. Fiz. i Khim, No. 1, pp. 140-141, (1967).

42. Verolemen, Y.F. and Osherovich, A., Optics and Spectroscopy (U.S.S.R) 25, pp. 258-259, (1968).

43. Popenoe, C.H. and Shumaker, J.B., Jr., J. Res. NBS 69A, p. 495, (1965).

44. Shumaker, J.B., Jr., and Popenoe, C.H., J. Opt. Soc. Am. 57,8, (1967).

45. Bates, D.R. and Damguard, A., Phil. Trans. Rog. Soc. London, Ser A 242, pp. 101-122, (1949).

46. Bues, I., Haag, T., and Richter, J., Tech. Report Inst. Experimentalphysik, Kiel Universität (1966-67) (1969).

47. Wende, B., Z. Physik 213, p. 341 (1968).

48. Richter, J., Z. Astrophysics 61, p. 47 (1965).

49. Chapelle, J. Sy, A., Cabannes, F., and Blandi, J., JQSRT 8, pp. 1201-16, (1968).

50. van Howelingen, D., and Kruitkof, A.A., JQSRT 11, p. 1235, (1971).

51. Wiese, W.L. and Shumaker, J.B., Jr., J. Opt. Soc. Am. 51, p. 937 (1961).

52. Griem, H.R., Kolb, A.C., and Shen, K.Y., Astrophys. J. 135, pp. 272-6 (1962).

53. Kepple, P., and Griem, H.R., Phys. Rev. 173, pp. 317-25 (1968).

54. Vidal, C.R., Cooper, J., and Smith, E.W., Astrophys. J. Suppl. No. 214, 25, pp. 37-136 (1973).

55. Greene, J., Astrophys. J., 130, p. 693 (1959).

56. Karzas, W.J. and Latter, R., Astrophys. J. Suppl VI (55), p. 167 (1961).

57. Schluter, D., Z. Astrophys., 56, p. 43 (1962).

58. Wende, B., Z. Physik, 198, p. 1. (1967).

59. Schnappauf, R., Z. Astrophys. 68, pp. 431-44 (1968).

60. Moore, C.E., Atomic Energy Levels, NBS Circ. p. 247, V.I., (1949).

61. Wright, A.E., Jr., Evans, D.L., Tankin, R.S., and Lambel, A.B., Argon Electron Transition Tables, ARL 67-0016 (1967).

62. Drawin, H.W., Z. Physik 228, p. 99 (1969).

63. Desai, S.V. and Corcoran, W.H., JQSRT 8, p. 1721 (1968).

64. Bourasseau, D., Cabannes, F., and Chapelle, J., J. Astron. and Astrophys. 9, p. 339 (1970).

65. Kolesnikov, V.N., Proc, P.H. Lebedev Phys. Inst. 30, p. 53 (1966).

66. Knoche, D.F., Eddy, T.L., and Mayer, T., "Contribution to the Question of Thermodynamic Equilibrium in Arcs", unpublished report.

67. Olsen, H.H., JQSRT 3, pp. 305-33 (1963).

68. Moore, C.E., NBS Circular, no. 467, Vols. I, II, III (1949, 1952, 1958).

69. Wiese, W.L., "Plasma Diagnostic Techniques", Eds., R.H. Huddlestone and S.L. Leonard, Academic Press, New York (1965).

70. Lorentz, H.A., "Proc Acad Sci Amsterdam", 8, 591 (1906).

71. Kolb, A.C. and Griem, H.R., Phys. Rev., 111, 514, (1958).

72. Spitzer, L., Phys. Rev., 58, 358, (1940).

73. Burkhardt, G., Z. Phys., 115, 592, (1940).

74. Behringer, K., Z. Phys, 246, 333, (1971).

75. Alpher, R.A. and White, D.R., Plasma Diagnostic Techniques, Eds., R.H. Huddlestone and S.L. Leonard, Academic Press, New York (1965).

76. Eddy, T.L. and Heberlein, J.V.R. (Eds.), NSF Workshop on Thermal Plasma Systems, Georgia Institute of Technology, Atlanta, May (1987).

76A. Ibid, Eddy, T.L., "Equilibrium and Nonequilibrium Considerations in Modeling", Ch. 9.1, pp 104-114.

76B. Ibid, Eddy, T.L., "Non-LTE Diagnostics via Emission Spectroscopy", Ch. 7.2, pp 74-79.

77. Wilson, R., JQSRT, 2, 477, (1962).

78. Shumaker, J.B., Jr. and Popenoe, C.H., Phys. Rev. Lett, 21, 1046, (1968).

79. Morris, J.C. and Krey, R.U., Phys. Rev. Lett, 21, 1042, (1968).

80. Key, D., JQSRT, 16, 69, (1975).

81. Blades, M.W., Spectrochimica Acta, 37B, no. 10, 869, (1982).

82. Gurvich, L.V., et. al, Technical Report, NASA-TN-D-4097, (1967).

83. Kuhn, H., Atomic Spectra, Academic Press (1962).

84. McBride, B.J. and S. Gordon, Technical Report, NASA-TN-D-4097 (1967).

85. Eddy, T.L., "Non-LTE and Multithermal Equilibrium in Subatmospheric Arc Plasmas", Ph.D. Thesis, University of Minnesota, Minneapolis, (1972).

86. McConkey, J.W. and Preston, J.A., J Phys. B., 6, L138, (1973).

87. Minnhagen, J., Opt. Soc. Am., 63, 1185, (1973).

88. Margenau, H. and Lewis, M., Rev. Mod. Phys., 31, 594, (1959).

89. Eddy, T.L., Pfender, E., and Eckert, E.R.G., "Spectroscopic Mapping of Non-Equilibrium Between Electron and Excitation Temperatures in a 1-atm Helium Arm", IEEE Trans., Plasma Sciences 1, pp. 31-42, (1973).

90. Farmer, A.J.D., and Haddad, G.N., Appl. Phys. Lett, 45, 1, (1984).

91. Nick, K.P., Richter, J., and Helbig, V., JQSRT, 32, no. 1, 1, (1984).

92. Shindo, H., and Imazu, S., JQSRT, 23, 605, (1980).

93. Seaton, M.J., Mont. Not. Roy. Astro. Soc., 118, 504, (1958).

94. Olsen, H.N., Phy. Rev., 124, 1703, (1961).

95. Shkarofsky, I.P., Johnston, T.W., and Bachynski, M.P., The Particle Kinetics of Plasmas, Addison-Wesley, (1966).

96. Üsold, A., Z. Astrophysik, 24, 355, (1948).

97. Drellishak, K.S., Knopp, C.F. and Cambel, A.B., Phys. Fluids, 6, 9, (1963).

98. Campel, A.B., Duclos, D.P., Anderson, T.P., Real Gases, Adacemic Press, (1962).

99. Wiese, W.L., Smith, M.W., and Miles, B.M., NSRDS-NBS-22, U.S. Govt. Printing Office, Washington, DC (1969)

100. Cho, K.Y., and Eddy, T.L., 39th Gaseous Electronics Conference, Madison, WI (1986).

101. Patch, R.W. "Components of a Hydrogen Plasma Including Minor Species", NASA TN D-4993, (1969).

102. Bauder, U.H., and Stephens, E.D., Rev. Sci, Inst. 43, 1341, (1972).

103. Maecker, H., Z. Naturforsch, 119, 457, (1956).

104. Hug, W.F., Evans, D.L., Tansin, R.S., and Campel, A.B., Technical Paper, ARL 66-0140 (1966).

105. Oklobdzija, V., and Konjevic, N., JQSRT, 14, 389, (1974).

106. Popiv, S., and Konjevic, N., JQSRT, 16, 15, (1976).

107. Larson, A.V., and Murray, R.T., Technical Paper, AEDC-TR-79-67, (1979).

108. Nester, O.H, and Olsen, H.N., SIAM Review, 2, 200, (1960).

109. Null, M.R., and Lozier, W.W., J Opt. Soc. Am., 52, 1156, (1962).

110. Cho, K.Y., Ph.D. Thesis, Georgia Institute of Technology, Atlanta, Georgia (in preparation).

111. Burgess, A., and Seaton, M.J., Mon. Not. Roy. Astro. Soc., 120, 121, (1960).

112. Eddy, T.L., "The Generalized Multighermal Equilibrium Model for Diagnostics and Modelling of High Temperature Gases" (in preparation).

113. Helbig, V., and Nick, K.P., J. Phys. B., 14, 3573, (1981).

114. Wiese, W.L., Kelleher, D.E., and Paquette, D.R., Phys. Rev. 6, pp. 1132-1153 (1972).

115. Cobine, J.D., "Gaseous Conductors", Dover Publ., New York, (1958).

116. Kolesnikov, V.N., Proc. P.H. Lebedev Phy. Inst., 30, 53, (1966).

117. Pfender, E., "Gaseous Electronics", Vol. 1, p. 291, Academic Press, (1978).

118. Drawin, H.W., Z. Phys. 146, pp. 295-313, (1956).

119. Gericke, W.E., Z. Astrophysik 53, pp. 68-79, (1961).

120. Malone, B.S. and Corcoran, W.K., JQSRT 6, pp. 443-449, (1966).

121. Wujec, T., Acta Phys. Polon. 36, p. 269, (1969).

Appendix A

Energy Levels and Degeneracies of Argon

ENERGY LEVELS AND DEGENERACIES OF ARGON INDCLUDING CONTRIBUTION OF ALL DIFFERENT BRANCHES.

ARGON NEUTRAL

N	G	E	G	E	G	E	G	E
3	1.	.0	1.	111667.9	3.	111818.1	9.	112750.2
	7.	113020.4	5.	112139.0	3.	114147.8	5.	113426.1
	7.	113716.6	5.	114641.0	7.	114822.0	5.	114805.2
	3.	115366.9						
4	5.	93143.8	3.	93750.6	1.	94553.7	3.	95399.9
	3.	104102.1	7.	105462.8	5.	105617.3	3.	106087.3
	5.	106237.6	1.	107054.3	3.	107131.8	5.	107289.8
	3.	107496.5	1.	108722.7	1.	118512.2	3.	118651.5
	9.	119023.7	7.	119212.9	5.	118906.7	3.	119847.8
	5.	119444.9	7.	119566.1	5.	120619.1	7.	120753.5
	5.	120600.9	3.	121012.0	3.	120188.3	5.	120188.7
	11.	120207.3	9.	120207.8	7.	120229.8	5.	120230.1
	7.	120250.2	9.	120250.2	7.	121653.4	9.	121653.4
	7.	121654.3	5.	121654.6				
5	5.	113468.6	3.	113643.3	1.	114861.7	3.	114975.1
	3.	116660.1	7.	116942.8	5.	116999.4	3.	117151.4
	5.	117183.7	1.	117563.0	3.	118407.5	5.	118469.1
	3.	118459.7	1.	118871.0	1.	121794.2	3.	121932.9
	9.	122036.1	7.	122160.2	5.	122087.0	3.	122514.3
	5.	122282.1	7.	122329.7	5.	123505.5	7.	123557.5
	5.	123373.0	3.	123815.5	3.	122686.2	5.	122686.4
	20.	122695.7	72.	122720.5	7.	122707.9	5.	122708.2
	7.	122717.9	9.	122717.9	7.	124135.7	9.	124135.7
	7.	124137.3	5.	124137.5	36.	124151.9		
6	5.	119683.1	3.	119760.2	1.	121096.7	3.	121161.4
	3.	121068.8	7.	121165.4	5.	121191.9	3.	121257.2
	5.	121270.7	1.	121470.3	3.	122609.8	5.	122635.1
	3.	122601.3	1.	122790.6	1.	123509.0	3.	123468.0
	9.	123653.2	7.	123773.9	5.	123808.6	3.	123815.0
	5.	123826.9	7.	123832.5	5.	125113.5	7.	125150.0
	5.	125066.5	3.	125286.3	3.	124041.2	5.	124041.4
	20.	124046.6	160.	124061.7	7.	124051.4	5.	124051.7
	7.	124058.4	9.	124058.4	7.	125482.7	9.	125482.7
	7.	125483.2	5.	125483.3	80.	125493.1		
7	5.	122440.1	3.	122479.5	1.	123873.1	3.	123882.3
	3.	123172.1	7.	123205.8	5.	123220.7	3.	123255.0
	5.	123261.6	1.	123385.1	3.	124643.5	5.	124658.5
	3.	124651.1	1.	124749.9	1.	124526.8	3.	124554.9
	9.	124609.9	7.	124649.6	5.	124604.0	3.	124788.4
	5.	124692.0	7.	124715.2	5.	126064.5	7.	126089.6
	5.	126053.2	3.	126161.9	3.	124857.3	5.	124857.4
	20.	124860.6	5.	126295.0	7.	124865.0	5.	124865.2
	7.	124868.8	9.	124868.8	7.	126294.9	9.	126294.9
	7.	126295.0	264.	124870.4	132.	126301.8		
8	5.	123903.3	3.	123936.0	1.	125334.8	3.	125353.3
	3.	124311.7	7.	124349.0	5.	124356.7	3.	124376.4
	5.	124381.0	1.	124439.4	3.	125783.8	5.	125791.9
	3.	125777.3	1.	125831.5	1.	125163.0	3.	125135.9
	9.	125219.9	7.	125269.5	5.	125283.0	3.	125376.9

	5.	125291.5	7.	125293.7	20.	126674.5	3.	125386.4
	5.	125386.4	9.	125388.7	11.	125388.7	7.	125391.0
	5.	125391.2	7.	125393.5	9.	125393.5	220.	126825.0
	384.	125395.0						
9	5.	124771.7	3.	124782.8	1.	126202.8	3.	126211.6
	3.	125039.6	7.	125054.1	5.	125059.8	3.	125072.6
	5.	125074.9	1.	125122.5	3.	126495.1	5.	126495.1
	3.	126495.1	1.	126524.2	1.	125595.1	3.	125613.1
	9.	125631.7	7.	125652.0	5.	125637.9	3.	125718.1
	5.	125671.5	7.	125680.5	0.	125700.0	0.	127130.0
	0.	127000.0	0.	125700.0	3.	125748.9	5.	125748.9
	9.	125750.4	11.	125750.4	7.	125752.8	5.	125753.0
	7.	125754.2	9.	125754.2	0.	127000.0	520.	125755.1
10	5.	125330.0	3.	125331.9	4.	126763.7	0.	126700.0
	3.	125505.5	7.	125519.9	5.	125521.0	3.	125531.9
	5.	125533.8	1.	125561.9	0.	126500.0	1.	125895.7
	3.	125898.6	9.	125922.5	7.	125932.6	5.	125906.6
	3.	126100.0	5.	125945.7	7.	125957.4	0.	127000.0
	0.	127410.0	0.	127100.0	56.	126009.9	672.	126012.5
11	8.	125711.0	24.	125849.8	40.	126145.5	840.	126203.0
	56.	126201.0						
12	56.	126346.3	24.	126081.9	40.	126303.7	8.	125980.5
	1024.	126202.3						
13	56.	126459.4	24.	126255.4	40.	126426.0	8.	126178.9
	1224.	126460.6						
14	56.	126549.1	24.	126388.3	40.	126522.4	8.	126329.4
	1440.	126550.0						
15	56.	126621.4	24.	126492.5	40.	126599.8	8.	126446.1
	1672.	126622.2						
16	56.	126680.6	24.	126575.7	40.	126662.8	8.	126538.4
	1920.	126681.2						
17	56.	126729.7	24.	126643.1	40.	126714.9	8.	126612.8
	2184.	126730.2						
18	56.	126770.8	24.	126698.5	40.	126758.3	8.	126673.5
	2464.	126771.2						
19	56.	126805.5	24.	126744.6	40.	126795.0	8.	126723.7
	2760.	126805.9						
20	56.	126835.2	24.	126783.4	40.	126826.2	8.	126765.8
	3072.	126835.6						
21	56.	126860.8	24.	126816.3	40.	126853.0	8.	126801.3
	3400.	126861.1						
22	56.	126882.9	24.	126844.5	40.	126876.2	8.	126831.6
	3744.	126883.2						
23	56.	126902.2	24.	126868.8	40.	126896.3	8.	126857.6
	4104.	126902.5						
24	56.	126919.2	24	126889.9	40.	126914.0	8.	126880.2
	4480.	126919.4						
25	56.	126934.2	24.	126908.3	40.	126929.6	8.	126899.9
	4872.	126934.3						

26	56.	126947.4	24.	126924.6	40.	126943.3	8. 126917.1
	5280.	126947.6					
27	56.	126959.2	24.	126938.9	40.	126955.6	8. 126932.3
	5704.	126959.4					
28	56.	126969.8	24.	126951.6	40.	126966.5	8. 126945.8
	6144.	126969.9					
29	56.	126979.3	24.	126963.0	40.	126976.4	8. 126957.8
	6600.	126979.4					
30	56.	126987.9	24.	126973.2	40.	126985.2	8. 126968.5
	7072.	126988.0					
31	56.	126995.6	24.	126982.4	40.	126993.2	8. 126978.1
	7560.	126995.7					
32	56.	127002.7	24.	126990.6	40.	127000.5	8. 126986.8
	8064.	127002.7					
33	56.	127109.0	24.	127109.0	40.	127109.0	8. 127109.0
	9999.	127109.0					

ENERGY LEVELS AND DEGENERACIES OF ARGON INDCLUDING
CONTRIBUTION OF ALL DIFFERENT BRANCHES.

ARGON FIRST ION

N	G	E	G	E	G	E	G	E
3	4.	.0	2.	1432.0	138.	176859.0	10.	179750.0
4	18.	136486.0	54.	158294.0	90.	186972.0	126.	195450.0
	10.	148732.0	30.	172117.0	50.	200161.0	70.	208922.0
	2.	167308.0	6.	192154.0				
5	18.	182755.0	54.	190629.0	90.	201244.0	126.	205050.0
	162.	205262.0	10.	195866.0	30.	203151.0	50.	216529.0
	70.	219272.0	90.	219280.0	2.	215065.0		
6	18.	200032.0	54.	204929.0	90.	209071.0	126.	212077.0
	162.	210680.0	198.	210680.0	10.	212933.0	30.	219954.0
7	18.	208155.0	54.	211023.0	90.	212820.0	720.	213862.0
	10.	221085.0						
8	18.	212430.0	54.	214112.0	90.	215320.0	990.	215962.0
9	18.	215016.0	54.	216129.0	90.	216954.0	1296.	217401.0
10	18.	216744.0	54.	217519.0	90.	218106.0	1638.	218431.0
11	18.	217956.0	54.	218517.0	90.	218950.0	2016.	219192.0
12	18.	218838.0	54.	219257.0	90.	219586.0	2430.	219722.0
13	18.	219500.0	54.	219822.0	90.	220077.0	2880.	220223.0
14	18.	220010.0	54.	220262.0	90.	220464.0	3366.	220581.0
15	18.	220411.0	54.	220612.0	90.	220775.0	3888.	220869.0
16	18.	220732.0	54.	220894.0	90.	221028.0	4446.	221105.0
17	18.	220992.0	54.	221126.0	90.	221237.0	5040.	221301.0
18	18.	221207.0	54.	221318.0	90.	221411.0	5670.	221465.0
19	18.	221386.0	54.	221480.0	90.	221558.0	6336.	221604.0
20	18.	221537.0	54.	221617.0	90.	221683.0	7038.	221723.0

21	18.	221665.0	54.	221734.0	90.	221791.0	7776.	221825.0
22	8550.	221913.0						
23	9360.	221990.0						
24	10206.	222058.0						
25	11088.	222118.0						
26	12006.	222171.0						
27	12960.	222218.0						
28	13950.	222260.0						
29	14976.	222298.0						
30	16038.	222332.0						
31	17136.	222363.0						
32	18270.	222391.0						
33	19440.	222417.0						
34	20646.	222440.0						
35	21888.	222462.0						
36	23130.	222481.0						
37	24408.	222516.0						
38	25722.	222516.0						
39	27072.	222531.0						
40	28458.	222546.0						
41	29880.	222559.0						
42	31338.	222571.0						
43	32832.	222583.0						
44	34362.	222593.0						
45	35928.	222603.0						
46	37530.	222613.0						
47	39168.	222621.0						
48	40842.	222629.0						
49	42552.	222637.0						
50	44298.	222644.0						
51	46080.	222651.0						
52	47898.	222658.0						

53	49752.	222664.0
54	51642.	222669.0
55	53568.	222675.0
56	55530.	222680.0
57	57528.	222685.0
58	59562.	222690.0
59	61632.	222694.0
60	63738.	222698.0
61	65880.	222702.0
62	68058.	222706.0
63	70272.	222709.0
64	72522.	222713.0
65	74808.	222716.0
66	77130.	222719.0
67	79488.	222819.9

ENERGY LEVELS AND DEGENERACIES OF ARGON INDCLUDING
CONTRIBUTION OF ALL DIFFERENT BRANCHES.

ARGON SECOND ION

N	G	E	G	E	G	E	G	E
3	5.	.0	3.	1112.0	1.	1570.0	5.	14010.0
	1.	33267.0	5.	113800.0	3.	114797.0	1.	115328.0
	100.	187000.0	60.	213000.0	40.	144900.0		
4	320.	197974.5	192.	211738.0	128.	180437.0		
5	500.	272245.0	300.	286009.0	200.	251155.0		
6	720.	303140.0	432.	316904.0	288.	282050.0		
7	980.	318877.0	392.	297787.0				
8	1280.	327965.0						
9	512.	306875.0						
10	648.	312594.0						
11	800.	316424.0						
12	968.	319114.0						
13	1152.	321076.0						
14	1352.	322550.0						
15	1568.	323686.0						
16	1800.	324579.0						
17	2048.	325294.0						
18	2312.	325876.0						
19	2592.	326356.0						
20	2888.	326756.0						
21	3200.	327093.0						
22	3528.	327379.0						
23	3872.	327625.0						
24	4232.	327837.0						
25	4608.	328022.0						
26	5000.	328184.0						
27	5408.	328326.0						
28	5832.	328452.0						

29	6272.	328452.0
30	6728.	328664.0
31	7200.	328753.0
32	7688.	328834.0
33	8192.	328907.0
34	8712.	328973.0
35	9248.	329033.0
36	9800.	329088.0
37	10368.	329138.0
38	10952.	329184.0
39	11552.	329226.0
40	12168.	329265.0
41	12800.	329301.0
42	13448.	329334.0
43	14112.	329364.0
44	14792.	329393.0
45	15488.	329420.0
46	16200.	329444.0
47	16928.	329467.0
48	17672.	329489.0
49	18432.	329509.0
50	19208.	329528.0
51	20000.	329546.0
52	20808.	329563.0
53	21632.	329579.0
54	22472.	329594.0
55	23328.	329608.0
56	24200.	329621.0
57	25088.	329633.0
58	25992.	329645.0
59	26912.	329656.0
60	27848.	329667.0
61	28800.	329677.0

62	29768.	329687.0
63	30752.	329696.0
64	31752.	329705.0
65	32768.	329713.0
66	33800.	329721.0
67	34848.	329728.0
68	35912.	329735.0
69	36992.	329742.0
70	38088.	329749.0
71	39200.	329755.0
72	39200.	329964.5

ENERGY LEVELS AND DEGENERACIES OF ARGON INDCLUDING
CONTRIBUTION OF ALL DIFFERENT BRANCHES.

ARGON THIRD ION

N	G	E	G	E	G	E	G	E
3	4.	.0	4.	21090.0	6.	21219.0	2.	34854.0
	4.	35035.0	50.	303616.0	10.	307314.0	90.	287315.0
4	160.	388965.0	32.	392664.0	288.	372665.0		
5	250.	428470.0	50.	432169.0	450.	412169.0		
6	360.	449929.0	72.	453628.0	648.	433629.0		
7	490.	462869.0	98.	466568.0	882.	446568.0		
8	640.	471267.0	128.	474966.0	1152.	454966.0		
9	810.	477024.0	162.	480723.0	1458.	460724.0		
10	1000.	481143.0	1800.	464842.0				
11	2178.	467890.0						
12	2592.	470207.0						
13	3042.	472011.0						
14	3528.	473442.0						
15	4050.	474597.0						
16	4608.	475542.0						
17	5202.	476325.0						
18	5832.	476981.0						
19	6498.	477536.0						
20	7200.	478011.0						
21	7938.	478419.0						
22	8712.	478772.0						
23	9522.	479081.0						
24	10368.	479352.0						
25	11250.	479591.0						
26	12168.	479803.0						
27	13122.	479992.0						
28	14112.	480161.0						
29	15138.	480312.0						

30	16200.	480449.0
31	17298.	480573.0
32	18432.	480685.0
33	19602.	480788.0
34	20808.	480881.0
35	22050.	480967.0
36	23328.	481045.0
37	24642.	481117.0
38	25992.	481184.0
39	27378.	481246.0
40	28800.	481303.0
41	30258.	481356.0
42	31752.	481405.0
43	33282.	481450.0
44	34848.	481493.0
45	36450.	481533.0
46	38088.	481570.0
47	39762.	481605.0
48	41472.	481638.0
49	43218.	481669.0
50	45000.	481698.0
51	46818.	481725.0
52	48672.	481751.0
53	50562.	481775.0
54	52488.	481798.0
55	54450.	481820.0
56	56448.	481840.0
57	58482.	481860.0
58	60552.	481878.0
59	62658.	481896.0
60	64800.	482399.0

ENERGY LEVELS AND DEGENERACIES OF ARGON INDCLUDING
CONTRIBUTION OF ALL DIFFERENT BRANCHES.

ARGON FORTH ION

N	G	E	G	E	G	E	G	E
3	1.	.0	3.	765.0	5.	2032.0	5.	16301.0
	216.	400279.0	108.	300279.0				
4	384.	533638.0	192.	433668.0				
5	600.	595364.0	300.	495364.0				
6	588.	549112.0						
7	768.	562234.0						
8	972.	571231.0						
9	1200.	577666.0						
10	1452.	582427.0						
11	1728.	586048.0						
12	2028.	588866.0						
13	2352.	591103.0						
14	2700.	592907.0						
15	3072.	594383.0						
16	3468.	595607.0						
17	3888.	596632.0						
18	4332.	597500.0						
19	4800.	598241.0						
20	5292.	598879.0						
21	5808.	599431.0						
22	6348.	599914.0						
23	6912.	600337.0						
24	7500.	600710.0						
25	8112.	601041.0						
26	8748.	601336.0						
27	9408.	601600.0						
28	10092.	601837.0						
29	10800.	602051.0						

30	11532.	602245.0
31	12288.	602420.0
32	13068.	602580.0
33	13872.	602726.0
34	14700.	602860.0
35	15552.	602983.0
36	16428.	603096.0
37	17328.	603200.0
38	18252.	603296.0
39	19200.	603385.0
40	20172.	603468.0
41	21168.	603544.0
42	22188.	603616.0
43	23232.	603682.0
44	24300.	603745.0
45	25392.	603803.0
46	26508.	603858.0
47	27648.	605099.0

Appendix B

Program Listing of ARGMTE and a Sample Output

```
      PROGRAM ARMTE (INPUT,OUTPUT,TAPE5=INPUT,TAPE6=OUTPUT)
      DIMENSION PI(10),TEOTAI(5),TXI(31),E(5,400),TXIP(3),XISP(3),
     1   GG(5,400), EI(5), Z(31,5), EIINF(5), WAVE(6), G(6), ENM(6),
     2   A(6), DEI(31), FNLEMC(31,6), FILEMC(31), CEMC(31), DELEI(31,5)
     3   ,SMQN(5),FOMQN(5),TEX(5),TEOTX1(5),TX20X1(5),TX30X2(5),
     4   TX40X3(5),TX50X4(5),EZERO(31,6),DH(31,5),DT(31),TX10XA(5),
     5   TQ(8),QEAT(8),TT(8),GIFT(8),TXI(6,3),XIS(6,3),WAVXI(6),
     6   ZHE(5),XTEX(33),XDA(33),XD1(33),XD2(33),XD3(33),XD4(33),
     7   XDE(33),XDTOT(33),WORDS(4),TN(33),KOUNT(5),NW(5,70),
     8   ZS(5,70,31),SEM(5,70,31),CECFB(31,6),CECEA(31,6),CECEI(31,6)
C     ---------------------------------------------------------------
C     ASSUMPTIONS- ONLY TRANSLATIONAL AND ELECTRONIC ENERGIES ARE CONSIDERED.
C     TA=TI
C     ---------------------------------------------------------------
      BOLTK=1.38054E-16
      NI=5
C  CHANE UNITS OF EH TO ERGS SO THAT IT IS COMPATIBLE WITH
C  BOLTK IN THE CONTIUUM CALCULATIONS.
      EH = 109735.8
      G11=6.0
      KNUM=0
      WT=39.944
      DO 6 I=1,5
 6    ZHE(I)=I*1.0
C     CONST  =(2.*3.14159*ELECTRON MASS*BOLTK/PLANKS CONSTANT**2)**1.5
      CONST=(2.*3.14159*9.1091E-28*1.38054E-16/6.6256E-27**2)**1.5
C
C     GENERATE TX1 (ATOM EXCITATION TEMPERATURE)
      TX1(1)=5000.
      DO 1 I=2,31
   1  TX1(I) = TX1(1)+(I-1.)*1000.
      DO 2 I=1,6
      DO 2 JJ=1,3
 2    XIS(I,JJ)=0.
C     ---------------------------------------------------------------
C           START READING THE DATA FILE
C     ---------------------------------------------------------------
      READ(5,4) WORDS
    4 FORMAT(4A5)
      READ(5,7) (TQ(I),I=1,8)
      READ(5,5) (QEAT(I),I=1,8)
      READ(5,7) (TT(K),K=1, 8)
      READ(5,7) (GIFT(K),K=1, 8)
    7 FORMAT (8F10.0)
    5 FORMAT(8E10.3)
C     PRESSURE IN BAR
      READ(5,15) IP,(PI(I), I=1,IP)
      READ(5,15) IA, (TEOTAI(I), I=1,IA)
      READ(5,15) I1, (TEOTX1(I), I=1,I1)
      READ(5,15) I2, (TX20X1(I), I=1,I2)
      READ(5,15) I3, (TX30X2(I), I=1,I3)
      READ(5,15) I4, (TX40X3(I), I=1,I4)
      READ(5,15) I5, (TX50X4(I), I=1,I5)
   15 FORMAT(I2,/4F8.4)
      READ(5,16) EIINF
   16 FORMAT (5(F10.3,2X))
      READ(5,79) ((GG(I,J),E(I,J),J=1,400),I=1,1)
   79 FORMAT(4(F7.0,1X,F9.2,2X))
      READ(5,79) ((GG(I,J),E(I,J),J=1,160),I=2,5)
      READ(5,89) (KOUNT(I),I=1,5)
   89 FORMAT(513)
      READ(5,88) ((NW(I,J),J=1,70),I=1,5)
   88 FORMAT(714)
      READ(5,18) (WAVE(I),G(I),ENM(I),A(I),I=1,6)
   18 FORMAT (F8.2,3X,F4.1,3X,F11.3,3X,E9.3)
      READ(5,3) WINI,WFIN,ZETAO,AA,BB
```

```
    3 FORMAT(2F7.1,F8.5,2E13.5)
      READ(5,19) (SMQN(I),I=1,5)
      READ(5,19) (FOMQN(I),I=1,5)
   19 FORMAT(5F5.1)
C    ------------------------------------------------------------
      DO 29 K=1,IA
      TEOTA = TEOTAI(K)
      DO 29 J1=1,I1
      DO 29 J2=1,I2
      DO 29 J3=1,I3
      DO 29 J4=1,I4
      DO 29 J5=1,I5
      DO 12 L=1,31
      TEX(1)=TX1(L)
      TE=TEOTX1(J1)*TX1(L)
      TA=TE/TEOTA
      TEX(2)=TEX(1)*TX20X1(J2)
      TEX(3)=TEX(2)*TX30X2(J3)
      TEX(4)=TEX(3)*TX40X3(J4)
      TEX(5)=TEX(4)*TX50X4(J5)
C    ------------------------------------
C    CALCULATE PARTITION FUNCTIONS
C    ------------------------------------
      SG=0.
      SEE=0.
C
      DO 621 IS=1,5
      DO 611 IZ=1,KOUNT(IS)
      ZS(IS,IZ,L)=0.
      IF(IZ-1) 607,607,608
  607 LS=1
  608 M=NW(IS,IZ)
      DO 610 KZ=LS,M
      IF(E(IS,KZ)-EIINF(IS)) 609,609,610
  609 ZS(IS,IZ,L)=ZS(IS,IZ,L)+GG(IS,KZ)/EXP(E(IS,KZ)*
     1    1.43879/TEX(IS))
      SG=SG+GG(IS,KZ)
      SEE=SEE+GG(IS,KZ)*E(IS,KZ)
  610 CONTINUE
      SEM(IS,IZ,L)=SEE/SG
      SG=0.
      SEE=0.
  611 LS=NW(IS,IZ)+1
      DO 615 J=1,KOUNT(IS)
      IF(J-1) 615,615,614
  614 ZS(IS,J,L)=ZS(IS,J,L)+ZS(IS,J-1,L)
      IF(IS.NE.1) GOTO 615
  615 CONTINUE
  621 CONTINUE
   12 CONTINUE
C     PRESSURE IN BAR
      DO 29 I=1,IP
      IPRES=I
      P = PI(I)
      KNUM=KNUM+1
      D1=1.0E+15
      D40D3=1.
      D30D2=1.
      D20D1=1.
C
      TEOTXA=TEOTX1(J1)
      TX10XA(2) = TX20X1(J2)
      TX10XA(3) = TX30X2(J3)
      TX10XA(4) = TX40X3(J4)
      TX10XA(5) = TX50X4(J5)
C   PRINT HEADING FOR PLASMA COMPOSITION
```

```
      IF(IPRES.NE.3) GOTO 81
C
      WRITE(6,9)
    9 FORMAT (1H1)
      WRITE(6,40)P,TEOTA,TEOTX1(J1),TX20X1(J2)
   40 FORMAT(4(/),2X,53HMULTI-THERMAL EQUILIBRIUM COMPOSITION OF ARGON P
     1LASMA,19X,10HPRESSURE =,F8.4,3HBAR,/,74X,10HTE/TA     =,F6.2
     2   ,/,74X,10HTE/TXA    =,F6.2,/,74X,10HTX1/TXA  =,F6.2,//,2X,
     3   3HTEX,4X,6(9HNUMBER OF,2X),7HNE/N1,A,3X,10HTOTAL PAR-,/,
     4   2X,5HDEG K,2X,9HATOMS PER,2X,8H1ST IONS,3X,8H2ND IONS,3X,
     5   8H3RD IONS,3X,8H4TH IONS,3X,9HELECTRONS,12X,10HTICLES PER,
     6   /,9X,3HCC.,8X,5(7HPER CC.,4X),10X,3HCC../)
C   ------------------------------------------------------------
C     START OF CALCULATIONS FOR ONE SET OF CONDITIONS
C   ------------------------------------------------------------
 81   DO 28 L=1,31
      KTR=1
      TEX(1)=TX1(L)
      TE=TEOTX1(J1)*TX1(L)
      TA=TE/TEOTA
      TEXOTA=TEX(1)/TA
      TEX(2)=TEX(1)*TX20X1(J2)
      TEX(3)=TEX(2)*TX30X2(J3)
      TEX(4)=TEX(3)*TX40X3(J4)
      TEX(5)=TEX(4)*TX50X4(J5)
C   ------------------------------------
C
C     APPROXIMATE ELECTRON DENSITY
      OE = SQRT((P*2.*1.0E6*(GG(2,1)))/(BOLTK*TA*(GG(1,1)
     1   ))*CONST  *TE**1.5/EXP(EIINF(1)*1.43879/TEX(1)))
   33 DEBYE=(4.0*3.14159*4.80298E-10**2*(DE/(BOLTK*TE)+D1*(1.+4.*D20D1+
     19.*D30D2*D20D1+16.*D40D3*D30D2*D20D1)/(BOLTK*TA)))**(-0.5)
C     LOWERING OF IONIZATION POTENTIAL FROM DEBYE THEORY, AFTER GRIEM.
C     ENERGY IN INVERSE CM.
      DELEI(L,1) = (4.80298E-10)**2/(1.9862E-16*DEBYE)
      DELEI(L,2) = 2.*DELEI(L,1)
      DELEI(L,3) = 3.*DELEI(L,1)
      DELEI(L,4) = 4.*DELEI(L,1)
      DELEI(L,5) = 5.*DELEI(L,1)
      EI(1)=EIINF(1)-DELEI(L,1)
      EI(2)=EIINF(2)-DELEI(L,2)
      EI(3)=EIINF(3)-DELEI(L,3)
      EI(4)=EIINF(4)-DELEI(L,4)
      EI(5)=EIINF(5)-DELEI(L,5)
C   ------------------------------------------------
C   EZERO IS E FROM GRD STATE OF ATOM TO GRD STATE OF ION
      EZERO(L,1)=0.0
      DO 20 N=1,5
      EZERO(L,N+1)=EZERO(L,N)+EI(N)
      DO 21 IL=1,KOUNT(N)
      IF(EI(N)-SEM(N,IL,L))93,93,21
 21   CONTINUE
 93   IF(IL.NE.1) GOTO 92
      Z(L,N)=ZS(N,IL,L)
      GOTO 20
 92   Z(L,N)=ZS(N,IL-1,L)
 20   CONTINUE
C   ---------------------------------------
C       CALCULATE SPECIES COMPOSITION RATIOS
C   ---------------------------------------------
      D10DA=(2.*CONST*TE**1.5/DE)**TEOTA*(Z(L,2)/Z(L,1))**(TEX(1)/TA)*
     1       EXP(-EI(1)*1.43879/TA)
      D20D1=(2.*CONST*TE**1.5/DE)**TEOTA*(Z(L,3)/Z(L,2))**(TEX(2)/TA)*
     1       EXP(-EI(2)*1.43879/TA)
      D30D2=(2.*CONST*TE**1.5/DE)**TEOTA*(Z(L,4)/Z(L,3))**(TEX(3)/TA)*
     1       EXP(-EI(3)*1.43879/TA)
```

```
      D40D3=(2.*CONST*TE**1.5/DE)**TEOTA*(Z(L,5)/Z(L,4))**(TEX(4)/TA)*
     1        EXP(-EI(4)*1.43879/TA)
      D1=DE/(1.+2.*D20D1+3.*D30D2*D20D1+4.*D40D3*D30D2*D20D1)
      DA=D1/D10DA
C
C   DEBYE-HUECKEL PRESSURE CORRECTION
C
      SIGNS=DA+DE+D1+D1*D20D1+D1*D20D1*D30D2+D1*D20D1*D30D2*D40D3
      PDHOP=(1./DEBYE)**3/(24.*3.14159*SIGNS)
      PCALC =(DA*BOLTK*TA+DE*BOLTK*TE+D1*BOLTK*TA*(1.+D20D1+D30D2*
     1   D20D1+D40D3*D30D2*D20D1))/1.0E6
      PCALC = PCALC - PDHOP*PCALC
C
C   TEST FOR CONVERGENCE
C
      KTR=KTR+1
      IF(KTR-1000)37,37,29
   37 CONTINUE
      IF(ABS((P-PCALC)/P)-1.E-9)32,32,30
   30 IF(ABS((P-PCALC)/P)-1.000)31,130,130
  130 DELDE = ABS(DE*((P-PCALC)/P)*1.2)
      DE = DE**2./DELDE
      GO TO 33
   31 DELDE = DE*((P-PCALC)/P)*.5
      DE=DE+DELDE
      GO TO 33
   32 CONTINUE
C
C   CALCULATE SPECIES COMPOSITION
C
      D2=D20D1*D1
      D3=D30D2*D20D1*D1
      D4=D40D3*D30D2*D20D1*D1
      DTOT=DA+DE+D1+D2+D3+D4
      DEODIA=DE*Z(L,1)/((GG(1,1))*DA)
      DEI(L) = DE
      DH(L,1)=DA
      DH(L,2)=D1
      DH(L,3)=D2
      DH(L,4)=D3
      DH(L,5)=D4
      DT(L) = DTOT
      IF(IPRES.NE.3) GOTO 83
C   ------------------------------------------------
      IF(L-6)44,41,42
   42 IF(L-16)44,41,43
   43 IF(L-26)44,41,44
   41 WRITE(6,141)
  141 FORMAT(1X)
   44    CONTINUE
         IF(D1.LE.1.D+00) D1=0.000
         IF(D2.LE.1.D+00) D2=0.000
         IF(D3.LE.1.D+00) D3=0.000
         IF(D4.LE.1.D+00) D4=0.000
C   ------------------------------------------------------
C   PRINT PLASMA COMPOSITION FOR EACH TEX FOR A GIVEN CONDITION
C   ------------------------------------------------------
      WRITE(6,45)TEX(1),DA,D1,D2,D3,D4,DE,DEODIA,DTOT,KTR
   45 FORMAT(1X,F6.0,8(1X,E10.5),I5)
   83 CONTINUE
C   ------------------------------------------------------
C   START CALCULATING EMISSION COEFFICIENTS FOR SELECTED
C   LINE , ION , AND CONTINUUM GIVEN BY DATA FILE
C   ------------------------------------------------------
C   ------  NEUTRAL LINES  ------
      DO 57 JJ=1,2
```

```
      FNLMCI = 1.9862E-16*A(JJ)*G(JJ)*DA/(4.*3.14159*WAVE(JJ)*
     1Z(L,1)*EXP(ENM(JJ)*1.43879/TEX(1)))*10.
   57 FNLEMC(L,JJ) = FNLMCI
C
C    ------  ION LINES  ------
C
      DO 58 JJ=3,4
      FILMCI = 1.9862E-16*A(JJ)*G(JJ)*D1/(4.*3.14159*WAVE(JJ)*
     1   Z(L,2)*EXP(ENM(JJ)*1.43879/TEX(2)))*10.
   58 FNLEMC(L,JJ)=FILMCI
C
C    ------  CONTINUUM EMISSION COEFFICIENTS  ------
C
      TXB = TEX(1)
      TC = TEX(1)
      ZI=Z(L,2)
      DO 59  JJ=5,6
      W=WAVE(JJ)
C
C     CALCULATE THE ELECTRON-ATOM CONTINUUM
C
      CALL INTERP(TQ, QEAT, 8, 3,TE,QEA )
      CECEA(L,JJ)= 2.20E-42*QEA*DE*DA*TE**1.5*(4+3*1.43879/W/1.0E-8/TE)*
     1EXP(-1.43879/W/1.0E-8/TE)
C
C     ACCOUNT FOR ADVANCE OF SERIES LIMIT (ERG)
C
      DELES=2.085E-17*ZHE(1)**0.8*DE**(0.2667)
      NPTS = 8
      NTERMS = 3
      IF (TE-1000000.) 650,650,645
  645 NTERMS = 2
  650 CONTINUE
      CALL INTERP(TT,GIFT,NPTS,NTERMS,TE,XIFF)
      CECEI(L,JJ)=5.44E-46*ZHE(1)**2*EXP(-DELEI(L,1)*1.43879/TXB)*
     1     (D1*DE*TE**(-.5)*XIFF*EXP(DELES/BOLTK/TE-1.43879/W/1.E-8/TE))
C
C     T CONT BASED ON RECOMBINATION TO HYDROGENIC LEVEL WITH QUANTUUM DEFECT
C     PRINCIPAL QUANT. NUMBERPNA AND AVERAGE ENERGY EN
C
      DO 912 NN=1,3
      TXIP(NN)=TXI(JJ,NN)
  912 XISP(NN)=XIS(JJ,NN)
      IF(W.LT.WFIN.AND.W.GT.WINI) GO TO 467
      WRITE(6,468)WINI,WFIN
  468 FORMAT(/1X,"WARNING: WAVELENGH OUT OF RANGE."
     1/5X,"THE PROGRAM IS SET UP TO HANDLE ONLY WAVELENGHS",
     25X,"BETWEEN",F8.0," AND",F8.0)
  467 ZETAL=ZETAO+AA*TXB+BB*W
      ZETA=EXP(ZETAL)
      CONST1=5.44E-46*ZHE(1)**2*EXP(-DELEI(L,1)*1.43879/TXB)
      CONST2=D1*DE**TEOTA*TE**(-1.5*TEOTA)
      CONST3=ZHE(1)**2*EH*1.43879*(2.*CONST)**(1-TEOTA)
      CONST4=1./Z(L,2)*(Z(L,1)/Z(L,2))**(TEXOTA-1.)
      CONST5=EXP(EIINF(1)*1.43879/TEX(1)*(TEXOTA-1)-1.43879/W/1.E-8/TXB)
      CECFB(L,JJ)=CONST1*CONST2*CONST3*CONST4*ZETA*CONST5
   59 FNLEMC(L,JJ)=CECFB(L,JJ)+CECEA(L,JJ)+CECEI(L,JJ)
C    ------------------------------------------------------------
      IF(L-31) 28,51,51
   51 IF(IPRES.NE.3) GOTO 82
      WRITE(6,70)P,TEOTA,TEOTX1(J1),TX20X1(J2)
   70 FORMAT(/,78X,F8.4,3F5.1)
C    ------------------------------------------------------------
C     PRINT PARTITION FUNCTIONS VS. TEX FOR A GIVEN SET OF
C     CONDITIONS.
C    ------------------------------------------------------------
```

```
      WRITE(6,52)P,TEOTA,TEOTX1(J1),TX20X1(J2)
   52 FORMAT(1H1,3(/),14X,28HINTERNAL PARTITION FUNCTIONS,10X,
     1   10HPRESSURE =,F8.4,1X,3HBAR,/,14X,8HOF ARGON,30X,
     2   10HTE/TA    =,F6.2,/,52X,
     3   10HTE/TXA   =,F6.2,/,52X,10HTX1/TXA  =,F6.2,//,14X,3HTEX,9X,
     4   4HATOM,6X,5HFIRST,6X,
     5   6HSECOND,5X,5HTHIRD,5X,6HFOURTH,/,14X,5HDEG K,19X,3HION,8X,
     6   3HION,8X,3HION,8X,3HION,/)
      WRITE(6,53)(TX1(LFA),(Z(LFA,N),N=1,5),LFA=1,31)
   53 FORMAT(5(13X,F6.0,F11.3,F11.3,F11.3,F11.3,F11.3,/),/,
     1       10(13X,F6.0,F11.3,F11.3,F11.3,F11.3,F11.3,/),/,
     2       10(13X,F6.0,F11.3,F11.3,F11.3,F11.3,F11.3,/),/,
     3        6(13X,F6.0,F11.3,F11.3,F11.3,F11.3,F11.3,/))
      WRITE(6,71)P,TEOTA,TEOTX1(J1),TX20X1(J2)
   71 FORMAT(51X,F8.4,3F5.1)
C    ------------------------------------------------------------
C     PRINT LINE AND CONTINUUM EMISSION COEFFICIENTS W/CC/STRAD
C    ------------------------------------------------------------
      WRITE(6,54)
   54 FORMAT  (1H1)
      WRITE(6,55)P,TEOTA,TEOTX1(J1),TX20X1(J2)
   55 FORMAT(3(/),14X,27HARGON EMISSION COEFFICIENTS,33X,10HPRESSURE =,
     1   F8.4,1X,3HBAR,/,14X,17H(WATTS/CC STERAD),43X,10HTE/TA    =,
     2   F6.2,/,74X,10HTE/TXA   =,F6.2,/,74X,10HTX1/TXA  =,F6.2,//,
     3                        14X,5HTEX  ,2X,7HNEUTRAL,4X,7HNEUTRAL,4X,
     4   2(7H  ION  ,4X),
     5   9HCONTINUUM,2X,9HCONTINUUM,2X,8HELECTRON)
      WRITE(6,812)(WAVE(KL),KL=1,6)
  812 FORMAT(14X,5HDEG K,2X,6(F7.2,4X),7HDENSITY/)
      WRITE(6,56)(TX1(LFA),(FNLEMC(LFA,JJ),JJ=1,6),DEI(LFA),LFA=1,31)
   56 FORMAT(5(13X,F6.0,1X,E10.3,1X,E10.3,1X,E10.3,1X,E10.3,1X,E10.3
     1   ,1X,E10.3,1X,E10.3,/),/,
     2       10(13X,F6.0,1X,E10.3,1X,E10.3,1X,E10.3,1X,E10.3,1X,E10.3
     3   ,1X,E10.3,1X,E10.3,/),/,
     4       10(13X,F6.0,1X,E10.3,1X,E10.3,1X,E10.3,1X,E10.3,1X,E10.3
     5   ,1X,E10.3,1X,E10.3,/),/,
     6        6(13X,F6.0,1X,E10.3,1X,E10.3,1X,E10.3,1X,E10.3,1X,E10.3
     7   ,1X,E10.3,1X,E10.3,/))
      WRITE(6,72)P,TEOTA,TEOTX1(J1),TX20X1(J2)
   72 FORMAT(73X,F8.4,3F5.1)
C
C    ---- USE SUBROUTINE PROPER TO CALCULATE THERMODYNAMIC
C         PROPERTIES VS. TEX                                    ----
C
   82 CONTINUE
      CALL PROPER(TX1,TEOTA,TEOTXA,TX10XA,P,DEI,DH,DT,Z,WT,
     1    WORDS,NI,EZERO,TN,IPRES)
   28 CONTINUE
   29 CONTINUE
      END
C ------------------------------------------------------------
      SUBROUTINE INTERP (X,Y,NPTS,NTERMS,XIN,YOUT)
      DOUBLE PRECISION DELTAX,DELTA,A,PROD,SUM
      DIMENSION X(8),Y(8),DELTA(10),A (10)
C
C          SEARCH FOR APPROPRIATE VALUE OF X
C
   11 DO 19 I=1,NPTS
      IF (XIN-X(I)) 13,17,19
   13 II=I-NTERMS/2
      IF(II) 15,15,21
   15 II = 1
      GO TO 21
   17 YOUT=Y(I)
   18 GO TO 61
   19 CONTINUE
```

```
      I1=NPTS-NTERMS+1
   21 I2=I1+NTERMS-1
      IF(NPTS-I2) 23,31,31
   23 I2=NPTS
      I1=I2-NTERMS+1
   25 IF (I1) 26,26,31
   26 I1=1
   27 NTERMS = I2-I1+1
C
C           EVALUATE DEVIATIONS DELTA
C
   31 DENOM = X(I1+1)-X(I1)
      DELTAX=(XIN-X(I1)) / DENOM
      DO 35 I=1, NTERMS
      IX= I1+I-1
   35 DELTA(I) = (X(IX) - X(I1)) / DENOM
C
C           ACCUMULATE COEFFICIENTS A
C
   40 A(1) = Y(I1)
   41 DO 50 K=2, NTERMS
      PROD = 1.
      SUM = 0.
      IMAX = K - 1
      IXMAX = I1 + IMAX
      DO 49 I=1, IMAX
      J = K - I
      PROD = PROD * (DELTA(K) - DELTA(J))
   49 SUM = SUM - A(J)/PROD
   50 A(K) = SUM + Y(IXMAX)/PROD
C
C           ACCUMULATE SUM OF EXPANSION
C
   51 SUM = A(1)
      DO 57 J=2, NTERMS
      PROD = 1.
      IMAX = J - 1
      DO 56 I=1, IMAX
   56 PROD = PROD * (DELTAX - DELTA(I))
   57 SUM = SUM + A(J)*PROD
   60 YOUT = SUM
   61 RETURN
      END
C -------------------------------------------------------------
      SUBROUTINE PROPER(TX1,TEOTA,TEOTXA,TX1OXA ,P,DE,DH,DT,ZX,WT,WORDS,
     1   NI,EZERO,TN,IPRES)
      DIMENSION TX1(31),TX1OXA(5)  ,TJ(5),TN(33),TTRANS(31),DE(31),
     1   DH(31,5),ZX(31,5),FLZT(5),FLZX(5),FLZON(5),GN(31),WTM(31),R(31)
     2   ,SN(31),HN(31),CPN(31),GAMMA(31),C(31),X(5),Y(5),A(5),XNV(56)
     3   ,TX1(31,5),DENS(31),DT(31),WTF(5),EZERO(31,6),WORDS(4)
     4   ,HORT(31),SOR(31),ZCOMP(31), CPGM(31),LNP(3),LNTN(31),
     5  ZPRES(31,3),DZDLT(31),DZDLP(31),CVN(31)
      REAL LNP,LNTN
C
C     INPUT VARIABLES MUST BE IN DEG K, BAR,CM**3,NI=1+NO. OF IONS
C     WORDS IS NAME OF GAS
C
      DO 29 I=1,5
   29 WTF(I)=1.0
      DO 2 L=1,31
      TX1(L,1)=TX1(L)
      DO 2 N=2,NI
      TX1(L,N)=TX1OXA(N)*TX1(L)
   2  CONTINUE
      DO 40 L=1,31
      TE=TEOTXA*TX1(L)
```

```
      TA=TE/TEOTA
      DENS(L)=(DT(L)-DE(L))*WT/6.02252E+23
      WTM(L)=(DT(L)-DE(L))*WT/DT(L)
      ZCOMP(L)=WT/WTM(L)
      LNP(IPRES)=P
      ZPRES(L,IPRES)=ZCOMP(L)
      R(L)=8.3143E+07/WTM(L)
      TTRANS(L)=P*1.0E+06/DENS(L)/R(L)
      FLZTE=ALOG(2.4148E+15*TE**1.5/DE(L))
      FLZONE=ALOG(2.)  +FLZTE
      AN=  DE(L)*1.38054E-16*TE/DENS(L)*(FLZONE+1.0)
      TNN=DE(L)*TE*(FLZTE+1.)
      TND=DE(L)*(FLZTE+1.)
      DO 6 N=1,NI
      IF(DH(L,N).GT.1.)   GOTO 2345
      FLZT(N)=0.
       GOTO 2347
 2345 FLZT(N)=ALOG(1.8793E+20*(WT*TA)**1.5/DH(L,N))
 2347 IF(N-1)  5,5,7
    5 FLZX(N)=ALOG(ZX(L,N))
      GO TO 9
    7 FLZX(N)=ALOG(ZX(L,N))-1.43879*EZERO(L,N)/TXI(L,N-1)
    9 FLZON(N)=FLZT(N)+FLZX(N)
      IF(TXI(L,N))  81,81,82
   81 TJ(N)=TA
      GO TO 83
   82 TJ(N)=(TA*(FLZT(N)+1.)+TXI(L,N)*ALOG(ZX(L,N)))/(FLZT(N)+1.
     1    + ALOG(ZX(L,N)))
   83 AN=AN+DH(L,N)*1.38054E-16*TJ(N)/DENS(L)*(FLZON(N)+1.0)
      TNN=TNN+DH(L,N)*TJ(N)*(FLZON(N)+1.0)
      TND=TND+DH(L,N)*(FLZON(N)+1.0)
    6 CONTINUE
      TN(L)=TNN/TND
      LNTN(L)=ALOG(TN(L))
      GN(L)=  AN-P*1.0E+06/DENS(L)
   40 CONTINUE
      DO 50 L=1,31
      SN(L)=DYDTP(GN,TN,L)
      HN(L)=-GN(L)+TN(L)*SN(L)
   50 CONTINUE
      IF(IPRES.NE.3)  RETURN
      DO 30 L=1,31
      CPN(L)=DYDTP(HN,TN,L)
      DZDLT(L)=DYDTP(ZCOMP,TN,L)
      DZDLP(L)=DZDP(ZPRES,LNP,L)
      CVN(L)=CPN(L)-R(L)*(ZCOMP(L)+TN(L)*DZDLT(L))**2/
     1    (ZCOMP(L)-P*DZDLP(L))
   30 CONTINUE
      DO 43 L=1,31
      IF(CVN(L))44,44,45
   44 IF(L.EQ.1)  CVN(L)=CVN(L+1)
      IF(L.EQ.31)  CVN(L)=CVN(L-1)
      IF(L.EQ.1.OR.L.EQ.31)  GO TO 45
      CVN(L)=(CVN(L-1)+CVN(L-1))/2.
   45 GAMMA(L)=ABS(CPN(L)/CVN(L)*ZCOMP(L))
      C(L)=SQRT(GAMMA(L)*R(L)*TN(L))
      DLRTN=TN(L)/R(L)*DYDTP(R,TN,L)
      CPGM(L)=(1.+GAMMA(L)*DLRTN)/(1.+DLRTN)
      HORT(L)=ZCOMP(L)*HN(L)/R(L)/273.16
      SOR(L)=ZCOMP(L)*SN(L)/R(L)
   43 CONTINUE
      DO 51 L=1,31
      DENS(L)=DENS(L)*1.0E+03
      HN(L)=HN(L)*1.0E-07
      SN(L)=SN(L)*1.0E-07
      GN(L)=GN(L)*1.0E-07
```

```
      CPN(L)=CPN(L)*1.0E-07
      CVN(L)=CVN(L)*1.0E-07
      R(L)=R(L)*1.0E-07
      C(L)=C(L)/100.
   51 CONTINUE
      WRITE(6,60)WORDS,P,TEOTA,TEOTXA,TX1OXA(2)
   60 FORMAT(1H1,3(/),14X,28HTHERMODYNAMIC PROPERTIES OF ,4A5,16X,
     1  10HPRESSURE =,F8.4,4H BAR,/,78X,10HTE/TA    =,F6.2,/,
     2  78X,10HTE/TEXA  =,F6.2,/,78X,10HTX1/TXA  =,F6.2,//,
     4  14X,5HTEXA ,8H  T EQIV,8H  T TRAN,11H   DENSITY ,11H  ENTHALPY
     5  ,9H  ENTROPY,11H  - GIBBS F,9H     CP  ,
     6  7H  GAMMA,9H     V     ,/,
     7  14X, 5HDEG K, 8H   DEG K, 8H   DEG K,11H   KG/M**3 ,11H   KJ/KG
     8  ,9H  KJ/KG K,4X,'KJ/KG  ',9H  KJ/KG K,2X,'EFF ',9H    M/S  ,/)
      WRITE(6,70) (TX1(L),TN(L),TTRANS(L),DENS(L),HN(L),SN(L),GN(L),
     1 CPN(L),GAMMA(L),C(L),L=1,31)
   70 FORMAT(5(13X,F6.0,2F8.0,2E11.3,F9.3,E11.3,F8.3,F8.3,F8.0,/),/,
     1       10(13X,F6.0,2F8.0,2E11.3,F9.3,E11.3,F8.3,F8.3,F8.0,/),/,
     2       10(13X,F6.0,2F8.0,2E11.3,F9.3,E11.3,F8.3,F8.3,F8.0,/),/,
     3       6(13X,F6.0,2F8.0,2E11.3,F9.3,E11.3,F8.3,F8.3,F8.0,/))
      WRITE(6,80)P,TEOTA,TEOTXA,TX1OXA(2)
   80 FORMAT(  84X,F8.4,3F5.1)
      WRITE(6,62)WORDS,P,TEOTA,TEOTXA,TX1OXA(2)
   62 FORMAT(1H1,3(/),14X,28HTHERMODYNAMIC PROPERTIES OF ,4A5,11X,
     1  10HPRESSURE =,F8.4,4H BAR,/,78X,10HTE/TA    =,F6.2,/,
     2  78X,10HTE/TEXA  =,F6.2,/,78X,10HTX1/TXA  =,F6.2,//,
     4  14X,5HTEXA ,8H  T EQIV,8H  T TRAN,11H   2ZH/RT  ,11H     2ZS/R
     5  ,11H       R      ,11H   CAP GAM ,5X,'Z',4X,'CV(KJ/KG-K)'/)
      WRITE(6,72) (TX1(L),TN(L),TTRANS(L),HORT(L),SOR(L)  ,R(L),CPGM(L),
     1 ZCOMP(L),CVN(L),L=1,31)
   72 FORMAT( 5(11X,3F8.0,4E11.3,F8.3,F9.3,/),/,
     1       10(11X,3F8.0,4E11.3,F8.3,F9.3,/),/,
     2       10(11X,3F8.0,4E11.3,F8.3,F9.3,/),/,
     3        6(11X,3F8.0,4E11.3,F8.3,F9.3,/))
      WRITE(6,80)P,TEOTA,TEOTXA,TX1OXA(2)
      RETURN
      END
C -------------------------------------------------------
C       FUNCTION DZDP  TO DIFFERENTIATE Z VS. P
C -------------------------------------------------------
      FUNCTION DZDP(Y,X,L)
      DIMENSION Y(31,3),X(3)
      CLM=((Y(L,2)-Y(L,1))*(X(3)-X(1))-(Y(L,3)-Y(L,1))*(X(2)-X(1)
     1  ))/((X(2)**2-X(1)**2)*(X(3)-X(1))-(X(3)**2-X(1)**2)*
     2  (X(2)-X(1)))
      B=((Y(L,2)-Y(L,1))-CLM*(X(2)**2-X(1)**2))/(X(2)-X(1))
      DZDP=B+2.*CLM*X(3)
      RETURN
      END
C -------------------------------------------------------
      FUNCTION DYDTP(YN,TN,L)
      DIMENSION YN(31),TN(31),X(5),Y(5),WTF(5),A(5),XNV(56)
      DOUBLE PRECISION YN,TN,X,Y,WTF,A,XNV
      DO 29 I=1,5
      A(I)=0.
   29 WTF(I)=1.0
      IF (L-2) 12,12,16
   12 DO 14 I=1,5
      X(I)= TN(I)
   14 Y(I)=YN(I)
      GO TO 26
   16 IF(L-30) 22,18,18
   18 DO 20 I=1,5
      X(I)=TN(26+I)
   20 Y(I)=YN(26+I)
      GO TO 26
```

```
   22 DO 24 I=1,5
      X(I)=TN(L-3+I)
   24 Y(I)=YN(L-3+I)
   26 CONTINUE
      CALL POLFIT(X,Y,WTF,5,4, 0,A,CHISQR)
      DYDTP =(A(2)+2.*A(3)*TN(L)+3.*A(4)*TN(L)**2)
      RETURN
      END
C -------------------------------------------------------------
      SUBROUTINE POLFIT(X,Y,SIGMAY,NPTS,NTERMS,MODE,A,CHISQR)
      DOUBLE PRECISION SUMX,SUMY,XTERM,YTERM,ARRAY,CHISQ
      DIMENSION X(5),Y(5),SIGMAY(5),A(5),SUMX(19),SUMY(10),ARRAY(10,10)
C     ACCUMULATE WEIGHTED SUMS
   11 NMAX=2*NTERMS-1
      DO 13 N=1,NMAX
   13 SUMX(N)=0.
      DO 15 J=1,NTERMS
   15 SUMY(J)=0.
      CHISQ=0.
   21 DO 50 I=1,NPTS
      XI=X(I)
      YI=Y(I)
   31 IF(MODE) 32,37,39
   32 IF(YI) 35,37,33
   33 WEIGHT=1./YI
      GO TO 41
   35 WEIGHT = 1. / (-YI)
      GO TO 41
   37 WEIGHT = 1.
      GO TO 41
   39 WEIGHT = 1. / SIGMAY(I)**2
   41 XTERM = WEIGHT
      DO 44 N=1,NMAX
      SUMX(N) = SUMX(N) + XTERM
   44 XTERM = XTERM * XI
   45 YTERM = WEIGHT * YI
      DO 48 N=1,NTERMS
      SUMY(N) = SUMY(N) + YTERM
   48 YTERM = YTERM * XI
   49 CHISQ =CHISQ + WEIGHT*YI**2
   50 CONTINUE
C     CONSTRUCT MATRICIES AND CALCULATE COEFFICIENTS
   51 DO 54 J=1,NTERMS
      DO 54 K=1,NTERMS
      N = J + K - 1
   54 ARRAY(J,K) = SUMX(N)
      DELTA = DETERM (ARRAY, NTERMS)
      IF (DELTA) 61, 57, 61
   57 CHISQR = 0.
      DO 59 J=1, NTERMS
   59 A(J) = 0.
      GO TO 80
   61 DO 70 L=1, NTERMS
   62 DO 66 J=1, NTERMS
      DO 65 K=1, NTERMS
      N = J + K - 1.
   65 ARRAY(J,K) = SUMX(N)
   66 ARRAY(J,L) = SUMY(J)
   70 A(L) = DETERM (ARRAY, NTERMS) / DELTA
C     CALCULATE CHI SQUARE
   71 DO 75 J=1, NTERMS
      CHISQ = CHISQ - 2.*A(J)*SUMY(J)
      DO 75 K=1, NTERMS
      N = J + K - 1
   75 CHISQ = CHISQ + A(J)*A(K)*SUMX(N)
   76 FREE = NPTS - NTERMS
```

```
   77 CHISQR = CHISQ / FREE
   80 RETURN
      END
C-------------------------------------------------------------
      FUNCTION DETERM (ARRAY,NORDER)
      DOUBLE PRECISION ARRAY,SAVE
      DIMENSION ARRAY(10,10)
C     CALCULATE THE DETERMINANT OF A SQUARE MATRIX
C     NORDER - ORDER OF DETERMINANT (DEGREE OF MATRIX)
C     THIS SUBPROGAM DESTROYS THE INPUT MATRIX ARRAY
C     DIMENSION STATEMENT VALID FOR NORDER UP TO 10
   10 DETERM=1.
   11 DO 50 K=1,NORDER
C     INTERCHANGE COLUMNS IF DIAGONAL ELEMENT IS ZERO
      IF (ARRAY(K,K)) 41, 21, 41
   21 DO 23 J=K, NORDER
      IF (ARRAY(K,J)) 31, 23, 31
   23 CONTINUE
      DETERM = 0.
      GO TO 60
   31 DO 34 I=K, NORDER
      SAVE = ARRAY(I,J)
      ARRAY(I,J) = ARRAY(I,K)
   34 ARRAY (I,K) = SAVE
      DETERM = - DETERM
C     SUBTRACT ROW K FROM LOWER ROWS TO GET DIAGONAL MATRIX
   41 DETERM = DETERM * ARRAY(K,K)
      IF (K- NORDER) 43, 50, 50
   43 K1 = K + 1
      DO 46 I=K1, NORDER
      DO 46 J=K1, NORDER
   46 ARRAY(I,J) = ARRAY(I,J) - ARRAY(I,K) * ARRAY(K,J)/ARRAY(K,K)
   50 CONTINUE
   60 RETURN
      END
```

MULTI-THERMAL EQUILIBRIUM COMPOSITION OF ARGON PLASMA

PRESSURE = 1.0000BAR
TE/TA = 1.00
TE/TXA = 1.00
TX1/TXA = 1.00

TEX DEG K	NUMBER OF ATOMS PER CC.	NUMBER OF 1ST IONS PER CC.	NUMBER OF 2ND IONS PER CC.	NUMBER OF 3RD IONS PER CC.	NUMBER OF 4TH IONS PER CC.	NUMBER OF ELECTRONS PER CC.	NE/N1,A	TOTAL PARTICLES PER CC.	
5000.	.14487E+19	.13106E+13	.00000E+00	.00000E+00	.00000E+00	.13106E+13	.90470E-06	.14487E+19	7
6000.	.12072E+19	.29205E+14	.00000E+00	.00000E+00	.00000E+00	.29205E+14	.24193E-04	.12073E+19	8
7000.	.10343E+19	.27021E+15	.56769E+02	.00000E+00	.00000E+00	.27021E+15	.26126E-03	.10348E+19	9
8000.	.90257E+18	.14416E+16	.21966E+05	.00000E+00	.00000E+00	.14416E+16	.15972E-02	.90545E+18	10
9000.	.79427E+18	.53107E+16	.23382E+07	.00000E+00	.00000E+00	.53107E+16	.66867E-02	.80489E+18	10
10000.	.69459E+18	.14988E+17	.10058E+09	.00000E+00	.00000E+00	.14988E+17	.21584E-01	.72456E+18	11
11000.	.59036E+18	.34386E+17	.22312E+10	.00000E+00	.00000E+00	.34386E+17	.58304E-01	.65913E+18	12
12000.	.47280E+18	.66154E+17	.29988E+11	.00000E+00	.00000E+00	.66154E+17	.14032E+00	.60511E+18	13
13000.	.34367E+18	.10813E+18	.27268E+12	.16611E+01	.00000E+00	.10813E+18	.31666E+00	.55993E+18	14
14000.	.21970E+18	.15086E+18	.18141E+13	.12475E+03	.00000E+00	.15087E+18	.69824E+00	.52143E+18	18
15000.	.12331E+18	.18220E+18	.93674E+13	.58034E+04	.00000E+00	.18222E+18	.15353E+01	.48774E+18	23
16000.	.63671E+17	.19693E+18	.39369E+14	.18179E+06	.00000E+00	.19701E+18	.33466E+01	.45765E+18	26
17000.	.32520E+17	.19887E+18	.13990E+15	.40360E+07	.00000E+00	.19915E+18	.70832E+01	.43067E+18	27
18000.	.17400E+17	.19390E+18	.43255E+15	.65959E+08	.00000E+00	.19476E+18	.14329E+02	.40650E+18	28
19000.	.10020E+17	.18562E+18	.11863E+16	.81986E+09	.00000E+00	.18800E+18	.27611E+02	.38483E+18	29
20000.	.62264E+16	.17519E+18	.29181E+16	.79544E+10	.00000E+00	.18103E+18	.50992E+02	.36536E+18	29
21000.	.41201E+16	.16218E+18	.64503E+16	.61194E+11	.39310E+02	.17508E+18	.91489E+02	.34783E+18	29
22000.	.28362E+16	.14548E+18	.12733E+17	.37528E+12	.11523E+04	.17095E+18	.16256E+03	.33201E+18	29
23000.	.19745E+16	.12449E+18	.22234E+17	.18366E+13	.23395E+05	.16897E+18	.29229E+03	.31767E+18	29
24000.	.13526E+16	.10034E+18	.34190E+17	.72301E+13	.33746E+06	.16874E+18	.54136E+03	.30462E+18	28
25000.	.89370E+15	.75870E+17	.46637E+17	.23398E+14	.35993E+07	.16921E+18	.10413E+04	.29264E+18	28
26000.	.56524E+15	.54208E+17	.57434E+17	.64241E+14	.29808E+08	.16927E+18	.20740E+04	.28154E+18	29
27000.	.34391E+15	.37155E+17	.65306E+17	.15465E+15	.20080E+09	.16823E+18	.42298E+04	.27119E+18	28
28000.	.20384E+15	.24882E+17	.70066E+17	.33582E+15	.11426E+10	.16602E+18	.87072E+04	.26151E+18	27
29000.	.11934E+15	.16553E+17	.72177E+17	.67201E+15	.56469E+10	.16292E+18	.17860E+05	.25245E+18	35
30000.	.69547E+14	.11270E+17	.72109E+17	.12549E+16	.24670E+11	.15925E+18	.36285E+05	.24396E+18	35
31000.	.49038E+14	.76782E+16	.70583E+17	.22137E+16	.96761E+11	.15549E+18	.72360E+05	.23601E+18	36
32000.	.29023E+14	.53089E+16	.67712E+17	.36963E+16	.34270E+12	.15182E+18	.14205E+06	.22857E+18	37
33000.	.17248E+14	.37173E+16	.63584E+17	.58469E+16	.11005E+13	.14843E+18	.27546E+06	.22160E+18	37
34000.	.10250E+14	.26225E+16	.58262E+17	.87486E+16	.32090E+13	.14541E+18	.53052E+06	.21505E+18	37
35000.	.60596E+13	.18522E+16	.51904E+17	.12360E+17	.85072E+13	.14277E+18	.10211E+07	.20890E+18	37

1.0000 1.0 1.0 1.0

INTERNAL PARTITION FUNCTIONS
OF ARGON

PRESSURE = 1.0000 BAR
TE/TA = 1.00
TE/TXA = 1.00
TX1/TXA = 1.00

TEX DEG K	ATOM	FIRST ION	SECOND ION	THIRD ION	FOURTH ION
5000.	1.000	5.325	7.904	4.023	6.239
6000.	1.000	5.419	8.158	4.064	6.669
7000.	1.000	5.490	8.393	4.134	7.032
8000.	1.000	5.546	8.615	4.233	7.350
9000.	1.000	5.591	8.827	4.362	7.637
10000.	1.000	5.628	9.029	4.515	7.899
11000.	1.001	5.658	9.221	4.689	8.140
12000.	1.003	5.684	9.405	4.881	8.364
13000.	1.006	5.707	9.579	5.086	8.573
14000.	1.017	5.726	9.745	5.301	8.767
15000.	1.039	5.743	9.902	5.522	8.949
16000.	1.082	5.759	10.052	5.749	9.120
17000.	1.157	5.772	10.194	5.978	9.280
18000.	1.280	5.785	10.330	6.208	9.431
19000.	1.472	5.798	10.459	6.438	9.573
20000.	1.754	5.812	10.583	6.666	9.707
21000.	2.153	5.827	10.702	6.891	9.834
22000.	2.697	5.848	10.816	7.114	9.953
23000.	3.416	5.876	10.927	7.333	10.066
24000.	4.340	5.917	11.035	7.548	10.174
25000.	5.500	5.975	11.141	7.759	10.276
26000.	6.926	6.059	11.246	7.966	10.373
27000.	8.647	6.178	11.351	8.167	10.465
28000.	10.691	6.343	11.457	8.365	10.552
29000.	13.083	6.568	11.565	8.557	10.636
30000.	15.846	7.010	11.683	8.745	10.716
31000.	22.821	7.461	11.803	8.928	10.792
32000.	27.156	8.043	11.934	9.106	10.865
33000.	32.010	8.781	12.074	9.280	10.934
34000.	37.399	9.704	12.228	9.450	11.001
35000.	43.336	10.842	12.399	9.615	11.065

1.0000 1.0 1.0 1.0

ARGON EMISSION COEFFICIENTS
(WATTS/CC STERAD)

PRESSURE = 1.0000 BAR
TE/TA = 1.00
TE/TXA = 1.00
TX1/TXA = 1.00

TEX DEG K	NEUTRAL 7147.04	NEUTRAL 4300.10	ION 4609.56	ION 4806.02	CONTINUUM 4200.00	CONTINUUM 6800.00	ELECTRON DENSITY
5000.	.255E-08	.251E-09	.300E-20	.161E-18	.103E-22	.765E-22	.131E+13
6000.	.363E-06	.571E-07	.234E-15	.599E-14	.784E-20	.356E-19	.292E+14
7000.	.122E-04	.269E-05	.736E-12	.111E-10	.938E-18	.311E-17	.270E+15
8000.	.167E-03	.475E-04	.311E-09	.315E-08	.318E-16	.836E-16	.144E+16
9000.	.125E-02	.433E-03	.343E-07	.255E-06	.461E-15	.101E-14	.531E+16
10000.	.605E-02	.246E-02	.147E-05	.852E-05	.363E-14	.693E-14	.150E+17
11000.	.209E-01	.965E-02	.312E-04	.148E-03	.180E-13	.307E-13	.344E+17
12000.	.537E-01	.276E-01	.383E-03	.153E-02	.604E-13	.942E-13	.662E+17
13000.	.104E+00	.588E-01	.301E-02	.104E-01	.143E-12	.208E-12	.108E+18
14000.	.154E+00	.938E-01	.161E-01	.494E-01	.244E-12	.334E-12	.151E+18
15000.	.176E+00	.115E+00	.624E-01	.172E+00	.309E-12	.404E-12	.182E+18
16000.	.166E+00	.115E+00	.187E+00	.470E+00	.312E-12	.394E-12	.197E+18
17000.	.140E+00	.102E+00	.464E+00	.107E+01	.274E-12	.338E-12	.199E+18
18000.	.112E+00	.854E-01	.101E+01	.217E+01	.225E-12	.273E-12	.195E+18
19000.	.880E-01	.700E-01	.197E+01	.397E+01	.179E-12	.216E-12	.188E+18
20000.	.688E-01	.568E-01	.354E+01	.673E+01	.141E-12	.169E-12	.181E+18
21000.	.536E-01	.457E-01	.586E+01	.106E+02	.109E-12	.133E-12	.175E+18
22000.	.411E-01	.362E-01	.890E+01	.153E+02	.839E-13	.103E-12	.171E+18
23000.	.306E-01	.277E-01	.123E+02	.203E+02	.628E-13	.786E-13	.169E+18
24000.	.218E-01	.203E-01	.154E+02	.243E+02	.453E-13	.578E-13	.169E+18
25000.	.147E-01	.140E-01	.173E+02	.264E+02	.311E-13	.406E-13	.169E+18
26000.	.937E-02	.911E-02	.178E+02	.262E+02	.204E-13	.272E-13	.169E+18
27000.	.569E-02	.565E-02	.170E+02	.242E+02	.129E-13	.176E-13	.168E+18
28000.	.334E-02	.338E-02	.153E+02	.212E+02	.806E-14	.111E-13	.166E+18
29000.	.193E-02	.199E-02	.133E+02	.179E+02	.501E-14	.701E-14	.163E+18
30000.	.111E-02	.116E-02	.113E+02	.148E+02	.320E-14	.453E-14	.159E+18
31000.	.642E-03	.682E-03	.939E+01	.120E+02	.207E-14	.295E-14	.155E+18
32000.	.373E-03	.402E-03	.771E+01	.966E+01	.137E-14	.196E-14	.152E+18
33000.	.218E-03	.238E-03	.624E+01	.765E+01	.923E-15	.132E-14	.148E+18
34000.	.127E-03	.140E-03	.495E+01	.596E+01	.633E-15	.906E-15	.145E+18
35000.	.737E-04	.825E-04	.385E+01	.454E+01	.438E-15	.624E-15	.143E+18

1.0000 1.0 1.0 1.0

THERMODYNAMIC PROPERTIES OF ARGON MIE

PRESSURE = 1.0000 BAR
TE/TA = 1.00
TE/TEXA = 1.00
TX1/TXA = 1.00

TEXA DEG K	T EQIV DEG K	T TRAN DEG K	DENSITY KG/M**3	ENTHALPY KJ/KG	ENTROPY KJ/KG K	- GIBBS F KJ/KG	CP KJ/KG K	GAMMA EFF	V M/S
5000.	5000.	5000.	.961E-01	.263E+04	5.350	.241E+05	.495	1.737	1345.
6000.	6000.	6000.	.801E-01	.311E+04	5.437	.295E+05	.497	1.718	1465.
7000.	7000.	7000.	.686E-01	.365E+04	5.520	.350E+05	.550	1.617	1535.
8000.	8000.	8000.	.600E-01	.423E+04	5.597	.405E+05	.625	1.534	1600.
9000.	9000.	8999.	.530E-01	.497E+04	5.684	.462E+05	.890	1.385	1616.
10000.	10000.	9997.	.471E-01	.613E+04	5.806	.519E+05	1.515	1.293	1657.
11000.	11000.	10990.	.414E-01	.819E+04	6.001	.578E+05	2.725	1.299	1771.
12000.	12000.	11971.	.357E-01	.118E+05	6.316	.640E+05	4.741	1.410	1989.
13000.	13000.	12936.	.300E-01	.178E+05	6.794	.705E+05	7.336	1.659	2359.
14000.	14000.	13892.	.246E-01	.263E+05	7.420	.776E+05	9.272	2.074	2916.
15000.	15000.	14851.	.203E-01	.357E+05	8.073	.854E+05	9.135	2.569	3578.
16000.	16000.	15828.	.173E-01	.440E+05	8.605	.937E+05	7.066	2.966	4165.
17000.	17000.	16819.	.154E-01	.498E+05	8.957	.103E+06	4.659	3.291	4655.
18000.	18000.	17820.	.140E-01	.535E+05	9.173	.112E+06	3.105	3.678	5144.
19000.	19000.	18823.	.131E-01	.563E+05	9.321	.121E+06	2.531	3.916	5503.
20000.	20000.	19826.	.122E-01	.589E+05	9.454	.130E+06	2.790	3.701	5526.
21000.	21000.	20825.	.115E-01	.621E+05	9.613	.140E+06	3.892	3.413	5481.
22000.	22000.	21818.	.107E-01	.669E+05	9.836	.149E+06	5.861	3.394	5660.
23000.	23000.	22802.	.986E-02	.740E+05	10.151	.159E+06	8.420	3.655	6114.
24000.	24000.	23779.	.901E-02	.837E+05	10.563	.170E+06	10.840	4.172	6835.
25000.	25000.	24753.	.819E-02	.954E+05	11.040	.181E+06	12.245	4.908	7782.
26000.	26000.	25728.	.745E-02	.108E+06	11.524	.192E+06	12.178	5.714	8806.
27000.	27000.	26710.	.683E-02	.119E+06	11.962	.204E+06	10.827	6.490	9802.
28000.	28000.	27699.	.633E-02	.129E+06	12.324	.216E+06	9.277	6.852	10458.
29000.	29000.	28694.	.594E-02	.138E+06	12.627	.228E+06	7.758	7.002	10918.
30000.	30000.	29692.	.562E-02	.145E+06	12.863	.241E+06	6.272	8.139	12099.
31000.	31000.	30692.	.534E-02	.151E+06	13.057	.254E+06	6.030	8.414	12614.
32000.	32000.	31691.	.509E-02	.157E+06	13.261	.267E+06	6.689	7.677	12341.
33000.	33000.	32688.	.485E-02	.164E+06	13.480	.281E+06	7.758	7.544	12527.
34000.	34000.	33683.	.462E-02	.173E+06	13.734	.294E+06	9.090	7.912	13149.
35000.	35000.	34674.	.439E-02	.183E+06	14.019	.308E+06	10.734	8.941	14344.

1.0000 1.0 1.0 1.0

THERMODYNAMIC PROPERTIES OF ARGON MTE

PRESSURE = 1.0000 BAR
TE/TA = 1.00
TE/TEXA = 1.00
TX1/TXA = 1.00

TEXA	T EQIV	T TRAN	2ZH/RT	2ZS/R	R	CAP GAM	Z	CV(KJ/KG-K)
5000.	5000.	5000.	.463E+02	.257E+02	.208E+00	.100E+01	1.000	.285
6000.	6000.	6000.	.547E+02	.261E+02	.208E+00	.999E+00	1.000	.289
7000.	7000.	7000.	.642E+02	.265E+02	.208E+00	.100E+01	1.000	.340
8000.	8000.	8000.	.744E+02	.269E+02	.208E+00	.101E+01	1.002	.408
9000.	9000.	8999.	.874E+02	.273E+02	.210E+00	.103E+01	1.007	.647
10000.	10000.	9997.	.108E+03	.279E+02	.213E+00	.105E+01	1.021	1.197
11000.	11000.	10990.	.144E+03	.288E+02	.220E+00	.110E+01	1.055	2.214
12000.	12000.	11971.	.208E+03	.303E+02	.234E+00	.120E+01	1.123	3.774
13000.	13000.	12936.	.313E+03	.326E+02	.258E+00	.140E+01	1.239	5.479
14000.	14000.	13892.	.462E+03	.356E+02	.293E+00	.170E+01	1.407	6.291
15000.	15000.	14851.	.629E+03	.388E+02	.332E+00	.199E+01	1.596	5.678
16000.	16000.	15828.	.773E+03	.413E+02	.365E+00	.208E+01	1.756	4.182
17000.	17000.	16819.	.875E+03	.430E+02	.387E+00	.196E+01	1.860	2.633
18000.	18000.	17820.	.941E+03	.441E+02	.400E+00	.179E+01	1.920	1.620
19000.	19000.	18823.	.990E+03	.448E+02	.407E+00	.164E+01	1.955	1.263
20000.	20000.	19826.	.104E+04	.454E+02	.413E+00	.158E+01	1.982	1.494
21000.	21000.	20825.	.109E+04	.462E+02	.419E+00	.168E+01	2.013	2.296
22000.	22000.	21818.	.118E+04	.473E+02	.429E+00	.194E+01	2.061	3.560
23000.	23000.	22802.	.130E+04	.488E+02	.445E+00	.231E+01	2.136	4.922
24000.	24000.	23779.	.147E+04	.507E+02	.467E+00	.278E+01	2.242	5.825
25000.	25000.	24753.	.168E+04	.530E+02	.494E+00	.330E+01	2.371	5.915
26000.	26000.	25728.	.189E+04	.554E+02	.522E+00	.374E+01	2.508	5.345
27000.	27000.	26710.	.210E+04	.575E+02	.548E+00	.399E+01	2.634	4.394
28000.	28000.	27699.	.227E+04	.592E+02	.570E+00	.385E+01	2.739	3.708
29000.	29000.	28694.	.243E+04	.607E+02	.587E+00	.350E+01	2.820	3.124
30000.	30000.	29692.	.255E+04	.618E+02	.599E+00	.357E+01	2.880	2.220
31000.	31000.	30692.	.265E+04	.627E+02	.610E+00	.350E+01	2.931	2.100
32000.	32000.	31691.	.277E+04	.637E+02	.620E+00	.327E+01	2.978	2.595
33000.	33000.	32688.	.289E+04	.648E+02	.630E+00	.342E+01	3.029	3.115
34000.	34000.	33683.	.304E+04	.660E+02	.643E+00	.387E+01	3.088	3.547
35000.	35000.	34674.	.321E+04	.673E+02	.658E+00	.471E+01	3.159	3.793

1.0000 1.0 1.0 1.0

Appendix C

Plasma Refraction Effects

The extent of refraction was checked by passing a laser beam at 6328Å through the arc plasma at various lateral (x) locations as shown in Fig. C.1 (excluding the lens). Refraction of the laser beam through the arc axis is negligible. The refraction first increases and then decreases as the arc is traversed laterally. Values of refractive shift, Δz, one meter from the arc center as a function of location and pressure, at 30A are given in Table C.1. The refractive shift is seen to be maximum at about 2/3 of the arc radius.

When a lens is placed in the optical path to focus the arc onto the slit of the spectrometer, the refracted rays are focused to a different location in the vertical plane than the unrefracted rays. The result is an effective refractive magnification factor, β_{refr}, which is smaller than the unrefracted magnification factor. The optical diagram is given in Fig. C.2 with r and r' indicating the unrefracted and refracted rays eminating horizontally from the object arrow point respectively. The refractive shift at the lens location is denoted by Δz_{refr}, with the apparent displacement of the object arrow point by $\Delta y'_I$.

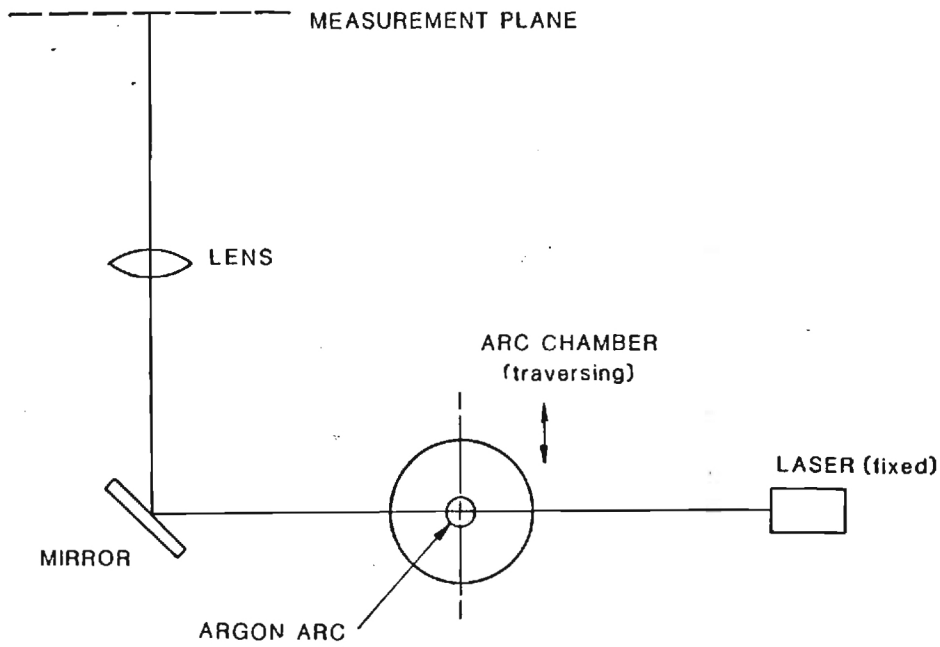

Figure C.1: Optical setup for measuring the refraction effects

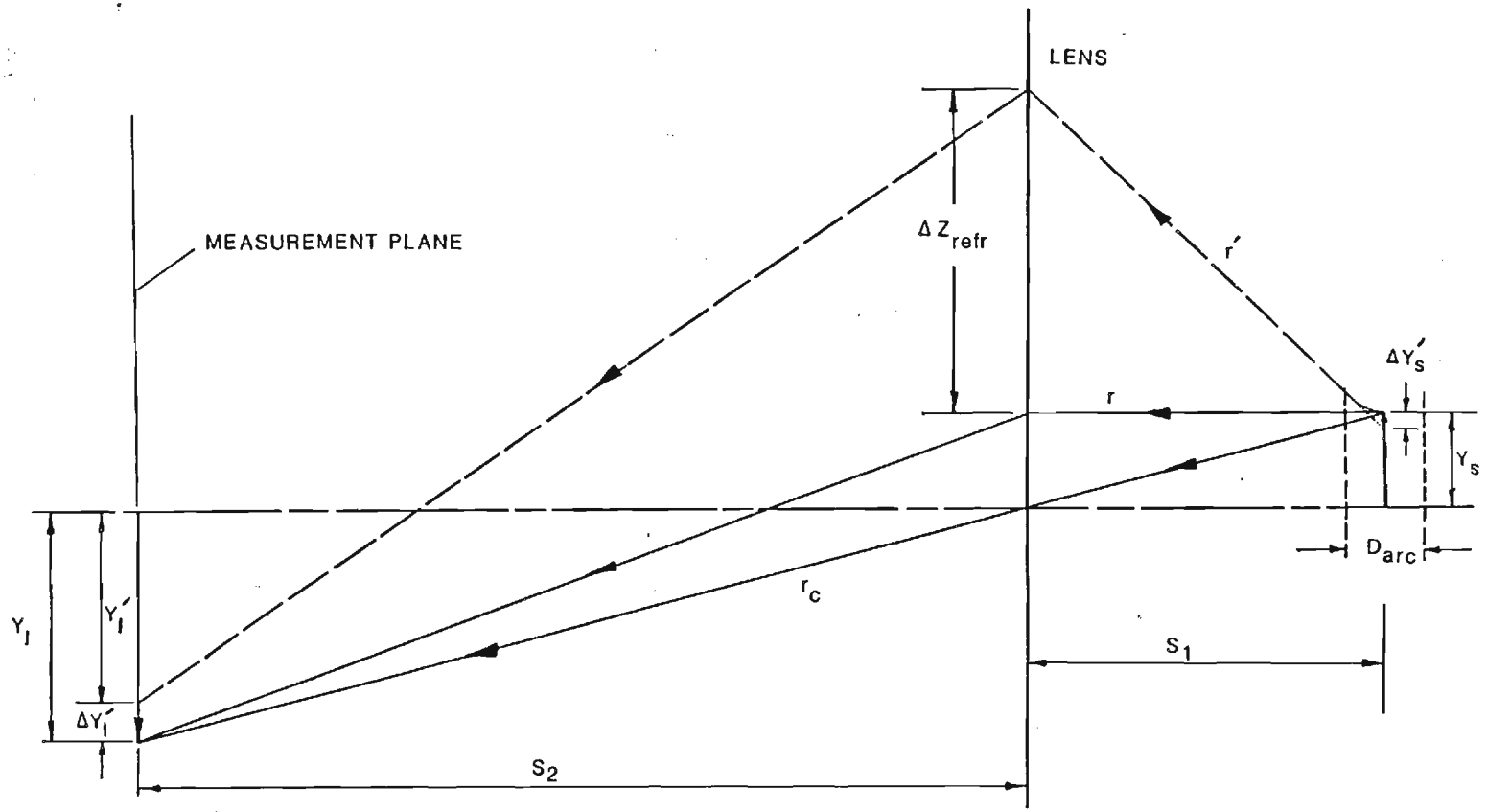

Figure C.2: Ray tracing technique used for determination of the net effect of refraction

Axial distances are large with respect to lateral distances and $D_{arc} << s_1$. Ray tracing geometry is used to determine β_{refr} from the following equations.

$$\beta = \frac{y_I}{y_S} = \frac{y'_I}{y'_s} = \frac{\Delta y'_I}{\Delta y'_s}$$

$$\frac{\Delta y'_s}{D_{arc}/2} \cong \frac{\Delta z_{refr}}{s_1 - D_{arc}/2}$$

$$\beta_{refr} = \frac{y'_I}{y_s} = \frac{y_I - \Delta y'_I}{y_s}$$

$$= \beta - \beta\frac{\Delta y'_s}{y_s} = \beta\left(1 - \frac{\Delta y'_s}{y_s}\right)$$

or

$$\frac{\beta_{refr}}{\beta} = 1 - \left(\frac{D_{arc}/2}{y_s}\right)\frac{\Delta z_{refr}[p,x]}{s_1 - D_{arc}/2}$$

If the maximum refractive shift comes from $x = y_s = D_{arc}/4$, and $D_{arc} << s_1$, then

$$\left.\frac{\beta_{refr}}{\beta}\right|_{maxshift} = 1 - \frac{2\Delta z_{refr}[p]}{s_1}$$

For $s_1 = 750$mm, and $\Delta z_{refr}[20bar] = 10$mm, then

$$\frac{\beta_{refr}}{\beta} \simeq 0.973$$

or less than 3% effect at the worst case. The effect at $p \leq 10$ bar would be much less than 1% and hence negligible.

Table C.1: Values of the refractive shift, Δz(mm), at I=30 amps.

	Pressure (bar)			
x(mm)	.....2.....	.....5.....	.....10.....	.....20.....
0	0	0	0	0
0.1	0	0.07	0.21	0.56
0.2	0	0.315	0.7	1.33
0.3	0	0.665	1.47	2.38
0.4	0.21	1.12	2.45	3.64
0.5	0.28	1.61	3.43	4.9
0.6	0.42	2.03	4.27	6.3
0.7	0.7	2.59	5.11	7.7
0.8	0.91	2.87	5.67	8.68
0.9	1.05	3.08	6.16	9.66
1	1.19	3.22	6.58	11.41
1.1	1.19	3.15	6.51	12.53
1.2	1.12	2.94	6.16	12.88
1.3	0.98	2.52	5.32	12.53
1.4	0.7	2.17	4.27	11.62
1.5	0.49	1.61	3.36	10.5
1.6	0.21	1.05	2.52	8.89
1.7	0.07	0.63	1.75	7.42
1.8	0	0.35	1.05	5.95
1.9	0	0.14	0.56	4.34
2	0	0	0.21	2.94
2.1	0	0	0	1.75
2.2	0	0	0	1.12
2.3	0	0	0	0.35
2.4	0	0	0	0

Appendix D

Program Listing of NTSAD

```
      PROGRAM NTSAD (INPUT,OUTPUT,TAPE5=INPUT,TAPE6=OUTPUT)
      DIMENSION G(400),X(100),Y(100),H(4),Z(400),XO(3),LQK(6),PDED(100),
     1  JQS(7),PDMOGI(400,7),CI(400),SI(400),EM(7),CNEW(100),PDIOG(150)
     2  ,WI(3),C(3,5,4),XNEW(100),HR(3,5),CLSS(4,400),TRATIO(150)
     3  ,CLLN(400),CLILC(3,400),YARRAY(400),XLINCH(400),XARRAY(100)
     4  ,YPLOT(100),XLK(3,400),CJCL(3),JQK(3),TEMP1(100),TEMP2(100)
     5  ,ABCFR(3,400),REFM(3),TPART(15),ZPA(15),ZPI(15),ZPII(15)
     6 ,CLIN(3,400),CLPOS(3,400),XLIN(3,400),CLSI(3,400),XLSI(3,400)
     7 ,CLABS(3,400),XLMM(3,400),XLXO(3,400),CLST(3,400),CLS2(3,400)
     8  ,COEFF(4),XL(400),CL(400),DARC(400),DFF(400),DCF(400),DII(100)
      CHARACTER * 69 WORDS
      CHARACTER YLABL*30
C ---------------------------------------------------------------
C     THE FOLLOWING ARE THE SOFTWARE SWITCHES
C
C     NSADCR = 0    IS USED FOR DATA HAVING ONLY THE DIRECT INTENSITY
C                   MEASUREMENTS. THIS SWITCH BYPASSES THE SUBROUTINE
C                   SADCOR (OF NBS).
C
C     NSADCR = 1    USES SADCOR TO ACCOUNT FOR ABSORPTION. NOTE THAT
C                   DATA SHOULD CONTAIN CHOPPED AND UNCHOPPED INTENSITIES
C
C     NSADCR = 2    THIS SWITCH BYPASSES SADCOR , ALTHOGH THE DATA
C                   CONTAINS CHOPPED AND UNCHOPPED INTENSITIES.
C
C     INSMTH = 0    DOES NOT SMOOTH THE RAW DATA UNTILL AFTER FOLDING.
C
C     INSMTH = 1    SMOOTHS THE ORIGINAL RAW DATA BEFORE PROCEEDING
C
C      NPRNT = 1    TURNS ON THE DETAIL PRINT-OUT OPTION
C
C      NPLOT = 1    TURNS ON THE PLOTTING OPTION. THIS ALLOWS
C                    THE USER TO PLOT THE LINE PROFILES, LTE ELECTRON
C                    DENSITY, LEVEL DENSITY, AND LTE TEPERATURES.
C      NABEL = 1    IT USES A 1-INTERVAL SMOOTHED DATA JUST
C                   BEFORE GOING THROUGH ABELLING
C      NABEL = 4    IT USES THE AVAILABLE 4-INT. SMOOTHED DATA.
C
C ---------------------------------------------------------------
C
C     SET THE SWITCHES
C
      NSADCR = 0
      INSMTH = 1
      NPRNT = 0
      NPLOT = 1
      NABEL = 1
C
C ---------------------------------------------------------------
C     UN-COMMENT THE FOLLOWING STATEMENTS IN PROG BELOW TO PLOT DATA
C
C                       CALL PLOTS (0.,2.,LZ+8)
C                  ALL  CALL PLOTIN(.................)
C                       CALL PLOT (0.0,0.0,999)
C---------------------------------------------------------------
C     INPUT GENERAL DATA
C
C     SMOOTH INPUT INTENSITIES WITH SOME COST: SEE SUBROUTINE SMOOTH
C
C      INPUT VARIABLE DEFINITIONS
C            ITYP   = 1 IF ARC POS. (X) VARIES OR 2 IF WAVELENGTH VARIES
C            MZ     = NO. OF CASES, USUALLY NO. OF LINES (<9 TO PLOT TEMP.)
C            PBAR   = PRESSURE IN BARS
C            WORDS  = DESCRIPTION OF EXPERIMENT. SEE OLD OUTPUTS.
C            EI     = IONIZATION POTENTIAL OF ATOM (INV. CM.)
C            EII    = IONIZATION POTENTIAL OF 1ST ION (INV. CM.)
```

```
C            G1A    = GROUND STATE DEGENERACY OF ATOM
C            G1I    = GROUND STATE DEGENERACY OF 1ST ION
C            G1I    = GROUND STATE DEGENERACY OF 2ND ION
C            TPART  = TEMPERATURE INTERVALS FOR Z-VALUES (K)
C            ZPA    = PARTITION FUNCTION FOR NEUTRAL ATOM
C            ZPI    = PARTITION FUNCTION FOR 1ST ION
C            ZPII   = PARTITION FUNCTION FOR 2ND ION
C ------------------------------------------------------------
C     NDPT IS THE NUMBER OF DATA POINTS IN DIMENSION
      NDPT=400
 5000 READ(5,210)ITYP,MZ,PBAR,WORDS
  210 FORMAT(I2,I3,F10.5,A64)
C     CONVERT UNITS OF PRESSURE FROM BARS TO DYNES PER CM2
C
      PRES = PBAR*1.0E+06
      NZ=MZ
      LZ=1
C     EI IN INV CM
      READ(5,1765) EI,EII,G1A,G1I,G1II
      EIINF=EI
 1765 FORMAT(2F15.3,3F5.1)
C
C     READ-IN THE VALUES FOR PARTITION FUNCTION OF THE NEUTRAL
C     THE FIRST AND THE SECOND ION.
C
      READ(5,1665)  (TPART(LFA),ZPA(LFA),ZPI(LFA),ZPII(LFA),
     1              LFA=1,11)
 1665 FORMAT(10(4F10.3,/),4F10.3)
C ------------------------------------------------------------
C     INPUT LINE CONSTANTS
C           WAVE    = WAVELENGTH OF LINE (ANGSTROMS)
C           LI      = 0 FOR NEUTRAL, 1 FOR ION, 2 FOR CONTINUUM
C           EI      = ENERGY OF UPPER LEVEL (INV. CM)
C           GI      = DEGENERACY OF UPPER LEVEL
C           AI      = TRANSITION PROBABILITY (PER SEC)
C           ERG     = AXIAL LOCATION, CASE NO., OR OTHER IDENTIFIER.
C           DRAD    = DESIRED OUTPUT RADIUS INTERVAL (MM) USUALLY .05
C           NC      = NO. OF CONTINUUM TRACES RUN IN LINE + CONT DATA
C           JQ      = NO. OF DATA POINTS
C           ZI      = CALIBRATION-SCALE FACTOR (PREFERRED UNITS ARE WATTS/SQ CM)
C           WI(IL)  = TRACE WAVELENGTH IDENTIFIER. USE TO PRORATE CONT.
C            XZ     = INITIAL X- POSITION (VOLTS)
C            XF     = FINAL   X- POSITION (VOLTS)
C            RFACTOR= CONVERSION FACTOR FROM VOLTS TO MM IN ARC POSITION
C            REFM   = REFLECTION EFFICIENCY OF THE SYSTEM
C           CL(K)   = INTENSITY/SCALE FACTOR AS FRACTION OF FULL SCALE
C           PO...   = PARTICLE DENSITY (CM**-3)
C
C ------------------------------------------------------------
      DO 1760 J=1,7
      JQS(J)=0.
      DO 1760 I=1,NDPT
 1760 PDMOG1(I,J)=0.
    2 READ(5,212)WAVE,LI,EI,GI,AI
  212 FORMAT (F10.3,I3,F15.3,F5.1,E12.3)
      READ(5,*)WAVE,ERG,DRAD,NC,JQ,ZI
      JQSAV=JQ
      SFAC=ZI
      IF(NPLOT.EQ.1) CALL PLOTS(0.,0.,LZ+8)
C-------------------------------------------------------------------
C     INITIALIZE VARIABLE ARRAYS
C
C     JQS IS THE NO. OF DATA POINTS FOR EACH INTENSITY PROFILE(JQ).
      DO 1761 J=1,4
      DO 1761 I=1,NDPT
 1761 CLSS(J,I)=0
```

```
      DO 1762 J=1,3
      DO 1762 I=1,NDPT
 1762 CLILC(J,I)=0
      DO 711 IL=1,3
      DO 711 I=1,5
      DO 711 J =1,4
      H(J) = 0.
  711 C(IL,I,J) = 0.
      DO 714 I=1,31
      X(I)=0.
  714 Y(I)=0.
      DO 713 I=1,NDPT
      CL(I) = 0.
      G(I)=0.
      CLLN(I)=0
      CI(I)=0
      SI(I)=0
      XL(I)=0
      DCF(I)=1.0
  713 Z(I)=0.
      EM(LZ) = E1
C-----------------------------------------------------------------------
C     INPUT LINE & CONTINUUM MEASUREMENTS
C
      DO 1001 IL=1,NC+1
      JQ=JQSAV
      JQK(IL)=JQ
      READ(5,355) W1(IL),XZ,XF,RFACTOR,REFM(IL)
  355 FORMAT(F10.3,4F10.5)
      IF(IL.GT.1) GO TO 361
      CALL HEADIN(WORDS,WAVE,L1,PBAR,NC,JQ,NSADCR,MZ,ERG,RFACTOR,
     *  REFM(1))
  361 WAVC=W1(IL)
  214 READ(5,215) (CL(K), K=1,JQ)
C-----------------------------------------------------------------------
C     CORRECT DATA HAVING NEGATIVE & POSITIVE VALUES
C     CL=-CL FOR HPDAS DATA  CL=CL FOR IBMDAS DATA
C
      IF(CL(JQ/2).GT.0.) GO TO 230
      DO 228 K=1,JQ
  228 CL(K)=-CL(K)
C
C     SET BASE LINE BY SUBTRACTING THE MIN VALUE FROM ALL DATA.
C
  230 RAWMIN=10.000
      DO 3 N2=1,JQ
      IF(CL(N2) .LT. RAWMIN) RAWMIN=CL(N2)
    3 CONTINUE
      DO 75  K=1,JQ
      CLIN(IL,K)=CL(K)
      CL(K)=CL(K)-RAWMIN
      CLPOS(IL,K)=CL(K)
   75 CONTINUE
  215 FORMAT (8F10.0)
C -----------------------------------------------------------------------
C      FIND MAX INTENSITY CL(K)  AND CORRESPONDING  X  VALUE.
C
      IF(IL.EQ.1) XZ1=XZ
      XL(1)=XZ-XZ1
      XLIN(IL,1)=XL(1)
      CJCL(IL)=(XF-XZ)/(JQ-1)
      DO 399 KP=2,JQ
      XL(KP)=XL(KP-1)+CJCL(1)
  399 XLIN(IL,KP)=XL(KP)
      WRITE(6,213) CJCL(IL)
  213 FORMAT(3X,'CJCL(IL) =',F10.5)
```

```
      XLMAXX=XL(1)
      CLMAX=CL(1)
      DO 80 K=2,JQ
      IF(CL(K).GT.CLMAX) GO TO 70
      GO TO 80
   70 CLMAX=CL(K)
      XLMAXX=XL(K)
      KMAX=K
   80 CONTINUE
C-----------------------------------------------------------------
C     ZERO INTENSITIES AND CUT OFF ZERO ENDS.
C     THE CRITERION FOR CUTTING THE ENDS CAN BE FINER (SMALLER)
C     IF THE EXPERIMENTOR FEELS THE DAS HAS GOOD PRECISION.
      IF(IL.GT.1) GO TO 229
C     SET ERROR CLEER
C
      CLERR=.002
C
C     FIND RANGE OF SIGNIFICANT VALUES
C
      CLHIGH=(CLMAX-(CL(1)+CL(JQ))/2)*CLERR
      DO 130 K=KMAX,JQ
      IF(CL(K+1).GT.CLHIGH)GO TO 130
      KHIGH=K
      CLHIGH=CL(K)
      XLHIGH=XL(K)
      GO TO 140
  130 CONTINUE
  140 CLLOW=(CLMAX-(CL(1)+CL(JQ))/2)*CLERR
      DO 150 K=KMAX,1,-1
      IF(CL(K-1).GT.CLLOW)GO TO 150
      KLOW=K
      CLLOW=CL(K)
      XLLOW=XL(K)
      GO TO 160
  150 CONTINUE
C
C     FIND AVERAGE OF END POINTS
C     DEFAULT IS THE AVERAGE OF THE END POINTS
C
  160 CLSUM=0.
      DO 170 K=1,KLOW-1
  170 CLSUM=CLSUM+CL(K)
      DO 180 K=KHIGH+1,JQ
  180 CLSUM=CLSUM+CL(K)
      CLZERO=CLSUM/(KLOW-1+JQ-KHIGH)
C
C     CORRECT FOR ZERO AND RESET TO LOW K WITH NEW JQ
C
  229 JQK(IL)=KHIGH-KLOW+1
      JQ=JQK(IL)
      DO 190 K=1,JQ
      CL(K)=CL(KLOW-1+K)-CLZERO
  190 XL(K)=XL(KLOW-1+K)
C -------------------------------------------------------------
C     THIS SECTION SMOOTHS THE RAWDATA BASED ON THE 1/4 1/3
C     AND 1/2 THE MAX INTENSITY AND FINDS THE MID POINT OF DATA
C
      IF(NPLOT.EQ.1) THEN
      IF(IL.EQ.1) CALL SYMBOL(1.5,1.,.2,WORDS,90.,64)
      ENDIF
      IF(INSMTH.EQ.1) CALL SMTHIN(XL,CL,CLMAX,XMID,JQ,NPLOT,IL)
C -------------------------------------------------------------
C THE FOLLOWING IS A SCHEME TO TAKE ONLY THE LOWER PROFILE
C OF INTENSITY BY INTERPOLATING FOR ODD OR EVEN POINTS IF
C NSADCR = 2
```

```
C
      IF(NSADCR.NE.2) GO TO 935
      IF(CL(JQ/2)-CL(JQ/2-1)) 944,944,942
 944  KMAX = JQ/2 - 1
      GO TO 943
 942  KMAX = JQ/2
  943 ODEV=FLOAT(KMAX)/2.
      IF(ODEV-FLOAT(KMAX/2)) 932,932,936
  932 ISTART=2
      CL(JQ)=CL(JQ-1)
      GO TO 937
  936 ISTART=3
      CL(1)=CL(2)
  937 DO 938 KOE=ISTART,JQ-1,2
  938 CL(KOE)=(CL(KOE+1)+CL(KOE-1))/2.
C
  935 DO 934 K=1,JQ
      CLS1(IL,K)=CL(K)
      XLS1(IL,K)=XL(K)
 934  CONTINUE
      XO(IL)=XMID
      IF(INSMTH.EQ.0) XO(IL) = XLMAXX
      WRITE(6,217)XO(IL)
  217 FORMAT(3X,'XO=  ',F15.5)
 1001 CONTINUE
C
C-----------------------------------------------------------------
C     IF NEED TO CORRECT FOR ABSORPTION: CALL SADCOR
C
      IF(NSADCR.NE.1) GOTO 801
      DO 1002 IL=NC+1,1,-1
      JQ=JQK(IL)
      WAVC=W1(IL)
      DO 720 K=1,JQ
      CL(K)=CLS1(IL,K)
  720 XL(K)=XLS1(IL,K)
      CALL SADAH(XL,CL,IL,JQ,DARC,DCF,REFM,NPRNT)
      DO 750 K=1,JQ
      CL(K)=DARC(K)
      CLABS(IL,K)=CL(K)
  750 ABCFR(IL,K)=DCF(K)
 1002 CONTINUE
C ---------------------------------------------------------------
C
C     THE FOLLOWING LOOP ( 1003 ) FOLDS THE INTENSITY CURVE ABOUT
C     THE MIDPOINT AND THEN SMOOTHS IT USING A 3RD DEGREE MULTI-
C     INTERVAL POLYNOMIAL. IT THEN ESTABLISHES THE INTERVAL BOUND-
C     RIES.
C
  801 DO 1003 IL=1,NC+1
      JQ=JQK(IL)
      DO 740 K=1,JQ
      IF(NSADCR.EQ.1) GO TO 941
      CL(K)=CLS1(IL,K)
      GO TO 740
 941  CL(K)=CLABS(IL,K)
  740 XL(K)=XLS1(IL,K)
C-----------------------------------------------------------------
C      CALCULATE X=(X-XO) AND SORT WITH INCREASING X
C
  800 DO 20 K=1,JQ
      XLMM(IL,K)=XL(K)*RFACTOR
      XL(K)=ABS(XO(IL)-XL(K))*RFACTOR
   20 CONTINUE
C-----------------------------------------------------------------
C     SORT INTENSITY VALUES BY PUTTING X VALUES IN INCREASING ORDER
```

```
C     SCHEME SORTS UNTIL IT REACHES A LARGER VALUE OF X
C     THE X VALUES MUST BE IN A CONTINUOUSLY DEC SERIES
C
      DO 24 I=1,JQ
      XLSAVE=XL(I)
      CLSAVE=CL(I)
      XMSAVE=XLMM(IL,I)
      DO 21 K=1,JQ-1
      IF (XLSAVE.LE.XL(K+1)) GO TO 22
      XL(K)=XL(K+1)
      CL(K)=CL(K+1)
      XLMM(IL,K)=XLMM(IL,K+1)
   21 CONTINUE
   22 XL(K)=XLSAVE
      CL(K)=CLSAVE
      XLMM(IL,K)=XMSAVE
   24 CONTINUE
      DO 225 J=1,JQ
      CLST(IL,J)=CL(J)
      XLXO(IL,J)=XL(J)
  225 CONTINUE
C-------------------------------------------------------
C     CALCULATE SMOOTHED DATA VALUES WITH LEAST SQUARES POLYNOMIAL
C
C     FIT DATA WITH UP TO 5 LSQ POLYNOMIALS
C     WITH A MINIMUM OF 20 DATA POINTS PER POLYNOMIAL
C     N = 4 FITS 3RD DEGREE POLYNOMIAL
C
      NQ = JQ
      N  = 4
      IF(IL.NE.1) GO TO 546
  546 DO 712 I=1,JQ
  712 G(I)=XL(I)
      NINT=JQ/20
      IF(NINT-5)330,331,331
  331 NINT=5
  330 NINT=NINT
      IF(IL.EQ.1) NSAV=NINT
      DO 550 I=1,NINT
      M=JQ/NINT
      GO TO (451,452,453,454,455),I
  451 MJ=M+5
      M1=1
      DO 465 J=1,MJ
  465 X(J)=G(J)*G(J)
      GO TO 458
  452 M1=M-5
      M=2*M+5
      GO TO 602
  453 M1=2*M-5
      M=3*M+5
      GO TO 602
  454 M1=3*M-5
      M=4*M+5
      IF(M-JQ) 602,602,441
  441 M = JQ
      GO TO 602
  455 M1=4*M-5
      M=JQ
  602 MJ=M-M1+1
      DO 466 J=1,MJ
      L=M1+J-1
  466 X(J)=G(L)
  458 DO 460 J=1,MJ
      L=M1+J-1
  460 Y(J)=CL(L)
```

```
C     POLFIT IS MODIFIED TO MAKE WEIGHT = 1 IF MODE = 0
      MODE = 0
  463 CALL POLFIT(X,Y,X,MJ,N,MODE,H,CHI)
      DO 227 J1=1,N
      C(IL,I,J1)=H(J1)
  227 CONTINUE
  550 CONTINUE
C-------------------------------------------------------
C     CALCULATE & PRINT COMPARISON OF RAW & SMOOTHED DATA
C     ESTABLISH THE INTERVAL BOUNRIES.
C
      M=JQ/NINT
      HR(IL,1)=0.
      HR(IL,2)=G(M)
      HR(IL,3)=G(2*M)
      HR(IL,4)=G(3*M)
      HR(IL,5)=G(4*M)
      CALL DATAPTY(G,CL,C,IL,HR,JQ)
C-------------------------------------------------------
C      PRINT OUT RAW TO SMOOTH DATA FOR EACH INTENSITY
C
      IF(NPRNT.EQ.0) GO TO 328
      WRITE(6,236)
  236 FORMAT(3H    ,'K  X(VOLTS) I RAW   I+CONST  I RAW SMOOTH  ABS COR',
     1 '  I UNABS  X(MM) SORT   X-XO SORT  I ABS/SORT  I SMOOTHED',/)
  328 DO 835 K=1,JQ
      CLS2(IL,K)=CL(K)
      IF(NPRNT.EQ.0) GO TO 835
      WRITE(6,245)K,XLIN(IL,K),CLIN(IL,K),CLPOS(IL,K),CLS1(IL,K)
     1 ,ABCFR(IL,K),CLABS(IL,K),XLMM(IL,K),XLXO(IL,K),CLST(IL,K)
     2 ,CLS2(IL,K)
  245 FORMAT(I5,10F10.5)
  835 CONTINUE
 1003 CONTINUE
C-------------------------------------------------------
C     CALCULATE PRORATED MEAN CONTINUUM UNDER LINE & NET LINE INTENSITY
C
      RADIUS = XL(JQ)
      JQ=RADIUS/DRAD
      JQS(LZ)=JQ
      NINT=NSAV
      M = JQ/NINT
      XL(1)=0.
      G(1)=XL(1)
      DO 820 K=2,JQ
      XL(K)=XL(K-1)+DRAD
  820 G(K)=XL(K)
      JQIL=JQ
      DO 837 IL=1,NC+1
      CALL DATAPTY(G,CL,C,IL,HP,JQ)
      DO 830 J=1,JQ
      IF(IL.GT.1.AND.CL(J).LT.0)CL(J)=0
      CLSS(IL,J)=CL(J)
      IF(IL.EQ.1.AND.CL(J).LT.0)THEN
      JQIL=J-1
      GO TO 833
      ELSE
      ENDIF
  830 CONTINUE
  833 JQ=JQIL
  837 CONTINUE
      IF(NC.LT.1) GO TO 862
      IF(NC.GT.1) GO TO 832
      CL5=0.
      CL4=1.0
      IL=2
```

```
      GOTO 836
  832 CL4=(WI(3)-WI(1))/(WI(3)-WI(2))
      CL5=(WI(1)-WI(2))/(WI(3)-WI(2))
      IL=3
  836 DO 840 I=1,NINT
      DO 840 K=1,N
  840 C(3,I,K)=CL5*C(3,I,K)+CL4*C(2,I,K)
      CALL DATAPTY(G,CL,C,IL,HR,JQ)
      DO 855 K=1,JQ
      CLSS(4,K)=CL(K)
  855 CONTINUE
      DO 860 I=1,NINT
      DO 860 K=1,N
      C(1,I,K)=C(1,I,K)-C(3,I,K)
  860 CONTINUE
  862 IL=1
      CALL DATAPTY(G,CL,C,IL,HR,JQ)
      DO 865 K=1,JQ
      CLLN(K)=CL(K)
      IF(CLLN(K).GT.CLSS(1,K)) CLLN(K) = CLSS(1,K)
      IF(CLSS(4,K).LT.0.) CLSS(4,K) = 0.
      IF(CLLN(K).LT.0.) GO TO 2092
  865 CONTINUE
      GOTO 2093
 2092 CLLN(K)=0.0
      JQ=K
 2093 JQS(LZ)=JQ
C
      IF(NPLOT.EQ.0) GO TO 893
C
C     PLOT LINE AND CONTINNUA
C
      PMAX = 0.
      DO 8827 K=1,JQ
 8827 IF(CLSS(1,K).GT.PMAX) PMAX = CLSS(1,K)
      PMAX = (INT(PMAX*10.)+1)/10.
      YLABL='RELATIVE INTENSITY!Z'
      CALL PLOTIN(XL,CLLN ,JQ,0.,PMAX,PMAX,2,YLABL,1,0.,0.,1)
      DO 8822 MA=1,100
 8822 YPLOT(MA)=CLSS(1,MA)
      CALL PLOTIN(XL,YPLOT,JQ,0.,PMAX,PMAX,2,YLABL,1,2.,0.,2)
      DO 8823 MA=1,100
 8823 YPLOT(MA)=CLSS(2,MA)
      CALL PLOTIN(XL,YPLOT,JQ,0.,PMAX,PMAX,2,YLABL,1,0.,0.,2)
      DO 8824 MA=1,100
 8824 YPLOT(MA)=CLSS(3,MA)
      CALL PLOTIN(XL,YPLOT,JQ,0.,PMAX,PMAX,2,YLABL,1,0.,0.,2)
      DO 8825 MA=1,100
 8825 YPLOT(MA)=CLSS(4,MA)
      CALL PLOTIN(XL,YPLOT,JQ,0.,PMAX,PMAX,2,YLABL,1,0.,0.,2)
C-------------------------------------------------------------
C
  893 IF(NPRNT.EQ.1) THEN
C
C      PRINT HALF-SIDE INTENSITIES AS SORTED BASED ON CJCL()=DEL X MEAS.
C
      WRITE(6,891)
  891 FORMAT(1H1,4X,'K       X(MM)      I(L+C)          I(C1)          I(C2)',
     1  '       I(C AVE)     I(L  NET) ',/)
      DO 890 K=1,JQ
      WRITE(6,892) K,XL(K),(CLSS(IL,K),IL=1,4),CLLN(K)
  892 FORMAT(1X,I4,1F11.3,5E13.5)
  890 CONTINUE
      ENDIF
C-------------------------------------------------------------
C     CALCULATE RADIAL EMISSION COEF FROM LATERAL INTENSITIES VIA ABEL INVER.
```

```
      IF(NABEL.EQ.4) THEN
       CALL ABEL4(G,CLLN(1),C,HR,DRAD,Z1,W1(1),L1,JQ,NINT,CI,SI)
      ELSE
      CALL ABELNO(G,CLLN,DRAD,W1(1),NTOLER,Z1,L1,JQ,CI,SI)
      IF(NPLOT.EQ.1)CALL PPLOT(XL,CLLN,JQ,1,0)
      ENDIF
C-------------------------------------------------------------
C CALCULATION OF LTE PARAMETERS FOR ION AND NEUTRAL LINES
C -------------------------------------------------------------
      WRITE(6,235)WORDS,W1(1),ERG,LZ
  235 FORMAT(1H1,/,A74,F8.2,3X,9HPOSITION ,F5.1,2HMM,3X,5HCASE ,I2,//,
     4  55X,37H.................LTE.................. ,/,
     1  5H     K,10H      I LAT,10H      I LSQ,10H  EM COEF ,
     2  10H    N(M)/G ,10HRADIUS(MM),10H       T    ,10H   T HIGH ,
     3  10H     NE     ,10H      NA    ,12H        NE/NA,/)
C ESTIMATE INITIAL TEMPERATURE.
      BOLTK=1.38049E-16
      TINC1=250.
      TINC2=10.
      ZDA=G1A
      ZDI=G1I
      ZDII=G1II
      JQL=JQ-1
      DO 233 K=1,JQL
      DELP=0.
      TINC = TINC1
      T=7000.
      NDONE=0
      JDONE=0
      JTEMP=0
      PDM=SI(K)*4.*3.1416*WAVE*1.0E-8/(1.986E-23*A1)
      IF(PDM) 2013,2013,2014
 2013 WRITE(6,2015)
 2015 FORMAT(3X,'ABORT DUE TO NEGATIVE PARTICLE DESITY')
      GOTO 233
 2014 CONTINUE
 2016 T=T+TINC
      IF(T.LT.35000.) GOTO 2018
      TEMP2(K)=35000.
      GO TO 2330
C FUN1 & FUN2 ARE THE RIGHT HAND SIDES OF THE SAHA EQN. FOR
C THE NEUTRAL AND ION RESPECTIVELY
C
 2018 CALL INTRP(TPART,ZPA,11,3,T,ZDA)
      CALL INTRP(TPART,ZPI,11,3,T,ZDI)
      CALL INTRP(TPART,ZPII,11,3,T,ZDII)
      IF(ZDA.LT.1.0) ZDA=1.0
      IF(JDONE.EQ.1) THEN
        DEBYE=(4.*3.14159*4.80298E-10**2*PDE/BOLTK*2./T)**(-.5)
        DELEI=4.80298E-10**2/1.9862E-16/DEBYE
        EI=EIINF-DELEI
      ENDIF
      FUN1=2.*ZDI/ZDA*2.416E15*T**1.5*EXP(-EI*1.4388/T)
      FUN2=2.*ZDII/ZDI*2.416E15*T**1.5*EXP(-EII*1.4388/T)
C
C  JUMP TO ION LINE CALCULATION IF LI .NE. 0 ----------
      IF (L1.NE.0) GOTO 2040
C
C ---THE FOLLOWING CALULATIONS ARE FOR NEUTRAL LINE -----
      PDA=PDM*ZDA/GI*EXP(E1*1.4388/T)
C MANIPULATING THE SAHA EQN. ALONG WITH THE EQN. FOR THE
C CONSERVATION OF PARTICLES , WE WILL GET A THIRD ORDER
C POLYNOMIAL IN NE
C      NE**3-FUN1*NA*NE-2.FUN1*FUN2*NA=0
C  DEFINE THE COEFFICIENTS.
C
```

```
C     SOLVING THE POLYNOMIAL BY ITERATION
      ITMAX=20
      PDE=(FUN1*PDA)**.5
      DO 7069 INE=1,ITMAX
      PDES=(FUN1*PDA*PDE+2.*FUN1*FUN2*PDA)**(1./3.)
      PERROR=ABS(PDE-PDES)/PDE
      IF(PERROR.LT.1.E-4) GOTO 7070
      PDE=PDES
 7069 CONTINUE
      PRINT*,'  ROOT OF NE WAS NOT FOUND AFTER ',ITMAX,' ITERATIONS'
 7070 PDI=FUN1*PDA/PDE
C                    ------------------------
      GO TO 2046
C
C  --- THE FOLLOWING SECTION IS FOR ION LINE CALCULATIONS. ---
C
 2040 PDI=PDM*ZDI/G1*EXP(E1*1.4388/T)
C SOLVE SAHA EQN. AND COSERV. OF PARTICLES FOR NE.
C
      PDE=.5*(PDI+SQRT(PDI**2+8*FUN2*PDI))
      PDA=PDI*PDE/FUN1
C                    ------------------------
 2046 PDII=FUN1*FUN2*PDA/PDE**2
      PCALC=(PDA+PDE+PDI+PDII)*BOLTK*T
      DELPS=DELP
      DELP=PCALC-PRES
      IF(NDONE.EQ.1) GOTO 3023
      IF(ABS(DELPS+DELP).GE.ABS(DELPS-DELP)) GOTO 2016
      IF(JDONE.EQ.1) GOTO 3022
      T=T-TINC
      TINC=TINC2
      JDONE=1
      DELP=DELPS
      GOTO 2016
 3022 T=(-DELPS)*TINC/(DELP-DELPS)+T-TINC
      NDONE=1
      GOTO 2018
 3023 IF(JTEMP.EQ.1) GOTO 3024
      TEMP1(K)=T
      PDE1=PDE
      PDI1=PDI
      PDII1=PDII
      PDA1=PDA
      DELPOP1=ABS(DELP/PRES)
      JTEMP=1
      NDONE=0
      JDONE=0
      TINC=TINC1
      GOTO 2016
 3024 TEMP2(K)=T
      PDE2=PDE
      PDI2=PDI
      PDII2=PDII
      PDA2=PDA
      DELPOP2=ABS(DELP/PRES)
C  --- CHOOSE THE PROPER TEMPERATURE (HIGH OR LOW) ---
      IF(TEMP1(K).GE.TEMP2(K)) GOTO 2043
 2330 T=TEMP1(K)
      PDE=PDE1
      PDI=PDI1
      PDII=PDII1
      PDA=PDA1
      GO TO 2044
 2043 T=TEMP2(K)
      PDE=PDE2
      PDI=PDI2
```

```
      PDII=PDII2
      PDA=PDA2
 2044 CONTINUE
      PDEODA=PDE/PDA
      PDMOG1(K,LZ)=PDM/G1
      TEX=T
      WRITE(6,239)K,CLLN(K),CI(K),SI(K),PDMOG1(K,LZ),XL(K),TEX,
     1  TEMP2(K),PDE,PDA,PDEODA
  239 FORMAT(I5,2F10.4,2E10.4,F10.3,2F10.0,2E10.4,E15.4)
      CL(K)=TEX
      PDED(K) = PDE
      DII(K)=PDII
  233 CONTINUE
C
      IF(NPLOT.EQ.1) THEN
      YLABL='ELECTRON DENSITY!Z'
      CALL PLOTIN(XL,PDED,JQL,1.E15,1.E18,1.E16,-100,YLABL,2,-8.5,4.5,1)
      YLABL='NM/GM!Z'
      YLABL = 'EMISSION COEF. W/(!2CM3/ST)!Z'
      PMAX = 0.
      DO 8828 K=1,JQ
 8828 IF(SI(K).GT.PMAX) PMAX=SI(K)
      PMAX=PMAX*1.2
      CALL PLOTIN(XL,SI,JQL,0.,PMAX,PMAX,3  ,YLABL,1,-4.,-4.5,1)
      YLABL='LTE TEMPERATURE!Z'
      CALL YTICKS(4,0)
      CALL PLOTIN(XL,TEMP1,JQL,0.,30000.,1000.,-50,YLABL,1,-8.5,4.5,1)
      CALL YTICKS(4,0)
C     CALL PLOTIN(XL,TEMP2,JQL,0.,30000.,1000.,-50,YLABL,1,0.,4.5,2)
      ENDIF
      LZ=LZ+1
  237 MZ=MZ-1
      IF(MZ)238,238,2
  238 CONTINUE
      IF(NPLOT.EQ.1) CALL PLOT(0.,0.,999)
C-------------------------------------------------------
      END
C-------------------------------------------------------
      SUBROUTINE POLFIT(X,Y,SIGMAY,NPTS,NTERMS,MODE,A,CHISQR)
C-------------------------------------------------------------
      DOUBLE PRECISION SUMX,SUMY,XTERM,YTERM,ARRAY,CHISQ
      DIMENSION X(NPTS),Y(NPTS),SIGMAY(NPTS),A(NTERMS),SUMX(19),
     1    SUMY(10),ARRAY(10,10)
C FIND MAXIMUM ELEMENT FOR WEIGHTING PURPOSES WHEN
C MODE IS NEGATIVE
      YMAX=Y(1)
      DO 777 II=1,NPTS
      IF(Y(II).LT.YMAX) GO TO 777
      YMAX=Y(II)
  777 CONTINUE
C     ACCUMULATE WEIGHTED SUMS
   11 NMAX=2*NTERMS-1
      DO 13 N=1,NMAX
   13 SUMX(N)=0.
      DO 15 J=1,NTERMS
   15 SUMY(J)=0.
      CHISQ=0.
   21 DO 50 I=1,NPTS
      XI=X(I)
      YI=Y(I)
C     WRITE(6,216)Y(I),X(I)
  216 FORMAT(F10.0,8X,F10.7)
   31 IF(MODE) 32,37,39
C WEIGHT VALUES LESS THAN .05(YMAX)
   32 YOYMAX=YI/YMAX
      IF(YOYMAX.GT..05) GO TO 322
```

```
      WEIGHT=(20.*YI/YMAX)**2
      GO TO 41
  322 WEIGHT=1
      GO TO 41
   33 WEIGHT=1./YI
      GO TO 41
   35 WEIGHT = 1. / (-YI)
      GO TO 41
   37 WEIGHT = 1.
      GO TO 41
   39 WEIGHT = 1. / SIGMAY(I)**2
   41 XTERM = WEIGHT
      DO 44 N=1,NMAX
      SUMX(N) = SUMX(N) + XTERM
   44 XTERM = XTERM * XI
   45 YTERM = WEIGHT * YI
      DO 48 N=1,NTERMS
      SUMY(N) = SUMY(N) + YTERM
   48 YTERM = YTERM * XI
   49 CHISQ =CHISQ + WEIGHT*YI**2
   50 CONTINUE
C     CONSTRUCT MATRICIES AND CALCULATE COEFFICIENTS
   51 DO 54 J=1,NTERMS
      DO 54 K=1,NTERMS
      N = J + K - 1
   54 ARRAY(J,K) = SUMX(N)
      DELTA = DETERM (ARRAY, NTERMS)
      IF (DELTA) 61, 57, 61
   57 CHISQR = 0.
      DO 59 J=1, NTERMS
   59 A(J) = 0.
      GO TO 80
   61 DO 70 L=1, NTERMS
   62 DO 66 J=1, NTERMS
      DO 65 K=1, NTERMS
      N = J + K - 1.
   65 ARRAY(J,K) = SUMX(N)
   66 ARRAY(J,L) = SUMY(J)
   70 A(L) = DETERM (ARRAY, NTERMS) / DELTA
C     CALCULATE CHI SQUARE
   71 DO 75 J=1, NTERMS
      CHISQ = CHISQ - 2.*A(J)*SUMY(J)
      DO 75 K=1, NTERMS
      N = J + K - 1
   75 CHISQ = CHISQ + A(J)*A(K)*SUMX(N)
   76 FREE = NPTS - NTERMS
   77 CHISQR = CHISQ / FREE
   80 RETURN
      END
      FUNCTION DETERM (ARRAY,NORDER)
      DOUBLE PRECISION ARRAY,SAVE
      DIMENSION ARRAY(10,10)
C     CALCULATE THE DETERMINANT OF A SQUARE MATRIX
C     NORDER - ORDER OF DETERMINANT (DEGREE OF MATRIX)
C     THIS SUBPROGAM DESTROYS THE INPUT MATRIX ARRAY
C     DIMENSION STATEMENT VALID FOR NORDER UP TO 10
   10 DETERM=1.
   11 DO 50 K=1,NORDER
C     INTERCHANGE COLUMNS IF DIAGONAL ELEMENT IS ZERO
      IF (ARRAY(K,K))  41, 21, 41
   21 DO 23 J=K, NORDER
      IF (ARRAY(K,J)) 31, 23, 31
   23 CONTINUE
      DETERM = 0.
      GO TO 60
   31 DO 34 I=K, NORDER
```

```
      SAVE = ARRAY(I,J)
      ARRAY(I,J) = ARRAY(I,K)
   34 ARRAY (I,K) = SAVE
      DETERM = - DETERM
C     SUBTRACT ROW K FROM LOWER ROWS TO GET DIAGONAL MATRIX
   41 DETERM = DETERM * ARRAY(K,K)
      IF (K- NORDER) 43, 50, 50
   43 KI = K + 1
      DO 46 I=KI, NORDER
      DO 46 J=KI, NORDER
   46 ARRAY(I,J) = ARRAY(I,J) - ARRAY(I,K) * ARRAY(K,J)/ARRAY(K,K)
   50 CONTINUE
   60 RETURN
      END
C-------------------------------------------------------
      SUBROUTINE DATAPTS(X,Y,A,IL,HR,JQ,DRAD2)
C-------------------------------------------------------
      DIMENSION X(JQ),Y(JQ),A(3,5,4),HR(3,5)
C     THIS SUBROUTINE CALCULATES DATA POINTS AT EVEN INTERVALS DRAD
C     FROM ANY SMOOTHED DATA IN THE FORM OF A POLYNOMIAL.
      X(1)=0
      DO 356 K=1,JQ
      X(K+1)=X(K)+DRAD2
      IF(X(K).GE.HR(IL,1))   I=1
      IF(X(K).GT.HR(IL,2))   I=2
      IF(X(K).GT.HR(IL,3))   I=3
      IF(X(K).GT.HR(IL,4))   I=4
      IF(X(K).GT.HR(IL,5))   I=5
      IF(I.GT.1) GO TO 350
      Y(K)=A(IL,I,1)+A(IL,I,2)*X(K)**2+A(IL,I,3)*X(K)**4+A(IL,I,4)
     1 *X(K)**6
      GO TO 356
  350 Y(K)=A(IL,I,1)+A(IL,I,2)*X(K)+A(IL,I,3)*X(K)**2+A(IL,I,4)*X(K)**3
  356 CONTINUE
      RETURN
      END
C-------------------------------------------------------
      SUBROUTINE DATAPTY(X,Y,A,IL,HR,JQ)
C-------------------------------------------------------
      DIMENSION X(JQ),Y(JQ),A(3,5,4),HR(3,5)
C     THIS SUBROUTINE CALCULATES Y DATA POINTS GIVEN X
C     FROM ANY SMOOTHED DATA IN THE FORM OF A POLYNOMIAL.
      DO 356 K=1,JQ
      DO 200 J1=1,4
      IF(X(K).GE.HR(IL,J1).AND.X(K).LE.HR(IL,J1+1)) GO TO 100
  200 CONTINUE
      I=5
      GO TO 300
  100 I=J1
  300 IF(I.GT.1) GO TO 350
      Y(K)=A(IL,I,1)+A(IL,I,2)*X(K)**2+A(IL,I,3)*X(K)**4+A(IL,I,4)
     1 *X(K)**6
      GO TO 356
  350 Y(K)=A(IL,I,1)+A(IL,I,2)*X(K)+A(IL,I,3)*X(K)**2+A(IL,I,4)*X(K)**3
  356 CONTINUE
      RETURN
      END
C -------------------------------------------------------------
      SUBROUTINE SMTHIN(XL,CL,CLMAX,XMID,JQ,NPLOT,IL)
C -----------------------------------------------------
C THIS SUBROUTINE FINDS THE MID-POINT OF THE INTENSITY
C CURVE FOR THE PURPOSE OF FOLDING. IT USES 1/4,1/2.3/4
C POINTS AND AVERAGES THEM. IT ALSO AVERAGES THE MIDPOINTS
C OF THE ABSORBED AND THE REABSORBED CURVE.
C
      DIMENSION CL(400),XL(400),XLK(400),XLJ(400),CLK(400),CLJ(400),
```

```
     1    SCLK(400),SCLJ(400),SXLK(400),SXLJ(400),H(5),DLK(400),
     2    DLJ(400),NPTK(4),NPTJ(4)
      CL14=1./4.*CLMAX
      CL12=1./3.*CLMAX
      CL34= 1./2.  *CLMAX
      KOON=1
      NJQ=JQ/2
      DO 11 I=1,NJQ
      K=I*2-1
      J=I*2
      CLK(I)=CL(K)
      CLJ(I)=CL(J)
      XLK(I)=XL(K)
   11 XLJ(I)=XL(J)
      NJ=NJQ/2
  713 DO 80 I=1,NJ
      IE=NJ*2-I+1
      IF(CL14.GE.CLK(I).AND.CL14.LE.CLK(I+1)) K14=I
      IF(CL12.GE.CLK(I).AND.CL12.LE.CLK(I+1)) K12=I
      IF(CL34.GE.CLK(I).AND.CL34.LE.CLK(I+1)) K34=I
      IF(CL14.GE.CLK(IE).AND.CL14.LE.CLK(IE-1)) KP14=IE
      IF(CL12.GE.CLK(IE).AND.CL12.LE.CLK(IE-1)) KP12=IE
      IF(CL34.GE.CLK(IE).AND.CL34.LE.CLK(IE-1)) KP34=IE
   80 CONTINUE
C
      DO 90 I=1,NJ
      IE=NJ*2-I+1
      IF(CL14.GE.CLJ(I).AND.CL14.LE.CLJ(I+1)) J14=I
      IF(CL12.GE.CLJ(I).AND.CL12.LE.CLJ(I+1)) J12=I
      IF(CL34.GE.CLJ(I).AND.CL34.LE.CLJ(I+1)) J34=I
      IF(CL14.GE.CLJ(IE).AND.CL14.LE.CLJ(IE-1)) JP14=IE
      IF(CL12.GE.CLJ(IE).AND.CL12.LE.CLJ(IE-1)) JP12=IE
      IF(CL34.GE.CLJ(IE).AND.CL34.LE.CLJ(IE-1)) JP34=IE
   90 CONTINUE
C
      XKM14=.5*(XLK(K14)+XLK(KP14))
      XKM12=.5*(XLK(K12)+XLK(KP12))
      XKM34=.5*(XLK(K34)+XLK(KP34))
C
      XJM14=.5*(XLJ(J14)+XLJ(JP14))
      XJM12=.5*(XLJ(J12)+XLJ(JP12))
      XJM34=.5*(XLJ(J34)+XLJ(JP34))
      XKO=1./3.*(XKM14+XKM12+XKM34)
      XJO=1./3.*(XJM14+XJM12+XJM34)
      XMID=.5*(XKO+XJO)
      IF(KOON.EQ.2) RETURN
      DO 110 I=1,NJQ
      IF(XMID.GE.XLK(I)) GO TO 110
      MMAX=I
      GO TO 140
  110 CONTINUE
C
C ------------------------------------------------------------
C THIS SECTION SMOOTHS INPUT DATA WITH 4TH DEGREE POLY-
C NOMIAL OVER FOUR INTERVALS
C
  140 INTER=4
      NPTK(1)=K12
      NPTK(2)=MMAX-K12
      NPTK(3)=KP12-MMAX
      NPTK(4)=NJQ-KP12
      NPTJ(1)=J12
      NPTJ(2)=MMAX-J12
      NPTJ(3)=JP12-MMAX
      NPTJ(4)=NJQ-JP12
      N2=0
```

```
      KTR=0
      NTERMS=5
      MODE=0
   12 KTR=KTR+1
      N1=N2+1
   13 N2=N1-1+NPTK(KTR)
      JCON=6
      NF=NPTK(KTR)+10
      IF(KTR.EQ.4) NF=NPTK(KTR)+5
      IF(KTR.NE.1) GO TO 87
      NF=NPTK(KTR)+5
      JCON=1
   87 DO 14 I=1,NF
      SCLK(I)=CLK(N1-JCON+I)
   14 SXLK(I)=XLK(N1-JCON+I)
      CALL POLFIT(SXLK,SCLK,SXLK,NF,NTERMS,MODE,H,CHI)
      DO 15 I=1,NPTK(KTR)
   15 DLK(N1-1+I)=H(1)+H(2)*SXLK(I+JCON-1)+H(3)*SXLK(I+JCON-1)**2+H(4)
     1      *SXLK(I+JCON-1)**3+H(5)*SXLK(I+JCON-1)**4
C
      IF(KTR.LT.INTER) GOTO 12
C
      N2=0
      KTR=0
      NTERMS=5
      MODE=0
  212 KTR=KTR+1
      N1=N2+1
  213 N2=N1-1+NPTJ(KTR)
      JCON=6
      NF=NPTJ(KTR)+10
      IF(KTR.EQ.4) NF=NPTJ(KTR)+5
      IF(KTR.NE.1) GO TO 287
      NF=NPTJ(KTR)+5
      JCON=1
  287 DO 214 I=1,NF
      SCLJ(I)=CLJ(N1-JCON+I)
  214 SXLJ(I)=XLJ(N1-JCON+I)
      CALL POLFIT(SXLJ,SCLJ,SXLJ,NF,NTERMS,MODE,H,CHI)
      DO 215 I=1,NPTJ(KTR)
  215 DLJ(N1-1+I)=H(1)+H(2)*SXLJ(I+JCON-1)+H(3)*SXLJ(I+JCON-1)**2+H(4)
     1      *SXLJ(I+JCON-1)**3+H(5)*SXLJ(I+JCON-1)**4
C
      IF(KTR.LT.INTER) GOTO 212
      KOON=2
C
C SET NEG. VALUES AND VALUES THEREAFTER TO ZERO AT BOTH ENDS.
      LKONT=0
      JKONT=0
      NJE=NJQ/2
      DO 492 K=1,NJE
      IF(LKONT.EQ.1) GO TO 493
      IF(DLK(NJE-K+1).GE.0.) GO TO 494
      KKMIN=NJE-K+1
      LKONT=1
  493 DLK(NJE-K+1)=0.
  494 IF(JKONT.EQ.1) GO TO 495
      IF(DLK(NJE+K).GE.0.) GO TO 492
      KKMAX=NJE+K
      JKONT=1
  495 DLK(NJE+K)=0.
  492 CONTINUE
C
      LKONT=0
      JKONT=0
      DO 692 K=1,NJE
```

```
      IF(LKONT.EQ.1) GO TO 693
      IF(DLJ(NJE-K+1).GE.0.) GO TO 694
      KKMIN=NJE-K+1
      LKONT=1
  693 DLJ(NJE-K+1)=0.
  694 IF(JKONT.EQ.1) GO TO 695
      IF(DLJ(NJE+K).GE.0.) GO TO 692
      KKMAX=NJE+K
      JKONT=1
  695 DLJ(NJE+K)=0.
  692 CONTINUE
C
      DO 17 I=1,NJQ
      K=I*2-1
      J=2*I
      CL(K)=DLK(I)
      CL(J)=DLJ(I)
   17  CONTINUE
      CCMAX=(CLMAX*10.+1)/10.
      IF(NPLOT.EQ.1) THEN
      IF(IL.EQ.1) THEN
      CALL PLOT(1,2,-3)
      CALL SIZE(1,5.,5.,1)
      CALL BOX(0.,5.,5,1,0.,CCMAX,.2,2)
      CALL XLABEL('!G ARC RADIUS (!2ARB. UNITS)!1!H!Z',0)
      CALL YLABEL('INTENSITY!Z',0)
      CALL SETSYM(0)
      CALL PPLOT(XLK,CLK,NJQ-1,1,0)
      CALL PPLOT(XLJ,CLJ,NJQ-1,1,0)
      CALL CURVE(XLK,DLK,NJQ-1,1,0,0)
      CALL SETDSH(0)
      CALL CURVE(XLJ,DLJ,NJQ-1,1,0,0)
      ENDIF
      ENDIF
      GO TO 713
       END

C-------------------------------------------------------------
      SUBROUTINE INTRP (X,Y,NPTS,NTERMS,XIN,YOUT)
C-------------------------------------------------------------
C     DOUBLE PRECISION DELTAX,DELTA,A,PROD,SUM
      DIMENSION X(15),Y(15),DELTA(15),A (15)
C
C          SEARCH FOR APPROPRIATE VALUE OF X
C
   11 DO 19 I=1,NPTS
      IF (XIN-X(I)) 13,17,19
   13 II=I-NTERMS/2
      IF(II) 15,15,21
   15 II = 1
      GO TO 21
   17 YOUT=Y(I)
   18 GO TO 61
   19 CONTINUE
      II=NPTS-NTERMS+1
   21 I2=II+NTERMS-1
      IF(NPTS-I2) 23,31,31
   23 I2=NPTS
      II=I2-NTERMS+1
   25 IF (II) 26,26,31
   26 II=1
   27 NTERMS = I2-II+1
C
C          EVALUATE DEVIATIONS DELTA
C
   31 DENOM = X(II+1)-X(II)
```

```
      DELTAX=(XIN-X(I1)) / DENOM
      DO 35 I=1, NTERMS
      IX= I1+I-1
   35 DELTA(I) = (X(IX) - X(I1)) / DENOM
C
C           ACCUMULATE COEFFICIENTS A
C
   40 A(1) = Y(I1)
   41 DO 50 K=2, NTERMS
      PROD = 1.
      SUM = 0.
      IMAX = K - 1
      IXMAX = I1 + IMAX
      DO 49 I=1, IMAX
      J = K - I
C      WRITE(6,98) PROD,DELTA(K),DELTA(J)
C98    FORMAT(/1X,"PROD.DELTA K J  ",3E15.5)
      PROD = PROD * (DELTA(K) - DELTA(J))
   49 SUM = SUM - A(J)/PROD
   50 A(K) = SUM + Y(IXMAX)/PROD
C
C           ACCUMULATE SUM OF EXPANSION
C
   51 SUM = A(1)
      DO 57 J=2, NTERMS
      PROD = 1.
      IMAX = J - 1
      DO 56 I=1, IMAX
   56 PROD = PROD * (DELTAX - DELTA(I))
   57 SUM = SUM + A(J)*PROD
   60 YOUT = SUM
   61 RETURN
      END
C -------------------------------------------------------------
      SUBROUTINE HEADIN(WORDS,WAVE,L1,PBAR,NC,JQ,NSADCR,MZ,ERG,
     *    RFACTOR,RE)
C -------------------------------------------------------------
C
C     THIS ROUTINE PRINT A HEADING IN THE BEGINNING OF THE OUTPUT
C     IT MOSTLY CONTAINS THE INPUT INFO. PLUS THE NAMES OF THE
C     SUBROUTINES TO BE USED ( I.E. SADCOR )
C
      CHARACTER * 69 WORDS
      WRITE(6,10)
   10 FORMAT(10(1X,/))
      PRINT*,'      ',WORDS
      PRINT*,'      ------------------------------------------------'
      PRINT*,'    '
      PRINT*,'      SPECTRAL LINE UNDER STUDY IS          ',WAVE,' A'
      IF(L1) 20,20,30
   20 PRINT*,'      THIS LINE IS                           NEUTRAL'
      GO TO 40
   30 PRINT*,'      THIS LINE IS                           ION'
   40 PRINT*,'      CHAMBER PRESSURE WAS                  ',PBAR,' BARS'
      PRINT*,'      NO. OF CONTINUUM TAKEN                ',NC
      PRINT*,'      NO. OF DATA POINTS TAKEN              ',JQ
      PRINT*,'      ARC AXIAL POSITION                    ',ERG
      PRINT*,'      RFACTOR WAS                           ',RFACTOR
      PRINT*,'      '
      IF(NSADCR-1) 50,60,50
   50 PRINT*,'      THE USER HAS CHOSEN TO BYPASS SADCOR ROUTINE'
      GO TO 70
   60 PRINT*,'      THE USER HAS CHOSEN TO USE SADCOR AND REFM = ',RE
   70   IF(MZ-1) 80,80,90
   90 PRINT*,'      THE USER HAS ATTEMPTED TO PROCESS ',MZ,' CASES TO '
      PRINT*,'      TO OBTAIN APPROXIMATE NON-LTE PROPERTIES'
```

```
 80   PRINT*,'  '
      PRINT*,'     ------------------------------------------------'
       PRINT*,'1'
      RETURN
      END
C -------------------------------------------------------------------
      SUBROUTINE PLOTIN(X,Y,KJQ,YMIN,YMAX,YTICK,ND,YLABL,ITYP,BEGX,BEGY,
     1  KPL)
C -------------------------------------------------------------------
      DIMENSION X(100),Y(100)
      CHARACTER YLABL*30
C
      JNUM=KJQ
      IF(ITYP.EQ.2) THEN
       DO 111 K=1,KJQ
 111   IF(Y(K).LE..000001) GOTO 112
 112   JNUM = K-1
      ENDIF
      IF(KPL.NE.1) GO TO 100
      CALL PLOT(BEGX,BEGY,-3)
      CALL SIZE(ITYP,3.,3.,.07)
      CALL BOX(0.,2.,.5,1,YMIN,YMAX,YTICK,ND)
      CALL BORDER
      CALL XLABEL('!GARC RADIUS!H (!2MM!1)!Z',0)
      CALL YLABEL(YLABL,0)
 100     CONTINUE
      CALL CURVE(X,Y,JNUM,1,0,0)
      RETURN
      END
C -------------------------------------------------------------------
      SUBROUTINE SADAH(XL,CL,IL,JQ,DARC,DCF,REFM,NPRNT)
C-------------------------------------------------------------------
C
C     THIS SUBROUTINE CALCULATES THE REFLECTION EFFICIENCY OF THE
C     SYSTEM BY ASSUMING THAT THE CONTINUUA ARE OPTICALLY THIN. IT
C     AVERAGES THE TWO VALUES OF THE  ** REFM ** FOR CONTINUUA AND
C     USES IT FOR LINE+CONT  DATA.
C
      DIMENSION CL(400),XL(400),REFF(400),DCF(400),DARC(400),CLAUX(400),
     1          REFM(3),REFFTS(400),DFF(400)
C
C     INTERPOLATE THE MISSING DATA POINTS AND CALL THEM ** CLAUX **
C
      CLAUX(1) = CL(2)
      CLAUX(JQ) = CL(JQ-1)
      DO 10 K=2,JQ-1
 10   CLAUX(K) = (CL(K-1) + CL(K+1))/2.
C
C     FIND THE SYSTEM REFL. EFFICIENCY
C
      DO 20 K=1,JQ
      IF(CLAUX(K).EQ.0..OR.CL(K).EQ.0.) THEN
      REFF(K) = 1.
      GO TO 20
      ENDIF
      IF(CLAUX(K).GT.CL(K)) THEN
      REFF(K) = CLAUX(K)/CL(K) - 1.
      ELSE
      REFF(K) = CL(K)/CLAUX(K) - 1.
      ENDIF
 20   CONTINUE
      IF(REFM(IL).EQ.1.) THEN
C
C     CALCULATE MEAN REFLECTION EFFICIENCY
CC          CALC. ONLY FOR CONTINUUM.
CC          VALID ONLY IF CONTINUUM IS OPTICALLY THIN OVER MOST OF PROFILE.
```

```
      IF(IL.EQ.1) THEN
      IF(REFM(IL+2).LT..1) REFM(IL+2)=REFM(IL+1)
      REFM(IL) = (REFM(IL+1) + REFM(IL+2))/2.
      GO TO 110
      ENDIF
CC          CALC. MEAN & STD. DEV. BASED ON ALL VALUES.
CC          RECALC. MEAN & STD. DEV. BASED ON VAL. < 1 STD. DEV.
CC          RECALC. MEAN & STD. DEV. BASED ON VAL. < 2 STD. DEV.
CC          RECALC. MEAN & STD. DEV. BASED ON VAL. < 3 STD. DEV.
      REFM1 = 1.0
      STDV=10000000.
      DO 100 I=1,7
      KTR = 0
      SUM = 0
      DO 80 K=1,JQ
      IF(ABS(REFF(K)-REFM1).GT.STDV) GOTO 80
      SUM=SUM+REFF(K)
      KTR=KTR+1
   80 CONTINUE
      REFM(IL)=SUM/KTR
      IF(I.LE.4) REFM(IL)=REFF(JQ/2)
      KTR=0
      SUM = 0
      DO 90 K=1,JQ
      IF(ABS(REFF(K)-REFM1).GT.STDV) GOTO 90
      SUM=SUM+(REFF(K)-REFM(IL))**2
      KTR = KTR + 1
   90 CONTINUE
      STDV=SQRT(SUM/(KTR-1))
      REFM1 = REFM(IL)
      WRITE(6,7001) IL,KTR,STDV,REFM
 7001 FORMAT(1X,'IL,STDV,REFM(1,2,& 3)=',2I5,4F10.3)
  100 CONTINUE
  110 CONTINUE
C
      ENDIF
C     CALCULATE ABSORPTION COEFFICIENT
C
      DO 30 K=1,JQ
      DFF(K) = REFM(IL)
      REFFTS(K) = REFF(K)
      IF(REFF(K).GT.REFM(IL)) REFF(K) = REFM(IL)
      DCF(K) = DFF(K)/REFF(K)
      IF(IL.NE.1) DCF(K)=1.
   30 CONTINUE
C
C     CORRECT THE INTENSITY DATA FOR ABSORPTION
C
      DO 40 K=1,JQ
      CLCORR = CL(K)
      IF(CL(K).GT.CLAUX(K)) CLCORR = CLAUX(K)
      DARC(K) = DCF(K) * CLCORR
   40 CONTINUE
      DARC(JQ) = DCF(JQ) * CL(JQ)
C
      IF(NPRNT.EQ.1) THEN
C
C     WRITE TITLE HEADER, FIT EFFICIENCY INFORMATION, & CONSTANTS
C
      WRITE(6,500) NIT, IT, PRES, WAVC, SFAC
C     WRITE OUT THE PARAMETERS
C
      PTSN = JQ
      PAGE = AMOD(PTSN,40.0)
      IPAGE = JQ / 40
      IF(PAGE .NE. 0.0) IPAGE = IPAGE + 1
```

```
      IMIN = 1
      IMAX = 40
      DO 35 J=1,IPAGE
      WRITE(6,510)
      DO 301 I=IMIN,IMAX
      WRITE(6,520) I,XL(I),CL(I),REFFTS(I),REFF(I),DFF(I),DCF(I),
     *  DARC(I)
  301 CONTINUE
      IF(J .NE. IPAGE) WRITE(6,535)
      IMIN = IMAX + 1
      IMAX = IMAX + 40
      IF(IMAX .GT. JQ) IMAX = JQ
   35 CONTINUE
      ENDIF
C-----------------------------------------------------------------------
C     FORMAT LABELS
C
  500 FORMAT(//1H1,22X,"SADCOR PROGRAM - MECHANICAL ENGINEERING",
     *       ", PLASMA LAB",//," ",39X,"DATA OUTPUT LISTING",///,
     *       " ",7X,"FIT TOOK",I3," ITERATIONS,"/,
     *       " ",7X,"NUMBER OF POINTS EXCLUDED IN FIT: ",I4,//
     *       " ",7X,"ARC PRESSURE, ATMS - ",F10.5,/
     *       " ",7X,"ARC WAVELENGTH, ANGSTROMS - ",F13.6,/,
     *       " ",7X,"INTENSITY SCALE FACTOR -",E12.5,//)
  510 FORMAT(" ",11X,"ARC LATERAL",6X,"RAW INPUT",8X,"RAW REFLECTION",
     *       4X,"FITTED REFLECTION",4X,"SELF-ABSORPTION",7X,
     *       "CORRECTED",/," ",12X,"POSITION",6X,"WAVE INTENSITY",
     *       7X,"EFFICIENCY",9X,"EFFICIENCY",11X,"CORRECTION",7X,
     *       "WAVE INTENSITY",/," ",89X,"FACTOR",/)
  520 FORMAT(" ",2X,I3,2(5X,F13.6),F9.3,F7.3,12X,F7.3,12X,
     *       F9.6,9X,F13.6)
  535 FORMAT("1",22X,"SADCOR PROGRAM - MECHANICAL ENGINEERING",
     *       ", PLASMA LAB",//)
C
      RETURN
      END
C-----------------------------------------------------------------------
      SUBROUTINE ABEL4(G,CLL,C,HR,DRAD,Z1,W,LI,JQ,NINT,CI,SI)
C-----------------------------------------------------------------------
C
C  THIS ROUTINE CONVERTS LATERAL INTENSITY TO RADIAL EMISSION
C  COEFFICIENT USING ABEL INVERSION. THIS PARTICULAR ROUTINE
C  USES 4-INTERVAL SMOOTHED INTENSITY.
C
      DIMENSION G(100),CI(100),SI(100),HR(3,5),C(3,5,9),
     *          LQK(6),Z(100)
C
C
      ML=NINT
      SISUM = 0.
      DO 571 I=2,JQ
      L=JQ+1-I
      IF(HR(1,ML)-G(L)) 560,560,565
  565 KPASS = 0
      ML=ML-1
      IF(I.EQ.2) NINT=ML
   560 SIL=0.
      LL=L
      IF(ML-NINT) 593,574,574
  593 IF(KPASS.EQ.1) GO TO 595
      LQK(ML)=L
      KPASS = 1
  595 LQ = LQK(ML)
      GO TO 575
  574 LQK(ML) = JQ
      LQ = JQ
```

```
575 R1=G(L)
    R2=G(LQ)
    DO 572 LM=ML,NINT
    IF(LM-1)573,573,850
573 S2=SQRT (G(LQ)*G(LQ)-G(L)*G(L))
    S1L=-1./3.14159*(2.*C(1,1,2)*S2+4.*C(1,1,3)*(S2**3/3.+G(L)*G(L)*
   1    S2)+6.*C(1,1,4)*(S2**5/5.+2./3.*G(L)*G(L)*S2**3+G(L)**4*S2))
    GO TO 580
850 Z(L)=G(L)
    Z(LL)=G(LL)
    Z(LQ)=G(LQ)
    S1=SQRT (Z(LL)*Z(LL)-Z(L)*Z(L))
    S2=SQRT (Z(LQ)*Z(LQ)-Z(L)*Z(L))
    WTEST=(R2+S2)/(R1+S1)
    IF(WTEST.GT.0.) GOTO 9501
    PRINT*,'  ****  WARNING  ****'
    PRINT*,  'THE ARGUMENT IN THE EMISSION COEFF. CALCULATION'
    PRINT*,'  IS NEGATIVE. SO THIS STEP IS BYPASSED'
    GO TO 580
9501 S1L=S1L-1./3.14159*(C(1,LM,2)*ALOG((R2+S2)/(R1+S1))+2.*C(1,LM,3)*
   1     (S2-S1)+3.*C(1,LM,4)*((R2*S2-R1*S1)/2.+Z(L)*Z(L)/2.*ALOG((R2
   2  +S2)/(R1+S1))))
 580 LL=LQK(LM)
    R1=G(LL)
    IF(LM-NINT+1)577,578,578
 577 LQ = LQK(LM+1)
    GO TO 530
 578 LQ=JQ
 530 R2=G(LQ)
 572 CONTINUE
    IF(ML-1)753,753,754
 753 Z(L)=G(L)*G(L)
    GO TO 755
 754 Z(L)=G(L)
 755 CI(L)=C(1,ML,1)+C(1,ML,2)*Z(L)+C(1,ML,3)*Z(L)*Z(L)+C(1,ML,4)*
   1   Z(L)**3
    SI(L)=S1L*Z1*10.
    IF(L1.EQ.2) SI(L)=SI(L)*W**2/2.9979E10/1.E8
    SISUM = SISUM + S1L
 571 CONTINUE
    SICHCK = SISUM * DRAD * 2.
    TOLER = ABS(SICHCK-CLL)/CLL * 100.
    NTOLER = TOLER + .5
C     PRINT*,'---- ----------------------------------------------------'
    PRINT*,'  ABELLING IS GOOD TO WITHIN  ',TOLER,' PERCENT '
C     PRINT*,'  ----------------------------------------------------'
    PRINT*, ' C.L. INTENSITY = ',CLL,'   CHECK INTENS. = ',SICHCK
    RETURN
    END
C ---------------------------------------------------------------
    SUBROUTINE ABEL(G,CLLN,DRAD,W,NTOLER,Z1,L1,JQ,CI,SI)
C---------------------------------------------------------------
C
C    THIS SUBROUTINE USES THE ABEL INVERSION  TO CONVERT THE LATERAL
C    INTENSITY TO RADIAL EMISSION COEFFICIENTS. THIS PARTICULAR
C    SUBROUTINE USES THE INTENSITY SMOOTHED BY 4-INTERVAL POLYNOMIAL.
C
     DIMENSION G(100),C(3,5,9),CI(100),SI(100),CLLN(100),X(100)
    *         ,Y(100),H(9),Z(100)
C
     NPOW=8
     YMIN=100.
     DO 6041 I=1,JQ
     X(I) = G(I) ** 2
     Y(I) = CLLN(I)
     IF(I.LT.25) GO TO 6041
```

```
      IF(Y(I).GT.Y(I-1)) GO TO 6047
      IF(Y(I).LT.YMIN) YMIN=Y(I)
 6041 CONTINUE
 6047 JQ=I-1
      IF(YMIN.EQ.100.) PRINT*,' ***** ERROR: YMIN=100 IN SUB ABEL'
      DO 6048 K=1,JQ
 6048 Y(K)=Y(K)-YMIN
      CALL POLFIT(X,Y,X,JQ,NPOW,0,H,CHI)
      DO 6042 I=1,NPOW
 6042 C(1,1,I) = H(I)
      DO 100 K=1,JQ
      CLLN(K)=H(1)+H(2)*X(K)+H(3)*X(K)**2+
     1         H(4)*X(K)**3+H(5)*X(K)**4+H(6)*X(K)**5+H(7)*X(K)**6+
     2   H(8)*X(K)**7
      PRINT*,' CLLN  Y  ', CLLN(K),Y(K)
      IF(K.LT.20) GO TO 100
      IF(CLLN(K).GT.CLLN(K-1)) GO TO 101
  100 CONTINUE
  101 JQ=K-1
      SISUM = 0.
      DO 571 I=2,JQ
      L=JQ+1-I
      SIL=0.
      LQ = JQ
  575 R1=G(L)
     3  +Q6*S2)+10.*H(6)*(S2**9/9.+4./7.*Q2*S2**7+
     4   Q4*S2**5+Q6*S2**3+Q8*S2)
     5  +12.*H(7)*(S2**11/11.+5./9.*Q2*S2**9+Q4*S2**7+Q6*S2**5
     6  +Q8*S2**3+Q10*S2)
     7  +14.*H(8)*(S2**13/13.+6./11.*Q2*S2**11+Q4*S2**9+Q6*S2**7
     8  +Q8*S2**5+Q10*S2**3+Q12*S2))
      Z(L)=G(L)*G(L)
      CI(L)=C(1,1,1)+C(1,1,2)*Z(L)+C(1,1,3)*Z(L)*Z(L)+C(1,1,4)*
     1   Z(L)**3
     2   +C(1,1,5)*Z(L)**4
      SI(L)=SIL*Z1*10.
      IF(L1.EQ.2) SI(L)=SI(L)*W**2/2.9979E10/1.E8
      SISUM = SISUM + SIL
  571 CONTINUE
      SICHCK = SISUM * DRAD * 2.
      TOLER = ABS(SICHCK-CLLN(1))/CLLN(1) * 100.
      NTOLER = TOLER + .5
C     PRINT*,'---- ----------------------------------------------------'
      PRINT*,'  ABELLING IS GOOD TO WITHIN  ',TOLER,' PERCENT '
C     PRINT*,'  ----------------------------------------------------'
      PRINT*, ' C.L. INTENSITY = ',CLLN(1),'   CHECK INTENS. = ',SICHCK
      RETURN
      END
C-----------------------------------------------------------------
      SUBROUTINE ABELNO(G,CLLN,DRAD,W,NTOLER,Z1,L1,JQ,CI,SI)
C-----------------------------------------------------------------
C
C    THIS SUBROUTINE USES THE ABEL INVERSION  TO CONVERT THE LATERAL
C    INTENSITY TO RADIAL EMISSION COEFFICIENTS. THIS PARTICULAR
C    SUBROUTINE USES THE INTENSITY SMOOTHED BY 4-INTERVAL POLYNOMIAL.
C
      DIMENSION G(100),C(3,5,9),CI(100),SI(100),CLLN(100),X(100)
     *         ,Y(100),H(9),Z(100),A(70,70),B(70,70),GG(100)
C
C
      NPOW=9
      DO 6041 I=1,JQ
      X(I) = G(I) ** 2
      Y(I) = CLLN(I)
      IF(I.LT.25) GO TO 6041
      IF(Y(I).GT.Y(I-1)) GO TO 6047
```

```
6041 CONTINUE
6047 JQ=I-1
     Y(JQ)=0.
     CALL POLFIT(X,Y,X,JQ,NPOW,0,H,CHI)
     DO 6042 I=1,NPOW
6042 C(1,1,I) = H(I)
     DO 100 K=1,JQ
     CLLN(K)=H(1)+H(2)*X(K)+H(3)*X(K)**2+
    1          H(4)*X(K)**3+H(5)*X(K)**4+H(6)*X(K)**5+H(7)*X(K)**6+
    2    H(8)*X(K)**7+H(9)*X(K)**8
 100  CONTINUE
      CLLN(JQ)=0.
      SISUM = 0.
       DO 110 K=1,JQ
       SUM=0.
       DO 200 N=K,JQ-1
       A(K,N)=1./(2.*N-1)*((N**2-(K-1)**2)**.5-((N-1)**2-(K-1)**2)**.5)
      IF(N.GT.K) GO TO 300
      B(K,N)=-A(K,N)
      GO TO 400
  300 B(K,N)=A(K,N-1)-A(K,N)
  400 SUM=SUM+B(K,N)*CLLN(N)
  200 CONTINUE
      SIL=-2./(3.14159*DRAD)*SUM
      SI(K)=SIL*Z1*10.
      SISUM=SISUM+SIL
  110 CONTINUE
      SICHCK = SISUM * DRAD * 2.
      TOLER = ABS(SICHCK-CLLN(1))/CLLN(1) * 100.
      NTOLER = TOLER + .5
C     PRINT*,'---- ----------------------------------------------------'
      PRINT*,'  ABELLING IS GOOD TO WITHIN  ',TOLER,' PERCENT '
C     PRINT*,'  ----------------------------------------------------'
C     PRINT*, ' C.L. INTENSITY = ',CLLN(1),'   CHECK INTENS. = ',SICHCK
      RETURN
      END
```

Appendix E

Electron Energy Equation

Because of the introduction of the new temperature, T_{exa}, an additional equation to those traditionally employed by two temperature models, is needed. This requirement is met by introducing the electron energy conservation equation. In stationary conditions the electron energy balance can be written as [30],

$$\sigma E^2 = \nabla \mathbf{q}_e + \phi_{elastic} + \phi_{inelastic} + q_{rad,e}$$

The left hand side represents the total input energy to electrons due to the present elecric field E and σ is the electron electrical conductivity. $\mathbf{q}_e$ is the electron heat flux vector which includes electron conduction and diffusion, and may be written as,

$$\mathbf{q}_e = -k_e \nabla T_e + \frac{5}{2} k T_e n_e < \mathbf{v}_e >$$

where k_e represents the thermal conductivity. $\phi_{elastic}$ corresponds to the electron energy losses due to elastic collisions with heavy particles and is given by

$$\phi_{elastic} = 3 \frac{m_e}{m_g} k n_e (T_e - T_g) \sum_h \overline{\nu}_{eh}$$

$\overline{\nu}_{eh}$ is the average frequency of elastic collisions between electrons and heavy particles of species h. For plasmas with only one degree of ionization, it can be written as,

$$\sum_h \overline{\nu}_e h = \left(\frac{3kT_e}{m_e} \right)^{1/2} (n_e Q_{ei} + n_a Q_{ea})$$

$\phi_{inelastic}$ represents the electron energy loss due to inelastic processes such as ionization,

$$\phi_{inelastic} = E_I \nabla . n_e < \mathbf{v}_e >$$

Finally, $q_{rad,e}$ is the radiative loss to the free-free and free-bound transitions.

In plasmas with cylindrical geometry where the gradients are only in the radial direction, the electron energy equation can be simplified to

$$\begin{aligned} \sigma E^2 &= (3m_e/m_g)k(T_e - T_g)n_e(3kT_e/m_e)^{1/2}(n_e Q_{ei} + n_a Q_{ea}) \\ &\quad -\frac{1}{r}\frac{d}{dr}(rk_e\frac{dT_e}{dr}) - (\frac{5}{2}kT_e + E_I)\frac{1}{r}\frac{d}{dr}(rAD_a\frac{dn_e}{dr}) + q_{rad,e} \end{aligned}$$

where D_a is the ambipolar diffusion coefficient, and A is a correction factor, the value of which lies between 1.1 and 1.3. This factor takes into account the role of atom density in the ambipolar diffusion flux [40]. A is given by,

$$A = \frac{n_a}{n_a + n_e}\left[1 - (\frac{n_e}{n_a})(\frac{dn_a}{dn_e})\right]$$

Electron energy equation requires transport properties which are taken from the following sources. Thermal conductivity k_e, electrical conductivity σ, and ambipolar diffusion coefficient D_a, are tabulated by DEVOTO [23], Q_{ei} from MITCHNER AND KRUGER corrected by KIHARA AND AONO[51], Fig.E.1, Q_{ea} from FROST AND PHELPS[38], Fig.E.2, and $q_{rad,e}$ from works of BAUDER[8].

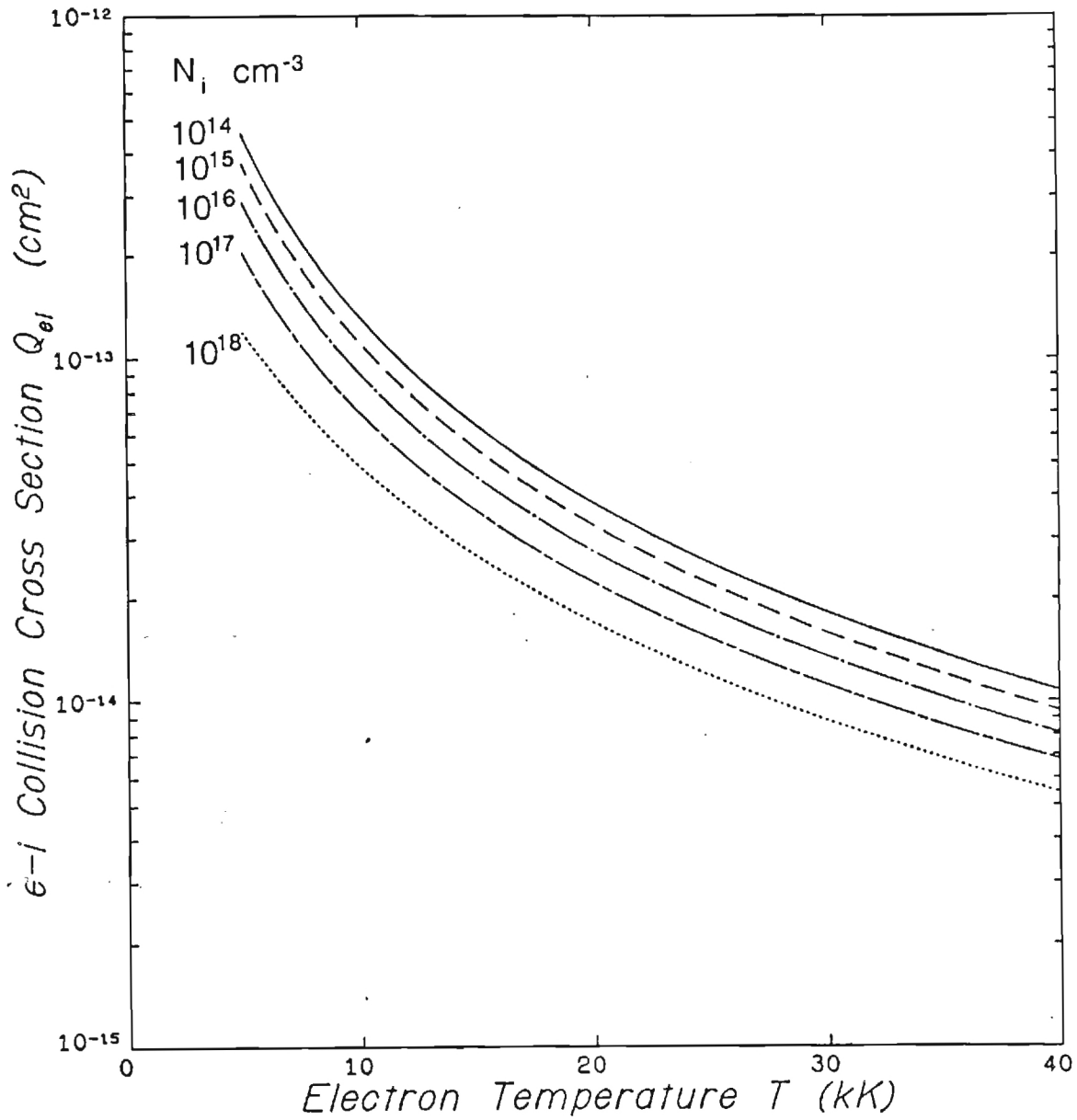

Figure E.1: Electron-ion collision cross section for various ion densities as a function of the electron temperature, from ref.[51].

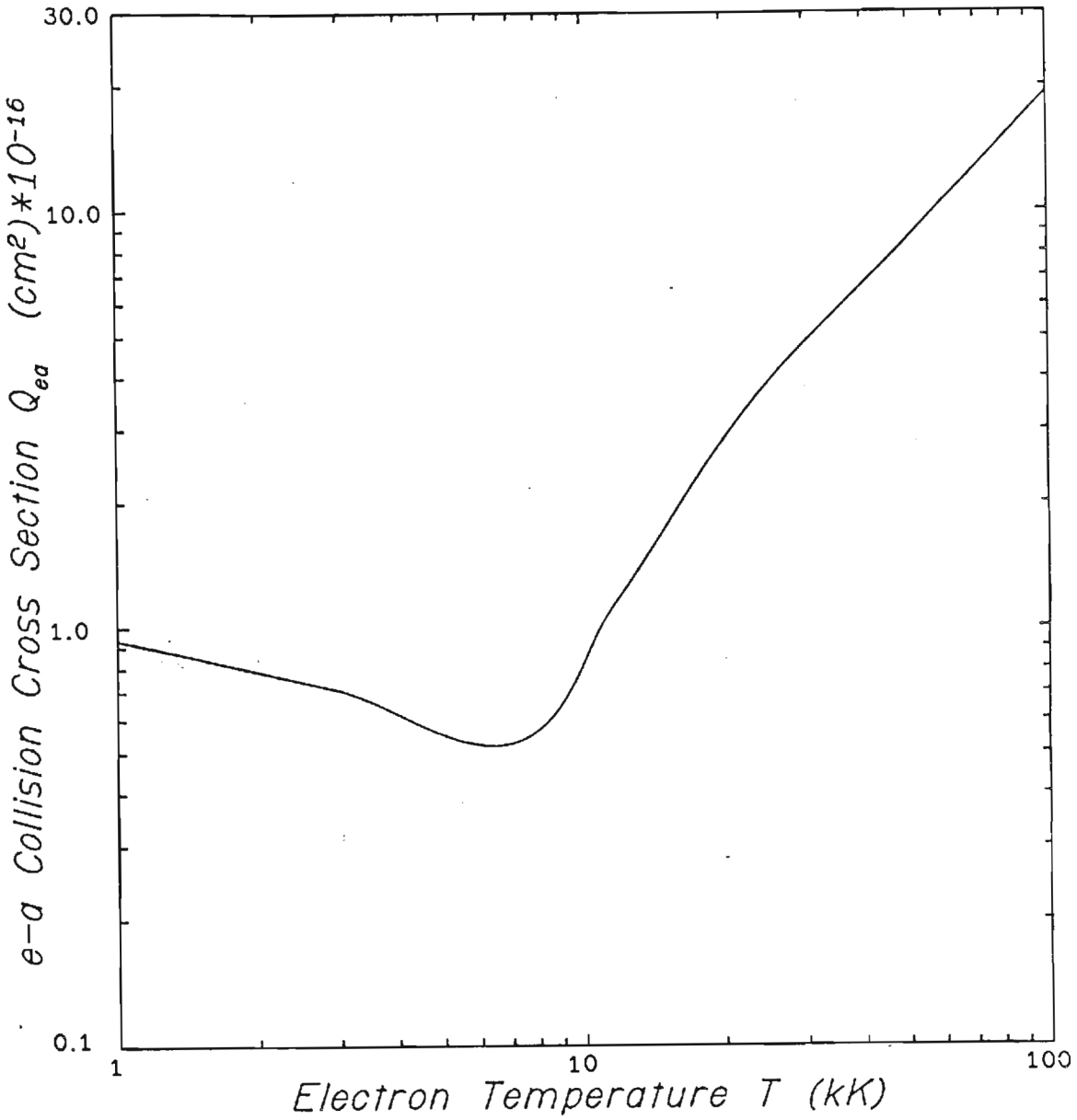

Figure E.2: Electron-atom collision cross section as a function of electron temperature, from ref.[38].